Thrust Layout Optimization for Masonry Structures

A thesis submitted to the University of Sheffield for the degree of Doctor of Philosophy

Kavinda Isuru Udayanga Nanayakkara

Department of Civil and Structural Engineering

January 2024

Dedicated to the memory of Henry Moseley, Alan Turing and Aaron Swartz—genius sacrificed to war, prejudice, and greed...

Acknowledgments

My work towards a degree of Doctor of Philosophy and this thesis would not have been successful if not for the guidance and support from many individuals who devoted their time and resources towards the success of this project.

I am deeply thankful to my research supervisors, Professor Matthew Gilbert and Dr Andrew Liew, for their guidance and support throughout the research project. With their constant guidance and motivation, this research project achieved greater heights. The technical input from Dr Linwei He, and the wider Layout Optimization group at the Department of Civil and Structural Engineering at the University of Sheffield, was useful for the successful completion of this work.

The generous funding from the Department of Civil and Structural Engineering at the University of Sheffield is gratefully acknowledged: if not for that, it would not have been possible to pursue this study.

My stay in Sheffield, two years of which was during a global pandemic and a political-economic collapse of my home country, would not have been as enjoyable and fruitful as it was if not for the wonderful group of friends and colleagues. Special thanks to the colleagues, over a period of four years, at the Department of Civil and Structural Engineering at the University of Sheffield—Farshid, Liang, Leanna, Adrien, Arthur, Kajanan, Oswald, Adam, Emma, Wengchao, Shanker, Lea—for all the beautiful moments shared.

Finally, I owe a huge debt of gratitude to my parents for this was not a project of four years, but decades in the making.

With the support from those who are mentioned here by name and otherwise, my research towards the Doctoral degree became a successful endeavour and it is my wish that its findings would be beneficial to science and mankind.

Abstract

Form-resistant structures are efficient structural systems that can contribute to addressing the adverse climate impacts of the construction industry by reducing material usage. Also, the availability of improved assessment and strengthening methods for masonry form-resistant structures can extend the life of many ageing buildings and other structures, ensuring these are not needlessly replaced at great cost to the planet.

Building on an observation by Hooke, Heyman's 'safe theorem' has been widely used to assess the safety of form-resistant structures. However, Heyman used a funicular thrust line to represent equilibrium, which has been found to be problematic in some cases. Seeking to improve upon the funicular thrust line, the notion of a 'thrust layout' is presented here. This can accurately represent the state of equilibrium while also enabling visualization of the flow of forces within a form-resistant structure. This is achieved by explicit consideration of block stereotomy and more realistic treatment of tensile forces.

A new automated analysis procedure, termed thrust layout optimization (TLO), is presented to allow identification of thrust layouts in masonry gravity structures comprising general arrangements of masonry blocks. The procedure employs a modified truss layout optimization with transmissible loads formulation and allows explicit consideration of sliding failures. A range of examples that demonstrate the efficacy of the TLO procedure are presented; these show that thrust line bifurcations can be automatically identified in problems involving openings, and that there is no need to estimate the 'ineffective area' in buttress wall problems, both issues encountered when using the traditional thrust line analysis method.

The TLO procedure is then extended to determine the optimal placement of auxiliary strengthening measures. While current practice is to use engineering intuition to determine the placement of strengthening measures, TLO provides a more robust physics-based approach, with clear visualization of force flows in strengthened structures.

සාරාංශය

ප්‍රතිරෝධී-ආකෘතියක් සහිත ව්‍යුහ (form-resistant structures) යනු ගොඩනගිලි අමුද්‍රව්‍ය භාවිතය අවම කිරීම මගින් ඉදිකිරීම් කර්මාන්තයේ අහිතකර පාරිසරික බලපෑම් අවම කරන කාර්යක්ෂම ව්‍යුහාත්මක පද්ධති (structural systems) වේ. තව ද, පෙදරේරුමය ප්‍රතිරෝධී-ආකෘතියක් සහිත ව්‍යුහ සඳහා වැඩිදියුණු කළ විශ්ලේෂණ ක්‍රම සහ සවිගැන්වීම් ක්‍රම යොදා ගැනීමෙන් බොහෝ පැරණි ගොඩනැගිලි සහ අනෙකුත් ඉදිකිරීම්වල ආයු කාලය දීර්ඝ කළ හැකි අතර එමගින් එම ඉදිකිරීම් පරිසරයට හානිකර ලෙසින් කඩා නොදැමෙන වග තහවුරු කරයි.

ප්‍රතිරෝධී-ආකෘති සහිත ව්‍යුහයක සුරක්ෂිත බව තක්සේරු කිරීමට, හූක් විසින් සිදු කරන ලද නිරීක්ෂණයක් පසුබිම් කරගෙන, හෙයිමන්ගේ 'ආරක්ෂිත ප්‍රමේයය' බහුලව භාවිත වේ. හෙයිමන්ගේ ආරක්ෂිත ප්‍රමේයයේ දී ප්‍රතිරෝධී-ආකෘති සහිත ව්‍යුහයක සමතුලිතතාවය නිරූපණය කිරීමට රැහැන් තෙරපුම් රේඛාව ක් (funicular thrust line) උපයෝගී කර ගනු ලැබේ. කෙසේ වෙතත් මෙම රැහැන් තෙරපුම් රේඛාවේ භාවිතය ගැටලු සහගත බව පසුව අනාවරණය කර ගැනිණ. මෙම අධ්‍යයනයේදී රැහන් තෙරපුම් රේඛාව වැඩිදියුණු කරමින් 'තෙරපුම් ජාලය' (thrust layout) නම් සංකල්පයක් ඉදිරිපත් කෙරේ. තෙරපුම් ජාලා නිවැරදිව සමතුලිතතාවය නිරූපණය කරන අතර නිසි පරිදි ව්‍යුහය තුළ බල ප්‍රවාහය (force flow) ද දෘශ්‍යමාන කරයි. තෙරපුම් ජාලා වලට මෙම හැකියාව ලැබෙනුයේ එය ගඩොලු රටාව එලෙසම නිරූපණයත්, ගඩොලුවල ආතන්‍ය බල ධාරිතාව වඩා යථාවාදීව නිරූපනයත් හේතුවෙනි.

පෙදරේරුමය ප්‍රතිරෝධී-ආකෘති සහිත ව්‍යුහ තුළ බල ප්‍රවාහ (එනම් තෙරපුම් ජාලා) හඳුනාගැනීමට තෙරපුම් ජාලා ප්‍රශස්තකරණය (thrust layout optimization) ලෙස හඳුන්වන නව ස්වයංක්‍රීය විශ්ලේෂණ ක්‍රියා පටිපාටියක් මෙහිදී ඉදිරිපත් කෙරේ. එය සම්ප්‍රේෂණය කළ හැකි බල (transmissible loads) සහිත නවීකරණය කරන ලද සැකිලි පිරිසැලසුම් ප්‍රශස්තකරණයක් (truss layout optimisation) භාවිතා කරන අතර ගඩොලු එකිනෙක මත ලිස්සා යාම මගින් වන කඩා වැටීම් සෘජුවම සලකා බැලීමට ඉඩ සලසයි. තෙරපුම් ජාලා ප්‍රශස්තකරණ ක්‍රියා පටිපාටියේ කාර්යක්ෂමතාවය පෙන්නුම් කරන උදාහරණ මාලාවක් මෙහි ඉදිරිපත් කර ඇත. අභ්‍යන්තර කවුළු සහිත ආකෘතිවල තෙරපුම් රේඛා බෙදීම් (bifurcations) ස්වයංක්‍රීයව හඳුනාගත හැකි බව සහ ආධාරක පවුරු (buttress wall) විශ්ලේෂණයේදී අකාර්යක්ෂම ප්‍රදේශය තක්සේරු කිරීම අනවශ්‍ය බව මේවා පෙන්නුම් කරයි. මේවා සම්ප්‍රදායික තෙරපුම් රේඛා විශ්ලේෂණ ක්‍රමය භාවිතයේදී පැන නගින දුර්වලතා වේ.

පසුව තෙරපුම් ජාලා ප්‍රශස්තකරණය ක්‍රියා පටිපාටිය පෙදරේරුමය ඉදිකිරීම්වල සවිගැන්වීම් ස්ථානගත කිරීම ප්‍රශස්ත කිරීම සඳහා වැඩි දියුණු කෙරිණ. සවිගැන්වීම් ස්ථානගත කිරීම නිර්ණය කිරීමේදී වර්තමාන පරිචය වන්නේ ඉංජිනේරු බුද්ධිය භාවිතා කිරීමයි. ඉන් ඔබ්බට යමින් වැඩි දියුණු කළ තෙරපුම් ජාලා ප්‍රශස්තකරණ (extended TLO) ක්‍රියා පටිපාටිය සවිගැන්වීම් මගින් ශක්තිමත් කරන ලද ව්‍යුහ තුළ බල ප්‍රවාහ පැහැදිලිව දෘශ්‍යකරණය කරමින් භෞතික විද්‍යා මූලධර්ම පදනම් කරගත් ප්‍රවේශයක් සපයයි.

Contents

List of Figures

List of Tables

Chapter 1

Introduction

Structural engineering and architecture professionals in the UK have declared a climate and biodiversity emergency, calling everyone in the building and construction industry into action towards a more responsible construction industry [1, 2]: In its annual global status report for building and construction [3], in 2022, the United Nations Environment Programme reports that the sector has accounted for around 37% of energy and process related carbon dioxide emissions, of which about 25% comes from building construction industry.

Amongst other things, the declaration by structural engineers calls for upgrading existing buildings for extended use, a shift to low embodied carbon materials, and minimization of wasteful use of resources in structural engineering design. Along similar lines, the United Nations' Sustainable Development Goals [4] identify 'sustainable cities and communities' (Goal 11) and 'responsible consumption and production' (Goal 12), in more general terms—reaching beyond the building and construction industry.

Within these frameworks, we can identify two paths for potential construction projects: (i) to assess and strengthen existing structures (Fig. 1.1a), thereby avoiding new construction; and (ii) when it is absolutely necessary to build anew, to design more sustainable buildings by using efficient structural forms and materials with low embodied carbon (Fig. 1.1b).

A considerable number of existing masonry housing, in the UK [7] and across the globe, are reaching their end of life. Their useful life can be extended by assessment of the current state of the structure and carrying out appropriate structural interventions as required. Although there are various methods for the assessment of load carrying capacity of structures, the identification of strengthening measures required is in most cases based on engineering intuition, rather than physics-based procedures.

Form-resistant structures are an efficient structural form as they fully utilize material at ev-

(a) (b)

Figure 1.1: Way forward for building and construction industry; (a) restore and strengthen existing structures—application of CFRP strips to strengthen a masonry vault (after [5]); (b) build efficiently with efficient structural forms and low carbon materials—15m span earthen shell roof (after [6]).

ery cross-section, as opposed to the commonly used column-beam frames, which are comparatively inefficient. Masonry gravity structures—from simple housing units to grand cathedrals—are also form-resistant structures. These structures, which are made of material stronger in compression than tension, predominantly carry the applied loads in compression. Nonetheless, they possess and use some tensile capacity in resisting externally applied loads. In fact, it has been shown that the optimal structural form to carry a uniformly distributed load across a single span above two fixed-pin supports will be predominantly in compression, but with some amount of tension allowed [8, 9].

It is typical for a form-resistant structure to be represented by a line of thrust (Fig. 1.2a) or a force (or thrust) network (Fig. 1.2b), for the purposes of analysis and form-finding. This network of forces is a discrete representation of a (possible) equilibrium force flow in an assembly of blocks or a continuum of material. Although these methods have been successfully applied in the design and analysis of form-resistant structures, they do not make use of the tensile strength capacity present in the material. It is also noted that the choice of the topology of the force network will influence the geometry of the optimal form [10], where the optimal solution sought can be the minimum volume structure, the closest fit to a target geometry, etc.

The discrete representation of forces in thrust lines and thrust networks makes it possible for them to be integrated with techniques such as ground structure layout optimization (LO), which were first developed for application to truss-like structures. Therefore, the possibility exists for the use of LO in the analysis and design of form-resistant structures. The use of a ground structure to identify the topology of a possible thrust network is a particularly interesting feature to be explored.

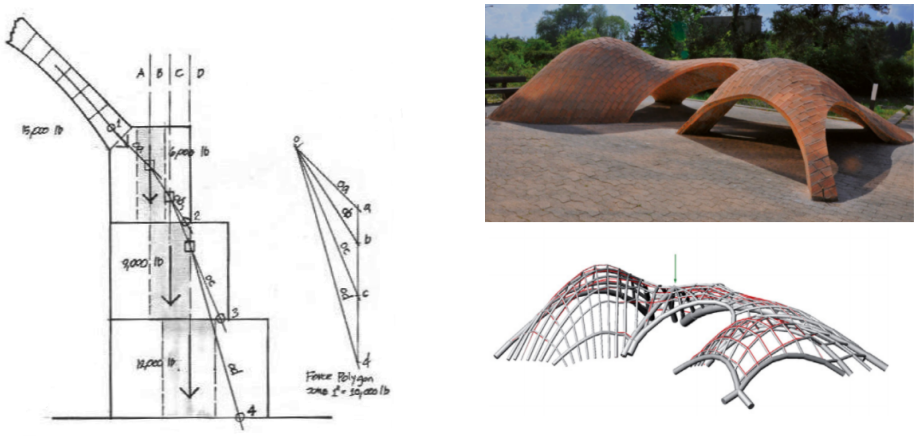

(a) line of thrust (b) thrust network

Figure 1.2: Representation of equilibrium of form resistant structures: (a) line of thrust for a stepped buttress under self-weight and thrust from an arch (after [11]); (b) thrust network used in the design of a free-form unreinforced tile vault, subjected to self-weight and a point load (after [12]).

In ground structure layout optimization, a ground structure representing all possible member connections (Fig. 1.3b) is defined within the design domain (Fig. 1.3a) and the optimization procedure picks up the appropriate members from the ground structure, under the constraints of equilibrium and yielding. Ground structure layout optimization, with its improvements—e.g., using a post-processing geometry optimization step to allow ground structure nodes to be moved (Fig. 1.3d)—has shown to be an efficient tool to identify optimal pin jointed structures [13] [14].

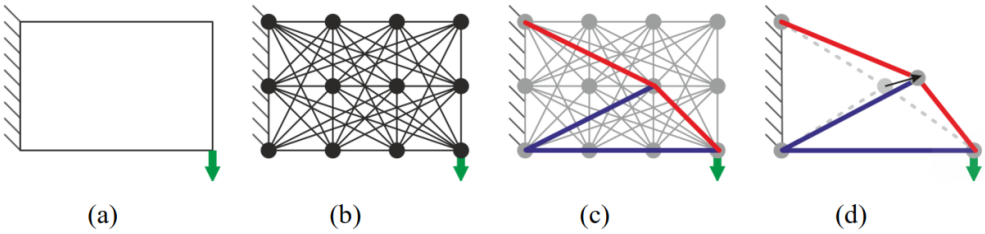

Figure 1.3: Steps in ground structure layout optimization: (a) design domain; (b) ground structure; (c) optimal layout found; (d) post-processing step of geometry optimization (after [15]).

The work presented here critically evaluates the methods used in practice for the assessment of form-resistant structures and seeks to make use of ground structure layout optimization to develop readily usable tools to assist engineers in addressing the demands of the climate emergency, within the building and construction industry.

Chapter 2

Motivation: The Climate Emergency

The United Nations defines climate change as "long-term shifts in temperatures and weather patterns" [16]. During the past 200 years of the post-industrialization era, the earth's temperature has risen by nearly 1^oC [17]. This directly impacts food production (due to increased and more severe draughts), displaces communities (due to rising sea levels), and threatens human and other life forms on earth (from increased heat-related illnesses in humans to acidification of the oceans threatening marine life) [18]. The earth's rising temperature is a result of human activities (Fig. 2.1) producing more greenhouse gases than the earth's systems can handle (i.e., safely absorb). These anthropogenic greenhouse gas emissions are also observed to be contributing towards the rising number and the severity of natural disasters across the globe: from droughts and wildfires to storms and flooding [19].

Recognizing the severity of the impacts of climate change and the urgency of making significant changes, not only at an individual level but also at local government, state government and global levels, declarations of 'climate emergency' have come about: the first such instance is by the city of Darebin in Australia [21] and now by nation-states (from Bangladesh [22] to the European Union [23]) and professionals (from medical [24] to engineering [25]). These declarations of climate emergency are of significance as they make addressing climate change a common goal and demand the governments (and the professionals) to prioritize the same: 'emergency' allude to the urgency of action. However, some drawbacks of the 'emergency' framing have been noted: e.g., technocratic governing leading to anti-democratic policies and action, higher political pressure leading to placebo policies [26].

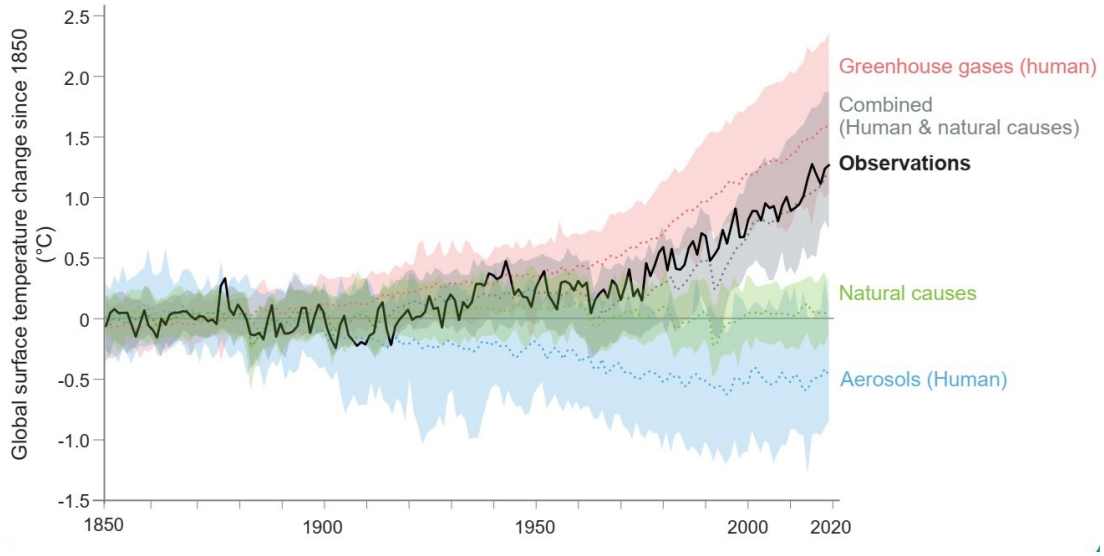

Figure 2.1: Evidence of anthropogenic climate change: The global temperatures observed can be reproduced only when human-caused emissions are considered. Solid/dashed lines show the average of the corresponding models and shading indicates the uncertainty ranges of the simulations. Average temperature between 1850-1900 as base temperature (after [20]).

The main greenhouse gases contributing to climate change are carbon dioxide and methane [16]. The main causes of these greenhouse gas emissions are power generation (for manufacturing industries, construction industry as well as domestic usage), transportation (from internal combustion engines), and food production (in various stages from land clearance to fertilizer production; farm equipment to methane emissions from cattle) [18]. Furthermore, deforestation exacerbates the effects of greenhouse gas emissions by limiting the capacity of the earth's systems to absorb greenhouse gases.

In its annual global status report for building and construction [3], in 2022, the United Nations Environment Programme (UNEP) reports that the sector has accounted for around 37% of energy and process-related carbon dioxide emissions (Fig. 2.2): of that, about 25% comes from building construction industry (i.e., about 9% of all global carbon dioxide emissions). The report highlights the importance of addressing the issue of embodied carbon in buildings so that it does not undermine the reductions achieved from energy efficiency. This is of particular importance in the African continent, as an estimated 70% of its 2040 building stock is yet to be built.

Paris Agreement reached at the 21st Conference of Parties (COP21) in Paris in 2015, is a landmark call for action towards reducing anthropogenic carbon emissions and mitigating effects of climate change. The Paris Agreement [27] recognizes the urgent threat of climate change and the parties agreed to "holding the increase in the global average temperature

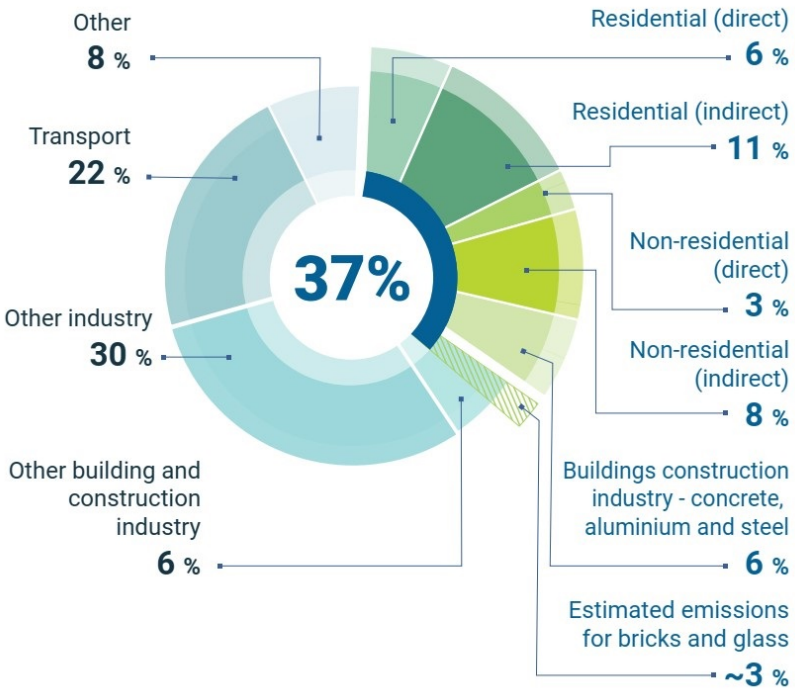

Figure 2.2: CO_2 emissions from building in 2010-2021: The building construction industry has contributed to ∼9% of global CO_2 emissions in the past decade. Emissions from construction materials include raw material preparation, processing and production. Other construction refers to infrastructure construction (after [3]).

to well below 2^oC above pre-industrial levels and pursuing efforts to limit the temperature increase to 1.5^oC above pre-industrial levels." The agreement also recognizes the principle of "common but differentiated responsibilities" noting the differences by country in their carbon emission, the level of development, and the degree to which the effects of climate change have been experienced. For instance, developed countries which are responsible for a major part of the global carbon emissions over the past 200 years and reaping benefits of the same (e.g., built large-scale industries, supply chains and research facilities) hold a responsibility towards developing technologies that could mitigate the future carbon footprint of developing countries, while assisting them in their development goals.

In the UK, its Climate Change Act of 2008 (amended in 2019) [28] commits the government "to ensure that the net UK carbon account for the year 2050 is at least 100% lower than the 1990 baseline": the UK's net zero target. Although legislation towards achieving net zero targets is still in works, the Institution of Structural Engineers-UK have made the commitment to "treat sustainability and the climate emergency with equal importance to life safety" [1], thus recognizing the importance and urgency of action towards net-zero emissions.

Historic England [7] reports that, in 2018, 5.1 million homes (21% of all homes) in England

were over 100 years old: This building stock consists of solid brick or stone masonry, or timber construction. And in the 2010-2018 period over 70,000 of the pre-1919 homes in England were demolished. The report notes a 60% saving on whole-life carbon emissions (by 2050) by opting for refurbishment and retrofits instead of demolition and new constructions. Furthermore, the UK Committee on Climate Change [29] notes retrofitting of existing homes as one of five key priorities for the UK housing sector in achieving the UK's net zero target. The Intergovernmental Panel on Climate Change (IPCC) in its 2022 summary for policymakers [30] notes the importance of renovation, retrofitting and repurposing existing buildings, whilst also noting the importance of low-emission construction materials, building typologies and form.

Noting the severity of climate change and the urgency to address the issue of anthropogenic greenhouse gas emissions, the need to urgently address the contribution of the global building construction sector is noted. One way of addressing this is by preserving the existing building stock so that no new constructions are needed: However, the need for new building stock in the developing economies is also noted. Noting that a major portion of the UK's building stock is of brick and stone masonry (and that a sizeable portion of that is ageing), the importance of having tools to assess the state of masonry gravity structures, and form-resistant structures in general, is recognized. Similarly, the need for the development of low-carbon building materials and typologies is noted, while recognizing stone masonry and stabilised earth block masonry to be such materials.

Chapter 3

Literature Review

Over the centuries, structural engineering designs have shifted from form-resistant systems; e.g., Inca rope bridges, to trusses, and then to concrete beam and slab systems. However, as the structural systems have progressed, the efficiency of the systems has reduced; hanging cables working purely in tension can carry more load per unit of material compared to an equivalent beam in bending (Fig. 3.1).

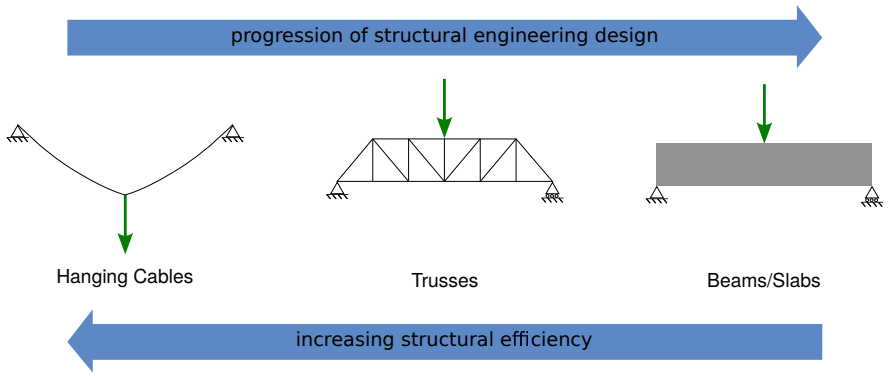

Figure 3.1: Hierarchy of structures.

Recalling our motivation of reducing the building and construction industry's impact on climate change, the structural efficiency of form-resistant structures, such as hanging cable models and arches, can be made use of. Furthermore, masonry gravity structures that form a major part of the existing building infrastructure in the UK and many other parts of the world can also be considered to be form-resistant. In the following sections, form-resistant structures and means of analysing them are explored in detail.

3.1 Form-resistant structures

Following Salvadori and Heller [31], form-resistant structures are defined as, "structures in which strength [*sic*] is obtained by shaping the material according to the loads they must carry", where here, the term strength refers to the load carrying capacity of the structure, not the strength of the material. For instance, consider the inclined columns in Colònia Güell and Park Güell (Fig. 3.2). If they were vertical columns, as typically found in column-beam frame structures, they would likely be subjected to bending and would either require increasing the material strength in tension (e.g., by having reinforcing steel) or increasing the size of the column. Instead, the same amount of material is used, without extra tensile reinforcement, by simply moving the material to where it is needed to carry the load as a compressive force. Note that this "form following force" approach reduces the amount of material used and allows for construction with natural materials, which, in most cases, are stronger in compression; e.g., stone, earthen material, etc.

(a) Colònia Güell (b) Park Güell

Figure 3.2: Form following force: inclined columns in Antoni Gaudi's designs are a classic example of form-resistant structures.

In designing the Colònia Güell, between 1898 and 1908, Antoni Gaudi used a hanging chain model to achieve this "form following force" objective [32], as shown in Fig. 3.3. As Robert Hooke previously observed, the form of a hanging chain (i.e., a catenary) inverted gives the form of an equivalent rigid arch, where the boundary forces (support reactions and

loading) and the internal force are also inverted in the process. Thus, the hanging chain, which carries only tensile forces, can be inverted to give an arch only in compression (Section 3.1.1). Thus, the process of letting a (nearly) weightless cable take its desired form when the corresponding loads are hung on it, realizes the idea of "form following force". Although not necessarily inspired by this observation by Hooke [32], Gaudi used the same idea, here via a network of cables.

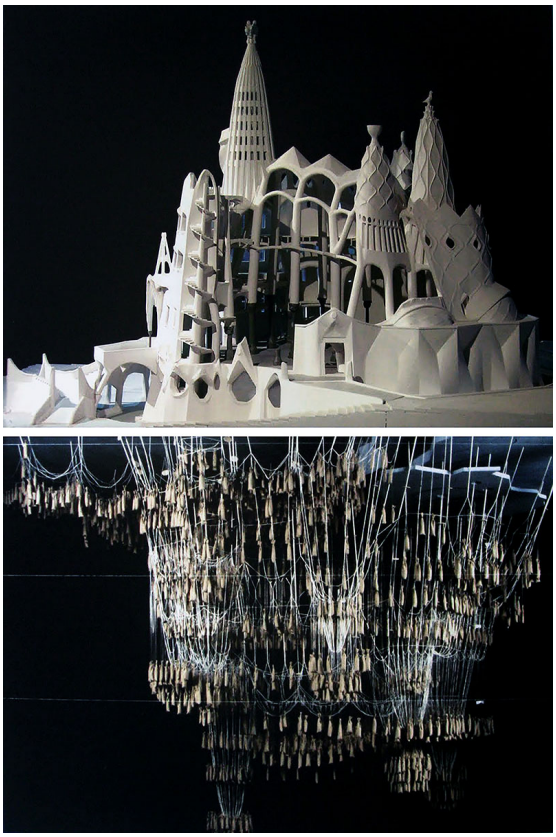

Figure 3.3: Form following force model generated via suspended cables: a CNC scale model (top), the geometry of which is generated from the (reconstructed) hanging chain model (bottom) for the Colònia Güell (after [32]).

A more comprehensive review of form-resistant structures (from their historical context in design philosophy to the development of design methodologies through rules-of-thumb to tools in the information age, to developments in material and construction technology) was presented in an article published by the author in *The Structural Engineer* (Annex A), also presented at a public lecture at the Institution of Structural Engineers [33, 34]. It is recognized that masonry gravity structures, with their varied traditions across the globe, form an important subset of existing form-resistant structures. This ageing stock of masonry gravity structures includes structures of historic value, such as historic cathedrals found across Europe, as well as residential units, all of which need to be properly assessed and their useful

life maximized.

The equilibrium methods commonly used for the analysis and design of form-resistant structures stem from Robert Hooke's observation of funicular forms. They were later formalized within the context of limit state design by Jacques Heyman, in his seminal work entitled 'The Masonry Arch' [35]. The following section gives a brief historical overview from Hooke's observation to Heyman's 'safe theorem', followed by a discussion of existing analytical methods used in the analysis of form-resistant structures.

3.1.1 A historical view: from Hooke to Heyman

The catenary

The English scientist Robert Hooke observed the analogy between the form of a catenary and that of an arch, and embedded his observation in the form of a Latin anagram in a 1663 paper. When deciphered and translated to English, the anagram reads, "As hangs the flexible line, so but inverted will stand the rigid arch" [36]. This intuition of Hooke, although not rigorously proven [36], implies that if a hanging cable fixed between two supports is solidified and then inverted, it would stand as a rigid arch (Fig. 3.4).

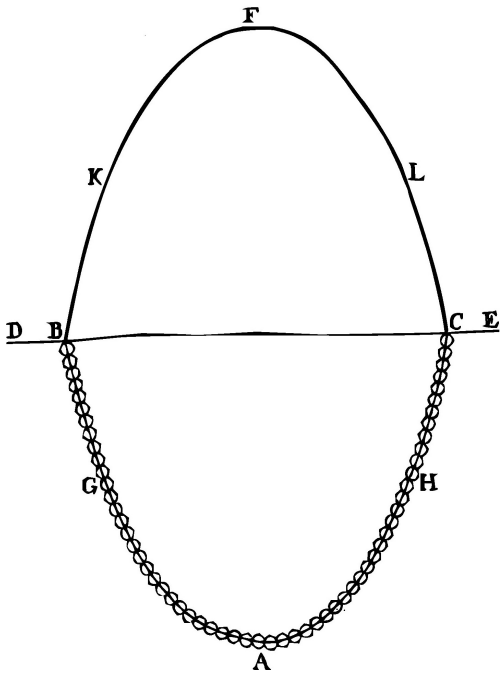

Figure 3.4: Form of a hanging chain (BGAHC) and its inverted rigid arch (DKFLE) (after [37]).

Moving a step further, the English mathematician David Gregory found the mathematical expression of the catenary and restated Hooke's observation thus: "none but the catenaria

is the figure of a true legitimate arch... And when an arch of any other figure is supported, it is because in its thickness some catenaria is included" [38, 39]. It is important to note that this simple restatement is significant in that it deviates from Robert Hooke's claim of the arch shape being a catenary, to one whereby the arch can be of any shape, though must contain one or more catenaries within it.

One famous early example of this idea being put into practice was by Poleni, in 1748, in his analysis of the dome of St. Peter's in Rome [40]. In analysing the cracked dome of St. Peter's, he divided the dome into a number of hemispherical lunes, following the meridional cracks in the dome. The stability of two opposing lunes forming an arch was considered. Then, a hanging chain model was constructed by loading a chain with loads corresponding to the distribution of the self-weight of the arch elements. The resulting form of the chain was found to be contained within the section of the arch (Fig. 3.5). Thus, he concluded that the meridional cracking observed would not lead to instability [39].

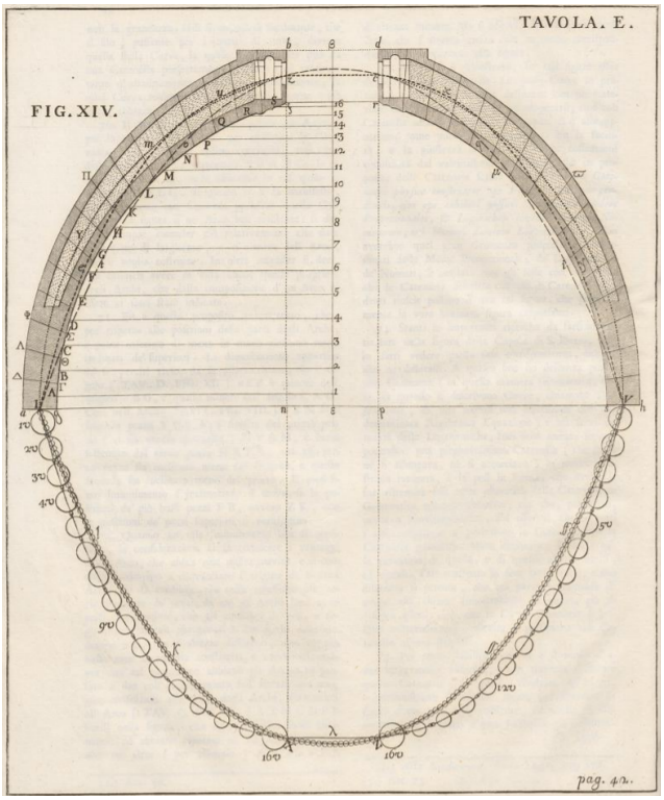

Figure 3.5: Using Hooke's observation for the analysis of masonry gravity structures: Poleni's investigation of St. Peter's Dome. A hanging chain contained within the section of the dome can be found, confirming its safety (after [37]).

Line of thrust

The development of graphic statics by Carl Culmann, and others (e.g., Simon Stevin, Pierre Varignon, etc.,) made it possible to geometrically construct the form of a catenary [36, 40, 41]; this graphical construction is called a funicular polygon (Fig. 3.6). Jacques Heyman, particularly in the application of his 'safe theorem' [39], used the funicular polygon as the thrust line representing the equilibrium of voussoirs forming an arch.

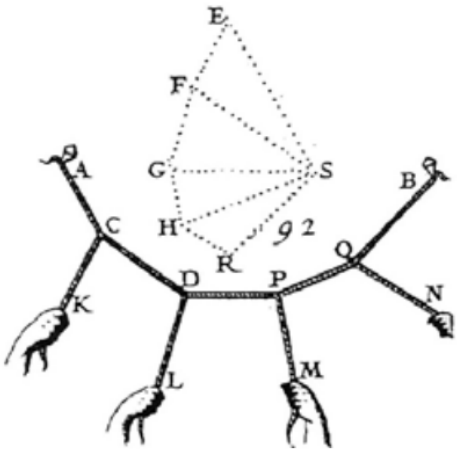

Figure 3.6: Graphical analysis of a funicular: the triangle EFS in the funicular polygon (indicated by dotted lines) correspond to the equilibrium of node C of the catenary, and similarly for other nodes (after [36]).

Barlow, in 1846, demonstrated the possibility of alternative positions for the line of thrust [39]. A model arch of six voussoirs, with each joint made up of four pieces of timber was considered (Fig. 3.7). By removing three of the four timber pieces in each of the joints, he visualized the different possible paths of the line of thrust.

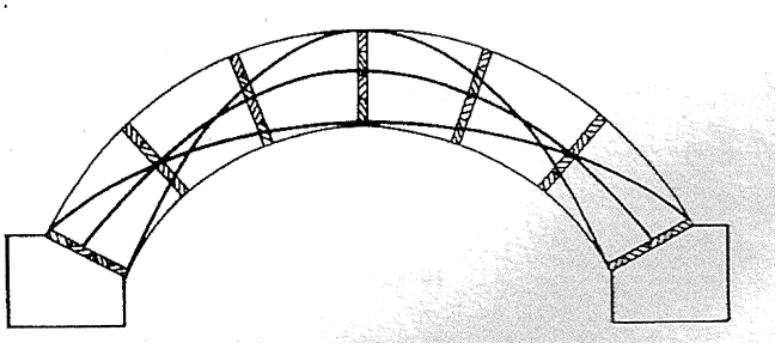

Figure 3.7: Barlow's experiment demonstrating the existence of multiple possible lines of thrust: each interface of a voussoir arch is made up of four timber pieces covering the full width, but only a quarter of the thickness of the arch. By removing these interface pieces (one or multiple at a time) and verifying the stability of the arch, the existence of multiple possible equilibrium states is demonstrated (after [39]).

With the possibility of having multiple possible thrust lines, the question of identifying the true line of thrust arises. Kurrer [40] notes previous attempts towards this end: (i) Moseley's principle states: "of all statically possible force systems in equilibrium, the one that prevails is the one in which the resistance is minimal"; and (ii) Navier's arch theory based on linear elastic theory. As Kurrer [40] further reports, the search for the true line of thrust was faced with much resistance and seen to be of purely academic interest, of no benefit to engineers. From an engineering perspective, the key issue is whether an arch is safe, with its imperfections, subjected to real loading conditions (which are variable) and real support conditions (which may yield and settle). The mathematical solution for the exact stress state of an ideal arch subjected to ideal boundary conditions was found to be of little use when the real behaviour of arches was considered; e.g., arches with settled abutments and visible cracks were observed to be functioning satisfactorily.

Heyman's safe theorem

Heyman [39] reformulated the thrust line method based on the theorems of plastic limit analysis to develop his 'safe theorem'. This, while not relying on the exact state of the stresses in the structure, provides a useful tool for practising engineers to assess the safety of form-resistant structures.

Theorems of limit analysis were originally presented for reinforced concrete by Gvozdev in 1936, and later for structural steelwork [40]. The advantages of plastic limit analysis are its simplicity, its ability to find bounds on the exact collapse load without consideration of deformations, and its ability to predict failure mechanisms.

The lower-bound (static) solution is a distribution of internal forces where: (a) the allowable forces are bounded by limit values (yield condition); and (b) internal forces are in equilibrium with external forces (equilibrium condition) (solution A, Fig. 3.8). In contrast, the upper-bound (kinematic) solution is associated with a collapse mechanism, where: (a) the equilibrium condition is satisfied; and (b) the assumed mechanism is valid (kinematic condition): solution B in Fig. 3.8, where while the above is satisfied, the yield condition is not satisfied. The lower-bound solution is always less than or equal to the true collapse load, whereas the upper-bound solution is always greater than or equal to this. The uniqueness theorem brings these together and states that if the upper-bound and lower-bound solutions are the same, i.e., the equilibrium, kinematic and yield conditions are all satisfied, then that solution is the true collapse load (solution C, Fig. 3.8).

Alternatively, the upper bound solution can be defined as a condition where the structure

collapses in a compatible plastic-failure mechanism for which the rate at which the external forces do work equals or exceeds the rate of internal dissipation [42]. This follows from an associated plastic flow rule where the plastic strain rate is in a direction normal to the yield surface. However, if the plastic strain rate is in a direction that is not normal to the yield surface due to the presence of a non-associative material then lower-bound and upper-bound solutions may not converge to a unique solution, thus leaving a 'duality-gap' [43].

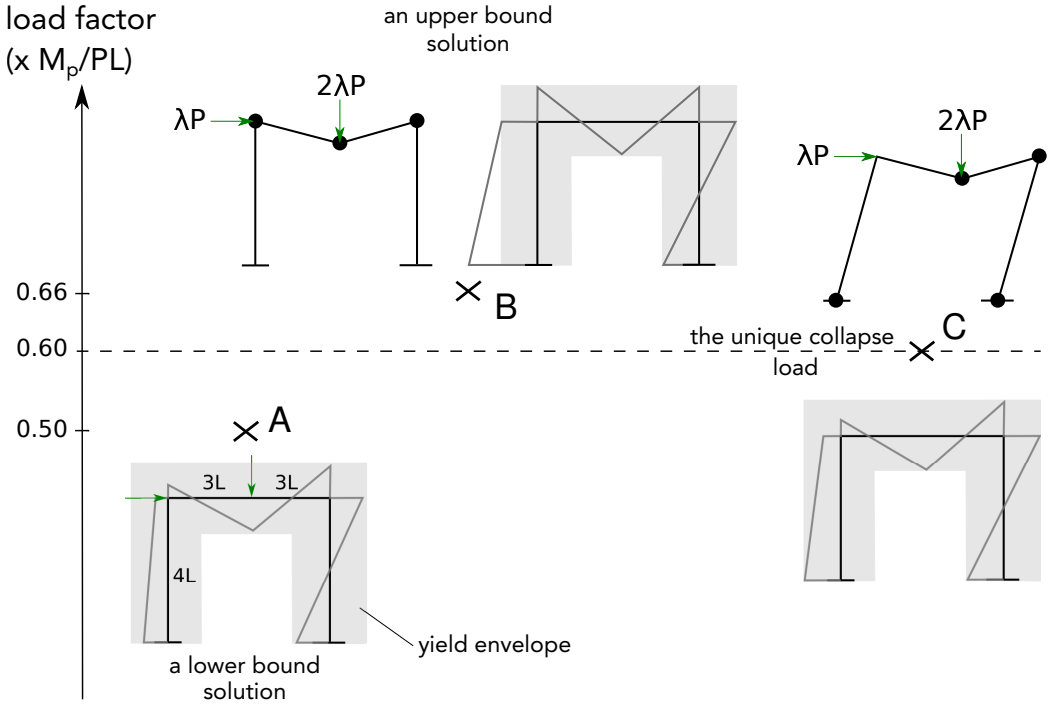

Figure 3.8: Limit analysis solutions for a frame subjected to vertical and horizontal loads: (A) a lower-bound solution with equilibrium and yield criteria satisfied; (B) an upper-bound solution with equilibrium and an admissible collapse mechanism; and (C) a solution corresponding to the unique collapse load, where equilibrium, yield and collapse mechanism criteria are all satisfied (moment capacity of all frame elements taken as M_p; yield envelopes shaded in grey).

According to Kurrer [40], the use of plastic limit analysis for arches was first suggested by Onat and Prager [44]; they apply both lower and upper-bound theorems to two-hinged steel arches. Around the same time, Kooharian [45] presented an application of plastic limit analysis to voussoir arches, with the assumptions of infinite compressive strength and zero tensile strength. While presenting the use of funicular thrust lines for lower-bound estimates, the emphasis was on determining the upper-bound by identifying an appropriate collapse mechanism. The lower-bound solution was used as a guide to locate the hinges.

The safe theorem presented by Heyman [35], with its general applicability to masonry load-bearing structures, has garnered wider attention than the aforementioned studies. While many of the basic ideas of Kooharian [45] were used, the emphasis was on establishing lower-

bound solutions, i.e., safe solutions. The concept of a geometrical factor of safety was presented as a measure of the capacity reserves available, whereas Kooharian [45] focussed on establishing an upper-bound collapse load estimate.

In arriving at his safe theorem, Heyman [39] made three assumptions in relation to material properties: (i) sliding failure cannot occur (i.e., friction between voussoirs is high enough to prevent this); (ii) the masonry has zero tensile strength; and (iii) the masonry has infinite compressive strength. Heyman [39] asserted that the first assumption is reasonable. However, it is possible to find cases where slippage has occurred in form-resistant structures; e.g., at the header of a flying buttress [46, 47] (Fig. 3.9). The assumption of zero tensile strength is conservative as masonry often has some tensile strength, albeit finite. Furthermore, with the interlocking of masonry units and the presence of friction, masonry can create apparent tension locally [48, 49, 50]. Assuming infinite strength of masonry is also often reasonable, as the stress levels in masonry structures are generally an order or two below the crushing strength in magnitude. However, both strength and friction criteria should be checked after an analysis to verify the reasonableness of these assumptions.

Figure 3.9: Failure due to slippage in a form-resistant structure: sliding near the head of a flying buttress at Saint-Julien in Royaucourt (after [47]).

Heyman [51] states his safe theorem as follows: "if a set of internal forces in a masonry structure can be found that equilibrate the external loads, and which lie everywhere within the masonry, then the structure is safe - in the sense that it cannot collapse under those loads". The "set of internal forces in equilibrium with external loads" is taken to be given by a line of thrust, with a line of thrust found to be fully contained within the structure indicating a safe

structure. In terms of limit analysis, this would be a lower-bound solution.

Heyman [39] concedes that the 'safe' line of thrust may or may not define the actual state of the structure. However, importantly, he states that once a valid thrust line is found, it will be still valid if the arch is subjected to small deformations, e.g., support movements (Ochsendorf [52] reports, from experiments, a significant 15.4% span increase at collapse in the case of a semi-circular arch of thickness to radius ratio of 0.23 (Fig. 3.10)). As such, the engineer need not know the true line of thrust, as long as he or she can find a possible equilibrium solution. This is indeed a key advantage of limit analysis over elastic analysis methods.

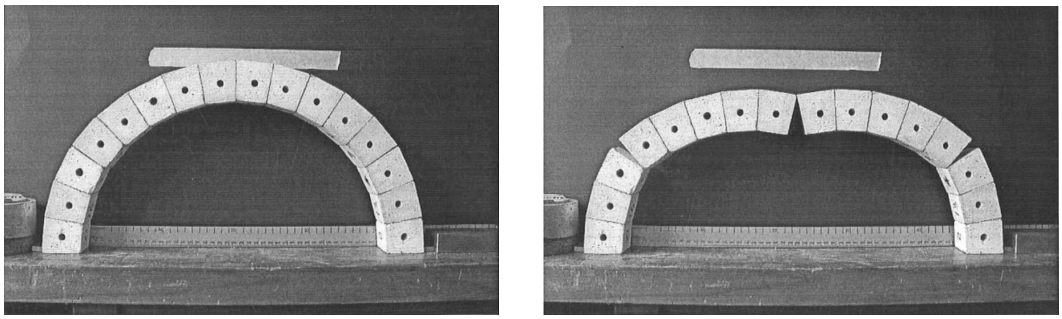

(a) (b)

Figure 3.10: Significant deformation of the supports can occur at failure: the semi-circular arch in (a), made of 16 blocks and thickness to radius ratio of 0.23, requires a 15.4% span increase at collapse (after [52]).

How this falls within the remit of limit analysis can be explained as follows. Once the centring of a masonry arch is struck, the arch exerts a horizontal thrust on the abutments and the abutments may yield. Cracks will appear on the intrados and extrados of the arch to permit this movement. These cracks are not necessarily dangerous and in fact, are an essential part of how the load-bearing structure responds to changes in the boundary conditions. Where the line of thrust touches the extrados or intrados, the cracks extend to almost the full thickness, creating a hinge. Once three such hinges are formed, the arch is statically determinate; the formation of (at least) one more hinge will turn the arch into a kinematically admissible mechanism (Fig. 3.11). At that point, there exists a valid line of thrust; i.e., equilibrium and yield conditions are satisfied and a valid mechanism exists, with the kinematic mechanism condition now satisfied. Thus, the arch has reached its unique collapse load, in this case, subjected to its self-weight only.

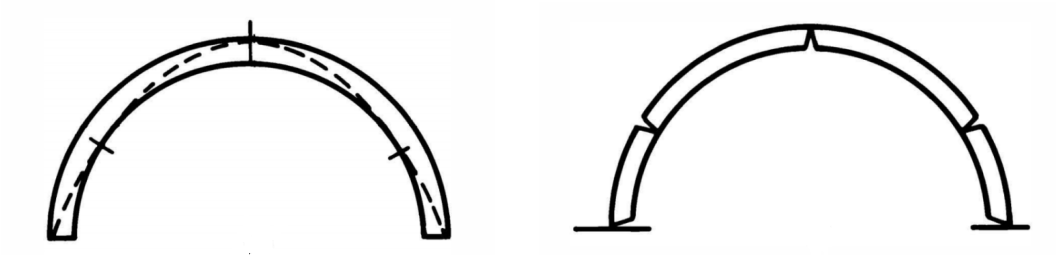

(a) (b)

Figure 3.11: An arch at its unique collapse load: (a) equilibrium satisfied as the line of thrust is contained within the arch; and (b) a valid mechanism as a sufficient number of hinges are formed, with the material at yield at hinge points. Hinges correspond to sections (or joints) where the line of thrust is touching the extrados or intrados (after [39]).

The yield condition for a material with no-tensile resistance, though which is infinitely strong in compression, is presented in Fig. 3.12a, where line OA and OB represent 'bending moment' $M = \pm hN$, with the arch thickness being $2h$ at the section (or the voussoir joint) considered and N being the normal component of the thrust force. A point within AOB represents a section where the line of thrust is fully within the masonry, a point on OA (or OB) is a hinge forming at the intrados (or extrados), and a point outside AOB is not possible due to the no tension condition. The yield criterion for a finite compressive strength material would be as in Fig. 3.12b, as the limited strength requires a growing 'crushing zone' as the thrust increases; now the normal force N cannot be at the edge of the section and thus the lever-arm gradually becomes smaller, from h to 0. However, the typically observed low compressive forces N suggest that it may be reasonable to instead use the region within OCE. Heyman also suggests conducting the analysis in a 'shrunk' arch thickness of (say) $2 \times 0.9h$, such that, by providing a margin of safety, the results obtained will almost always be safe.

The minimum arch thickness that can safely carry a given load is termed the limit thickness, for the given load and geometry; for a semi-circular arch under its self-weight, the limit thickness would be approximately 1/18 of the span. Following this, Heyman [39] proposes the concept of a 'geometrical factor of safety' for arches, which is an arch thickness to limiting thickness ratio (Fig. 3.13); he suggests a value of 2 under the most unfavourable loading condition. This proposed geometric factor of safety contrasts with the collapse load factor used in the plastic limit analysis of steel and reinforced concrete structures; as such the geometrical factor of safety appears to be seldom used in engineering practice.

It is clear that this approach is based primarily on the stability criterion and not the material strength criterion (although the latter is accounted for in the yield criterion); hence the safety of a masonry structure is made a matter primarily of geometry. Heyman [39] notes that this is

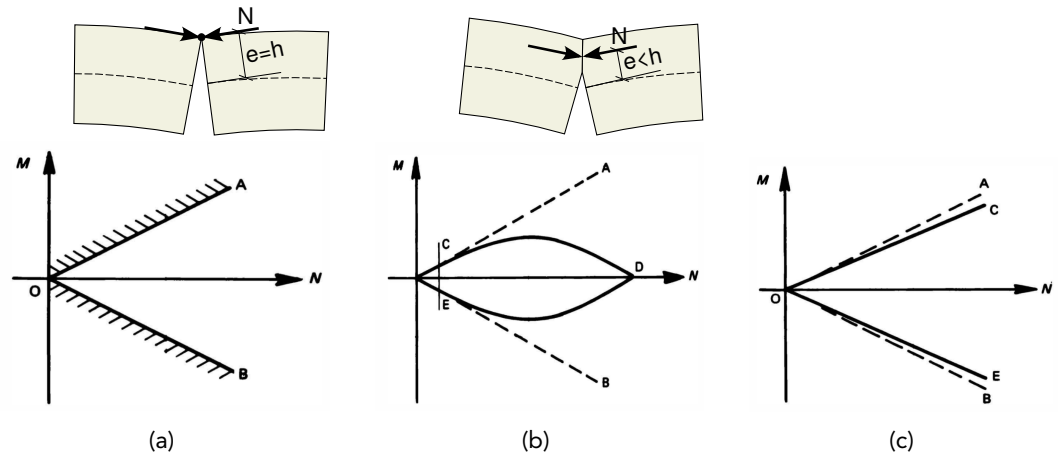

Figure 3.12: Yield criterion for masonry: (a) assuming infinitely strong masonry in compression; (b) accounting for finite compressive strength of masonry via a crushing zone; and (c) considering low operational forces in masonry. Yield criteria presented in $M - N$ domain where 'bending moment' $M = Ne$; N is the normal force component of the thrust at the joint considered; e is the eccentricity of the normal force N from the centre-line at the section considered (adapted from [39]).

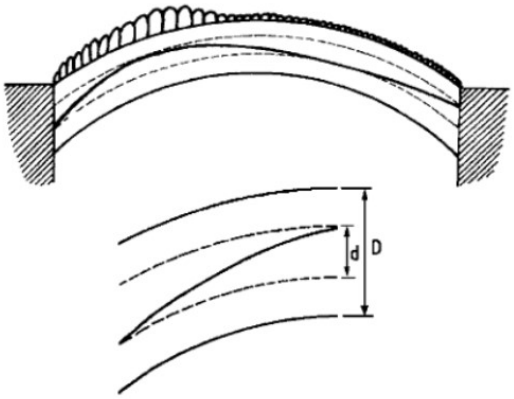

Figure 3.13: Geometrical safety factor for arches - defined as the ratio of the arch thickness (D) to limiting thickness (d) (after [53]).

in fact the case, as the stresses in a masonry arch at failure are much lower than that required for material failure. Huerta [38] shows that an arch of medium sandstone (density $20\,kN/m^2$ and crushing strength $20\,N/mm^2$) will require a span of $640\,m$ to have both the strength and stability criterion reached at the same time, in the absence of a factor of safety. None of the known, built or planned, masonry bridges come close to the aforementioned limit of $640\,m$; the stone arch bridge of Fong-Huan in China (built in the 1970s) spans $120\,m$, whilst the bridge over Adda in Trezzo (built in the 1370s) spans $72\,m$, and Da Vinci's proposed single arch bridge over the Golden Horn in Istanbul (1500AD) spans $240\,m$.

3.1.2 A review of tools in current practice

Existing methods for the analysis of form-resistant structures are now reviewed, taking into consideration the complexity of the idealization, and in turn, the analysis process and their performance in predicting the collapse load (Fig. 3.14). Based on the complexity of the idealization, they can be broadly categorized as: (i) a discretized force system - i.e., thrust lines, thrust networks, strut-and-tie model, etc.; (ii) a rigid block assembly; or (iii) an elastic continuum - i.e., finite element models, discrete element models, etc. As will be evident later, discretized force systems and rigid block systems can be identified as geometric methods whereas elastic continuum methods are stiffness-based methods.

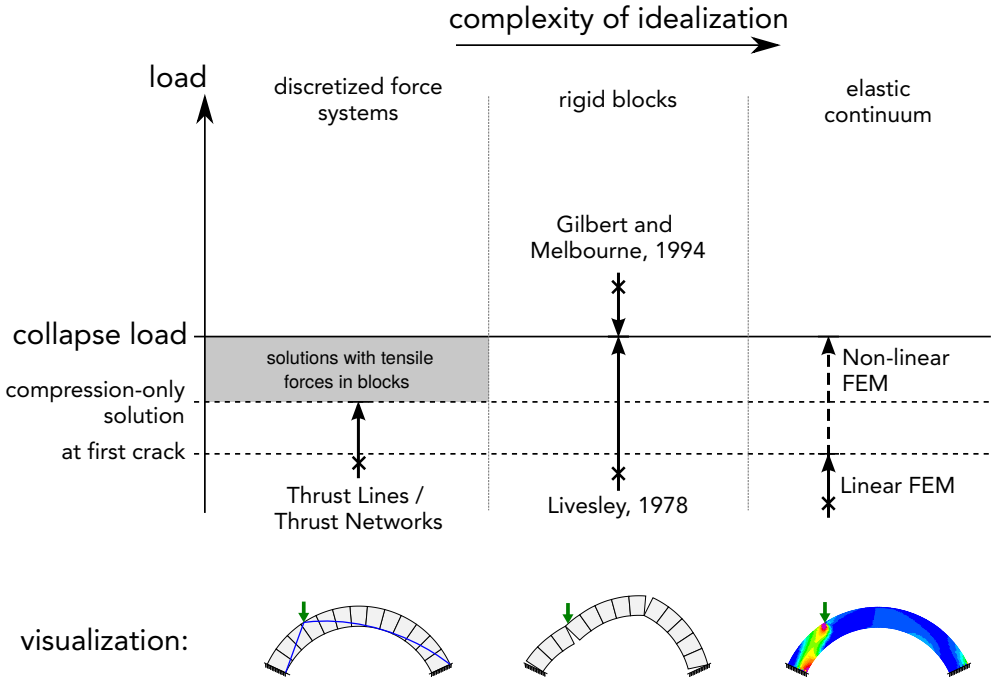

Figure 3.14: Framework for the review of current tools in practice to analyse form-resistant structures: methods in increasing complexity of idealization exist, from discrete force systems to elastic continuum, giving lower and upper-bound estimates of the exact collapse load. The thrust line method and Linear-FEM have limitations in achieving the exact collapse.

Thrust lines

Thrust lines, discussed thus far, are a discrete representation of equilibrium forces within a form-resistant structure. Heyman's safe theorem, along with the funicular thrust lines used to represent the equilibrium, provide a quick and easy method to assess the safety of form-resistant structures, including masonry gravity structures.

The traditional thrust line method will give a lower-bound solution (Fig. 3.14) as a funicular thrust line fully contained within the structure is taken to guarantee a solution in equilibrium

without violating the yield criterion (with the assumption that the kinematics are such that the associativity of flow rule holds). However, not accounting for the finite, but present, tensile capacity of the block material may result in collapse load estimates lower than the exact value; i.e., give a compression-only solution (Fig. 3.14). One way to account for this is by constraining the thrust line only at block interfaces, thus assuming no tensile failure of the blocks themselves.

The thrust line method is not without fault: although a visual method, it lacks clarity when e.g., a thrust line passes through internal voids of a structure (i.e., should the thrust line in this case be taken as 'fully contained within the structure'?). Certain special cases require special treatment; e.g., a masonry buttress requires determination of an ineffective zone of masonry [54, 52, 55]; the treatment of friction as infinite has been noted to be unsatisfactory, e.g., at the head of the flying buttress [47, 46]. Furthermore, some limitations of the usage of funicular thrust lines have been noted, specifically due to it not properly considering the block stereotomy [56, 57, 58], discussed in detail in Chapter 4.

Force/Thrust networks

A force network for a vault or dome can be seen as the three-dimensional equivalent of a line of thrust for an arch. O'Dwyer [53] first presented an application of force networks for the analysis of three-dimensional masonry forms (Fig. 3.15). A force network, satisfying equilibrium at nodes of the force network and the nodes contained within the structure, is looked for by solving a linear programming problem; the problem is made linear by assuming the horizontal thrust forces *a priori*, and the linear programming problem is solved repeatedly at different horizontal thrusts to obtain the optimal solution.

Block and Ochsendorf [59] later extended force networks to incorporate force densities, presented by Schek [60], to linearize the nodal equilibrium equations. This extension, termed Thrust Network Analysis (TNA), is presented as a form exploration tool for form-resistant structures. It uses reciprocal figures by J. Clerk [61], matrix analysis of indeterminate frameworks by Pellegrino and Calladine [62], and graphic statics.

In addition to the above 'geometric stiffness' methods, 'dynamic equilibrium' methods have also been used to solve force network systems (taxonomy following Veenendaal and Block [63]). In dynamic equilibrium methods, the motion of the structure is followed through time under applied loads; i.e., a flat grid of members (with elasticity and damping) connected at nodes are allowed to deform under gravity, and the position of the nodes are updated at each time step [64, 65]. While dynamic relaxation methods involve material properties

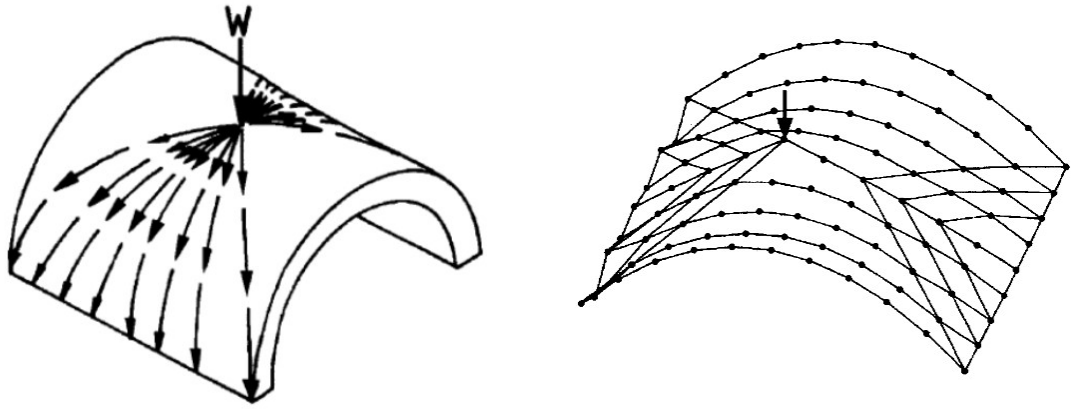

(a) (b)

Figure 3.15: Force network for a masonry barrel vault: (a) a possible load path for a point load applied on a barrel vault; and (b) the optimal force network obtained by O'Dwyer [53].

and iterative solution (that may lead to convergence issues), it avoids the inversion of the connectivity matrix, which is a required step in the geometric stiffness methods; the dynamic equilibrium method only requires the inversion of the mass matrix, which is a diagonal matrix.

In general, force (thrust) network approaches improve upon the slicing method used by Poleni and Heyman, by allowing for more efficient load paths. However, the solution still depends on the topology of the chosen network [10, 66]. While O'Dwyer [53] leaves the user to identify the principal load paths, Oval et al. [67, 68, 69, 70] present a rule-based approach (founded on heuristics identified from experience) for the meshing process.

Thus, although force (thrust) network approaches provide a means of designing and analysing three-dimensional form-resistant structures, they are limited by the topology of the network chosen. Furthermore, as the method follows on from the traditional thrust line method for two-dimensional analysis, it inherits the same shortcomings.

Strut-and-tie method

The 'strut-and-tie' method was introduced by Prof. Schlaich and his colleagues for the analysis of reinforced concrete structures [71]. When the applied loads and geometry are likely to result in geometrical and statical discontinuities (e.g., in corbels, deep beams and pile caps), it is appropriate to model the internal forces as being concentrated in regions of concrete compression struts, steel tension ties, and nodal zones.

More recently, the strut-and-tie method has been applied to masonry structures; e.g., [72, 73, 74]. In contrast to the discrete force methods following the thrust line method, the strut-and-tie method accounts for the tensile capacity present in masonry gravity structures.

However, improper consideration of tensile capacity leads to overestimation of the load capacity.

To generate appropriate strut-and-tie models for masonry, Roca et al. [72] present a set of rules and specific strut-and-tie models, based on previous experimental and numerical results. Palmisano and Elia [74] employ the evolutionary structural optimization (ESO) method to identify the 'most plausible' strut-and-tie model, i.e., the solution with the lowest total strain energy. Foraboschi and Vanin [73] present an alternative approach involving an 'evolutive' strut-and-tie model in which the model is updated by removing ties as they reach a limiting tensile strain (Fig. 3.16).

Although the application of the strut-and-tie method is noted for considering the tensile capacity within masonry, the need to reliably know the mode of failure, *a priori*, makes it an involved process for general application (i.e., for structures other than walls), in some cases needing complex finite element models as a pre-processing step.

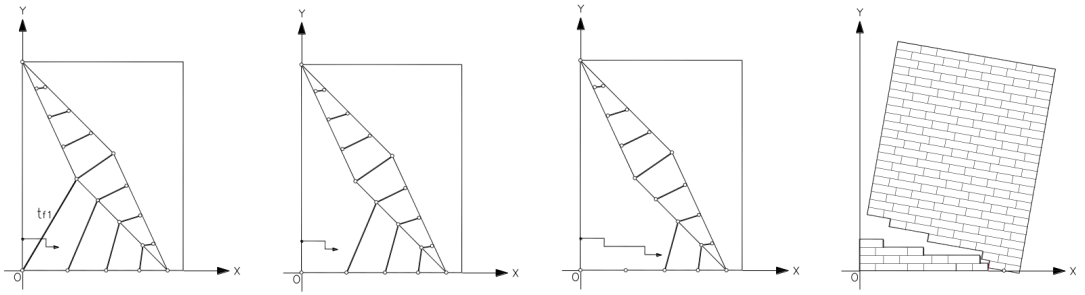

Figure 3.16: Evolutive strut-and-tie model for masonry: a masonry wall is subject to an in-plane lateral load at the top corner, and fails in flexure. Tie members reaching their tensile capacities are removed during the evolution process (a-c), prior to failure (d) (after [73]).

Membrane analysis

Membrane theory of shells is applicable to thin shells where either no bending is possible (i.e., the shell is not stiff enough) or the loading is low in comparison to the self-weight which is reliably resisted by the shell with the given geometry, giving rise to primarily normal stresses and negligible shear stresses. Under the assumption of smoothly distributed loading, membrane theory can be applied to assess the state of stress in thin shells.

Masonry shells—e.g., vaults and domes—can be analysed assuming a no-tension elastic membrane. This governing equation—i.e., Pucher's equation in Eq. (3.1)—combines the shell geometry ($\mathbf{z}(x, y)$ in Fig. 3.17), loading (p_z, p_x, p_y), and the stress state—which is given as a

stress function (ψ)—i.e., the Airy potential [75, 76, 77, 78].

$$\left(\frac{\partial^2\psi}{\partial x^2} - \int p_y dy\right)\frac{\partial^2 z}{\partial y^2} - 2\frac{\partial^2\psi}{\partial x\partial y}\frac{\partial^2 z}{\partial x\partial y} + \left(\frac{\partial^2\psi}{\partial y^2} - \int p_x dx\right)\frac{\partial^2 z}{\partial x^2} = p_x\frac{\partial z}{\partial x} + p_y\frac{\partial z}{\partial y} - p_z \quad (3.1)$$

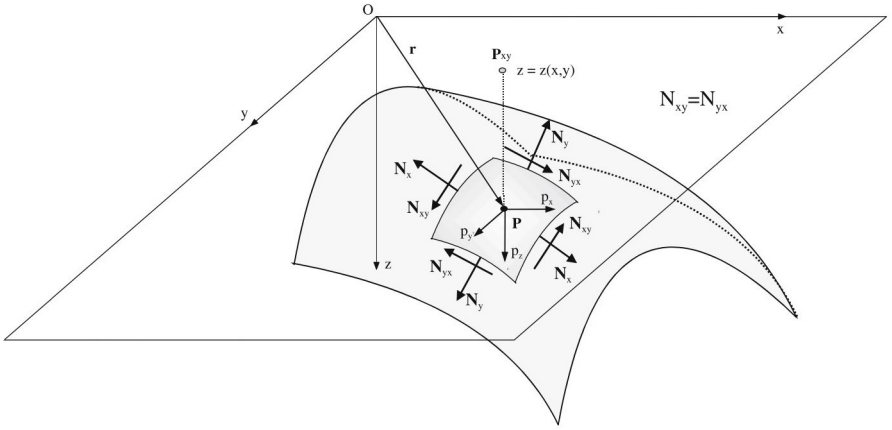

Figure 3.17: Surface element of a membrane shell - where the element at point $\mathbf{P}(x, y)$ at elevation $\mathbf{z}(x, y)$ is subjected to external loading (p_z, p_x, p_y). $\mathbf{N}_{ij}$ are membrane forces (after [76]).

Thus, to analyse a masonry structure, it is possible to find the geometry of a membrane that is fully contained within the structure, along with a stress function satisfying the no-tension condition [76]. Baratta and Corbi [76] show that, given only vertical loading is present and the shell geometry is convex, equilibrium implies the fulfilment of the no-tension condition. However, determining a valid membrane geometry and a stress function is much easier when the geometry of the shell is simpler and some intuition of the nature of the stress function exists (e.g., a barrel vault); the process is much more difficult when applied to free-form shells.

Chiang and Borgart [78] propose an iterative procedure for solving Pucher's equation, where the geometry and the stress function are given as radial basis functions and thus, the problem is re-formulated as a least-square regression problem. Similarly, Fraternali [77] employs an iterative strategy where the geometry (constrained within the extrados and intrados) is updated while checking the no-tension condition through the concavity of the stress function.

Barsi et al. [79] note a mapping from thrust lines to membranes: the membrane solution, which is a continuous representation of equilibrium, emerges when the size of the blocks is made infinitesimally small in the corresponding force network problem (Fig. 3.18).

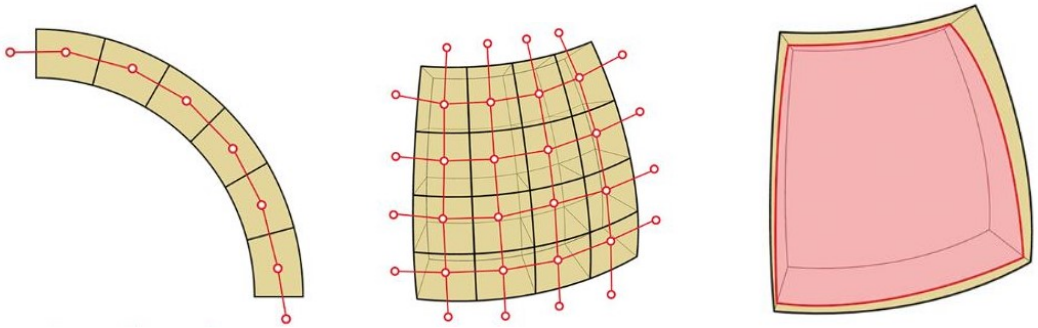

Figure 3.18: From funicular polygon to membrane solution: (a) funicular polygon, in 2D, and (b) thrust network, in 3D, are discrete representations of equilibrium in block assemblies, whereas in (c) the membrane is a continuum representation of equilibrium, where blocks are made infinitesimally small (after [79]).

Similarly, there is a relationship between force networks and Airy stress functions. Note here, that the force networks are referring to pin-jointed structures in general, with no restriction on the nature of the force. Then, the structure can be converted to an equivalent self-stressed structure (by replacing external forces with pin-jointed members), which is in turn a projection of a polyhedral function (Fig. 3.19). The polyhedral function is an Airy stress function, where the changes in slopes between adjacent faces give the forces in the members, while the convexity/concavity of the polyhedral functions indicates the compressive/tensile nature of forces [80, 81].

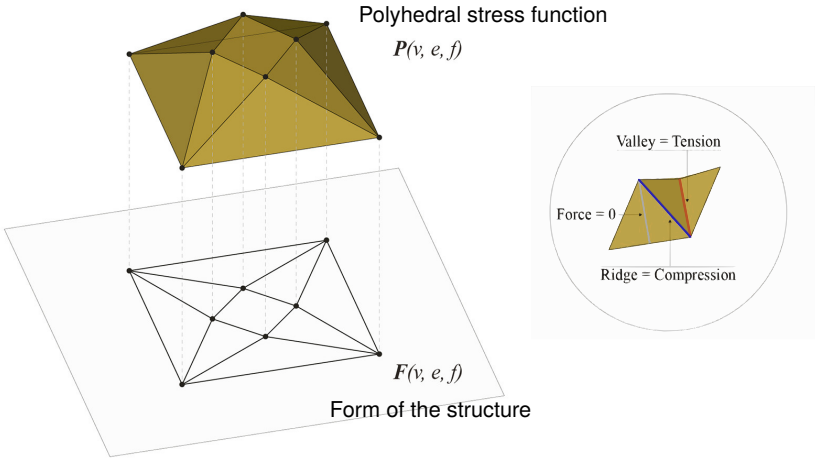

Figure 3.19: From force network to Airy stress function: polyhedral stress function (P) represents the forces of the structure, while its projection gives the form (F) of the structure. The change of slope in P gives the magnitude of the force in the corresponding member, while the nature of the change in slope (ridge/valley) corresponds to the nature of the force (compression/tension) (adapted from [81]).

Thus, the equivalence of the solution of discrete force networks and continuum mem-

branes is noted. The equivalence exists in Airy stress functions defining the state of stress as well. The difference in the complexity of the solution in the two formulations, discrete and continuum, is also noted. However, unlike other elastic continuum methods in Fig. 3.14, the solution does not require stiffness properties of the material and remains a geometric problem.

Rigid block method

Livesley [82] presents a computational limit analysis procedure to determine the collapse load of a structure made of rigid blocks. In this work, the equilibrium of the structure is imposed along with yield constraints, for normal and shear forces, at block interfaces, adopting a lower-bound approach. Solving the resulting linear programming problem gives the collapse load factor. It is possible to plot the failure mode (Fig. 3.20) and to draw the corresponding line of thrust using the stress resultants from the analysis. The method was later extended to treat three-dimensional cases [83].

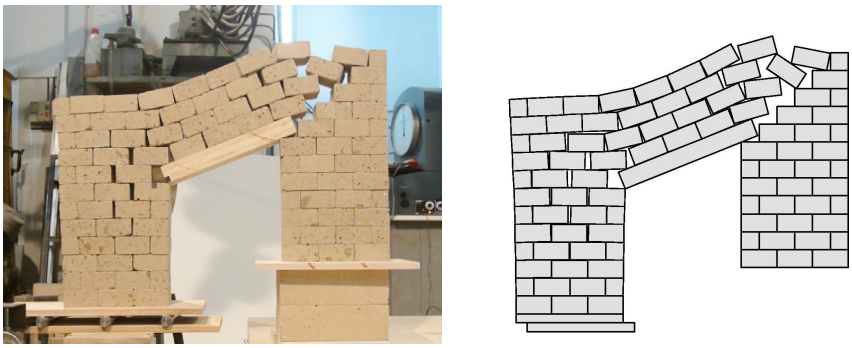

(a) (b)

Figure 3.20: Rigid block method of analysis applied to masonry gravity structures: comparison of the failure mode of a wall specimen from: (a) an experimental investigation; and (b) the rigid block method of analysis (after [84]).

Livesley [82] further extends the procedure to account for friction at the interfaces, considering Coulomb friction with no cohesion; i.e., $-n\mu \leq t \leq n\mu$, where n and t are normal and shear (friction) forces and μ is the friction coefficient. However, the linear programming algorithm used assumes the normality rule, whereas Coulomb friction does not obey the normality rule. Thus the rigid block method (when solved 'naively') will assume deformation in the direction of the resultant of the normal and the shear force at the interface, whereas, in reality, with Coulomb friction, the deformation will be along the shear direction (Fig. 3.21). This may result in the failure mechanism being incorrectly identified. This error can be corrected by re-solving the problem by replacing constraint $-n\mu - t = u \leq 0$ with $t = t_A$, where

t_A is the result obtained from the first solution.

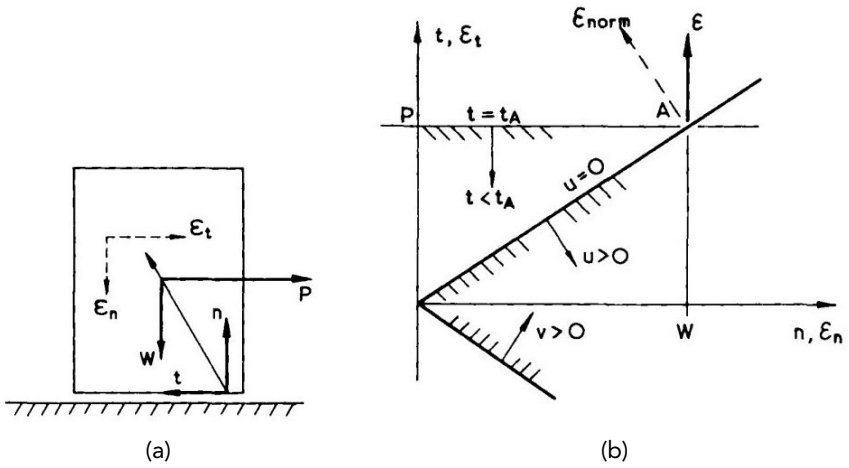

Figure 3.21: Coulomb friction and the normality rule: (a) normal, n, and shear, t, force component of a block on a rough surface; and (b) corresponding yield surface in n, t space and the direction of the normal deformation ϵ_{norm}. Corrected yield surface PA, for failure at a shear force $t = t_A$, is also indicated (after [82]).

In addition to the deformations being incorrect, the assumption of the normality rule can result in the collapse load being overestimated. This is when the failure load is affected by the kinematics. Such situations can be checked by inspecting the work done at interfaces, considering the corrected failure mechanism; a positive work done at interfaces will indicate an overestimated collapse load. That is, if Coulomb friction is held, only the friction will be doing work and that would be negative work as the friction force is in a direction opposite to the motion of the block. If no work is done at interfaces then the estimated collapse load is correct, despite the assumption of normality.

In contrast to the equilibrium formulation of Livesley [82], but still considering rigid block assemblies, Gilbert and Melbourne [85] present an equivalent kinematic formulation. Minimization of virtual work is carried out with kinematically admissible deformation fields for the rigid blocks (with sliding failure initially assumed not to occur) and the mechanism corresponding to the exact collapse mechanism is found. The formulation is made linear by assuming small deflections, thus enabling the use of linear programming solvers. It is noted that a solution may not exist if either the form is 'geometrically locked' (i.e., the arch will not fail in a hinged mechanism), or the structure is already unstable under its own self-weight.

The procedure was extended to incorporate sliding between rigid blocks, assuming the normality rule to hold. Thus, similar shortcomings as discussed for the equilibrium formulation exist. However, it is noted that many problems involving arches will give the exact collapse loads, while, in general, the obtained collapse load will be an upper bound on the exact

collapse load [85].

Furthermore, as indicated in Fig. 3.14, the rigid block method does not give any indication as to how forces flow within the rigid blocks. However, considering resultant forces at the interfaces, it is possible to generate a thrust line.

Finite element analysis

Linear finite element (FE) analysis is not well suited to the analysis of masonry gravity structures. The linearity condition of materials and geometry is insufficient to model the real behaviour of masonry gravity structures; e.g., no-tension and orthotropic material, presence of cracks, yielding of abutments, etc. Block et al. [86] demonstrate the inability of linear FE analysis to differentiate between an unstable arch geometry (Fig. 3.22a) and a stable one (Fig. 3.22b). While FE analysis cannot say anything conclusive about the stability of the arch, limit analysis can clearly indicate the instability of the form through the presentation of a line of thrust. Nonetheless, linear FE can give a lower-bound estimate of collapse load, considering the initiation of the first crack [86].

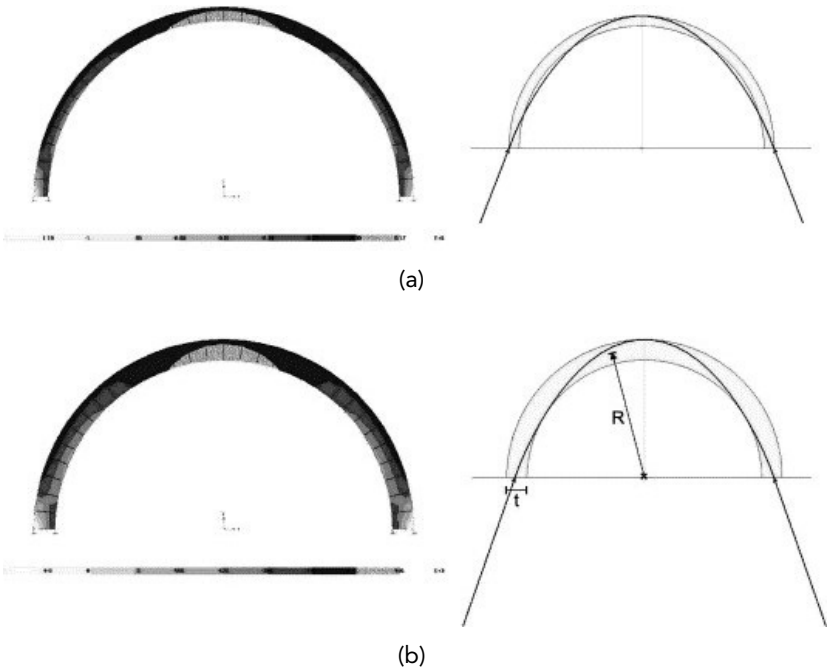

Figure 3.22: Linear-elastic finite element (FE) analysis (left) versus limit state analysis (right), for arches with: (a) an unstable geometry, $t/R = 0.08$; (b) a stable geometry $t/R = 0.16$. While the FE results cannot distinguish between the stable and unstable geometries, the thrust line clearly indicates instability as it moves out from the arch section (after [86]).

Non-linear FE analysis can incorporate the complexities in masonry behaviour, both in terms of geometry and material. Masonry can be modelled under two idealization strategies:

(i) macro-modelling; and (ii) micro-modelling, often further categorized into detailed and simplified micro-models. Macro-modelling considers a fictitious homogeneous orthotropic continuum material model, forgoing a detailed description of the interaction between individual blocks and mortar joints (Fig. 3.23). The material parameters of the continuum (i.e., constitutive model) can be determined via numerical homogenization along with experimental results from testing of individual components or simple wallettes or cores from masonry panels. Lourenço and Rots [87], and later others, demonstrate how the damage laws can be incorporated in the constitutive laws. Isotropic criteria have been preferred in these continuum damage finite element models for their mathematical simplicity, although orthotropic models have been also proposed (e.g., Pelà et al. [88]). However, macro modelling results in damage described as spreading over a large volume, whereas real damage tends to be localized in the form of cracks. Roca et al. [89] notes new developments enabling more realistic damage distributions.

Micro-modelling explicitly differentiates between block and interface material behaviour and hence is the more accurate tool, but carries a considerable computational cost. Various simplified micro models have been developed in an attempt to address this: e.g., Lotfi and Shing [90] modelled mortar joints with zero-thickness interface elements with a dilatant constitutive module capable of simulating the initiation and propagation of interface fracture under normal (both compressive and tensile) and shear stresses; Lourenço and Rots [87] propose a multi-surface interface-based model where sliding, tensile cracking and compressive crushing are concentrated to the interfaces.

An intermediate homogenization solution can be realized by first analysing a micro model to set up the unit element of a macro model. Primarily there are two approaches; one based on micromechanical deformation mechanisms, and the second based on a polynomial expansion of stress fields [91]. In the latter masonry is assumed to be rigid, perfectly plastic materials with associative flow rule [92]. Milani et al. [93] analyse masonry vaults considering a six-node triangular curved element with a suitable FE homogenization procedure.

Discrete element method

The discrete element method (DEM) was first introduced by Cundall and Hart in the 1970s, and first applied to the assessment of masonry structures by Pagnoni in the mid-1990s [89]. Roca et al. [89] give a list of DEM applications for the analysis of masonry structures, including load-bearing walls, stone bridges, arches, etc., but notes that the application of DEM to complex structures is a controversial topic.

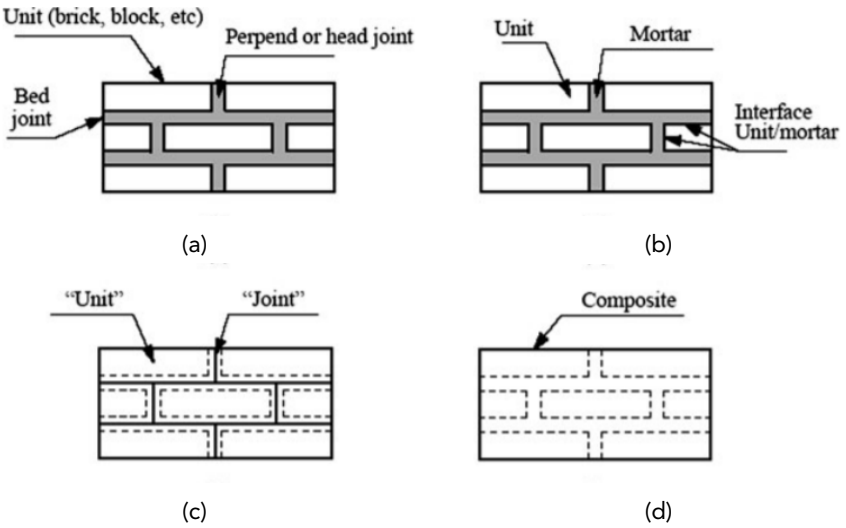

Figure 3.23: Modelling strategies for masonry structures: (a) real masonry; (b) detailed modelling strategy; (c) simplified micro-modelling strategy; (d) macro-modelling strategy (after [89]).

DEM models material as an assemblage of distinct units allowed to displace and rotate, including complete detachment from each other, and automatically detect contact between the distinct units as the calculation progresses. While different classifications of DEM formulations have been observed, the following are the most commonly identified types: (i) distinct element methods; (ii) discontinuous deformation analysis (DDA) methods; (iii) discrete finite element methods (DFEM); and (iv) non-smooth contact dynamics..

Distinct element models directly derive from work by Cundall and Hart. They use a soft contact formulation (i.e., all deformations occur at the surface of the blocks) and explicitly solve the equations of motion. The blocks can be assumed rigid or deformable. In the latter case, they are divided into equal strain elements. This was implemented in the UDEC code [94] and later extended to 3D as 3DEC.

DDA method was developed by Shi and Goodman [95] for rock engineering and was later applied to masonry [96]. DDA uses deformable blocks (having a uniform stress and strain state) with rigid contacts [89, 97]. Contacts are no tension, allow no penetration, and follow Coulomb's law [98].

There have been various attempts at combining FEM with ideas from DEM. Munjiza et al. [99] developed a DFEM formulation to simulate fracturing problems, using deformable blocks. Mamaghani et al. [100] presented DFEM for masonry assemblies using zero-thickness interface elements, where the finite deformations are concentrated at interfaces that have no tensile strength and obey the Mohr-Coulomb yield criterion.

Non-smooth contact dynamics (NSCD) models consider contact dynamics, where the motion of bodies is simulated considering energy dissipation due to the impact between the bodies, with contacts possessing friction and zero tensile resistance; these have also been successfully applied in the analysis of masonry gravity structures [49].

Commentary

In summary, the complex material behaviour and difficulty in characterizing masonry properties due to their variability bring a degree of complexity to the solution process and uncertainty to the results obtained via stiffness-based methods [98]. Additionally, stiffness-based methods methods tend to require significant computational power and user expertise to set up the models involved. In contrast, the geometry-based methods (e.g., thrust line and rigid block methods) avoid the use of material properties and form the problem as a problem primarily of geometry, involving easy-to-understand equilibrium formulations. Nonetheless, shortcomings in the thrust line and rigid block methods are also recognized.

3.2 Mapping from thrust lines to layout optimization

The discretized force systems mentioned earlier (thrust lines and their derivative forms) have a close relationship with the ground structure layout optimization (LO) method used in the optimization of trusses. This relationship is due to the graphic statics (GS) used in thrust lines, their derivative methods, and their close mapping to LO. First, a brief introduction to graphic statics (in Section 3.2.1) and ground structure layout optimization (in Section 3.2.2) is provided, considering two-dimensional cases. This is followed by a mapping between GS and LO for the case of trusses in Section 3.2.3; thereafter, this mapping is extended in Section 3.2.4 to the analysis of arches, vaults, and domes, the traditional triad of form-resistant structures.

3.2.1 Graphic statics

Graphic statics (GS) is the usage of graphical methods (i.e., visualizations such as graphs, charts and diagrams) to study forces in equilibrium. For instance, GS can be used to determine forces in a pin-jointed bar structure loaded at joints, such as a truss.

A force diagram, which is dual to the form (geometry) of the truss, is constructed when analysing a truss via graphic statics. Consider the pin-jointed-bar structure in Fig. 3.24(a) carrying a horizontal load P at node A and vertical load W at node C, and supported at nodes E and F. The corresponding force diagram is shown in Fig. 3.24(b). The links in the

force diagram are vectors representing the internal forces in the members of the truss, and the corresponding links and members are parallel to each other (following Cremona's convention; Maxwell drew dual diagrams with corresponding members perpendicular to each other). Following vector summation, if all the forces on a node of the truss are in equilibrium, then the corresponding force vectors would form a closed polygon in the force diagram, as in the triangle representing the force equilibrium of node D shaded in the force diagram in Fig. 3.24(b).

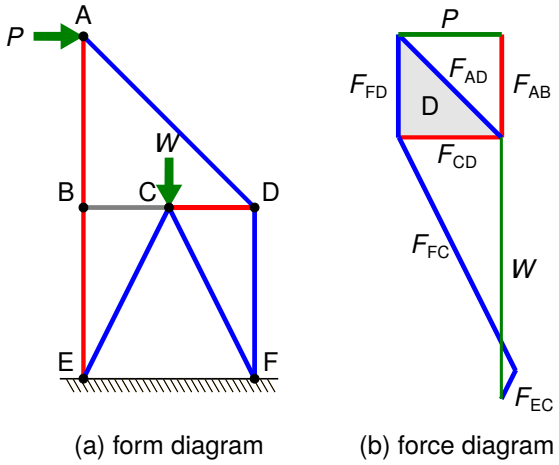

Figure 3.24: Graphic static (GS) analysis of a truss structure: considering the structure shown in (a), the dual force diagram satisfying equilibrium can be constructed as in (b). The equilibrium of a node in (a) is represented by a closed polygon of forces in (b), as indicated by the polygon shaded in (b) that corresponds to the equilibrium of node D in (a). (Members in red and blue represent tensile and compressive forces respectively; the member in grey carries no force.)

When the structure is statically determinate, as in the case in Fig. 3.24, the dual force diagram is unique up to a scale. If the structure is statically indeterminate, the force diagram generated is not unique. Changing the length (i.e., the force) in the set of independent branches of the force diagram will give rise to different possible force paths (solutions) in the indeterminate system. The number of independent force branches is equal to the degree of statical indeterminacy of the structure. Fig. 3.25 shows two possible force diagrams for a statically indeterminate structure, with a single degree of statical indeterminacy. Here, the force branch F_{AB} is taken as the independent force branch, changing the length of which changes the force diagram. Note that, in this example, any branch could have been taken as the independent branch to alter the force diagram.

Graphic statics has been extended to three-dimensional cases via two approaches. Following Rankine, the force diagram can be presented as an assembly of polyhedral cells where closed polyhedrons represent nodal equilibrium with the face areas representing the forces in

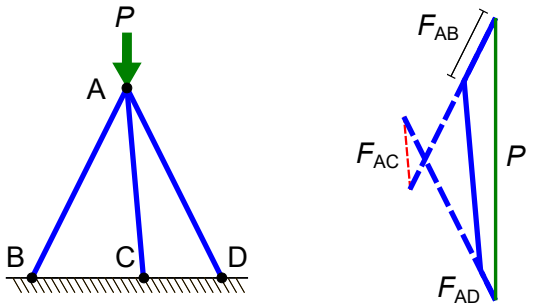

(a) form diagram (b) force diagram

Figure 3.25: Graphic static (GS) analysis of a statically indeterminate truss structure: considering the structure shown in (a), the dual force diagram satisfying equilibrium can be constructed as in (b). The force diagram is not unique: by changing the length of branch F_{AB} the force diagram changes by changing the forces in the members of the structure. Two possible solutions are indicated in solid and dashed lines. (Members in red and blue represent tensile and compressive forces respectively.)

members perpendicular to the corresponding face [101]. Alternatively, following Cremona, a three-dimensional force diagram where the corresponding members in form and force diagrams are parallel to each other can be constructed [102, 103].

Millar et al. [104] and McRobie et al. [105] present a graphic stability analysis using Maxwell-Minkowski diagrams (in 2D), constructed by translating pieces in the form diagram [106], and Maxwell-Williot diagrams, constructed by translating pieces in the force diagram to give a displacement diagram [107]. By calculating the internal work done (in the self-stressed form) the stability of the structure is determined; a positive work done indicates a stable structure. With the graphical presentation of the work done via Maxwell-Minkowski, and Maxwell-Williot diagrams, it is possible to manipulate the form and force diagrams to adjust the stiffness of the structure, with the diagrams giving visual feedback. However, the increasing complexity of the form, force, and other graphs as the complexity of the structure increases is to be noted; some of these may be alleviated with the aid of modern visualization tools.

3.2.2 Ground structure layout optimization procedure

The ground structure layout optimization (LO) process was originally developed to identify minimum volume truss structures [13, 108, 109, 110, 111]. It considers the plastic analysis of a truss with an unknown form (i.e., here, all truss members are stressed to their yield strength) to determine the optimal form of the truss by solving an optimization problem.

In Fig. 3.26, the problem of determining the minimum volume truss within the design space (shaded in grey), while adhering to the boundary conditions (i.e., loads P and W, and the support at base) is considered. First, a set of nodes, dispersed across the physical design

space, is generated. They are then connected to each other with links, which also remain inside the design domain. This collection of nodes and links is called the 'ground structure' (Fig. 3.26b). The links in the ground structure represent potential members of the structure and have an area of zero or a positive number; the links with non-zero areas at the end of the optimization process represent the members present in the optimal structure.

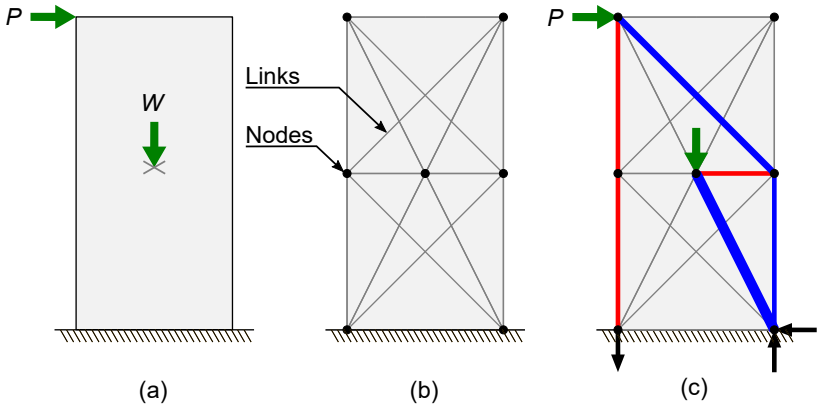

Figure 3.26: Ground structure layout optimization (LO) procedure: (a) specified design domain with loading and support conditions; (b) nodes linked by potential members, creating a 'ground structure'; and (c) optimal (minimum volume) layout identified by solving the underlying layout optimization problem. (Tension and compression forces are shown in red and blue, respectively, with line thickness proportional to force magnitude.)

The optimization problem (Eq. (3.2)) is formulated and solved with the objective of finding the minimum volume truss structure possible within the ground structure defined (Eq. (3.2a)), under the constraints of equilibrium at nodes (Eq. (3.2b)), and members yielding at their material strength (Eq. (3.2c)). As both the objective function and the constraints are linear with respect to the variables, this is a linear programming problem.

$$\min_{a,q} \quad V = l^T a \tag{3.2a}$$

$$\text{s.t.} \quad Bq = f \tag{3.2b}$$

$$-\sigma^- a \leq q \leq \sigma^+ a \tag{3.2c}$$

$$a \geq 0 \tag{3.2d}$$

where, V is the volume of the force network, $l = [l_1, l_2, ..., l_m]^T$ is a vector of link lengths, $a = [a_1, a_2, ..., a_m]^T$ is a vector containing the member cross-sectional areas of links, B is $2n \times m$ equilibrium matrix containing direction cosines (see [112]), $q = [q_1, q_2, ..., q_m]^T$ is a vector containing internal forces of the links, $f = [f_{1x}, f_{1y}, f_{2x}, f_{2y}, ..., f_{nx}, f_{ny}]^T$ is a vector containing the external loads applied at nodes, n is the number of nodes, m is the number of

links, and σ^+ and σ^- are limiting tensile and compressive stresses respectively.

The basic formulation of the LO problem presented here for the two-dimensional case can be readily extended to the three-dimensional case by including the nodal equilibrium equations in the third spatial dimension, in Eq. (3.2b). Furthermore, the basic formulation of the LO problem has been improved by using an adaptive 'member-adding' process to reduce the computational cost of the process [13]; also rationalization via geometry optimization has been added as a post-processing step to produce more practically viable structures [113], and is discussed in more detail in Section 3.3.

3.2.3 Trusses

Application of GS and LO techniques to truss structures can be compared, considering their formulation and application (Table 3.1). Aspects of the problem formulation (i.e., how the geometry, equilibrium, and stability of trusses are represented) and how this is applied (i.e., how these tools are used in engineering analysis and design) are compared.

Table 3.1: A mapping from graphic statics to ground structure layout optimization, considering trusses.

	Graphic statics (GS)	Ground structure layout optimization (LO)
Design problem	Can explore a design space	An optimal solution emerges
Analysis problem	Formulated as an analysis problem; determine the member forces	Can be formed as an analysis problem
Equilibrium	Enforce equilibrium at nodes	Enforce equilibrium at nodes and yield in members
Stability	Graphic stability	Destabilizing loads
Geometry / Topology	Nodes in continuous space, with fixed topology/connectivity	Nodes in predefined positions with topology emerging from the process

Both GS and LO can be used in the design of trusses, but the output from the two methodologies is different. The GS formulation, in combination with form-force duality, allows a designer (architect or engineer) to explore a wide range of feasible solutions and choose a form that fits other design requirements as well. In contrast, LO looks for a unique solution(s) that optimizes a given objective, typically, minimizing the volume of the structure, while satisfying feasibility.

To ensure the feasibility of a solution, GS imposes equilibrium at pin joints (nodes) by having closed polygons in the corresponding force diagram. Similarly, feasible solutions in LO

also need to satisfy equilibrium. However, this is done by explicitly considering equilibrium via equations for the balance of forces. In addition, as a unique solution is searched for, LO formulation will include other constraints, such as yielding of members at their strength capacity when volume minimization is the objective.

The explorable design space in GS is restricted by the topology of the truss, which is decided *a priori*. In contrast, in the LO process, the optimal topology emerges from the ground structure, with inactive members having zero force (and thus zero cross-sectional area). Furthermore, nodes in LO have fixed coordinates whereas nodes in GS can be moved within the design space while different geometries are being explored (but the topology is fixed). LO can address this by increasing the number of nodes in the ground structure. However, this may result in an increased computational cost, i.e., CPU time and memory. This can be alleviated by rationalization via geometry optimization (allowing nodes to move) and a member-adding process (reducing computational time by considering only a subset of all members).

Both GS and LO problems can be formulated as analysis problems, e.g., to verify the structure's ability to safely carry a given loading. In the case of GS, this is a straightforward exercise of constructing a dual force diagram, with all polygons corresponding to the nodal equilibrium condition being closed. In the case of LO, the problem can be formulated as a load maximization problem, with the member areas being fixed and the magnitude of loading being a variable.

Stability is not explicitly considered in the basic formulation of either method. However, recent research has introduced methods to incorporate stability checking. McRobie and colleagues [104, 105] present graphic stability using Maxwell-Minkowski and Maxwell-Williot diagrams, briefly discussed in Section 3.2.1. In LO, a pragmatic method is to add destabilizing loads to check the stability of the truss, typically added as separate load cases.

3.2.4 Arches-vaults-domes

While graphic statics (GS) based methods have been widely used in the design and assessment of form-resistant structures, application of ground structure layout optimization (LO) to such problems is more limited [114, 115, 116]. Application of GS to the analysis of form-resistant structures follows from Hooke's observation and Heyman's safe theorem and is discussed in detail in Section 3.1.1 and Section 3.1.2. A potential mapping between GS and LO for its application to the analysis and design of form-resistant structures is presented in Table 3.2.

Table 3.2: A potential mapping from graphic statics to ground structure layout optimization, considering forms in compression.

	Graphic statics (GS)	Ground structure layout optimization (LO)
Design problem	Find a compression-only thrust network of the desired form	Given the loading and supports, a minimum volume form emerges
Analysis problem	Find a thrust network to fit within the structure	-
Equilibrium	Enforce equilibrium at nodes with no tension allowed; self-weight loads move in the direction of gravity	Enforce equilibrium at nodes, with tension allowed; self-weight considered as transmissible loads
Geometry / Topology	Nodes in continuous space, with fixed topology/connectivity	Nodes in predefined positions with topology emerging from the process

The main challenge in extending GS and LO to form-resistant structures is how the self-weight loads are handled. In GS, this restricts the movement of nodes to the direction of gravity, as now the self-weight loads are lumped at nodes. In contrast in LO, where nodes are fixed at coordinates, this effect is reproduced using transmissible loads; i.e., loads shareable between multiple nodes [8, 114]. Furthermore, Fairclough et al. [117] introduce equal stress catenary members where the self-weight of long-span members is properly accounted for, as opposed to masses lumped at nodes. This novel approach has been used to find optimal forms for long-span bridges.

The stringent no-compression condition is typically used in the analysis of form-resistant structures. This is ensured by using force networks mimicking hanging chains and nets. Here, as was noted previously in Section 3.1.2, the dependence of the results on the topology of the force network is also recognized. In LO, compression-only conditions can be imposed by giving the members in the underlying LO problem zero (or negligible) tensile strength.

In the design problem (in contrast to the analysis problem) the self-weight is not yet known, as the structure is unknown at the start. Thus, in TNA (the most commonly used GS-based formulation for the design of form-resistant structures) a self-weight updating strategy is employed [118]. Although a similar approach is possible in an LO formulation, the fact that the emergent solution is not a surface brings in additional challenges (Fig. 3.27a). However, recently, Bołbotowski [116] presented a mathematical formulation to solve the optimal vault problem, where the least volume compression-only vault (also a surface) is sought (Fig. 3.27b); here, the topology of the force network and the form (i.e., the elevation) are determined simultaneously, representing a major breakthrough in the field.

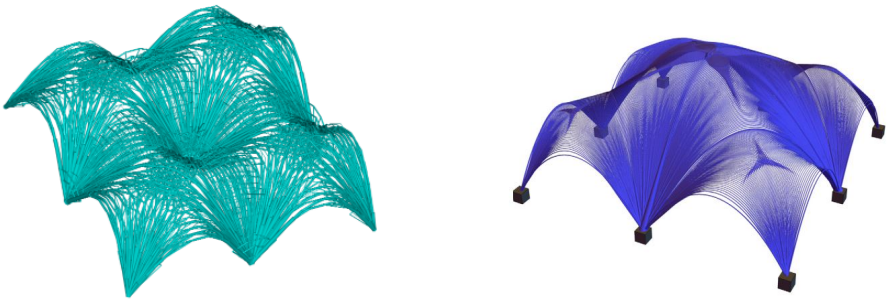

(a) (b)

Figure 3.27: Optimal volume vault occupying a cuboidal design domain in the presence of uniformly distributed transmissible loads: (a) from Gilbert et al. [114]; and (b) from Bołbotowski [116]. (Note that the structure in (a) is supported at a central point, in addition to the eight corner points used in (b).)

In summary, mapping GS and LO indicates the potential for LO to be used in the analysis of form-resistant structures. The ability of LO to include tensile forces (with controls on the force magnitude) and the fact that there is no need to define the topology of the force network *a priori* is potentially a major benefit.

3.3 Layout optimization techniques

Ground structure layout optimization, referred to here as LO, is one of many layout optimization techniques in use. However, its use of a ground structure and the plastic limit assumption of members make it unique. In the following section, developments in ground structure layout optimization are further expanded upon from Section 3.2.2, and other layout optimization techniques are also briefly introduced.

3.3.1 Ground structure layout optimization

Gilbert and Tyas [13] significantly reduced the computational cost (CPU time and memory) of the standard LO process (presented in Section 3.2.2) by using a 'member adding' solution procedure based on the dual formulation of the LO problem. This allows optimization to initially consider a limited number of potential members and, as the optimization progresses, 'add' members (to the reduced ground structure) that are likely to make the structure more optimal. This makes it possible for LO to handle problems involving very large ground structures.

He and Gilbert [14] proposed a post-processing step involving geometry optimization to simplify the solution obtained from the standard LO problem; the standard LO solution

is rationalized by allowing the nodes to move and merge, with new nodes created where members cross over. Although the proposed rationalization process is more effective than the simple rationalization technique involving the use of joint length penalties, due to the non-linear non-convex nature of the geometry optimization procedure, there is no guarantee of obtaining a globally optimal solution.

He et al. [15] propose the use of a further post-processing step to minimize structural complexity. In this case, the number of members connected to a node can potentially be controlled; e.g., members connected to nodes that have more than n_{max} connecting members can be penalized, where n_{max} is a user-defined parameter. In this case, the presence or otherwise of members (for the complexity measure) is represented by the use of a smooth Heaviside projection, with the member area projected to discrete integers, 0 and 1. The presented design optimization allows users to obtain near-optimal solutions for problems involving structural complexity constraints, with these having volumes within a user-specified percentage of the volume of the optimal solution of the corresponding problem involving no structural complexity constraints.

Furthermore, an advantage of using a plastic formulation in the LO problem is that multiple load cases can be handled easily [109]; an elastic formulation results in statically indeterminate structures under multiple load cases, meaning that compatibility of deformations needs to be explicitly considered. Note that the geometry post-processing procedure presented by He et al. [15] can also handle multiple load cases.

Ground structure layout optimization has been used with transmissible loads, where the load position of the applied load is also optimized; i.e., the line of action of a load is specified and the exact point(s) of application is determined as part of the optimization. This may yield solutions more optimal than when the location of the load application is specified *a priori* (Fig. 3.28).

Transmissible loads can be applied using one of two strategies: (i) a rigid bar approach, where the load is transferred to the structure via rigid, cost-free bars; and (ii) a migrating loads approach, where the load is shared between nodes along the line of action of the load (Fig. 5.2). Although both methods have been used, the rigid bar approach is only valid for funicular nets (either in compression or tension), with members oriented at a specific angle to the line of loading action. When the resulting structure is fully stressed, with mutually orthogonal members in tension and compression, the rigid bar approach will artificially strengthen the structure, resulting in spurious solutions [120].

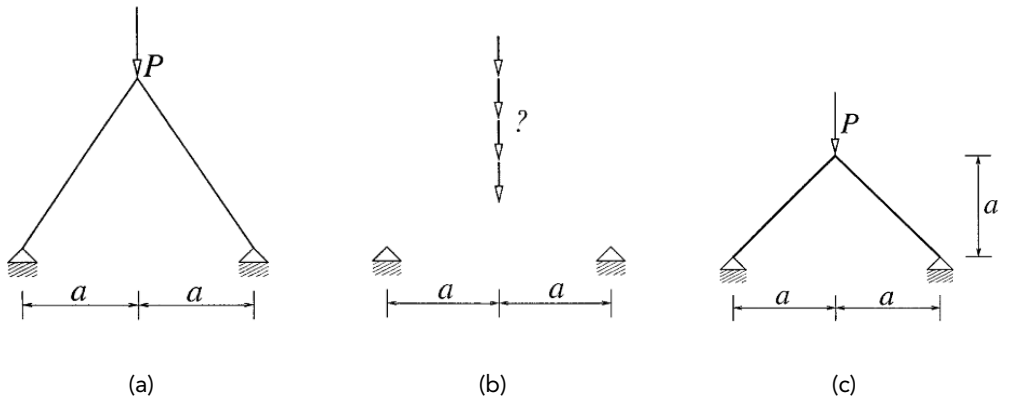

Figure 3.28: Solutions obtained using fixed vs transmissible loads: (a) optimal structure obtained when specifying a point load at a fixed location; (b) a transmissible load, acting along a vertical line of action; (c) optimal structure obtained when using this transmissible load, with the optimization process now finding the optimal position of the load as well as the optimal structure (after [119]).

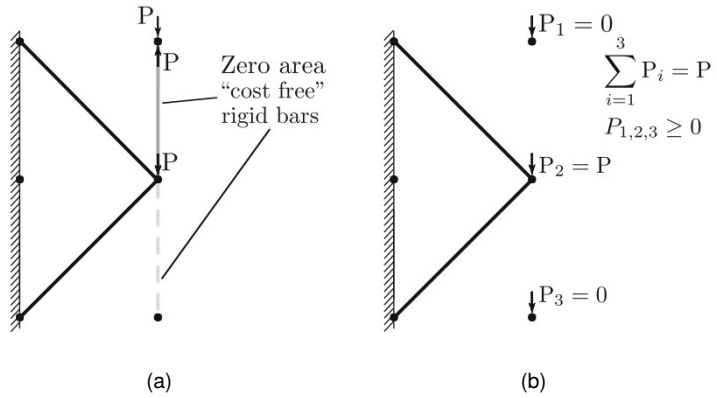

Figure 3.29: Strategies for application of transmissible loads in LO: (a) rigid bar approach; and (b) migrating load approach (after [120]).

3.3.2 Growth method

The growth method presented by Martínez et al. [121] is a topology optimization method that starts with a simple initial structure satisfying the boundary conditions (restraint and loading) and iteratively adds new joints and members until the optimal structure is found (Fig. 3.30).

The growth process is controlled by heuristics: (a) the number of crossovers created by newly added members, and (b) the number of new members connected to the new nodes created. In the latter case, preference is given to members that are close to being orthogonal to existing members. Furthermore, the procedure is only presented for single-load case scenarios. Thus the versatility of the method is doubtful, specifically when more general (i.e., structures other than Michell trusses) and more complex problems are involved.

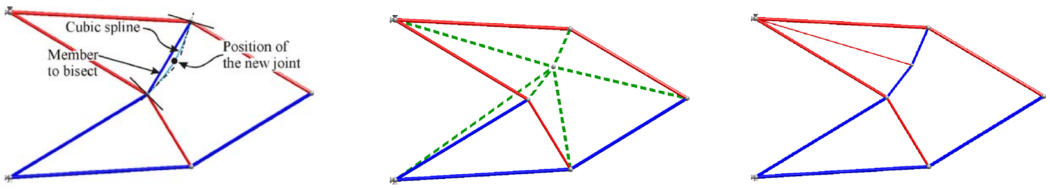

Figure 3.30: An iteration of the growth method for truss topology optimization: (a) new node position is found; (b) potential new members are identified; (c) optimal structure with new node and new member(s) found (after [121]).

Generalized shape optimization

In contrast to the above methods, where the layout is determined by the size of the elements in a ground structure, the topology optimization problem can also be formulated as a material distribution problem [122]. Bendsøe and Kikuchi [123] and Suzuki and Kikuchi [124] find the optimal distribution of an anisotropic material constructed by the distribution of small holes in a homogeneous isotropic material, i.e., introducing microscopic voids in a domain of micro-cells to create a porous medium (Fig. 3.31). Typically, the underlying analysis problem is solved via the finite element method, with finite elements overlapping the micro-cells.

The objective of optimization is to minimize compliance, subject to equilibrium and volume of material used (volume fraction) constraints. The effective material properties depend on the size and the orientation of the holes and are determined by using an explicit relationship between the material mechanical properties, computed using homogenization, and the porosity (or density). Thus, the density of the cell becomes the design variable, effectively converting the problem of determining topology into one of determining the sizes (i.e., densities) of the cells.

Suzuki and Kikuchi [124] present a solution for the two-bar frame problem, considering a grid of 40×96 finite elements (Fig. 3.32). The solution is dependent on the volume fraction, where a larger volume fraction leads to a thicker solution and vice versa. Similarly, it is noted that using an insufficient volume fraction may lead to a non-continuous solution (a checker-board pattern), while very high-volume fractions will lead to denser structures [125]. Furthermore, the solutions are influenced by other process parameters, such as the penalty power that relates the porosity of a unit cell to its compliance, and the filter radius used to avoid disconnected solutions.

The homogenization method described above, which involves the use of a continuously varying material density field, can be converted into a discrete domain; i.e., at any given location material is either present (1) or absent (0), using a penalty function to push intermediate

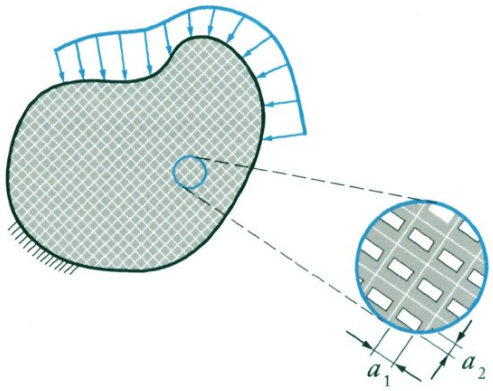

Figure 3.31: Generalized shape optimization: design domain with boundary conditions, where the design space is filled with quadratic micro-cells containing rectangular holes (after [125]).

densities to extreme values. Solid Isotropic Microstructure/Material with Penalization (SIMP) is one such approach, where 'porous' elements are suppressed (pushed to be a solid or void element) using a penalty function. This results in a solution with solid and void regions only, making the results more practical, albeit sub-optimal [126, 127].

Xie and Steven [128] present an evolutionary topology optimization procedure, termed Evolutionary Structural Optimization (ESO); this builds on the works of Bendsøe and Kikuchi [123] and others. In ESO, an optimal structure is produced by removing inefficiently used material; i.e., material subject to low-stress or with low-strain energy. This methodology is largely based on intuition, and lacks a sound theoretical basis [129].

An improvement on ESO, Bidirectional Evolutionary Structural Optimization (BESO), allows the addition of material to alleviate high-stress areas, in addition to eliminating material from low-stress areas [130] (Fig. 3.33). Noting the possibility of obtaining sub-optimal results after complete removal of material from the design domain ('hard kill'), Huang and Xi [131] present an alternative ('soft kill') BESO method, which allows previously removed material to be reinstated at later iterations in the optimization procedure.

3.3.3 Boundary-based methods

Shape optimization techniques have also been used to find optimal structures [132]. However, these have drawbacks in that they can only explore the boundary shapes of an existing topology (i.e., they cannot create new holes in the structure); also FE re-meshing can be problematic. In contrast, the level set method provides a topology optimization methodology based on boundary variation but is able to generate new topologies as well.

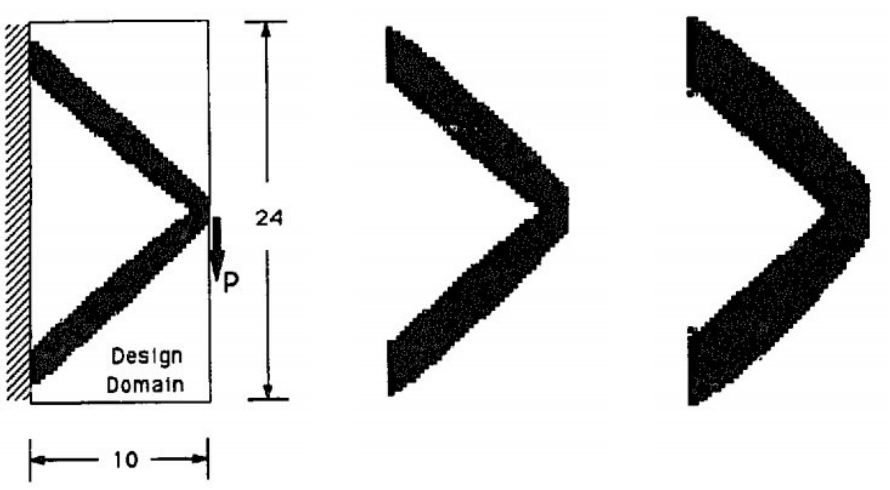

Figure 3.32: Generalized shape optimization with homogenization for the two-bar example: solutions for the two-bar frame problem with increasing volume fractions (after [124]).

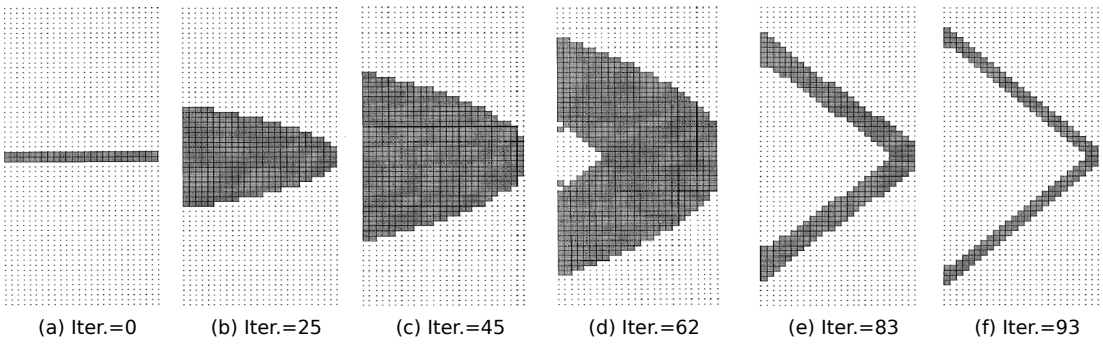

Figure 3.33: BESO method applied to the two-bar example: (a)-(f) results obtained at different iterations (after [130]).

Wang et al. [133] present a structural topology optimization method based on the level set method to represent the boundaries of the structural form as the optimization process progresses (Fig. 3.35). The level-set method provides an implicit way of representing interfaces as a set of contours in a scalar field; the movement of the interface is represented by the evolution of the scalar field. Using the level set method allows easy, robust, and efficient representation of complex boundaries, with the ability for complex topologies to form, including bodies containing holes, or split into multiple pieces.

The optimization problem minimizes some physical properties of the structure (e.g., the strain energy of the structure), subject to equilibrium constraints and a limit on the maximum admissible volume of the design domain (Fig. 3.34). The design variable is the boundary of the structure, represented implicitly by a level-set. The equilibrium equations can be imposed using an FE analysis.

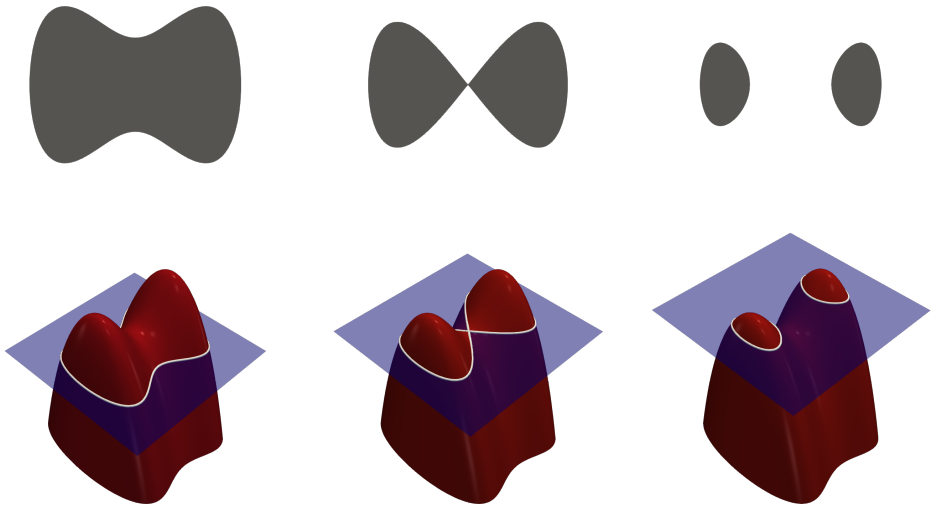

Figure 3.34: An illustration of the level-set model: level set function (red surface) gives the well-behaved boundary (in grey) as the flat plane (in blue) moves upward (after [134]).

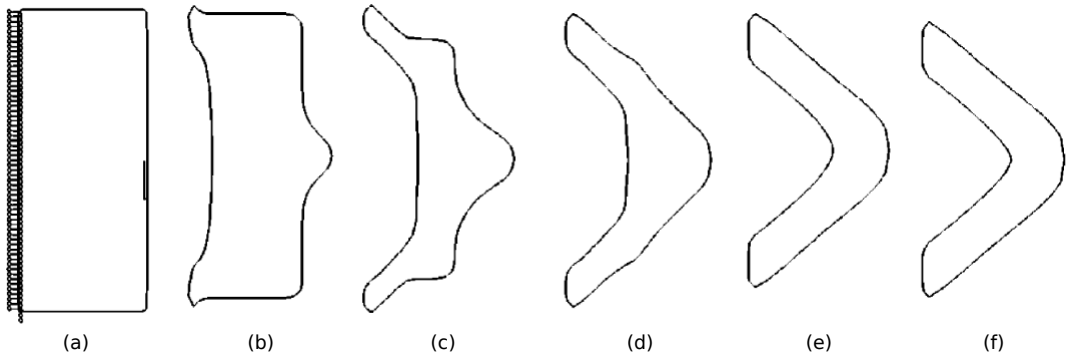

Figure 3.35: Level set method applied to the two-bar example: (a)-(f) results of different level set optimization iterations, transitioning from a solid initial design without holes (after [133]).

3.3.4 Commentary

Considering the available methods, the ground structure layout optimization procedure appears to have most potential when considering the analysis of form-resistant structures, given its ability to handle transmissible loads, large networks, and to generate new topologies. While other methods of generating topologies are available, their reliance on underlying finite element models (which are computationally expensive and may require user expertise) and also the need for tuning parameters (which lack physical meaning) make them less attractive for the current application. In contrast, LO provides a simple, physically explainable, optimization problem formulation that can be solved via linear programming (LP), allowing it to be solved using robust commercially available LP solvers.

3.4 Concluding remarks

3.4.1 Key observations

In summary:

- Form-resistant structures are efficient structural systems that have been used for centuries, mostly in the form of masonry gravity structures. Design and analysis methods to assess form-resistant structures have stemmed from Robert Hooke's observation of a the form of a hanging chain and later, have been formalized into the thrust line method and other similar discretized force systems in use today.

- Existing analysis methods for masonry gravity structures range from discretized force systems (e.g., thrust lines and derivative methods), to rigid block methods, to elastic continuum analysis methods (e.g., finite element (FE) methods) and discrete element methods. While the thrust line method is simpe to use, the information provided by the method is, at times, not intuitive and lacks clarity. In contrast, although FE models can give detailed information on the state of stress, they require material stiffness properties that are variable and difficult to estimate, require user expertise, and are computationally expensive. As such, the need for rapid, easy-to-use, assessment tools, which provide reliable information on how a structure carries load, is clear.

- The ground structure layout optimization (LO) method, which to date has been primarily used for the analysis of trusses, bears similarities to graphic statics (GS) methods used to generate thrust lines in the analysis of form-resistant structures. The mapping between the two suggests that LO has the potential to form the basis for a new analysis tool for form-resistant structures. In comparison to other layout optimization procedures, ground structure-based layout optimization is attractive as it is simple (does not require an FE solver and can be solved using linear programming) and versatile (has shown the potential to handle transmissible loads, multiple load cases, and new member types).

3.4.2 Research gaps

From the review of current literature, the following research gaps have been identified.

- While thrust lines methods are easy-to-use for the analysis of form-resistant structures, they may not give the exact collapse load as the limited tensile strength within blocks is not explicitly included. This leads to the question, can the inclusion of tensile forces

in thrust lines improve their ability to accurately predict collapse loads? Would the inclusion of tensile forces in a thrust line analysis improve the visualization of force flows within form-resistant structures?

- The ground structure layout optimization (LO) method appears to have the potential to automatically generate thrust lines; i.e., force flows within form-resistant structures, and this has not been explored previously. This thus poses the questions: how can thrust lines be generated via layout optimization, and what benefits would this bring?
- The mapping between graphic statics and LO points to the potential for truss stability considerations be treated in an improved manner in LO. However, this is out of the scope of the current study, and hence is not explored further.

Chapter 4

From Thrust Lines to Thrust Layouts

Preface

Following Hooke's observation and Heyman's safe theorem, the thrust line method is widely applied to the analysis and design of masonry gravity structures and other form-resistant structures. However, there is contention as to what is to be considered as a thrust line—there are competing notions and nomenclatures in usage. In this chapter, it is attempted to untangle the different notions of thrust lines and identify the differences between them. Recognizing the benefits of the different notions of thrust lines a novel concept of thrust layouts, building upon thrust lines, is presented.

The content of this chapter was originally prepared for a journal paper: Nanayakkara, K.I.U., Liew, A., Gilbert, M. (2023), 'Thrust layouts in masonry gravity structures', International Journal of Solids and Structures (in preparation).

Abstract

Heyman's 'safe theorem' is widely used to assess the safety of masonry gravity structures. In its original incarnation, a funicular thrust line—i.e., a hanging chain—was used to represent a possible flow of forces through a structure, though this was later found to be problematic in some cases. Following the work of Moseley, a line of resistance has also been used as a thrust line. However, although this provides a valid representation of equilibrium, it does not facilitate clear visualization of a flow of forces in a structure, making it less intuitive than a funicular thrust line. With the aim of addressing shortcomings associated with funicular thrust lines, the notion of a 'thrust layout' is also considered here. This can accurately represent a state of equilibrium while also enabling visualization of a flow of forces within a structure. Thrust layouts also allow explicit consideration of the tensile forces that can (or cannot) be reasonably sustained in a masonry construction (e.g., within constituent blocks but not across weak joints).

4.1 Introduction

Robert Hooke (1635-1703) observed the correspondence between a hanging chain and a rigid arch and stated 'As hangs the flexible line, so but inverted will stand the rigid arch' [35, 36, 135]. Thus originated the idea of a 'funicular' to represent the equilibrium of an arch. In 1748, Poleni successfully applied this to the analysis of the cracked dome of St. Peter's in Rome [135].

Since then, thrust lines generated from funiculars have been extensively used in the analysis of masonry gravity structures, such as arches, vaults, and domes. Here, such thrust lines generated from funiculars will be referred to as 'funicular thrust lines', where the funiculars can be from physical hanging chain/cloth models [32, 136, 137], graphic statics [36, 59, 136, 138], or various other numerical methods (e.g., particle spring models [64, 65]). The usage of funicular thrust lines was further popularized by the development of Heyman's 'safe theorem' [35], as this placed it within the realm of limit analysis, giving structural engineers the confidence to use it in everyday practice. Here, it is noted that a thrust line may not represent the exact state of the structure, where these masonry gravity structures are highly statically indeterminate a thrust line would only show one possible flow of forces within the structure. As Heyman [39] notes, and experimental evidence suggest [52], this is sufficient to guarantee the safety of masonry gravity structure.

However, as was later noted by Heyman himself [57, 139], along with others, funicular thrust lines unintentionally assume the structure to be made up of equivalent vertical strips of material, rather than using the actual block stereotomy present. If care is not exercised then this assumption may lead to unsafe designs—e.g., when analysing a masonry buttress, the masonry effective in resisting the external loads needs to be determined first to prevent ineffective material from being inadvertently 'lifted up' to the thrust line, leading to an over-estimation of the load carrying capacity [52, 54].

The usage of thrust lines is further complicated by the different notions of thrust lines that arise from Moseley's 'line of resistance' and 'line of pressure', where the latter coincides with what is here referred to as a funicular thrust line [135, 58]. Although the subtle but important distinctions between the two have been previously noted, they have both been referred to as 'thrust lines'*, and used in the application of Heyman's safe theorem (e.g., the line of resistance is used as the thrust line in [136, 140, 141], whilst the line of pressure / funicular thrust line is used for this purpose in [36, 39, 142])

Drawing upon previous attempts to resolve these issues (e.g., [57, 58, 79]), a thorough discussion is provided here. In addition, the notion of a 'thrust layout' is introduced, which allows new light to be shed on the various notions of thrust lines. Thrust layouts are a valid representation of equilibrium (as is the line of resistance) and a valid force flow (as is the line of pressure / funicular thrust line) of masonry gravity structures, thus providing a means of bringing together the current competing notions.

Issues related to frictional contacts in thrust lines are noted but not explored in depth in this work. Heyman's safe theorem assumes infinite friction capacity at masonry block interfaces, notwithstanding that frictional failures in masonry gravity structures have been previously observed, e.g., sliding failure at the head of a flying buttress [47]. In this case Bagi [143] has pointed out that rigid block systems can fail even when an equilibrium solution exists and the sliding resistance is not exceeded anywhere, with additional kinematic conditions needing to be considered to make Heyman's safe theorem truly 'safe' in this case.

In this contribution, the limitations of using funicular thrust lines are first carefully considered. Then, to remedy these, thrust layouts are introduced. Two observations on detecting erroneous funicular thrust lines are also presented.

*In this chapter, the term 'thrust lines' is used as an umbrella term for all usages of thrust lines. Furthermore, 'thrust lines' and 'lines of thrust' are considered interchangeable terms, referring to the same.

4.2 Funicular thrust line

A funicular thrust line (or a 'line of pressure') is defined here as a funicular polygon representing a possible state of equilibrium of a masonry gravity structure. It can be generated from a hanging chain model or from an equivalent graphic static or numerical procedure. Formal definitions of these are as follows.

Definition 1. A **funicular polygon** is an open or closed polygon that takes the form of a (weightless) cable acted upon at a number of points by forces in various directions. (see Fig. 4.1)

Figure 4.1: A funicular polygon generated by hanging loads on a cable or thread (in blue), the weight of which is negligible.

Definition 2. A **funicular thrust line** is a funicular polygon, where the forces acting upon the cable represent the boundary conditions of a masonry gravity structure (i.e., external loading, self-weight, and support reactions), and the cable represents one possible state of equilibrium of the masonry gravity structure.

Jacques Heyman, in his eponymous 'safe theorem', used funicular thrust lines to represent the equilibrium of a masonry gravity structure [35], with the zero tensile capacity yield criterion satisfied when these thrust lines are completely contained within the extent of the structure. Thus, if a funicular thrust line subjected to self-weight and external loading can be contained entirely within the structure, it can be deemed safe; see Fig. 4.2.

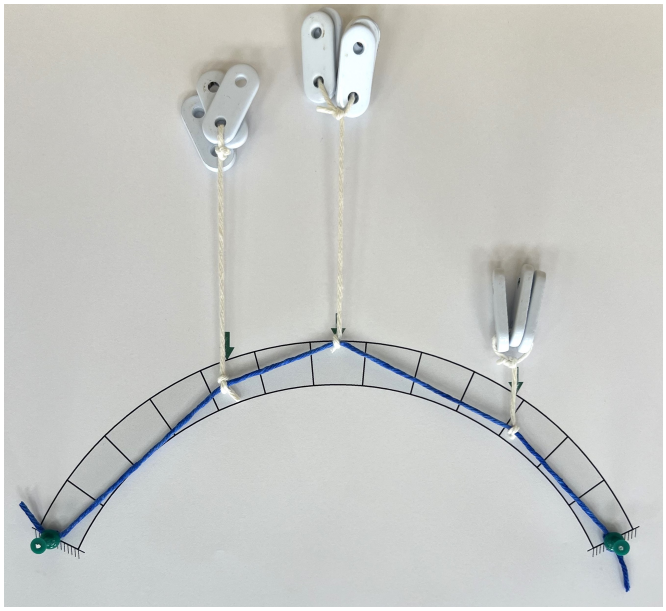

Figure 4.2: Heyman's safe theorem: the funicular thrust line (in blue), generated by a hanging chain model (inverted), is fully contained within the arch section; assuming the self-weight of the arch is negligible, the arch can be considered safe.

4.2.1 Assumption of equivalent vertical-strips

Heyman [57] notes that his earlier work (i.e., [35]) "unintentionally" assumes the voussoirs to have vertical cuts between them. He concludes that, although the safe theorem can reasonably be applied to e.g., a monolithic arch, it fails to account for the effects of cuts, or interfaces, between voussoirs (*la coupe des pierres* or block stereotomy).

For instance, consider the segmental arch shown in Fig. 4.3. A funicular thrust line, shown in blue, is generated considering the weight of the voussoirs, lumped at their mass centres. As noted previously, the usage of a funicular unintentionally assumes a series of vertical strips, with lines of action that pass through the centres of mass of the real voussoirs present. Figure 4.3 indicates the geometry of the real voussoirs, and the corresponding equivalent vertical strips (shown shaded in grey) for two voussoirs, A and B.

Now consider the funicular thrust line segments within those voussoirs, real and equivalent, and the corresponding thrusts at their interfaces (see the inset figures in Fig. 4.3b). As seen in inset (i), the thrust line segment within the voussoir (blue line) and the thrusts at the interfaces (green arrows) do not exactly coincide, leaving an offset; i.e., they are inconsistent, albeit only slightly. This inconsistency implies that the funicular thrust line is not a valid representation of the equilibrium of the voussoir, and thus the arch.

Also, note that the self-weight of voussoir A is applied to the thrust line at a point beyond its extent. Thus the trajectory of the thrust line would change (to match that of the thrust at

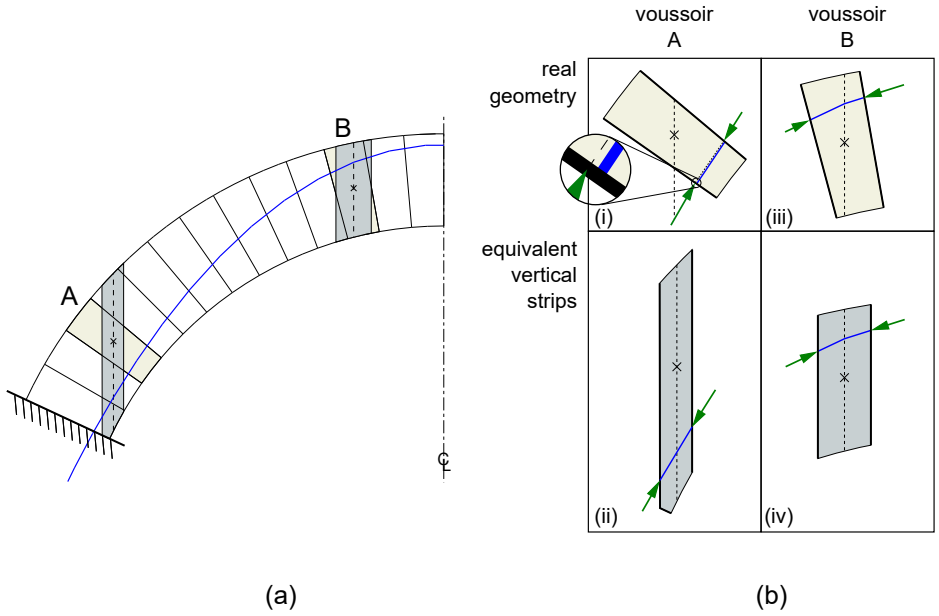

Figure 4.3: Funicular thrust lines unintentionally assume a series of equivalent vertical strips instead of the actual voussoir stereotomy: funicular thrust line within voussoir (a) is not consistent with the thrust at the interfaces, whereas it is for the assumed equivalent vertical strip; in contrast, for voussoir (b), the funicular thrust line within both the voussoir and the equivalent vertical strip are consistent with the thrust at interfaces.

the interface) only after the point of application of this self-weight force. This leads to the thrust line within the block being inconsistent with the thrust at the interfaces.

However, as shown in inset (ii) of Fig. 4.3b, the funicular thrust line and the thrusts at interfaces are consistent for the corresponding equivalent vertical strip. Note that the self-weight is now applied to the thrust line within the extent of the equivalent vertical strip; this is guaranteed to be the case when the lines of actions of self-weight are parallel to the voussoir interfaces. Thus the equilibrium representation of a funicular thrust line is only strictly valid for equivalent vertical strips.

Nevertheless, the geometry and orientation of the voussoirs can be such that the static equilibrium representation of a thrust line is still valid. For instance, consider voussoir B in Fig. 4.3. As seen in inset (iii) the funicular thrust line and the thrusts at interfaces are in this case consistent with the real voussoir. This is in fact guaranteed to be the case if the line of action of the self-weight of the voussoir does not cross a radial joint (i.e., the line of action of the self-weight remains within the corresponding block).

4.2.2 Implicit tensile strength

Now consider the segmental arch shown in Fig. 4.4. A funicular thrust line (corresponding to one possible flow of forces) is also constructed, shown in a blue solid line, considering

self-weights lumped at the centres of mass of the voussoirs.

Now observe in Fig. 4.4 the positions of the centres of mass (marked with an $\times$) relative to the funicular thrust line. It is evident that some of the mass centres lie above the funicular thrust line, while others lie below. This implies that struts in compression are required to transfer the self-weight of voussoirs to the thrust line, as indicated by blue vertical lines running from the centres of mass in Fig. 4.4. Similarly, ties in tension are required to transfer the self-weight loads in cases where the centres of mass of voussoirs are below the funicular thrust line; see red vertical lines in Fig. 4.4. Thus, this construction of a funicular thrust line implicitly assumes that tensile forces can be resisted by the masonry.

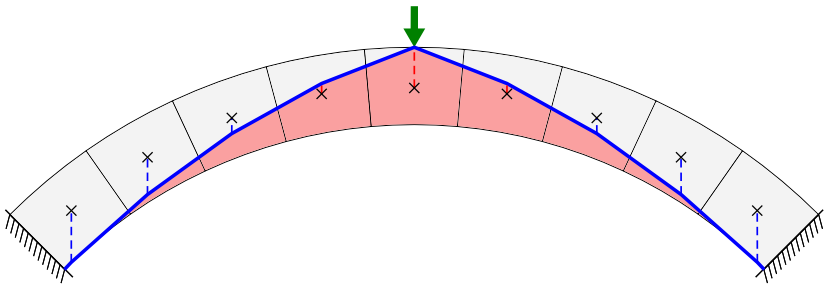

Figure 4.4: Implicit tension in funicular thrust lines: Funicular thrust lines assume tensile forces to transfer the self-weight loads from their points of application to the thrust line, as indicated by red verticals where the self-weights are lumped at the centres of mass of the voussoirs. Equivalently, when the self-weight is considered distributed, the areas below the funicular thrust line (shaded in pink) will be in tension in the vertical direction. Similarly, blue indicates compressive forces.

By extension, if the self-weight were to be considered distributed, instead of being lumped at the centres of mass, the material below the thrust line, shaded in pink, is carrying self-weight loads in tension (in the vertical direction), and the material above the thrust line is carrying these in compression (in the vertical direction).

In summary, funicular thrust lines (i) assume equivalent vertical strips instead of the real voussoir configuration, which is likely to lead to an invalid representation of the state of equilibrium of the structure; and (ii) implicitly assume tensile forces can be resisted by the voussoirs, although this is not made explicitly clear to the users, though no tensile forces are allowed in the funicular thrust line itself.

For a typical example involving a segmental arch subjected to self-weight and other vertical loads, the aforementioned shortcomings may lead to conservative predictions of safety. Consider for example the two voussoirs shown in Fig. 4.5, where the voussoirs share a common interface, have self-weights W_A and W_B, and are subjected to thrust forces F_A and F_B. Here, the funicular thrust line considered (and shown in a solid blue line) moves outside the

two-voussoir configuration indicating according to Heyman's safe theorem that the structure will not stand due to the absence of a valid equilibrium solution. However, the structure is safe: the three forces on each of the voussoirs (self-weight, external thrust force, and the thrust between the voussoirs) create closed force polygons (see force diagram in Fig. 4.5) guaranteeing equilibrium, and all thrust forces are contained within corresponding interfaces ensuring the yield condition for masonry is not violated. Thus, here, the funicular thrust line indicates an unsafe structure even when the structure is safe, therefore leading to a conservative assessment of safety.

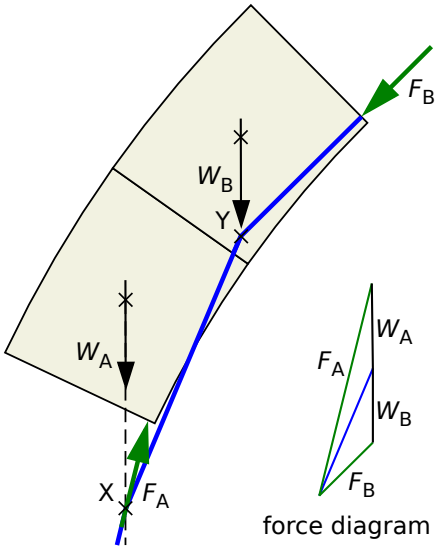

Figure 4.5: Funicular thrust line in two-voussoir example: although an equilibrium solution exists, the funicular thrust line moving outside the extent of the assembly indicates an unsafe solution. (The two voussoirs are of weight W_A and W_B, share an interface, and are subjected to thrusts F_A and F_B.)

Alternatively, assuming infinitely rigid blocks (which was not an explicit assumption of Heyman [35]) would rectify the issues caused by the assumption of vertical strips and implicit tensile strength [144]. However, thrust lines generated with this assumption would no longer be a funicular thrust line: they would align with the notion of line of resistance.

4.3 Line of resistance

In 1843 Moseley [145] presented the notion of a 'line of resistance' to represent a possible state of equilibrium of 'a structure made of uncemented stone' (the same notion was in 1907 also presented by Milankovich, though in this case referred to as *die druckkrve* [146, 147]).

Definition 3. A **line of resistance** is a geometrical locus of points-of-application of the resultant thrust forces that develop at interfaces within a masonry arch or other structure.

Revisiting the two-voussoir example, now consider a line of resistance. The line of resistance drawn as a solid purple line in Fig. 4.6 is constructed by first determining the points-of-application of thrust at each interface (marked X, Y, Z) and then connecting them by line segments.

Thus a line of resistance is a valid equilibrium representation that explicitly considers block stereotomy. However, it does not necessarily align with the thrust trajectory at interfaces; this happens if and only if the interfaces are vertical [146, 147]. Thus, it can be argued that a line of resistance does not represent a valid force flow within the structure. Also, as a line of resistance does not follow the thrust force vectors, it is visually less intuitive than a funicular thrust line and does not make it clear to a structural engineer how the structure could safely carry the applied loads.

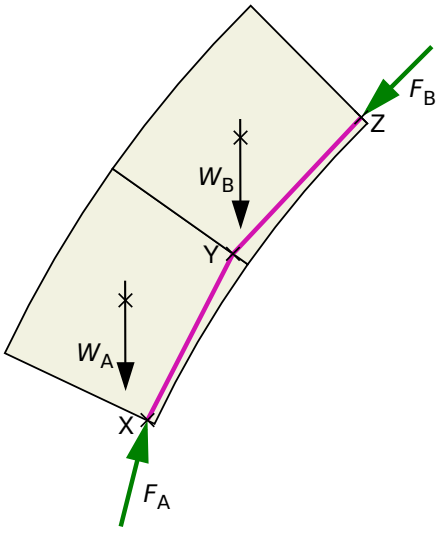

Figure 4.6: Line of resistance in two-voussoir example: although the line of resistance is fully contained within the structure, it does not correspond to a force flow as the line segments do not align with the corresponding thrusts at the interface.

Furthermore, a convenient, albeit non-rigorous, way of checking for sliding failure is to check the angle of incidence of a thrust line at an interface against the angle of friction of the material; e.g., see [145, 46]. Now, since a line of resistance representing a thrust line does not reflect the actual thrust trajectory, such a geometrical check is not possible.

Finally, given that vertical strips are implicitly assumed in the case of funicular thrust lines, it follows that a line of resistance and the corresponding funicular thrust line will coincide if, and only if, the interfaces between masonry blocks are vertical (i.e., are aligned parallel to the direction of gravity loading).

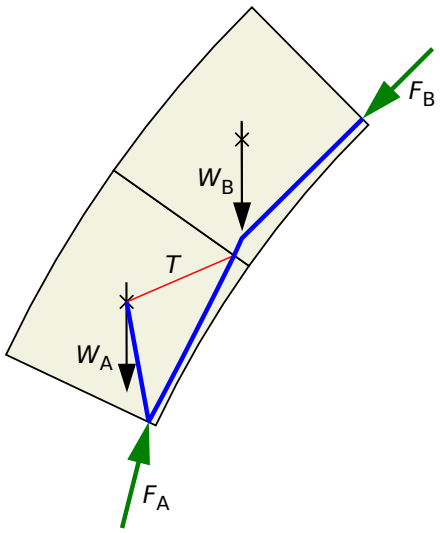

Figure 4.7: Thrust layout in two-voussoir example: the thrust layout is fully contained within the structure and properly corresponds to a force flow.

4.4 The thrust layout

Now consider the network of forces in Fig. 4.7 for the same two-voussior example considered earlier. The network is fully contained within the structure; its links align with the force vectors and the forces satisfy equilibrium constraints for each of the voussoirs, and hence in turn the whole assembly. Therefore, this network of forces is both a valid representation of equilibrium and a meaningful visualisation of force flow. This network of forces is here termed the 'thrust layout'.

The thrust layout is formally defined below:

Definition 4. A **thrust layout** is a network of forces in equilibrium, representing a possible flow of forces in an assembly of blocks, where:

1. compressive forces of any magnitude are allowed;
2. self-weight forces must be transferred to the network within the extent of the corresponding masonry block;
3. tensile forces are allowed within blocks, but not across the weak interfaces that lie between them.

Note the presence of a tensile link in the force network shown in Fig. 4.7, and in the definition of a thrust layout. It was previously observed that tensile forces are implicitly associated with funicular thrust lines; instead here these forces are explicitly shown, and can usually be

carried provided that some, albeit limited, tensile capacity can be transmitted within a given masonry block.

Taking a thrust layout to be a natural extension of a funicular thrust line, the condition of infinite compressive forces is adopted here and two additional constraints are introduced: (i) self-weight is assumed to be transferred to a thrust layout within the extent of a given block; (ii) tension is explicitly allowed within the extents of a given block. The effects of these additional constraints are explored further in the following sections.

4.4.1 Transferring self-weight to the thrust layout within the extent of a given block

Consider the simple two-block example shown in Fig. 4.8a, which shows a small block stacked on a larger block. An increasing horizontal load P is applied at the top left corner of the top block, which will eventually overturn that block about its bottom right corner, opening up the weak interface between the two blocks. One may construct a hanging chain model (Fig. 4.8b), or a corresponding graphic static funicular thrust line (Fig. 4.8c), considering the self-weights of the blocks, W_A and W_B, to be lumped at their mass centres. Both methods predict the same collapse load, of $P = P_1$.

However, the force flow represented by this funicular thrust line is not admissible in the real structure, since it implicitly assumes that a tensile force can be transmitted across a weak interface, which in reality is not possible. This error is easily detected when the forces carrying self-weight from the mass centres to the funicular thrust line are plotted (see Fig. 4.8c), whereas not so obvious in the physical hanging chain model (see Fig. 4.8b).

This erroneous funicular thrust line can be corrected by ensuring the self-weight load corresponding to a given block is mobilized only within the extent of that block. A valid thrust layout is presented in Fig. 4.8d, where the self-weight of the bottom block W_B is not transmitted up to the main thrust line, but instead is directly transferred down to the supporting ground. In this solution equilibrium of each individual block is satisfied, and hence so is the equilibrium of the whole structure. Also, the yield condition is satisfied at all interfaces (i.e., no tension is applied across weak interfaces), with the solution also corresponding to a valid collapse mechanism (where the top block rotates about the bottom right corner, as in Fig. 4.8a), thus giving the exact collapse load, of $P = P_2$.

Contrary to the commonly held belief that thrust line solutions will always be conservative, the solution of $P = P_1$ given by the funicular thrust line in Fig. 4.8c, is higher than the exact

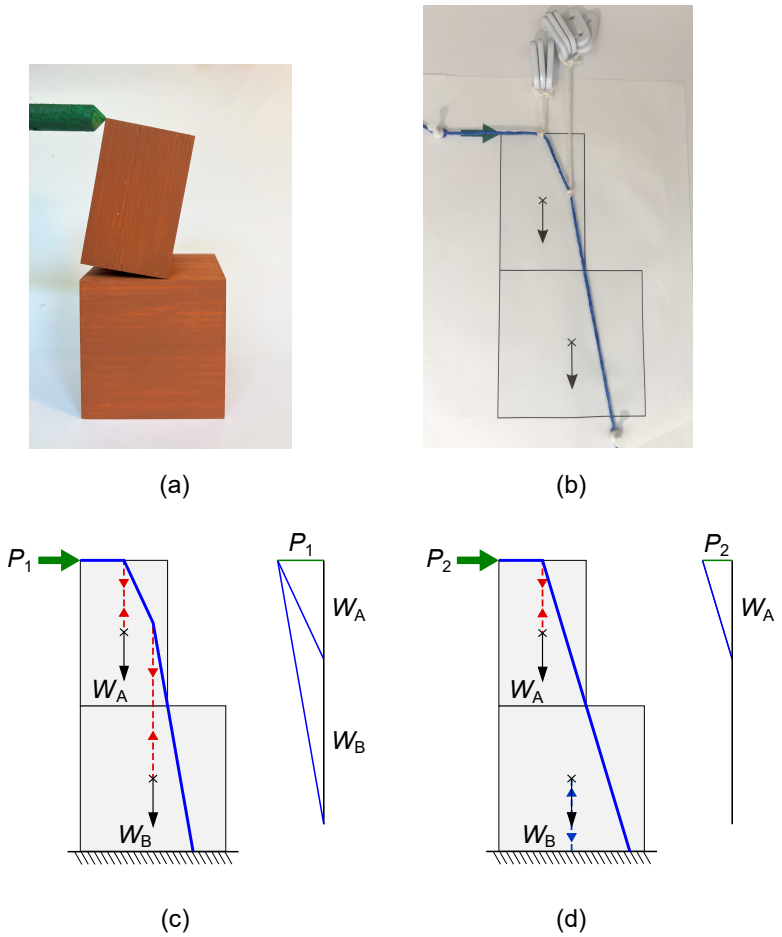

Figure 4.8: Mobilizing self-weight load within the extent of a given block: (a) experimentally observed failure mechanism when a horizontal load P is applied at the top left corner of the top block; (b) physical hanging chain model at failure, with $P = P_1$; (c) corresponding graphic statics model, with again $P = P_1$; (d) thrust layout model, with now $P = P_2$, where $P_2 < P_1$; in this case the self-weight of the bottom block is carried directly by the supporting ground whereas the funicular thrust line implicitly assumes that a tensile force can be transmitted across the weak interface between the blocks, inadmissible in the physical model. (Compression and tension forces are shown in blue and red respectively.)

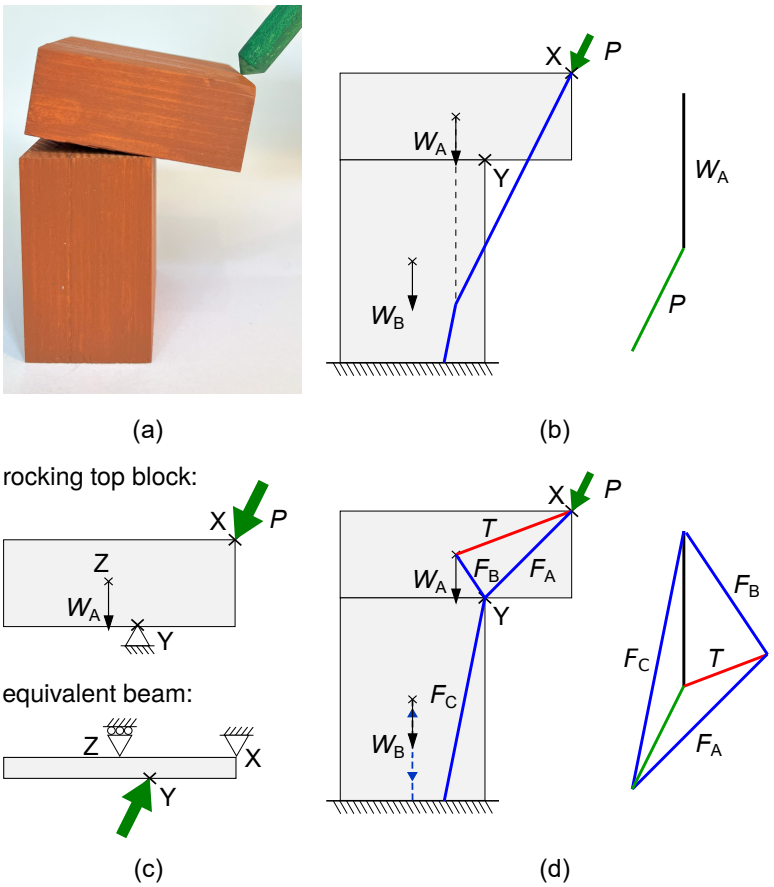

Figure 4.9: Incorporating tension explicitly: (a) experimentally observed failure mechanism when an inclined load P is applied at the top right corner of the top block; (b) a thrust line lying entirely within the structure cannot be constructed; (c) observing the equivalence of the rocking top block (in the physical model) to a beam in bending, the requirement for tensile forces to be present inside the block is noted; (d) a valid thrust layout incorporating tensile forces is constructed. (Compression and tension forces are shown in blue and red respectively.)

collapse load of $P = P_2$, since the self-weight of the bottom block will help resist the applied load.

4.4.2 Incorporating tension explicitly

Now consider another example involving two blocks, where in this case the top block overhangs the bottom block (Fig. 4.9a). The two block assemblage is in this case subjected to an inclined load applied to the top right corner of the overhanging block.

Firstly, an attempt is made to construct a funicular thrust line for this example (Fig. 4.9b). For this, a compressive force along the line of action of the external load P is required, in order to satisfy equilibrium at point X. However, this compressive force would move outside of the structure before intersecting the line of action of the self-weight W_A of the top block (indicated in a dashed line). Thus a funicular thrust line fully contained within the structure cannot be constructed.

Yet the physical model (Fig. 4.9a) suggests that a valid solution must exist. Investigating this further, a free body diagram for the rocking top block is drawn (Fig. 4.9c); observe the top block rocking about point Y in the physical model. This is equivalent to a beam subjected to a point load in bending. The presence of bending in the beam suggests that tensile forces must be mobilized in the block, likely to be in the upper portion of the block. Following this intuition, a force network that includes a tensile force (i.e., a thrust layout) is constructed (Fig. 4.9d), where the forces are in equilibrium and the network is fully contained within the structure.

Thus, a valid thrust layout is constructed by explicitly allowing tensile forces within constituent blocks, where a funicular thrust line would have suggested an unstable structure under the given loading. Note that the thrust layout presented in Fig. 4.9d is one of many possible valid thrust layouts.

4.5 Identifying erroneous funicular thrust lines

The two examples studied in the previous section demonstrate the limitations of using a funicular thrust line to represent the equilibrium of block assemblies. Now, considering the geometry of the funicular thrust line, the two examples are re-examined to see if general rules can be found to detect erroneous funicular thrust lines.

4.5.1 Case 1: collapse load over-estimation

Consider the example shown in Fig. 4.8, now reproduced in Fig. 4.10. Observe the funicular thrust line changing its orientation, from being horizontal at the loading point to being near-vertical as the self-weight of the constituent blocks is transferred to it. This is the general behaviour observed in funicular thrust lines in regions where no external horizontal load is applied; e.g., see the arches in Fig. 4.3 and Fig. 4.4.

Now consider the equilibrium of the bottom block in Fig. 4.10. The block is in equilibrium under three forces: the thrust from the top block, F_A; the reaction from the ground, F_B; and

self-weight, W_B. These equilibrating forces meet at a point above the block (point Z), but this still lies within the structure.

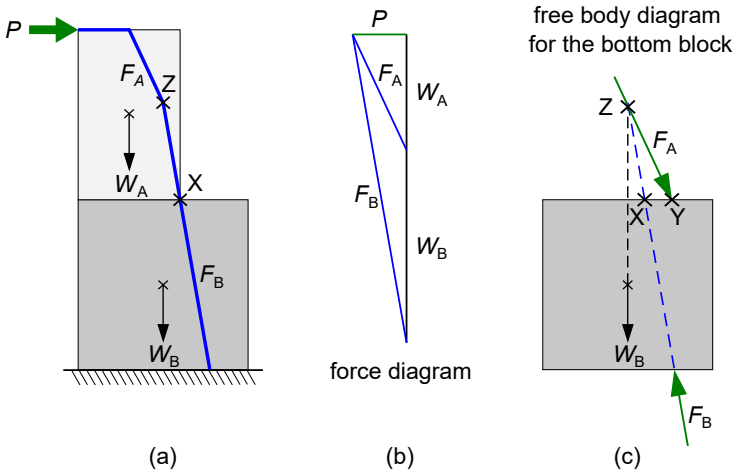

Figure 4.10: Over-estimation of the collapse load by the funicular thrust line: Although the thrust line is fully contained within the structure, the equilibrium of the bottom block is not valid: The thrust F_A between the blocks is outside the interface between the two blocks—passing through point Y, in the free body diagram. Note the equilibrating forces of the bottom block coincide at a point above the block.

The funicular thrust line approaching point Z follows the trajectory of the thrust force vector F_A, and then changes orientation, becoming more vertical. The deflected thrust line then intersects the block boundary at point X, whereas the thrust force vector F_A, when extrapolated, goes on to intersect the block boundary at point Y. Thus, the (deflected) funicular thrust line intersects the block boundary at a point some distance within where the real thrust would intersect the block boundary.

This means, in a limiting case where the funicular thrust line is on the boundary of the structure (point X in Fig. 4.10), the thrust itself would likely be outside (point Y). Hence the equilibrium representation of the funicular thrust line is not valid.

4.5.2 Case 2: collapse load under-estimation

Now, consider the example shown in Fig. 4.9, now reproduced in Fig. 4.11. The funicular thrust line in Fig. 4.11 is only partially contained within the structure.

The top block in Fig. 4.11 is in equilibrium under three forces: the externally applied load, P; the thrust from the bottom block, F_B; and the self-weight, W_A. These forces intersect at a point below the block (point Z), but still within the structure.

The funicular thrust line following external load P changes its orientation towards the vertical at point Z and then follows the trajectory of the thrust F_B. This results in the funicular

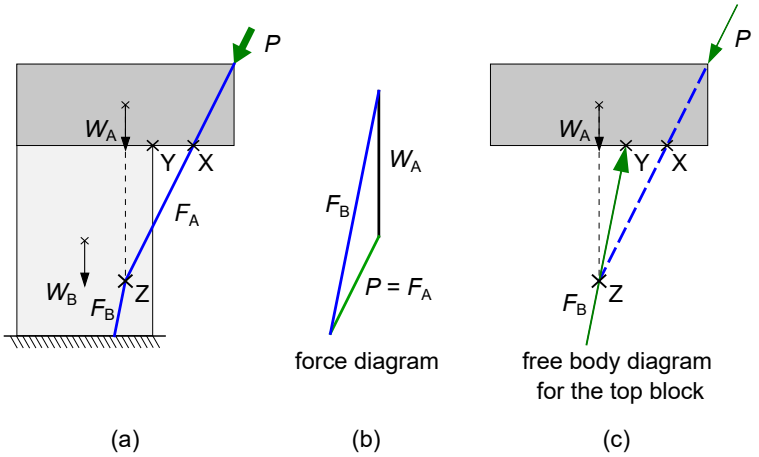

Figure 4.11: Under-estimation of the collapse load by the funicular thrust line: Although the funicular thrust line lies outside the structure, the equilibrium of the blocks and the structure is satisfied: Thrust force F_2 between the blocks lies within the interface between the two blocks—passing through point B. Note the equilibrating forces of the top block coincide at a point below the block.

thrust line intersecting the block boundary at point X, which is exterior to the point where the thrust F_B is being applied on the block (point Y).

This means, that, even when the funicular thrust line is outside the structure, there may still exist a valid equilibrium solution. That is the case here as point Y is on the boundary of the structure.

4.6 Discussion

Thrust layouts can be used for the analysis of masonry gravity structures where the block stereotomy is known; a structure is safe if a thrust layout fully contained within the structure can be found. One method of generating thrust layouts is by starting with a hanging chain model, and then using the two observations noted to identify locations where either an alternative load path is required or tension needs to be introduced; i.e., add struts and add/remove extra ties from the hanging chain model. However, this would be impractical where the geometry is complex and a large number of constituent blocks are involved. For such cases, user-friendly computer tools will be required to automatically generate thrust layouts, as has been the case for the generation of funicular thrust lines, e.g., [64, 86, 148].

Masonry gravity structures are generally statically indeterminate and thus have multiple possible 'safe' load paths. Knowing one of these would be satisfactory for an engineer to assess an existing structure (or to verify the design of a new one). In other words, although

only one load path may exist in reality, knowing that particular load path is not necessary.

The thrust layout optimization (TLO) procedure presented recently by Nanayakkara et al. [149] automates the generation of thrust layouts. The presented numerical method solves an underlying linear programming (LP) problem, taking advantage of efficient and widely available LP solvers. Furthermore, the TLO procedure also takes account of the limited frictional capacity of block interfaces, albeit implicitly assuming associative friction. Thus the concerns of Bagi [143] are not addressed here, though this could be remedied by adopting an iterative solution scheme, e.g., the approach proposed in [150].

While noting that funicular thrust lines implicitly assume vertical tension-weak planes, Heyman suggests that a funicular thrust line would be valid for a monolithic continuum [57]. However, testing on monolithic arches made of rammed earth suggests that the failure planes of the arch are unlikely to be vertical [151, 152]. This suggests that a methodology which automatically identifies critical failure planes (e.g., [153, 154]) would be more appropriate for the analysis of form-resistant continua (e.g., arches formed using rammed earth construction).

Thrust networks are the equivalent three-dimensional extension of funicular thrust lines, and similar shortcomings exist there too. Fantin and Ciblac [155] extend thrust networks with additional 'partial branches' to account for solutions where the forces on a block do not converge to a point, whereas thrust networks restrict the domain of acceptable solutions to where all forces on a block coincide at a point. This, however, does not appear in the two-dimensional problem as the blocks are in equilibrium under only three forces and therefore must meet at a point to satisfy equilibrium. Furthermore, Barsi et al. [79] map the funicular thrust lines to the classic membrane solution (in 3D) and the line of resistance to thrust surfaces (in 3D).

4.7 Conclusions

Heyman's 'safe theorem' is widely used in the assessment of masonry gravity structures. In developing his theorem, Heyman used a funicular thrust line to represent the equilibrium of a masonry gravity structure. However, as noted in this contribution, there are limitations associated with using a funicular thrust line to represent the state of equilibrium of a masonry gravity structure. These limitations arise from not taking account of block stereotomy, which can lead to either under- or over-estimation of the collapse load of a masonry gravity structure, contrary to the commonly held belief that the thrust line method will generally give safe solutions. Furthermore, the implicit reliance on tensile strength when working with funicular

thrust lines is not clear to users.

Here, the notion of a 'thrust layout' is proposed. Block stereotomy is explicitly taken into account in a thrust layout, with tensile forces allowed within constituent blocks, but not across the weak interfaces between blocks. Thrust layouts can be used in the application of Heyman's safe theorem to any structure, as this now appropriately represents the equilibrium of the structure. Furthermore, similar to funicular thrust lines, thrust layouts visualize a flow of forces within a structure. Thus, in contrast to the 'line of resistance' presented by Moseley, a thrust layout enables the structural engineer to clearly grasp how a masonry gravity structure safely carries applied loads.

Authors' Contributions

KIUN conceptualized the paper, carried out the investigation, and generated the visualizations in consultation with MG and AL. KIUN wrote the original draft, which was reviewed and edited by AL and MG.

Chapter 5

Thrust Layout Optimization (TLO)

Preface

Generation of thrust layouts presented in Chapter 4 can be automated so that practising engineers can readily use it for the analysis of masonry gravity structures, and other form-resistant structures. Using the mapping between the graphic statics used to generate the traditional funicular thrust lines and the ground structure layout optimization, a novel procedure termed thrust layout optimization (TLO) is presented.

The TLO procedure presented is further extended to include a post-processing geometry optimization rationalization process (GO), inspired by the same presented for trusses by He and Gilbert [113]. This post-processing procedure was used to improve the visual clarity of thrust layouts. Technical details of the procedure are provided in Annex B.

The content of this chapter was originally prepared for a journal paper: Nanayakkara, K.I.U., Liew, A., Gilbert, M. (2023), 'Application of thrust layout optimization to masonry structures', Proceedings of the Royal Society A 479 (2273), 20230053. The text presented in this chapter includes the following additions to the original text: (i) a note on the nature of the thrust lines generated, found on lines 11-13 on page 72, (ii) a note on the relative importance of internal and boundary node densities, on lines 9-14 on page 85, and (iii) a note on the effects of material strength limits on the presented results, on lines 5-11 on page 92.

Additional examples of the application of TLO are provided in Annex C, which is a paper presented at the Structural Analysis of Historical Constructions conference held in Kyoto in September 2023: Nanayakkara, I., Liew, A., Gilbert, M. (2024). 'Thrust Layout Optimization for the Analysis of Historic Masonry Structures'. In: Endo, Y., Hanazato, T. (eds) Structural Analysis of Historical Constructions. SAHC 2023. RILEM Bookseries, vol 46. Springer.

Abstract

A new automated analysis procedure designed to overcome limitations of the traditional thrust line analysis method for masonry gravity structures is presented. The procedure, termed thrust layout optimization (TLO), is capable of automatically identifying admissible thrust lines in masonry gravity structures comprising general arrangements of masonry blocks. The procedure employs a modified truss layout optimization with transmissible loads formulation, which means that an initial thrust line layout does not need to be specified in advance. Highly visual output is generated, allowing areas where tensile strength has been implicitly assumed to be clearly identified, which is beyond the scope of traditional thrust line analysis. Also, sliding failures can be modelled without difficulty. Finally, examples are used to demonstrate the efficacy of the TLO procedure; these show that thrust line bifurcations can be automatically identified in problems involving openings, and that there is no need to estimate the ineffective area in buttress wall problems, both issues for the traditional thrust line analysis method.

5.1 Introduction

Traditional load-bearing masonry structures have been used for millennia in construction, ranging in scale from individual dwelling houses to viaducts and cathedrals. Many of these structures have considerable historic value, and, to ensure they remain safe and fit for purpose, effective assessment methods are required [40, 89]. The current climate emergency is also leading to renewed interest in stone masonry as a low embodied carbon means of construction [156, 157] and this also makes it important that these structures are not needlessly demolished and replaced, at considerable cost to the environment.

To confirm the stability of masonry gravity structures, thrust line methods have been used since at least the time of Poleni [32]. As first pointed out by Hooke [39], 'as hangs the flexible line, so but inverted will stand the rigid arch'. This suggests that if a line of thrust can be found that lies entirely within the thickness of a masonry arch then the structure will be stable (neglecting the possibility for sliding failure or material crushing). This observation led to the development of the thrust line method, which has also been widely used in design, perhaps most famously by Gaudi when designing the Colònia Güell church near Barcelona [32]. In this case a geometrically complex physical cable-net model was constructed to ensure the network of supports, ribs and vaults forming the building were appropriately proportioned

to ensure stability.

More recently computer based methods have been used to assess the stability of masonry constructions. Although finite element analysis methods have proved popular in a wide range of engineering disciplines, traditional linear elastic finite element analysis is of limited use in the case of traditional masonry gravity structures, principally due to the typically minimal tensile stresses that can safely be sustained by masonry materials. Conversely, non-linear finite element methods, although powerful, are generally too computationally expensive and demanding of operator expertise for routine use. Similarly, although discrete element [158] methods, including non-smooth contact dynamics (NSCD) [49], can be applied to masonry problems, the iterative solution procedure and requirement for the use of small timesteps makes them comparatively computationally expensive when a static analysis is involved.

Thus limit analysis approaches have proved popular, principally due to their ability to rapidly and directly analyse the collapse limit state. Building on the work of Kooharian [45] and Heyman [35], Livesley [82] proposed a rigid block limit analysis method, later extended by workers such as Ferris and Tin-Loi [159], Orduna and Lourenco [160] , Gilbert at al. [150] and Nodargi et al.[161] to treat problems involving non-associative sliding friction between blocks. Although usually used to identify instantaneous collapse mechanisms, rigid block analysis problems involving gross displacements can also be handled (e.g. [162, 163]).

However, rigid block methods require a masonry construction to be split either into constituent units, of which there are usually many, or into macro-blocks (e.g. [164]) to approximately represent these. In the latter case, since failure planes must coincide with the interfaces between blocks, there is a danger of over-estimating the stability of a given masonry construction when a number of physical units are represented by a single macro block. Also, particularly when treating complex geometries, it is not straightforward to infer a continuous line of thrust from the output—e.g. in the recent contribution by Iannuzzo et al. [163] the lines are discontinuous.

As an alternative to explicitly discretizing a masonry structure into constituent blocks, in recent years there has been a resurgence in interest in thrust line methods, now taking advantage of various computer based implementations. Notably, building on work by O'Dwyer [53], Block and Ochsendorf [165] developed the thrust network analysis (TNA) procedure to provide a rapid means of analysing and designing three-dimensional vaulted masonry structures. Using TNA the geometry of a predefined network of thrust lines is adjusted until a stable solution is found, in which the thrust lines lie entirely within the masonry. TNA can be used to evaluate the safety of masonry structures by computing a geometric safety fac-

tor, or, by considering limiting horizontal thrusts at the supports, a 'stability domain' that describes admissible stress states [166]. However, the dependence of the results obtained on the topology of the initially defined thrust network remains an issue.

However, the thrust line method, whether undertaken by hand or via computer, has a number of inherent limitations. For example, to enable the self-weight of masonry lying below a thrust-line to be mobilized (i.e. be effectively 'lifted up') it is implicitly assumed that the masonry possesses a degree of tensile resistance, but this is not necessarily transparent to the user. Consequently, to avoid non-conservative outcomes, an inclined crack may need to be introduced when modelling masonry buttresses [54, 55, 56], and results are also sensitive to the way in which the masonry is discretized into blocks [57], something that is not always obvious to users. Furthermore, the usual assumption that the masonry possesses unlimited friction capacity can lead to non-conservative predictions of stability; e.g. even though a line of thrust can be identified that fits entirely within the masonry, sliding failure at the head of a flying buttress may lead to premature failure [46, 47]. Premature, friction-induced, failure may also arise in multi-ring arches [167]. Finally, when complex geometries are involved (e.g. consider a gothic cathedral) it is often necessary to analyse parts of the structure separately and to then combine these to check overall stability, a somewhat cumbersome process [55].

In this paper, a new computational means of identifying admissible thrust lines in masonry gravity structures is proposed to overcome the aforementioned issues. The proposed procedure takes advantage of powerful layout (or 'topology') optimization techniques that have already been successfully used to automate the so-called 'strut and tie' method of design for reinforced concrete structures, where the goal is to identify tensile and compressive force paths in deep beams and other elements, enabling efficient layouts of tensile reinforcement to be identified [168]. In a traditional unreinforced masonry structure the goal is somewhat different, with the priority being to identify compressive force paths, with self-weight effects handled appropriately. Topology optimization has been little used previously in the field of masonry structures, with a rare example being usage in [169] to identify regions of compression for use in subsequent nonlinear finite element pushover analyses of masonry walls. In the present contribution it will be shown that a formulation employing truss layout optimization [13, 108], used in tandem with transmissible loads [8, 120], can be built on to directly identify compressive force paths and to establish margins of safety. It will be shown that this requires the introduction of interfaces to represent weak masonry joints, thereby allowing both tensile and sliding failures to be modelled, as well as changes to the optimization objective function.

The present chapter is organized as follows. In Section 5.2 the development of the thrust

layout optimization formulation is outlined, with this then applied to a wide range of example problems in Section 5.3; in Section 5.4 conclusions are drawn.

5.2 Thrust layout optimization method

5.2.1 Standard ground structure layout optimization (LO) procedure

The standard 'ground structure' layout optimization method was originally developed to identify optimal (minimum volume) truss structures [13, 108, 109, 110, 111]. The process involves the steps of: (i) specifying a design domain and boundary conditions—i.e. loading and support conditions (Fig. 5.1a); (ii) positioning nodes across the design domain, then interlinking these with potential members to form a 'ground structure' (Fig. 5.1b); and (iii) using linear programming (LP) to find the optimal structure to carry the applied loads (Fig. 5.1c). (Note that the basic LO formulation may result in structures that are in unstable equilibrium with the applied loads, e.g. see the structure shown in Fig. 5.1c.)

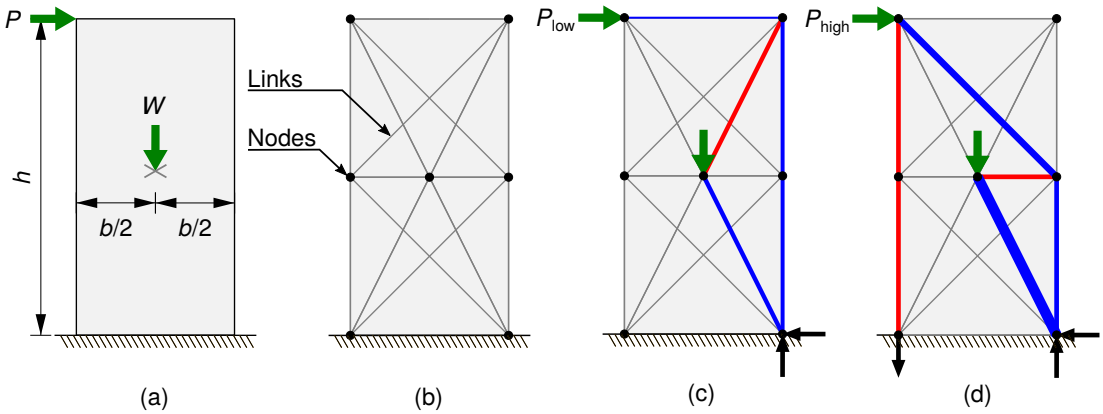

Figure 5.1: Standard 'ground structure' truss layout optimization (LO) procedure: (a) specified design domain, loading and support conditions; (b) nodes linked by potential members, creating a 'ground structure'; (c) optimal (minimum volume) layout identified by solving the underlying layout optimization problem; (d) optimal solution when a higher horizontal load is applied, involving the need for a support reaction that would be inadmissible if tension could not be transmitted to the support. Optimized truss layouts shown for values of P_{low}, P_{high}, W, h, b, σ_{t} and σ_{c} of 1, 2, 4, 2, 1, 1 and 100 respectively. Tension and compression forces shown in red and blue respectively, with line thickness proportional to force magnitude.

In terms of mathematics, for a problem involving a ground structure comprising n nodes and m potential members, the associated underlying LP problem formulation that involves finding the minimum volume truss structure (or 'truss-like' flow of forces) can be written as follows:

$$\min_{\mathbf{a},\mathbf{q}} \quad V = \mathbf{l}^{\mathrm{T}}\mathbf{a} \tag{5.1a}$$

$$\text{s.t.} \quad \mathbf{B}\mathbf{q} = \mathbf{f} \tag{5.1b}$$

$$-\sigma_{\mathrm{c}}\mathbf{a} \leq \mathbf{q} \leq \sigma_{\mathrm{t}}\mathbf{a} \tag{5.1c}$$

$$\mathbf{a} \geq \mathbf{0}, \tag{5.1d}$$

where V is the volume of the truss structure; $\mathbf{l} = [l_1, l_2, ..., l_m]^{\mathrm{T}}$ is a vector of ground structure member lengths and $\mathbf{a} = [a_1, a_2, ..., a_m]^{\mathrm{T}}$ is a vector of member cross-sectional areas. Force equilibrium is imposed at nodes by Eq. (5.1b), where $\mathbf{B}$ is a $2n \times m$ matrix containing direction cosines, $\mathbf{q} = [q_1, q_2, ..., q_m]^{\mathrm{T}}$ is a vector of internal member forces, and $\mathbf{f} = [f_{1x}, f_{1y}, f_{2x}, f_{2y}, ..., f_{nx}, f_{ny}]^{\mathrm{T}}$ is a vector of external applied loads. Yield constraints are enforced for each member by Eq. (5.1c), where σ_{t} and σ_{c} are limiting tensile and compressive stresses respectively. Truss members are constrained to have zero or positive cross-section area in Eq. (5.1d). Since the objective function Eq. (5.1a) and all constraints are linear with respect to the optimization variables—member areas $\mathbf{a}$ and internal forces $\mathbf{q}$—this is therefore a LP problem, that can be solved efficiently using modern LP solvers.

However, the problem setup shown in Fig. 5.1 can alternatively be interpreted as a means of determining an admissible flow of forces in a loaded masonry gravity structure, here comprising a single stone block of height h, breadth b, and weight W, resting on a rough horizontal base. In this case the design domain in Fig. 5.1a now represents the extent of the block, with the self-weight of the block applied as a downward load W at its centre of mass. A horizontal external load P is applied at the top left corner. The generated minimum volume truss structure shown in Fig. 5.1c now corresponds to an admissible pattern of internal forces, where in this case the horizontal load P_{low} is (just) capable of overturning the block. Application of a larger horizontal load, P_{high}, corresponds to a solution involving support reactions that cannot be sustained by the masonry, assuming that the interface at the base of the block possesses zero tensile strength (Fig. 5.1d). This basic conceptual model will be developed further in subsequent sections of the present paper.

5.2.2 Interface nodes representing weak masonry bonds

In the standard ground structure layout optimization solution shown in Fig. 5.1d, the node at the bottom left of the domain is supported and so can sustain an upward force; similarly the

node at the bottom right of the domain can sustain a downward force. However, if the desire is to represent the stability of a stone block, as considered at the end of the previous section, the upward (tensile) force present at the left support cannot be sustained, assuming that the interface between the base of this block and the support cannot resist tension. To appropriately represent the required behaviour at block-to-block and block-to-support interfaces, interface nodes can now be introduced.

Interface nodes share the same physical location at a weak interface, but with each being associated with one of the adjacent blocks. This gives rise to node pairs that are each connected via a normal force q_{n} and a shear force q_{s}, respectively aligned perpendicular and parallel to the interface. The weak interface is enforced by constraining the normal force to always be compressive, Eq. (5.2b), and the shear force to be limited by the normal force and friction coefficient between blocks at the interface, Eq. (5.2c).

To incorporate interfaces, mathematical formulation Eq. (5.1) is modified by replacing Eq. (5.1b) with the following equilibrium and yield constraints:

$$\mathbf{B}\mathbf{q} + \mathbf{B_n}\mathbf{q_n} + \mathbf{B_s}\mathbf{q_s} = \mathbf{f} \tag{5.2a}$$

$$\mathbf{q_n} \leq \mathbf{0} \tag{5.2b}$$

$$\mu\mathbf{q_n} \leq \mathbf{q_s} \leq -\mu\mathbf{q_n}, \tag{5.2c}$$

where in Eq. (5.2a) interface equilibrium matrices $\mathbf{B_n}$ and $\mathbf{B_s}$ are introduced, containing direction cosines on the basis of notional zero-length members oriented respectively perpendicular and parallel to the corresponding interface. Both matrices are of size $2n \times p$, where p is the number of interface node pairs. Also $\mathbf{q_n} = [q_{n,1}, q_{n,2}, ..., q_{n,p}]^{\mathrm{T}}$ is the interface normal force vector and $\mathbf{q_s} = [q_{s,1}, q_{s,2}, ..., q_{s,p}]^{\mathrm{T}}$ is the interface shear force vector. Finally, μ is the static friction coefficient for block-to-block and block-to-support interfaces.

5.2.3 Transmissible self-weight loads

Returning to the example shown in Fig. 5.1, when this was interpreted as a single block gravity structure analysis problem, the self-weight of the block was assumed to be applied at the centre of mass, leading to somewhat convoluted patterns of internal forces being identified. However, when constructing a funicular polygon using the traditional thrust line method, self-weight loads are allowed to move along their lines of action, permitting identification of simpler, compression-only, patterns of internal forces. This is something that can be reproduced in layout optimization by the use of 'transmissible' loads [8, 119, 120]. These are

loads that are shared across multiple nodes lying along a given vertical line of action when self-weight loads are involved.

To illustrate the concept, in Fig. 5.2a, the self-weight in the single stone block example is now modelled using two vertical strips of material. The self-weight of each strip can be considered as a transmissible load, with this shared between nodes lying along its line of action (Fig. 5.2a and b), as opposed to being fixed at its centre of mass (as in Fig. 5.1). As the number of strips (or transmissible load lines) and the number of nodes on a strip are increased, it is evident that the solution will tend towards the form of a traditional thrust line solution—see Fig. 5.2c, where here 25 transmissible load lines have been employed, with σ_{t} and σ_{c} set respectively to 1 and 100 to identify a thrust layout where compressive forces are dominant. Note that, unlike a traditional thrust line, here the thickness of the line corresponds to the magnitude of force. Also note that here it is necessary to increase the number of vertical strips to obtain a more faithful representation of self-weight effects.

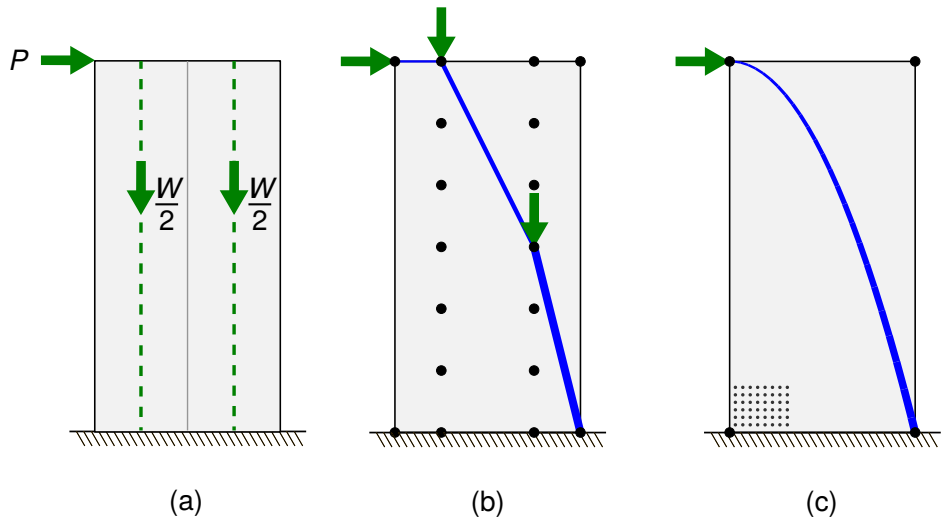

Figure 5.2: Including self-weight via transmissible loads: (a) discretization of the self-weight of a notional masonry block via two vertical strips; (b) positions of nodes along transmissible load lines and the resulting optimal force flow; (c) optimal force flow obtained using a finer resolution—with block self-weight now discretized via 25 transmissible load lines and using a post-processing geometry optimization rationalization step to improve clarity (after [113]).

In comparison to constraint Eq. (5.1b), which was used when generating Fig. 5.1, introduction of transmissible self-weight loads w requires these to be separated from externally applied loads f in the equilibrium equation—see Eq. (5.3a) below. Also, the self-weight loading applied to a given node (denoted w) now needs to be represented by an optimization variable, with the total self-weight load associated with each transmissible load group ($\bar{w}$) fixed for a given discretization by constraint Eq. (5.3b). Finally, constraint Eq. (5.3c) is also needed in order to avoid spurious solutions from being identified (see [120] for an explanation of why

this is necessary):

$$\mathbf{Bq} - \mathbf{w} = \mathbf{f} \tag{5.3a}$$

$$\mathbf{Hw} = \bar{\mathbf{w}} \tag{5.3b}$$

$$\mathbf{w} \geq \mathbf{0}, \tag{5.3c}$$

where, $\mathbf{w} = [0, w_1, 0, w_2, ..., 0, w_n]^{\mathrm{T}}$ is the nodal self-weight load vector. Note that as self-weight loads are applied in the vertical direction, only vertical equilibrium constraints are affected. Also $\bar{\mathbf{w}} = [\bar{w_1}, \bar{w_2}, ..., \bar{w_g}]^{\mathrm{T}}$ is the load group vector, where g is the number of transmissible self-weight load groups in the problem and $\bar{w_i}$ is the total load applied in transmissible load group i. Binary matrix $\mathbf{H}$ specifies which nodal load components in $\mathbf{w}$ belong to which load group in $\bar{\mathbf{w}}$, where $\mathbf{H}$ is of size $g \times 2n$ and is given by:

$$\mathbf{H}_{ij} = \begin{cases} 1 & \text{if load component } j \text{ exists in load group } i \\ 0 & \text{otherwise.} \end{cases} . \tag{5.4}$$

5.2.4 Proposed thrust layout optimization (TLO) procedure

The developments described in the preceding sections provide the basic foundations for a new analysis method for masonry gravity structures, henceforth termed thrust layout optimization (TLO). The method builds on the standard ground structure truss layout optimization method by (i) introducing interface nodes to represent weak interfaces; and (ii) representing self-weight loads as transmissible loads. However, several further developments are required to realise the TLO procedure; these include changes to the optimization objective function, and are described in this section.

As with the standard truss layout optimization procedure, TLO first requires that the extent of the problem domain and the nature of loading and boundary conditions are prescribed (Fig. 5.3a). However, in this case the problem domain is bounded by the outline of the masonry gravity structure, and the presence of weak interfaces between blocks need to be identified. Nodes are generated in both the interior and at boundaries of blocks, while interfaces are populated with interface nodes. Links are created between all nodes in the same block (Fig. 5.3b). These links, representing potential internal force paths, are allowed to take any compression force, but the maximum tensile force is limited by a value $q^{\mathrm{t}}_{\max}$, to reflect the non-zero, albeit usually relatively low, tensile strength of masonry blocks. Self-weight loading is applied as transmissible loads, with the line of action constrained to lie within any given

block (Fig. 5.3c). This prevents the self-weight of a given block being 'lifted up' across a weak interface.

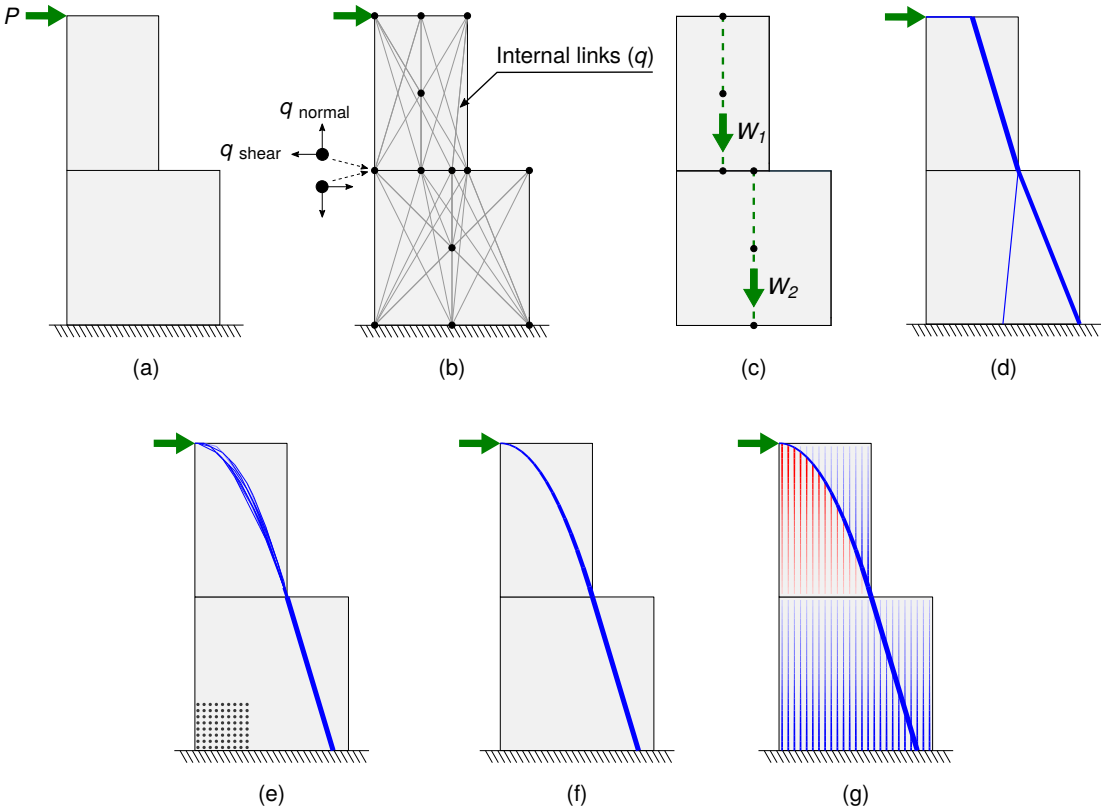

Figure 5.3: Application of proposed thrust layout optimization (TLO) procedure to a simple two block problem: (a) geometry of blocks and location of external load P and support; (b) problem discretized via nodes and links; (c) masonry self-weight represented by transmissible loads W_1 and W_2; (d) collapse load and thrust layout found by solving the associated layout optimization problem; (e) thrust layout obtained when using a finer resolution nodal grid (as indicated); (f) thrust layout obtained after also performing a post-processing geometry optimization rationalization step; and (g) layout with transmissible self-weight vectors also plotted—compression and tensile transmissible self-weight vectors are shown in blue and red, respectively, with line thicknesses representing the magnitude of the forces.

When assessing the stability of a masonry gravity structure, a common goal is to seek the magnitude of applied load that can be applied before collapse occurs. To achieve this, rather than seeking the minimum volume truss associated with Eq. (5.1), the objective of the optimization needs to be changed to one of finding the collapse load factor (the multiplier on a given load required to trigger failure). This can be achieved by maximizing the load factor subject to equilibrium and yield constraints, using the defined ground structure and set of transmissible self-weight loads created—resulting in the modified formulation given in

Eq. (5.5) below:

$$\max_{\mathbf{q},\mathbf{q_n},\mathbf{q_s},\mathbf{w},\lambda} \quad \lambda \tag{5.5a}$$

$$\text{s.t.} \quad \mathbf{Bq} + \mathbf{B_n q_n} + \mathbf{B_s q_s} - \mathbf{w} - \lambda \mathbf{f} = \mathbf{0} \tag{5.5b}$$

$$\mathbf{Hw} = \bar{\mathbf{w}} \tag{5.5c}$$

$$\mathbf{q} \leq q^{\mathrm{t}}_{\max} \mathbf{1} \tag{5.5d}$$

$$\mathbf{q_n} \leq \mathbf{0} \tag{5.5e}$$

$$\mu \mathbf{q_n} \leq \mathbf{q_s} \leq -\mu \mathbf{q_n} \tag{5.5f}$$

$$\mathbf{w} \geq \mathbf{0} \tag{5.5g}$$

$$\lambda \geq 0, \tag{5.5h}$$

where λ is the load factor on the externally applied loads, and other terms are as defined previously. Thus the factor on externally applied loads is maximized under the constraints of (i) static equilibrium at nodes—Eq. (5.5b) and Eq. (5.5c); (ii) a maximum tensile force allowed within blocks Eq. (5.5d), with no tensile forces allowed across weak interfaces Eq. (5.5e); and (iii) interface friction force limited by friction coefficient, Eq. (5.5f). The linear nature of the objective function and constraints means that the problem can be solved using LP.

Finally, although solving Eq. (5.5) will determine the collapse load factor, the associated solution may include spurious self-equilibriating force networks, since these are not explicitly penalized in Eq. (5.5). This will in turn lead to thrust layouts that are not visually clear. To address this, a volume minimization post-processing step can be performed, with the computed load factor constrained to lie at the value found in the load evaluation step. This is carried out using the basic layout optimization formulation presented in Eq. (5.1), with interface nodes (Eq. (5.2)) and transmissible self-weights (Eq. (5.3)) now also included in the model. Outcomes from the process are shown in (Fig. 5.3d-e). A further post processing geometry optimization rationalization step (after [113]) can help further improve the visual clarity of the force flow; see Fig. 5.3f. Furthermore, in addition to the thrust lines obtained via the TLO process (shown in Fig. 5.3d-f), the vertical self-weight vectors hidden by the assumed transmissibility of self-weight loads can also be optionally plotted to provide additional visual information; see Fig. 5.3g. These transmissible self-weight vectors are force vectors indicating the force in the notional link required to move the self-weight either up or down from its original position to where it is transmitted to, the former requiring tensile links and the latter compressive links.

5.2.5 Software implementation

To enable 2D mesh geometries created in a CAD environment to be efficiently converted into an appropriate data structure for use with the developed TLO procedure, a suitable digital workflow was developed. Thus the software Rhinoceros [170] was used to prepare the presented examples, with an export process developed to transfer vertex and face data. The TLO procedure itself was implemented as a computational algorithm using the Python programming language [171], making use of the numerical package NumPy [172], geometry package Shapely [173] and linear programming solver MOSEK [174].

When working with problems involving large numbers of discrete blocks, it is important to employ a robust and efficient data structure for: (i) tracking connectivity between vertices, edges, faces and links; (ii) storing information on loads, degrees-of-freedom and internal forces as properties; (iii) performing efficient algorithmic operations and manipulations on the underlying geometry; and (iv) saving, loading and editing instances of the data structure through the optimization pipeline. Thus for data handling, a hybrid data structure was created to facilitate storing of information and performing operations on geometric data through vertices, edges, faces and links, where the links are the straight lines connecting vertices. Thus the general purpose open-source half-edge data structure OpenMesh [175] was used for the management of vertices, edges and faces, and NetworkX [176] was used for handling link connectivity.

5.2.6 Verification of method

To verify the proposed method, two simple example problems are now considered: (i) a simple two block problem (Fig. 5.4); (ii) a semicircular arch problem (Fig. 5.5).

Considering first the two block problem shown in Fig. 5.4, this comprises a solid block (breadth 3 units; height 5 units; width 2 units) stacked on a larger solid block (breadth 5 units; height 5 units; width 2 units). The blocks are composed of masonry with a unit weight of 2 units. The stack of blocks is subjected to a horizontal point load at the top left corner as indicated. Two cases are considered: (i) assuming the interfaces possess infinite friction capacity (Fig. 5.4a-b); and (ii) that the friction coefficient at the interfaces is 0.25 (Fig. 5.4c-d). In the former case the failure load is found to be 18, with the top block overturning (Fig. 5.4a-b), while in the latter case the failure load is found to be 15, with the top block sliding (Fig. 5.4c-d).

The correctness of these values can be verified via simple analytical calculations or rigid

block analysis software, confirming the ability of TLO to correctly determine the failure load for problems with or without frictional failure. Here the LimitState:GEO software package [177], which implements the discontinuity layout optimization method [178, 179], was used to perform the rigid block analysis calculations. For the overturning block case, the TLO thrust layout shows forces passing through the bottom right corner of the top block (Fig. 5.4a), coinciding with where the rigid block model indicates overturning failure of this block occurs (Fig. 5.4b). In contrast, in the sliding block case (Fig. 5.4c), the thrust line bifurcates and spreads over a region at the block interface.

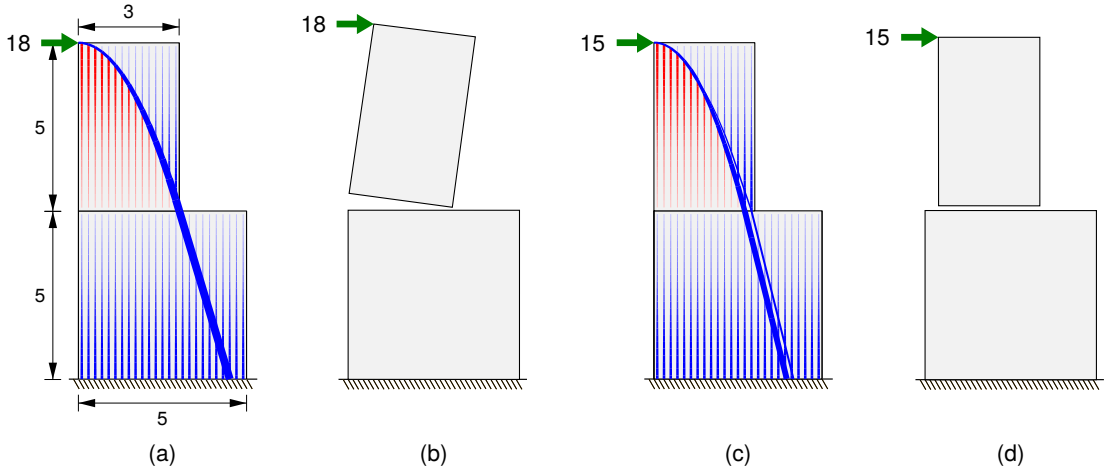

Figure 5.4: Two block problem - influence of friction: (a) TLO solution assuming infinite friction; (b) corresponding rigid block mechanism; (c) TLO solution assuming coefficient of friction of 0.25; (d) corresponding rigid block mechanism (blocks have width of 2 units and unit weight of 2 units; thrust layouts obtained using internal and boundary node spacings of 0.2 and 0.1 units respectively; layouts then rationalized via geometry optimization post-processing step, with transmissible load vectors also plotted; rigid block solutions obtained independently using LimitState:GEO software [177]).

Considering next a semicircular arch with a centreline radius (R) of 10 m , unit width and unit density. In this case the minimum arch thickness t required to carry its self-weight can be determined for any given friction coefficient by trying a range of different arch thicknesses; results are shown in Fig. 5.5. For friction coefficients higher than 0.395, a minimum arch thickness ratio (t/R) of 10.68 % was obtained. This matches well with the minimum arch thickness ratio of 10.75 % obtained by Ocshendorf [56], assuming a continuum arch (the difference is because a continuum arch can fail at any radial plane whereas weak planes were here positioned between the 27 voussoirs assumed to form the arch). At friction coefficients smaller than 0.31 the minimum thickness required was found to rise rapidly as the arches undergo sliding failure. In contrast, at friction coefficients greater than 0.395 failure is due to hinging, with a mixed mode of sliding and hinging failure in the intermediate range. Across the

full range of friction coefficients considered, the results obtained using TLO were found to coincide perfectly with the numerical results obtained previously by Gilbert et al. [150].

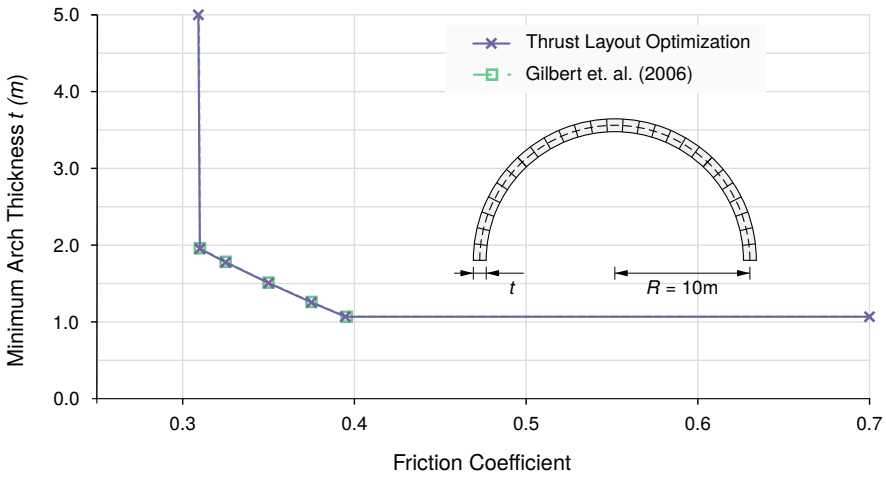

Figure 5.5: Semicircular arch problem: minimum arch thickness required for stability under self-weight for various coefficient of friction values, showing agreement between TLO results and those of Gilbert et al.[150] (arch contains 27 voussoirs).

5.2.7 Commentary

In his seminal work Heyman [39] presented the funicular polygon (i.e. a graphic static construction of a hanging chain) as a line of thrust that could be used to check the safety of a masonry gravity structure; this has subsequently been widely adopted by practicing engineers. However, more recently, it has been pointed out that the funicular polygon may not always represent a valid thrust line [57, 58, 139]. The issue stems from the fact that the arrangement of the interfaces, or joints, between blocks (termed the 'stereotomy') is not explicitly considered in the construction of a funicular polygon. Instead, as demonstrated in [57, 146, 147], a given arch or other structure is implicitly taken to be made up of a series of vertical strips of material. This is likely to lead to incorrect predicted collapse loads, as the importance of stereotomy on the latter has previously been demonstrated [58, 154]. Furthermore, this may lead to situations where a self-weight load is inadvertently assumed to be transferred upwards across a weak interface, leading to an overestimated predicted load carrying capacity. In contrast, in the TLO procedure weak interfaces are explicitly considered, preventing this from occurring. Thus a thrust layout obtained by TLO can be viewed as a corrected thrust line solution, with the corresponding computed collapse load converging towards the exact limit load as the numerical discretization is refined. Also, in a TLO solution, the flow of the principal forces remains clearly evident, with, in the interests of transparency, transmissible

self-weight loads also plottable if required.

Note that in the literature various means of constructing a thrust line are described, leading to differences in the form of the thrust line itself; see [58, 79]. Here, a funicular polygon is used for this purpose (after Heyman [35]). Of the different forms of thrust line, the funicular polygon compares well with the thrust layouts described herein, with both providing a clear means of visualizing force-flows.

5.3 Examples

A selection of illustrative examples and applications are presented in this section to demonstrate the efficacy of the proposed TLO method. Results are compared with those from traditional thrust line and rigid block analysis methods. All computations were performed on a PC employing an Intel(R) Core(TM) i7-8700 processor running at 3.20 GHz under Microsoft Windows 10. A Python implementation of the TLO method has been made available to accompany the paper, along with detailed nodal coordinate and connectivity information for all the example problems described (see Data Accessibility statement). The nodal spacings used to generate the thrust layouts presented were selected primarily to ensure visual clarity, given that the computed TLO collapse loads can be observed to be comparatively insensitive to the nodal spacing used, providing a reasonable number of nodes are used—see results from the parametric study conducted in the case of Example (5.3.1), which involves a flat arch on stone columns. For the volume minimization post-processing step of the TLO runs a material strength ratio ($\sigma_t : \sigma_c$) of 1:100 was set to penalize the presence of tensile forces. For the range of material strength ratios typically observed for stone masonry, this has been observed to have little effect on the visualization, i.e., where the tension is present remains unaffected while the amount of tension present may slightly vary.

In the case of some examples, traditional thrust line solutions are also presented for comparative purposes. These are funicular polygons drawn at the point of incipient collapse, identified using custom written code written in Matlab R2019b, taking advantage of its optimization toolbox. Rigid block models were also created for some examples; in this case the analyses were performed using the commercially available LimitState:GEO software package [177].

In the case of both the traditional thrust line solutions and the TLO solutions, compressive and tensile forces are plotted respectively using blue and red lines. In the case of the traditional thrust line solutions, thrust lines are plotted with uniform thickness whilst in the case of

the TLO solutions the line thickness is varied to reflect the magnitude of the forces involved, scaled linearly from 0.05 at $q_{\min}$ to 1.0 at $q_{\max}$. In the interests of visual clarity, forces q lower than $q_{\min}$ are not plotted, with $q_{\min}$ set as 0.001 $q_{\max}$, and forces below 0.05 $q_{\max}$ plotted in a progressively lighter colour shade. Finally, in the case of some TLO plots, transmissible load vectors are also plotted; in this case the associated line thickness is scaled up by a factor of 5 relative to other force vectors to ensure these are visible. Finally, the post-processing geometry optimization rationalization step described in [113] is employed to improve visual clarity as required.

5.3.1 Illustrative examples

Capabilities of the proposed TLO method are first explored via three illustrative examples, consisting of: (i) stacked blocks with voids; (ii) a segmental arch with and without voids; and (iii) a flat arch on stone columns.

Stacked blocks with voids

This problem consists of two hollow blocks placed on top of each other, subjected to a horizontal force at the top left corner of the upper block, as shown in Fig. 5.6. The predicted collapse load and visual representation of internal forces obtained using TLO is compared with those obtainable using the traditional thrust line and rigid block methods.

Firstly, consider the traditional thrust line analysis solutions shown in Fig. 5.6a-b. These show thrust lines that pass through the internal void, with it not being clear whether these are acceptable—given that Heyman's safe theorem [35] requires thrust lines to 'lie wholly within the masonry'. In the first thrust line solution (Fig. 5.6a) the stereotomy of blocks is not considered, leading to an unrealistically high collapse load estimate of 27.6 units. This arises from 'lifting up' of the lower block across the weak interface between blocks. When this weak interface is explicitly modelled, e.g., by only considering equilibrium of the upper block, the traditional thrust line method then yields a more realistic collapse load (of 14.4 units, Fig. 5.6b). This can be shown to be the exact collapse load for this problem, and is also predicted by the TLO and rigid block method (Fig. 5.6c-d respectively).

Considering now the TLO solution (Fig. 5.6c), this explicitly respects block stereotomy (by including no-tension interfaces and allowing transmisibility of self-weight only within blocks) and also successfully identifies a force flow that remains entirely within the material volume, passing from the externally applied load through to the supports. The TLO solution also

correctly indicates that some intrinsic tensile strength of the masonry block material needs to be mobilized. In comparison, although the rigid block limit analysis solution shown in Fig. 5.6d depicts the critical collapse mechanism, no information about the internal distribution of forces within the structure is provided.

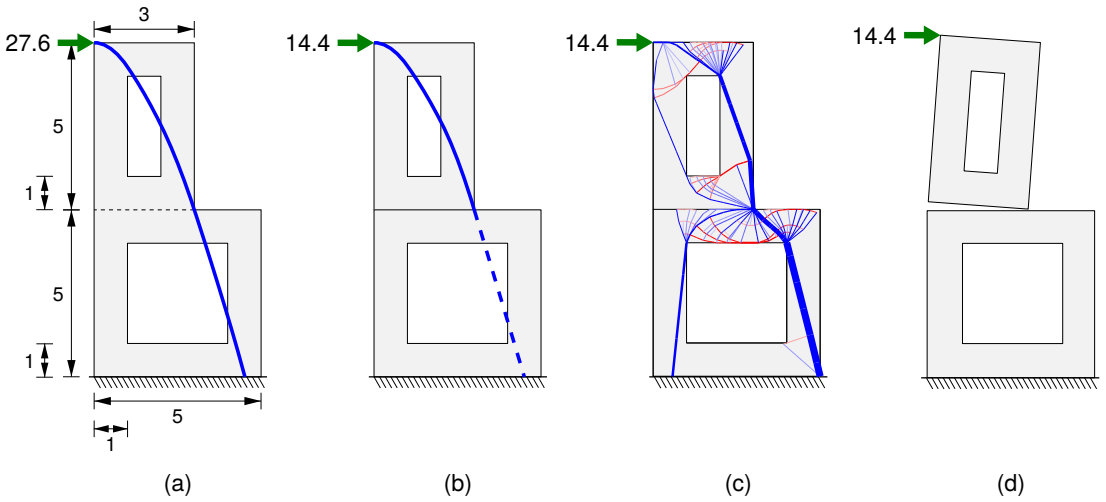

Figure 5.6: Stacked blocks with voids - solutions obtained via: (a) traditional thrust line method, assuming monolithic masonry; (b) traditional thrust line method, only considering upper block; (c) TLO, showing a force flow that is confined to areas where material is present; (d) rigid block analysis method, showing collapse mechanism only (blocks have width of 2 units and a unit weight of 2 units; thrust lines obtained using 0.2 unit wide vertical strips; thrust layouts obtained using internal and boundary node spacings of 0.2 units and $q^{\mathrm{t}}_{\max}$ = 0.005; thrust layout rationalized via geometry optimization post-processing step; infinite friction assumed at interfaces between blocks; note that although the thrust lines in (a) and (b) are qualitatively similar, they are not identical).

Segmental arch

The next example involves two segmental arches composed of a number of equally sized voussoirs, one solid and one including three internal holes positioned on the arch centreline; see Fig. 5.7. Both arches are subjected to an offcentre point load, as indicated. To ensure no sliding failures occur, a friction coefficient of 1 is assumed.

Firstly, the traditional thrust lines shown in Fig. 5.7a and b both lie entirely within the masonry, not passing through the holes in the case of the structure shown in Fig. 5.7b. However, these correspond to very conservative estimates of collapse load (P of 39.8 kN for the solid arch and 27.6 kN for the arch with holes). By recognising that the blocks do possess some tensile strength, the traditional no tension condition can instead be enforced only at interfaces between blocks, resulting in the thrust line solutions shown in Fig. 5.7c and d, which correspond to significantly higher collapse loads (P of 62.4 kN for the solid arch and 57.4 kN

for the arch with holes). However, the thrust lines no longer lie entirely within the masonry, rendering the status of these solutions potentially unclear.

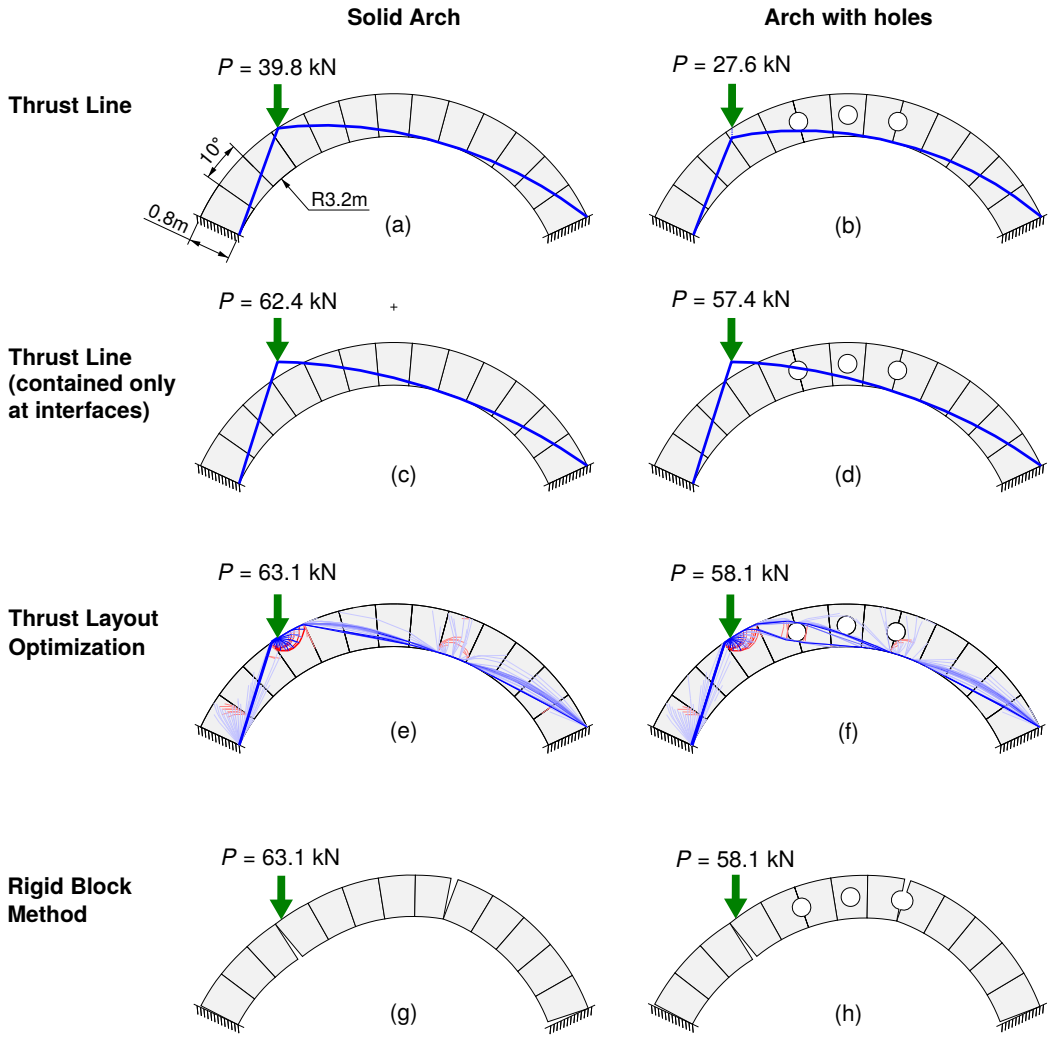

Figure 5.7: Segmental arch - solutions obtained via: (a-b) traditional thrust line method; (c-d) thrust line method with thrust constrained at block interfaces only; (e-f) TLO, showing force flows confined to areas where material is present; (g-h) rigid block method, showing collapse mechanisms only (arch span: 5.80 m, rise 1.85 m, width 0.1 m, unit weight: 25 kN/m^3; circular voids on arch centreline at locations indicated have diameter of 0.35 m; collapse load P in kN applied 0.72 m from left support; thrust lines obtained assuming self-weight lumped at block centroids; thrust layouts obtained using internal and boundary node spacings of 0.05 m and $q^{\mathrm{t}}_{\max}$ = 250 N; thrust layout tensile force line thickness scaled by a factor of 2 for emphasis).

Considering now the corresponding TLO solutions, shown in Fig. 5.7e and f, the predicted collapse loads (P of 63.1 kN for the solid arch and 58.1 kN for the arch with holes) are similar to those obtained via thrust line analysis with the no tension condition enforced only at block interfaces*, though force flows that remains entirely within the material volume are now clearly

*The slight difference between the collapse loads predicted via traditional thrust line analysis (see Fig. 5.7c and d) and TLO (see Fig. 5.7e and f) is due to the thrust line analysis not considering block stereotomy, instead assuming the arches to be formed using notional vertical strips [57]. This issue is further explored in (5.3.1), the flat arch on stone columns example.

identified. Specifically, areas of the blocks where tensile strength is required are now evident (e.g., where the traditional thrust lines lie outside the thickness of the arch), and the bifurcation of the thrust line around one of the internal voids (see Fig. 5.7f) now effectively verifies the reasonableness of allowing the traditional thrust line to pass through this (see Fig. 5.7d). Thus TLO provides a new, and potentially extremely valuable, perspective on how forces flow in such structures. Finally, although the collapse loads predicted via rigid block limit analysis are the same as the TLO method (compare Fig. 5.7e-f with Fig. 5.7g-h), no information about the internal distribution of forces within the structure is provided when using this method.

Flat arch on stone columns

The next example, involving a flat arch supported by two stone columns, demonstrates that the collapse load predicted using the thrust line method can be significantly in error, even when the thrust line is constrained to lie within the thickness of the masonry only at interfaces. The structure is shown in Fig. 5.8 and is made up of five equally sized blocks, plus associated springing blocks. To ensure no sliding failures occur, a friction coefficient of 1 is assumed.

Firstly, a traditional thrust line analysis solution, with the thrust line lying entirely within the thickness of the masonry, is shown in Fig. 5.8a. However, while this solution appears qualitatively reasonable, it is evident that the associated collapse load is low, at P = 10.1 kN. When the thrust line is constrained only to lie within the thickness of the masonry at block interfaces, a higher associated collapse load, of P = 16.2 kN, is obtained, as shown in Fig. 5.8c. However, this is still significantly lower than the predicted collapse load of P = 45.1 kN obtained when using TLO (see Fig. 5.8e), with the correctness of this solution verified using the rigid block method (see Fig. 5.8f). The discrepancy in computed collapse loads is a consequence of the thrust line solutions being represented by funicular polygons, derived by discretizing the structure using vertical strips of material [57], with here each strip having a width of 0.05 m. These solutions can be reproduced using the rigid block method by introducing vertical cracks at locations where the thrust line touches the edges of the masonry; thus the rigid block solution shown in Fig. 5.8b corresponds to the thrust line solution shown in Fig. 5.8a. Similarly, when the keystone crack is omitted, the rigid block solution shown in Fig. 5.8d is obtained, corresponding to the less constrained thrust line solution shown in Fig. 5.8c. (The collapse loads shown in Fig. 5.8c and d are not exactly the same—16.191 kN in (c) and 16.171 kN in (d), with the small difference being due to the two sides of the keystone block being slightly off from vertical.)

In contrast, when using TLO, weak interfaces are explicitly taken into account, with a lim-

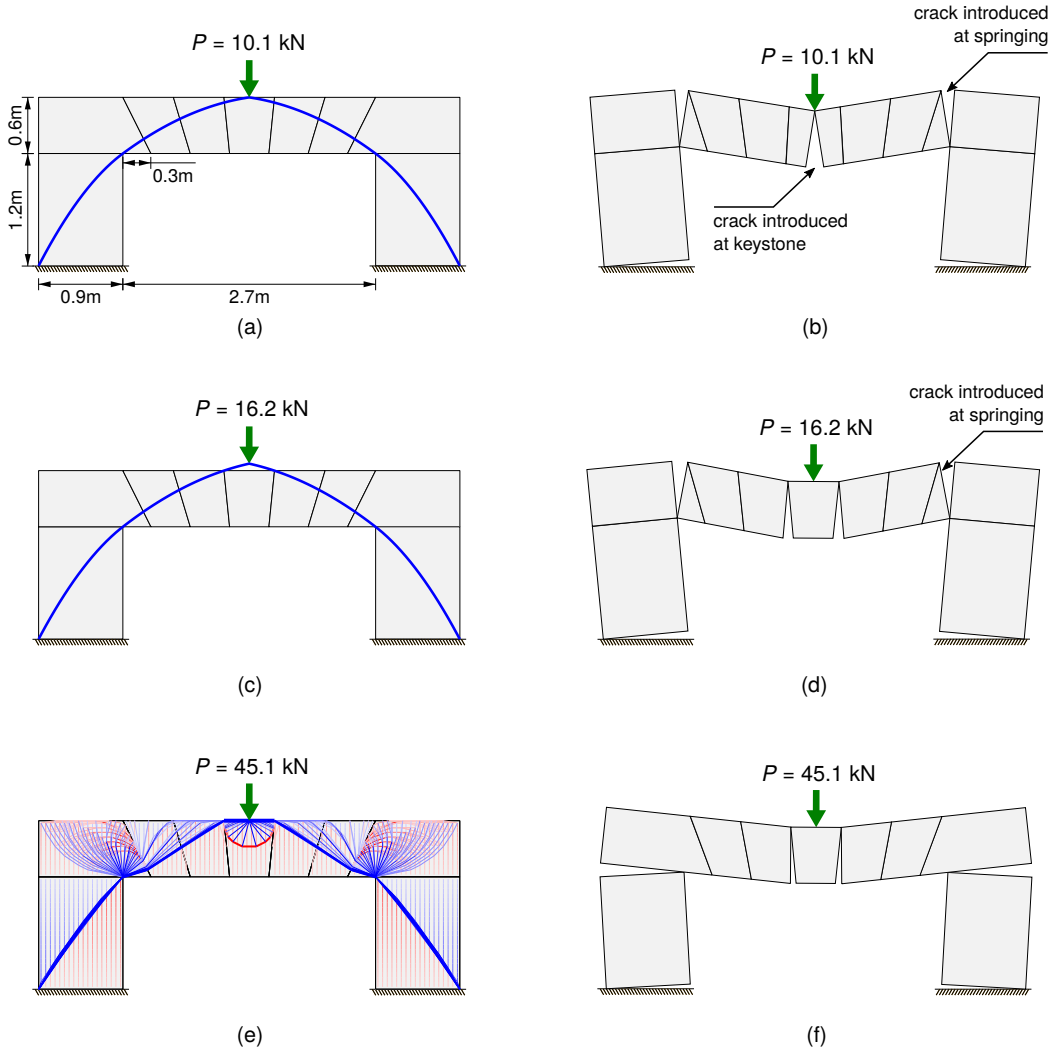

Figure 5.8: Flat arch on stone columns - solutions obtained via: (a) traditional thrust line method; (b) rigid block method, after three extra vertical failure planes added; (c) thrust line method with thrust constrained at block interfaces only; (d) rigid block method, after two extra vertical failure planes added; (e) TLO, showing force flows confined to areas where material is present (transmissible self-weight vectors also plotted); (f) rigid block method, with no extra failure planes added to provide agreement with TLO solution, since that takes actual block stereotomy into account (all five blocks in the arch have a top breadth of 0.54 m and a bottom breadth of 0.42 m; a width of 1 m and material unit weight of 25 $\mathrm{kN/m^3}$ are assumed; thrust lines obtained using vertical strips of 0.05 m width; thrust layouts obtained using internal and boundary node spacings of 0.05 m and 0.01 m respectively and $q^{\mathrm{t}}_{\mathrm{max}}$ = 250 N).

ited amount of tension inside blocks permitted as part of the formulation. While the resulting TLO solution (see Fig. 5.8e) includes thick blue lines reminiscent of a traditional thrust line, tensile forces are now also evident in the keystone and springing blocks, providing an indication as to how the self-weight of the latter are mobilized. In the keystone block, the thrust layout resembles the form of the optimal half-wheel truss structure, whereas in each springing

block the thrust layout resembles an optimal Michell cantilever truss structure [180]. In addition, transmissible self-weight vectors are also shown in Fig. 5.8e, making the transmissible load representation of the self-weight of the masonry clear.

It is also of interest to investigate the sensitivity of the TLO solutions for this example to both the selected nodal density and the maximum allowed tensile force, $q^{\mathrm{t}}_{\max}$. Thus Fig. 5.9 shows how the computed collapse load converges towards the exact value, of P = 45.1 kN, as the nodal density is increased for a range of values of $q^{\mathrm{t}}_{\max}$. It is evident that for higher $q^{\mathrm{t}}_{\max}$ values, convergence occurs at lower nodal densities, with the computed collapse load converging to the exact collapse load at a very low nodal density when $q^{\mathrm{t}}_{\max}$ = 1000 N. The increase in internal node density reduces the self-weight on an internal node (and within the transmissible load groups) and therefore reduces the demand for explicit tensile forces within blocks. Similarly, the increase in boundary node density allows more points for the compressive thrust line to pass across blocks, thereby reducing the need for force layouts involving tensile forces.

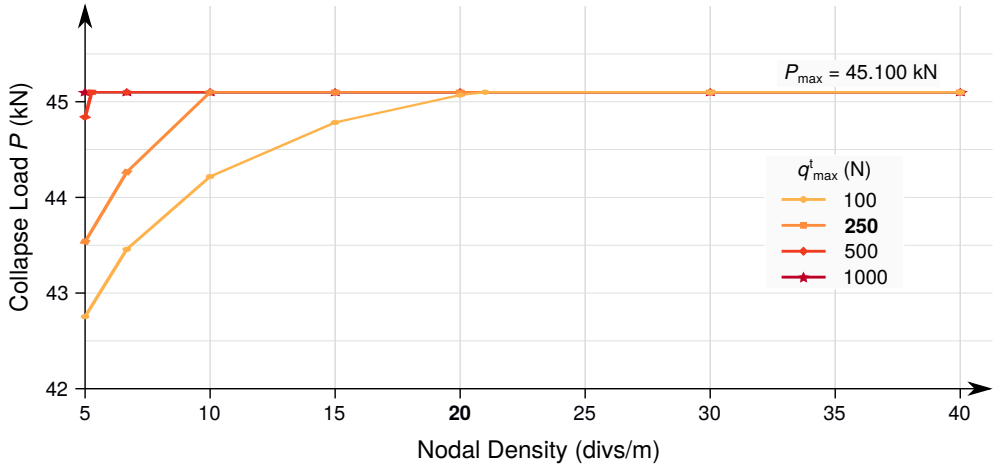

Figure 5.9: Flat arch on stone columns: computed collapse load vs nodal density for a range of maximum allowed tensile force values, $q^{\mathrm{t}}_{\max}$ (quoted nodal density is the reciprocal of the internal node spacing; boundary node spacing is 0.2 $\times$ internal node spacing; values in bold used to generate Fig. 5.8e).

As an alternative to considering the maximum tensile force, $q^{\mathrm{t}}_{\max}$, the thickness of material required to carry this can instead be considered, calculated assuming the masonry blocks possess finite but low tensile strength, here taken as 1 $\mathrm{N/mm^2}$. Thus Fig. 5.10 shows how the computed collapse load varies with required stressed thickness, for a range of different nodal densities. It is evident that a very low required stressed thickness of 0.25 mm (equivalent to $q^{\mathrm{t}}_{\max}$ = 250 N) is required in order for the solution to converge to the exact rigid block collapse load in this case. This stressed thickness is several orders of magnitude smaller than

the physical dimensions of the structure, and is well within the limits of what could safely be carried by most stone materials. Also, when even lower maximum stressed thickness values are used (e.g., 10^{-5} mm, equivalent to $q^{\mathrm{t}}_{\mathrm{max}}$ = 0.01 N) it is evident from Fig. 5.10 that the solutions lie in close proximity to the compression-only thrust line solution of Fig. 5.8a. (Note though that the compression-only TLO solution will at the limit lie below the corresponding thrust line method solution. This is because the transmissibility of the block self-weight is constrained at interfaces when using TLO, such that 'pulling up' the weight of lower blocks to the main part of the thrust line will require a finite, albeit small, tensile capacity.)

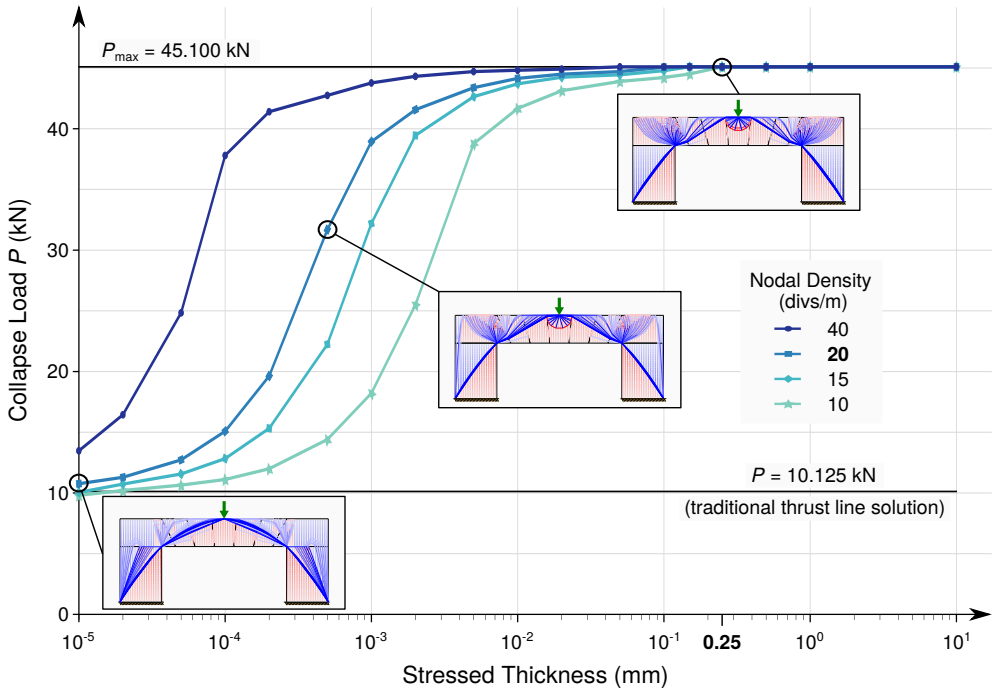

Figure 5.10: Flat arch on stone columns: computed collapse load vs stressed thickness, for a range of nodal densities (stressed thickness indicated based on an assumed tensile strength of 1N/mm^2; values in bold used to generate Fig. 5.8e).

Finally, the CPU time required to obtain TLO solutions for a range of nodal densities are summarised in Table 5.1, with the associated number of links and nodal interface pairs also shown. Note that internal nodes are positioned on a Cartesian grid while boundary nodes are uniformly spacing though with extra boundary nodes added to model load transmissibility. It is observed that although the exact collapse load can be obtained using a coarse nodal density, the use of finer nodal densities often allows the flow of forces to be more clearly visualized, albeit at higher computational cost.

Table 5.1: Flat arch on stone columns: CPU time for solutions at different nodal densities (nodal density with respect to internal nodes; boundary node spacing is $\times 0.2$ internal node spacing; $q^{\mathrm{t}}_{\max}$ of 250 N ; values in bold used in Fig. 5.8e).

Nodal density (divs/m)	Nodes	Links	Interface pairs	Collapse load (kN)	CPU time (s)†	
					Load eval.	Vol. min.
5	1,091	61,672	264	43.536	0.4	3.1
6.67	1,430	106,641	326	44.265	0.6	6.3
10	2,261	274,726	470	45.100	2.0	9.9
15	3,968	858,443	776	45.100	5.7	24.5
20	**5,628**	**1,769,939**	**990**	**45.100**	**15.2**	**48.6**
30	9,645	5,465,060	1,384	45.100	49.1	122.4
40	15,146	13,713,614	1,984	45.100	139.8	476.8

†: LP time as reported by the solver; load evaluation with full ground-structure; volume minimization with member adding starting with a minimal ground structure—see [112]

5.3.2 Applications

The TLO method is now applied to two rather more practical masonry structures, namely (i) a two-ring arch, and (ii) a masonry buttress wall.

Two-ring arch

This examples involves a two ring brickwork arch rib load tested to collapse in the laboratory by Melbourne and Gilbert [167]. The specific arch rib considered here incorporated a continuous sand joint between the two rings of brickwork to replicate a structure in the field with debonded arch rings; see Fig. 5.11. The material unit weight was reported to be 23.7 $\mathrm{kN/m^3}$ and the friction coefficient of the sand joint to be 0.53.

(a) (b) (c)

Figure 5.11: Two-ring arch - experimental testing: (a) initial setup; (b) hinges forming; (c) collapse of structure (arch has 3 m span, 0.75 m rise, 215 mm thickness and 215 mm width and is subject to point load 0.84 m from left abutment [167]).

Firstly, considering the traditional thrust line analysis method, to bound the solution from above the arch can be represented by a single 215 mm thick arch ring. Thus, assuming the thrust line is constrained only at weak radial interfaces, the predicted collapse load is 3.79 kN,

and the corresponding thrust line solution is shown in Fig. 5.12a. Alternatively, by constructing a separate thrust line for each arch-ring, the solution can be bounded from below, with the predicted collapse load now 1.15 kN (based on 0.55 kN being carried by the top ring and 0.60 kN carried by the bottom ring, and no interaction between rings), and the corresponding thrust line solution is shown in Fig. 5.12b.

In contrast, when using TLO the combined effects of both rings can be modelled directly. The TLO solution for this problem is shown in Fig. 5.12c, with the corresponding predicted collapse load being 1.48 kN, which closely matches the experimentally obtained value of 1.5 kN [167]. Whereas the thrust line method is able to successfully bracket the experimental value, the upper and lower bound thrust line solutions (3.79 kN and 1.15 kN) are too far apart to be practically useful.

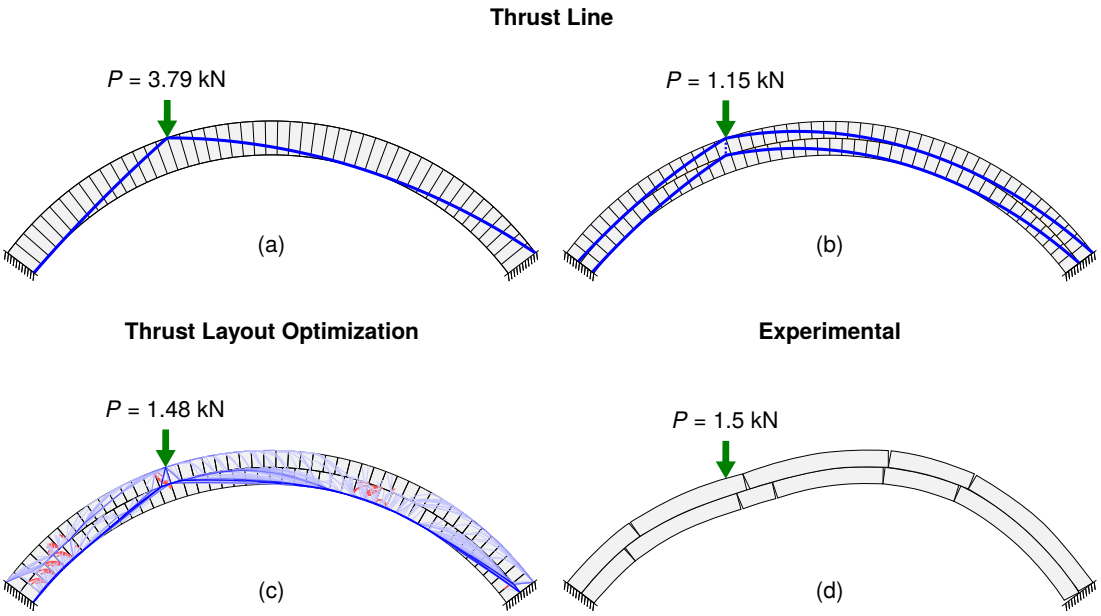

Figure 5.12: Two-ring arch - solutions obtained via: (a) traditional thrust-line method, assuming single monolithic arch ring; (b) traditional thrust-line method, determining separate thrust lines for each arch ring; (c) TLO, showing associated force flows; (d) experimental test, showing observed failure mechanism [167] (thrust lines obtained assuming self-weight lumped at block centroids; thrust layouts obtained using internal and boundary node spacings of 0.01 m and 0.005 m respectively and $q^{\mathrm{t}}_{\max}$ = 1 N; thrust layout tensile force line thickness scaled by a factor of 2 for emphasis).

The TLO solution shown in Fig. 5.12c also provides an indication as to how the load is being carried, here indicating that the loading is primarily carried by the bottom arch ring, with the main thrust hugging the intrados near the left hand support and in the three-quarter span region, also touching the extrados of the bottom arch ring directly below the loading point and at the right hand support. These appear broadly in line with the experimentally observed mechanism; see Fig. 5.12d.

Masonry buttress

When the traditional thrust line method is applied to structures such as leaning towers [54] and buttresses [52] an additional step is generally required in order to identify how much of the masonry will be effective in resisting the applied loading; e.g., see Fig. 5.13. A benefit of TLO is that this is not required when the structure is modelled using the appropriate discretization of blocks (size, aspect-ratio and stacking pattern) and friction capacity, since the effective (and ineffective) regions can in this case be identified automatically. Alternatively, were a buttress wall to be modelled as a continuum using TLO then plotting the transmissible self-weight load vectors would likely cause the engineer to quickly question this representation, as the self-weight of sections of the wall being 'lifted up' would be clearly visible. Furthermore, this suggests that only the region of masonry lying below the thrust line would need to be faithfully modelled - and hence also to a potential staged approach to modelling, in which the masonry is only modelled in detail in regions where an initial analysis has indicated that this is necessary.

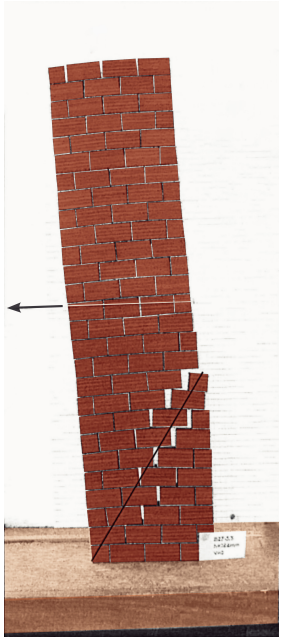

Figure 5.13: Masonry buttress - horizontal mid-height load test: blocks below diagonal black line deemed ineffective in resisting the load (test carried out by Ochsendorf [52], reproduced here as a colourized image).

Here the masonry buttress in Fig. 5.14a is considered; this has a base width of 0.54 m and a total weight of 19.05 kN, acting along a line of action at 0.30 m distance from the left-hand corner. An external load, inclined to the horizontal at an angle $\tan^{-1} 1.25$, is applied at a height of 1.68 m. This loading is representative of the load applied from a flying buttress.

The material unit weight is 18 $\mathrm{kN/m^3}$ and a unit width of buttress is assumed.

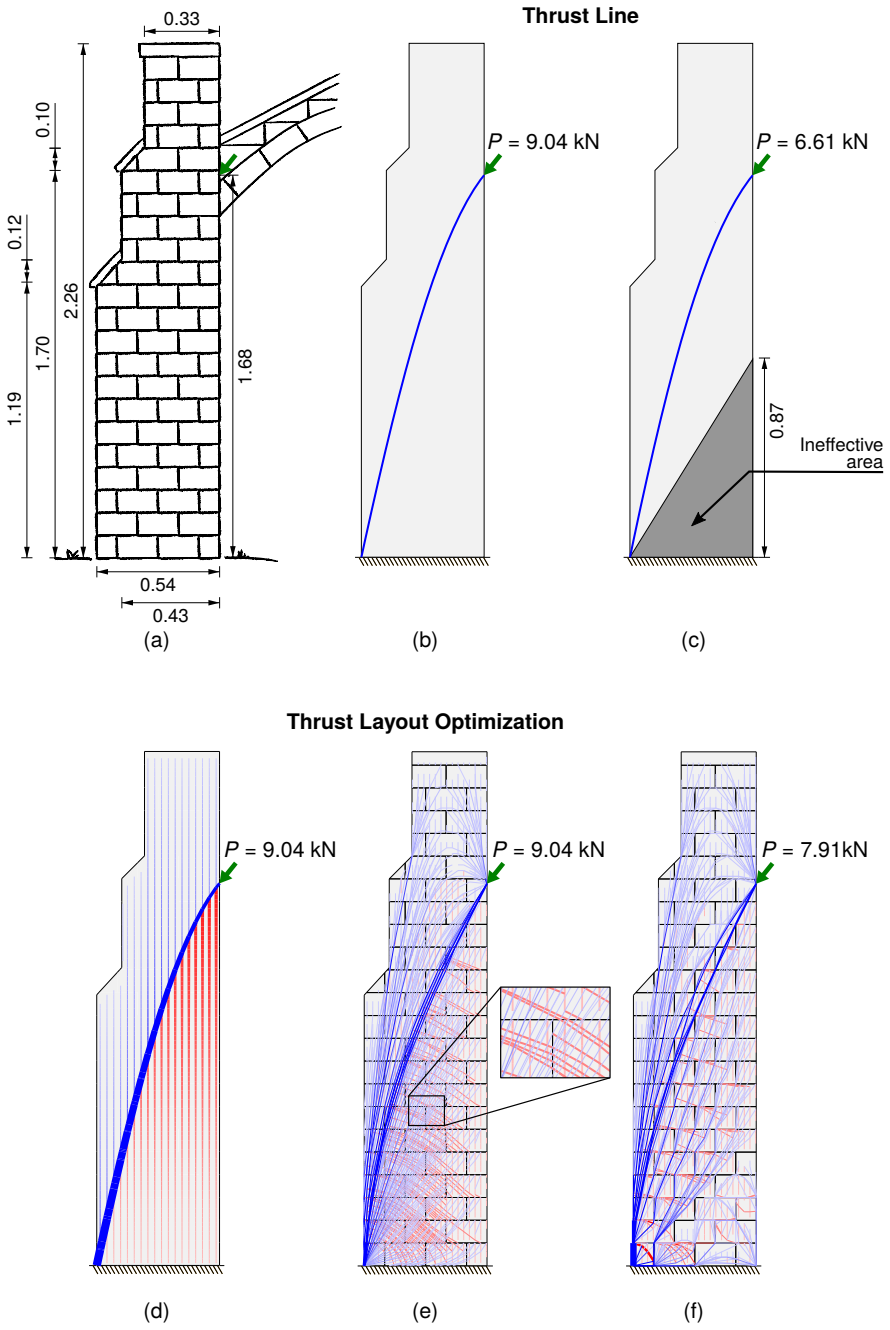

Figure 5.14: Masonry buttress: of geometry shown in (a) and assessed using (b) traditional thrust line method; (c) traditional thrust line method considering fracture of the buttress; TLO, considering the structure (d) as a continuum, rationalized via a geometry optimization post-processing step and with transmissible load vectors plotted; (e) as a block assembly with infinite friction resistance; (f) as a block assembly with friction limited by a friction coefficient of 0.7 (thrust lines obtained using vertical strips of 0.03 m width; thrust layouts in continuum obtained using internal and boundary node spacings of 0.03 m; thrust layouts in block assembly obtained using internal and boundary node spacings of 0.025 m and 0.01 m respectively; $q^{\mathrm{t}}_{\mathrm{max}}$ = 150 N; tensile force line thickness scaled by a factor of 2 for emphasis; links with forces lower than 0.0001 f_{max} not plotted; all dimensions in metres.)

Using the traditional thrust line method, a collapse load of 9.04 kN is predicted for the buttress (Fig. 5.14b), reducing to 6.61 kN if an ineffective area of the structure is assumed (using the method proposed by Ochsendorf [52]; see Fig. 5.14c). In this example, the fracture giving the ineffective area extends to 0.87 m above ground level.

Modelling the structure as a continuum in TLO reproduces the traditional thrust line method collapse load of 9.04 kN, but how the self-weight loading is carried is now clearer (Fig. 5.14d). Taking account of the masonry bonding pattern but assuming infinite joint friction capacity, the same collapse load of 9.04 kN is predicted via TLO. However, the self-weight load is now mobilzed via a different mechanism (see Fig. 5.14e). The figure inset gives a closer view of the flow of forces, which suggest that tensile forces are being transmitted across block interfaces, even though these have been prescribed to be non-tensile resistant; this arises from the frictional resistance of block interfaces. This is also influenced by the aspect ratio of the blocks and the adopted bonding (interlocking) pattern, a phenomenon previously investigated by Bacigalupo et al. [48], and more recently in [50, 181].

When the friction coefficient is set to a realistic value, in this case 0.7, the predicted collapse load reduces to 7.91 kN. The resulting thrust layout in Fig. 5.14f indicates that the self-weight of several blocks in the bottom-right corner are now not 'lifted up' to the main line of compression that runs from the applied load down to the supports. However this region is not fully inactive, and does contribute to resisting the applied load. This suggests that the method proposed by Ochsendorf provides a conservative estimate of the load capacity (amounting to 84 % of the TLO solution in this case). This is because it does not consider the tensile strength of the blocks or the bonding pattern, with the degree of under-estimation becoming more significant as blocks become larger.

5.3.3 Commentary

In several of the examples considered in this section it has been demonstrated that frictional (sliding) failures at interfaces between blocks can readily be modelled in the TLO procedure. However, it is worth noting that although the flow rule is not explicitly specified in the TLO formulation presented, the use of a maximization step in the procedure means that the friction is implicitly assumed to be associative (i.e. that any sliding movement will be accompanied by dilation (see e.g., [82]), with the angle of dilation equal to the angle of sliding friction, i.e., $\tan^{-1}\mu$). Although this behaviour is not physically realistic, and can lead to over-estimates of the safety of a given structure, the degree of any over-estimation is likely to be relatively

modest when the structure is discretized using a large number of blocks [153]. Also, this issue could potentially be addressed by replacing the single maximization step used in the presented TLO method with an iterative procedure, similar to that proposed for use with rigid block limit analysis by Gilbert et al. [150].

It is noted that for typical masonry gravity structures, of the sort considered in the examples presented herein, the material strength limits in both compression and tension are unlikely to be reached. Load carrying capacity estimates from TLO will only be strictly valid in such cases. In extreme cases where material strength is likely to be reached, safety needs to be verified by considering stress resultants (at nodal points) and checking them against material failure criteria. However, by visualising a possible flow of forces, TLO points towards how the structure can be strengthened, if needed.

Finally, although two-dimensional examples have been used to demonstrate the capability of the TLO procedure, this is in principle readily extendable to three-dimensional problems. The procedure can also potentially be extended to be applicable to retrofit design problems, allowing optimally placed strengthening measures to be identified in existing masonry gravity structures.

5.4 Conclusions

A new procedure has been developed that allows both the safety of masonry gravity structures to be evaluated and the transmission of internal forces to be clearly visualized. The procedure builds on a truss layout optimization with transmissible loads formulation, using this to model self-weight, and with interfaces included in the formulation to model weak masonry joints. The new procedure is herein termed thrust layout optimization (TLO):

- Although the traditional thrust line analysis method has proved useful for many years, it has some limitations. For example, block stereotomy is not considered, leading to self-weight being 'lifted up' across weak interfaces. Also, unlimited friction capacity is usually assumed, leading to sliding failures not being identified. The TLO procedure overcomes these limitations by considering block stereotomy, the low (but finite) tensile strength of blocks, and the limited friction capacity of interfaces, to furnish the exact collapse load for any given problem. Furthermore, TLO eliminates the need for case specific assumptions, which are very often required when using the traditional thrust line method (e.g., estimating the ineffective area in a buttress wall, or postulating potential load paths in a multi-ring arch).

- The thrust layouts identified via TLO provide a rich visual representation of force flows in masonry gravity structures. The procedure takes on board the limited tensile capacity of masonry blocks and makes no prior assumptions about the topology of thrust layouts. This enables visualizion of forces flowing around internal holes, with the force flows associated with blocks rocking about vertices often resembling classical Michell structures; more familiar funicular thrust line solutions can also be identified. It is also possible to plot transmissible self-weight vectors, eliminating ambiguity as to how self-weight forces are mobilized.
- The TLO procedure thus provides a fully automated means of generating a thrust layout and determining the associated collapse load for any given problem, comprising an arbitrary arrangement of masonry blocks. Computed collapse loads are found to be comparatively insensitive to the chosen numerical discretization (spacing of nodes) and the tensile force allowed within masonry blocks, with exact solutions obtainable at modest computational cost by taking advantage of efficient and widely available linear programming (LP) solvers.

Although a range of sophisticated non-linear analysis methods are now available for masonry structures, these are generally too demanding of computer time and operator expertise for routine use. This means that there remains a need for simple and intuitive analysis models, which provide clear and reliable results. Since the proposed TLO procedure successfully overcomes a number of the known weaknesses of the traditional thrust line analysis method, it has the potential to form an invaluable part of the tool-sets of engineers responsible for analysing masonry gravity structures.

Authors' Contributions

KIUN programmed the methods described, taking advantage of a software codebase developed by AL. KIUN performed the numerical runs, on the suggestion of, and in consultation with, MG and AL. All authors contributed to writing the initial draft of the paper and approved the final version.

Acknowledgements

The authors thank Dr Linwei He for his advice and for making available a Python script for rationalizing the generated layout optimization solutions via geometry optimization.

Data Accessibility

A Python script and accompanying data files have been made available to enable the solutions obtained herein via the TLO procedure to be replicated: https://dx.doi.org/10.15131/shef.data.21836541.

Chapter 6

Extended TLO with Auxiliary Strengthening Measures

Preface

TLO formulation is readily extended to determine optimal strengthening measures for form-resistant structures, including masonry gravity structures. This is a natural extension of the TLO procedure by extending the ground structure to include the domain of auxiliary strengthening measures. Furthermore, the formulation is readily extended to account for multiple load cases, including seismic loading as well.

This chapter is written in the format of a manuscript for potential publication in a journal.

Abstract

Recognising the need to extend the useful life of buildings and infrastructure of masonry construction and to preserve historic masonry structures that are part of our cultural heritage, tools capable of assessing their load-carrying capacity and determining the best placement of strengthening measures are needed. While current practice is to determine these based on engineering intuition, more robust physics-based methods are required given the complex geometries and loading conditions encountered and the need to minimize the usage of the additional material used in strengthening works. The thrust layout optimization (TLO) procedure developed to estimate the collapse load and to generate force flows (i.e., thrust layouts) within masonry gravity structures is here extended to consider auxiliary strengthening measures. The TLO procedure is reformulated to find the optimal placement of such strengthening measures, for a loading regime, and to visualize the corresponding thrust layout. Small increases in the collapse load relative to the unstrengthened construction can be achieved by introducing strengthening measures to locally inhibit the formation of masonry hinges. Less intuitively obvious strengthening measures emerge when higher load-carrying capacities are required. The rationale of these can be explained with the aid of visualization of the corresponding thrust layouts. Furthermore, the extended formulation containing an auxiliary strengthening domain can readily be used to design new masonry structures, incorporating an external metallic structure to carry additional tensile and compression forces.

6.1 Introduction

The world is facing a climate emergency caused by the anthropogenic emission of greenhouse gases [18], with the construction industry being one of the major contributors [3]. The demolition of existing structures is exacerbating the situation, increasing the demand for new construction and creating material waste; e.g., between 2010-2018, 70,000 houses of masonry construction in the UK were demolished [7]. At the same time, historic masonry structures form an essential part of the world's collective cultural heritage, ranging from the grand arches of the Sassanian Empire in the 3rd Century CE to Saint Peter's Basilica in Rome in the 17th Century CE [135]. Assessment of their load-carrying capacity and making any necessary corrective measures to strengthen them is essential for the preservation of this cultural heritage [89]. Thus, the need to strengthen masonry gravity structures has two main drivers: (i) the need to increase the useful life of our existing housing stock, much of which is

constructed of masonry, and (ii) the need to preserve our important cultural heritage.

Repairing and strengthening have been carried out on both historical and modern masonry structures, where damage may have been due to years of weathering or an incident such as an earthquake. Retrofit and repair techniques used in current practice include repointing, grout/epoxy injection, anchoring, tying, overlays (e.g., textile-reinforced mortar), bracing, internal/external reinforcement (steel bars, CFRP, etc.) and post-tensioning, each with their specific advantages and disadvantages [182, 183, 184]. It is noted that repointing and grout/epoxy injection will only restore the original load-carrying capacity of masonry gravity structure, whereas the other methods can improve load-carrying capacity by introducing additional tensile members or imposing confinement to the system [182, 183].

Repair and retrofit techniques have been successfully carried out over the years on various masonry structures, such as bridges [185, 186], domes [187, 188], and buildings and towers [189, 190, 191]. However, there is no widely accepted means of determining the most suitable strengthening intervention (i.e., of determining the optimal placement or pattern and amount of additional material) and in practice, this is often guided by 'expert opinion'. Usually, the strengthening measures adopted are justified by analysis of a model of the strengthened structure, but the selection of the strengthening measures and their positioning is usually based on intuition [192], or some often narrowly scoped experimental evidence [193, 194].

A need for a more rigorous, physics-based, approach to determine the placement of strengthening is needed. This is driven by (i) the increased complexity of structural geometries and typologies and complex loading scenarios, (ii) the need to reduce material usage, and (iii) the potentially detrimental effects of over-strengthening. The ability of masonry to form cracks is a desirable behaviour, whereby the structure can safely adapt to changing boundary conditions, e.g., support movements [195]. As evident by Poleni's analysis of St. Peter's dome, a masonry structure can still be safe in its cracked state [196], requiring no further intervention. However, severe over-strengthening will inhibit this capacity of crack adaptation in masonry gravity structures [193, 197].

Basilio et al. [198] attempted to identify optimal strengthening solutions for a semi-circular arch, such as the optimal width, length and location of CFRP strips. However, the results obtained were based on a limited number of strip widths and assumed strengthening at the surface of the masonry only. Although the results give some insights on behaviour, the study was limited in scope. Krevikas and Tiantafillou [199] presented details of an early attempt to automatically determine the optimal placement of strengthening measures, where a strut-and-tie model was used to determine the optimal volume of strengthening measures. However, the

topology of the strut-and-tie model was user-defined, though guided by results from a finite element model.

Bruggi and Taliercio [200] developed a procedure based on topology optimization to determine the optimal placement of strengthening measures in masonry gravity structures. The presented procedure determines the placement of strengthening measures by maximizing overall stiffness, given a volume fraction of strengthening measures (though the influence of the specified volume fraction on the results obtained is noted). A similar methodology was presented by Bruggi et al. [201], though in that case using minimization of the volume of strengthening elements as the objective function. However, both these methodologies are limited to surface strengthening (i.e., disregard the possibility of more radical external strengthening measures) and rely on involved numerical simulations requiring user expertise and reliable determination of the material stiffness properties.

Fraternali et al. [197], Carpentieri et al. [202] presented a tensegrity-based approach for finding the "optimal" reinforcement for masonry structures subjected to multiple load cases. They represented the masonry structure as a minimal mass system of masonry rods in compression that was reinforced via tensile elements. The procedure proposed starts with an initial network of prescribed members. Thus, similar to the issues faced in thrust network analysis [10, 66], the choice of the topology of the underlying network will inevitably influence the optimal solution found.

Gilbert [203] outlined the potential for the optimal placement of strengthening measures to be identified by combining a rigid block analysis model for the masonry with a ground structure-based truss layout optimization procedure, solving a simple linear programming problem to obtain the optimal placement of external strengthening measures. As a fully connected ground structure is used, the solution obtained will tend to be increasingly optimal as a more densely populated ground structure is used. However, an in-depth study of the potential of this approach was not presented. The Thrust Layout Optimization (TLO) procedure [149], which similarly uses ground structure layout optimization to obtain force flows within masonry gravity structures could potentially be extended to find optimal strengthening measures. This would now allow identification of both internal, external and surface strengthening measures, and would also provide users with the ability to visualize the new force flows in the system, altered via the addition of strengthening measures.

The present contribution is organized as follows. In Section 6.2 the TLO formulation is extended to include optimal strengthening measures and, to extend its range of applicability, also seismic loading. Thereafter, a range of example problems are considered in Section 6.3;

their implications are discussed in Section 6.4; and in Section 6.5 conclusions are drawn.

6.2 Thrust layout optimization (TLO)

The TLO procedure adapts the standard ground structure layout optimization (LO) method, which has long been used for the optimization of trusses. TLO extends LO by incorporating: (a) transmissible self-weight loads, and (b) interface node pairs to model weak joints (interfaces) in masonry. In the following sections, the basic TLO procedure is outlined and then extended to account for strengthening measures and seismic loading.

6.2.1 The basic TLO formulation

The TLO procedure for the analysis of masonry gravity structures is presented in detail in [149]; a summary is provided here. In the basic TLO formulation, the maximum load factor subject to equilibrium and yield constraints is sought for an assembly of blocks with given boundary conditions (Fig. 6.1a), using a ground structure defined (Fig. 6.1b) and a set of transmissible self-weight loads (Fig. 6.1c). The optimization formulation is as follows:

$$\max_{\mathbf{q},\mathbf{q_n},\mathbf{q_s},\mathbf{w},\lambda} \quad \lambda \tag{6.1a}$$

$$\text{s.t.} \quad \mathbf{Bq} + \mathbf{B_n q_n} + \mathbf{B_s q_s} - \mathbf{w} - \lambda \mathbf{f} = \mathbf{0} \tag{6.1b}$$

$$\mathbf{Hw} = \bar{\mathbf{w}} \tag{6.1c}$$

$$\mathbf{q} \leq q^{\mathrm{t}}_{\max} \mathbf{1} \tag{6.1d}$$

$$\mathbf{q_n} \leq \mathbf{0} \tag{6.1e}$$

$$\mu \mathbf{q_n} \leq \mathbf{q_s} \leq -\mu \mathbf{q_n} \tag{6.1f}$$

$$\mathbf{w} \geq \mathbf{0} \tag{6.1g}$$

$$\lambda \geq 0, \tag{6.1h}$$

where λ is the load factor on the externally applied loads: $\mathbf{B}$ is a $2n \times m$ matrix containing direction cosines, $\mathbf{q} = [q_1, q_2, ..., q_m]^{\mathrm{T}}$ is a vector of internal member forces, where n is the number of nodes in the ground structure and m the number of internal links: Interface equilibrium matrices $\mathbf{B_n}$ and $\mathbf{B_s}$ are $2n \times p$ matrices containing direction cosines on the basis of notional zero-length members oriented respectively perpendicular and parallel to the corresponding interface, where p is the number of interface node pairs: $\mathbf{q_n} = [q_{n,1}, q_{n,2}, ..., q_{n,p}]^{\mathrm{T}}$ is

the interface normal force vector and $\mathbf{q_s} = [q_{s,1}, q_{s,2}, ..., q_{s,p}]^{\mathrm{T}}$ is the interface shear force vector: and $\mathbf{f} = [f_{1x}, f_{1y}, f_{2x}, f_{2y}, ..., f_{nx}, f_{ny}]^{\mathrm{T}}$ is a vector of external applied loads. Self-weight loads, which are all in the vertical direction, are given by $\mathbf{w} = [0, w_1, 0, w_2, ..., 0, w_n]^{\mathrm{T}}$ is the nodal self-weight load vector: $\bar{\mathbf{w}} = [\bar{w_1}, \bar{w_2}, ..., \bar{w_g}]^{\mathrm{T}}$ is the load group vector, where g is the number of transmissible self-weight load groups in the problem and $\bar{w_i}$ is the total load applied in transmissible load group i. Binary matrix $\mathbf{H}$ specifies which nodal load components in $\mathbf{w}$ belong to which load group in $\bar{\mathbf{w}}$, where $\mathbf{H}$ is of size $g \times 2n$ and is given by:

$$\mathbf{H}_{ij} = \begin{cases} 1 & \text{if load component } j \text{ exists in load group } i \\ 0 & \text{otherwise.} \end{cases} . \tag{6.2}$$

Finally, the maximum tensile force in internal links is limited by a value $q^{\mathrm{t}}_{\max}$, and μ is the static friction coefficient for block-to-block and block-to-support interfaces.

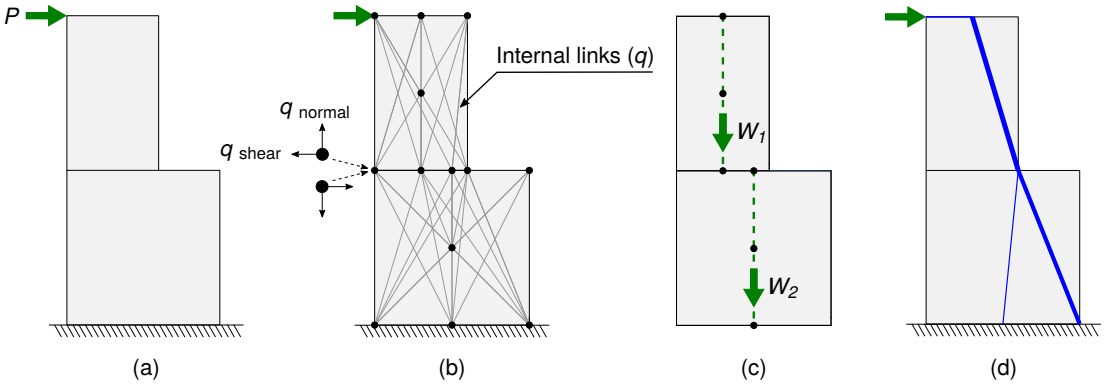

Figure 6.1: Application of the TLO procedure to a simple two-block problem: (a) geometry of blocks and location of external load *P* and support; (b) problem discretized via nodes and links; (c) masonry self-weight represented by transmissible loads W_1 and W_2; (d) collapse load and thrust layout found by solving the associated layout optimization problem (compression and tensile forces are shown in blue and red, respectively, with line thicknesses representing the magnitude of the forces).

6.2.2 Extended TLO formulation incorporating strengthening measures

The TLO process considers a ground structure that defines the domain of all possible links (i.e., thrusts). The links of the ground structure are restricted to be within each individual block making up the structure, such that links crossing weak joints or extending beyond the boundaries of the structure are not allowed. As was observed by Nanayakkara et al. [149], and as the commonly understood nature of masonry gravity structures dictates, the load carried by the structure is limited by its geometry and stereotomy, such that no amount of increase in the compressive strength of the masonry blocks will give a higher load capacity. However,

an increase in load capacity can be achieved via the introduction of additional strengthening links (i.e., additional load paths), which are external to the structure and which can cross weak interfaces.

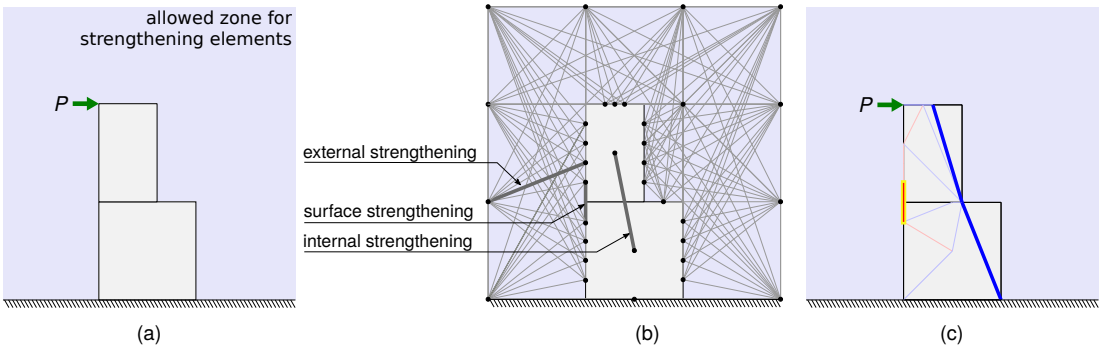

Figure 6.2: Application of the proposed extended TLO procedure to a simple two-block problem: (a) problem definition now including a surrounding zone where strengthening elements are allowed; (b) ground structure to additionally include external, surface and internal strengthening elements; (d) thrust layout with optimal placement of strengthening measures found by solving the associated layout optimization problem (compression and tensile forces are shown in blue and red, respectively, with line thicknesses representing the magnitude of the forces; strengthening elements highlighted in yellow).

The extended TLO formulation considers an extended ground structure (see Fig. 6.2), where the additional links correspond to strengthening elements, and seeks to find minimum volume strengthening measures for a prescribed level of applied loading, subject to equilibrium and yield constraints. The modified optimization formulation can be written as follows:

$$\min_{\mathbf{q},\mathbf{q_n},\mathbf{q_s},\mathbf{q_{rf}},\mathbf{a_{rf}},\mathbf{w}} \quad V_{rf} = \mathbf{l_{rf}}^{\mathrm{T}}\mathbf{a_{rf}} \tag{6.3a}$$

$$\text{s.t.} \quad \mathbf{Bq} + \mathbf{B_n q_n} + \mathbf{B_s q_s} + \mathbf{B_{rf} q_{rf}} - \mathbf{w} = \mathbf{f} \tag{6.3b}$$

$$\mathbf{Hw} = \bar{\mathbf{w}} \tag{6.3c}$$

$$\mathbf{q} \leq q^{\mathrm{t}}_{\max}\mathbf{1} \tag{6.3d}$$

$$\mathbf{q_n} \leq \mathbf{0} \tag{6.3e}$$

$$\mu\mathbf{q_n} \leq \mathbf{q_s} \leq -\mu\mathbf{q_n} \tag{6.3f}$$

$$-\sigma_{\mathrm{c,rf}}\mathbf{a_{rf}} \leq \mathbf{q_{rf}} \leq \sigma_{\mathrm{t,rf}}\mathbf{a_{rf}} \tag{6.3g}$$

$$\mathbf{w} \geq \mathbf{0}, \tag{6.3h}$$

where V_{rf} is the volume of the strengthening elements; $\mathbf{l_{rf}} = [l_1, l_2, ..., l_{\mathrm{m_{rf}}}]^{\mathrm{T}}$ is a vector of ground structure strengthening member lengths and $\mathbf{a_{rf}} = [a_1, a_2, ..., a_{\mathrm{m_{rf}}}]^{\mathrm{T}}$ is a vector of strengthening member cross-sectional areas; $\mathbf{B_{rf}}$ is a $2n \times m_{\mathrm{rf}}$ matrix containing direction

cosines for strengthening members, $\mathbf{q_{rf}} = [q_1, q_2, ..., q_{\mathrm{m_{rf}}}]^{\mathrm{T}}$ is a vector of strengthening member forces, where m_{rf} is the number of strengthening links: $\sigma_{\mathrm{t,rf}}$ and $\sigma_{\mathrm{c,rf}}$ are limiting tensile and compressive stresses respectively of strengthening links: and other terms are as defined previously.

Therefore, the optimization seeks to find the group of strengthening measures that consume the least volume of material under the constraints of: (i) static equilibrium at nodes (Eq. (6.3b) and Eq. (6.3c)); (ii) a maximum tensile force allowed within blocks, Eq. (6.3d), with no tensile forces allowed across weak interfaces, Eq. (6.3e); (iii) the interface friction force limited by friction coefficient, Eq. (6.3f); and (iv) strengthening links must be at or below their yield strength Eq. (6.3g). The extended formulation remains linear and thus can be solved using linear programming solvers. Similar to the TLO procedure, once the optimal placement of strengthening measures has been found, a volume minimization process is carried out to obtain a visually clear thrust layout within the masonry structure. This is carried out with the areas of the reinforcing links (a_{rf}) fixed at the values found in the previous step.

In the basic formulation described above, all the different types of strengthening links are treated the same, not taking into account the practicalities of installing them. However, the latter can be accounted for by using a comprehensive cost function rather than the volume of the strengthening measures as the objective function.

6.2.3 Extended TLO formulation to model seismic loading

To extend the range of applicability of the TLO procedure, it is now extended to consider the seismic loading by considering an equivalent horizontal acceleration (a_v) applied to the mass of the material. The equilibrium constraints are adjusted as below, where external loads (if present) are fixed at their given values.

$$\mathbf{Bq} + \mathbf{B_n q_n} + \mathbf{B_s q_s} - \mathbf{w} = \mathbf{f} \tag{6.4a}$$

$$\mathbf{Hw} = \mathbf{k}^T \bar{\mathbf{w}} \tag{6.4b}$$

$$\mathbf{w} \geq \mathbf{0}, \tag{6.4c}$$

where, $\mathbf{w} = [w_{1x}, w_{1y}, w_{2x}, w_{2y}, ..., w_{nx}, w_{ny}]^{\mathrm{T}}$ is the nodal self-weight load vector; the load group vector is $\bar{\mathbf{w}} = [\bar{w_1}, \bar{w_2}, ..., \bar{w_{gr}}]^{\mathrm{T}}$ where the first gr_x load groups correspond to seismic loading in horizontal direction (x) and the next gr_y load groups correspond to self-weight load in gravity (y) direction (and $gr = gr_x + gr_y$); $\mathbf{k} = [a_h, a_h, ..., a_h, 1, 1, ..., 1]^{\mathrm{T}}$ is the seismic

coefficient vector, where the first n_x elements are a_h the horizontal acceleration and the next n_y elements are unity (i.e., correspond to self-weight). a_h is a new variable and is the parameter being maximized, in the determination of the seismic loading capacity of a structure. The binary matrix $\mathbf{H}$ is as earlier, and the constraint on Eq. (6.4c) also follows from the TLO formulation presented earlier. Note that formulation in Eq. (6.4) can be readily extended to consider vertical seismic loading as well, by appropriately changing the seismic coefficient vector $\mathbf{k}$.

Here, seismic loading is also considered a transmissible load. Thus the horizontal and vertical components of forces applied to the same mass can potentially be mobilized at different locations. While this is not strictly true in practice, it has been observed that this gives a clearer visualization of force flows and appears not to greatly affect collapse load estimates.

6.3 Numerical examples

In the following section, examples are used to explore the capabilities of the extended TLO formulation. Firstly, three examples are used to demonstrate the capability of the extended TLO formulation to determine the optimal placement of strengthening measures in masonry gravity structures, considering strengthening of: (i) a flat arch on stone columns; (ii) a semi-circular arch with strengthening element exclusion zones; and (iii) a wall with openings subjected to seismic loading. In a final example involving a stone beam, the extended TLO procedure is applied to the design of a structure with external tension zones.

6.3.1 Flat Arch

A flat arch on stone column example, following Nanayakkara et al. [149], is used here to explore the optimal placement of strengthening measures in masonry gravity structures, using the extended TLO formulation.

In this case, the flat arch can safely carry a mid-span point load P of 45.1 kN without any additional strengthening, and the corresponding thrust layout indicates a collapse mechanism where the keystone is hinging about its top corners and the springing blocks hinge about the internal corners of the corresponding stone columns; see Fig. 6.3a. As intuition suggests, the load-carrying capacity could be increased if the masonry hinges that are opening could be suppressed. The extended TLO formulation incorporating strengthening measures indicates an increase in the load capacity P to 150 kN if the springing blocks are physically joined to the columns; see Fig. 6.3b. While this can be achieved in many ways, the theoretical optimal

is to have straps carrying tension (24.5kN at P=150 kN) at the outer surface, across the joints between the blocks.

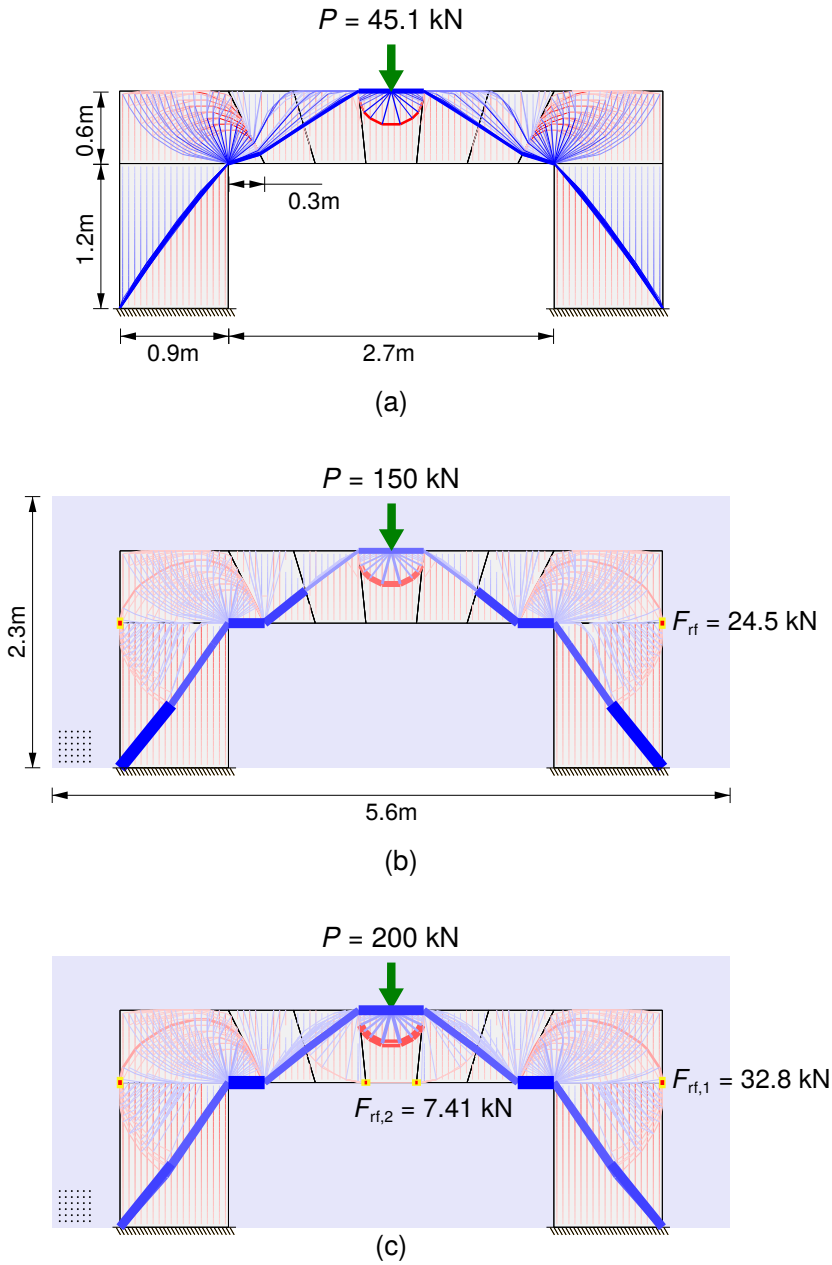

Figure 6.3: Strengthening a flat arch: (a) a flat arch with a collapse load estimate of 45.1 kN; (b) the flat arch optimally strengthened to carry an increased load of 150kN; (c) the flat arch optimally strengthened to carry an increased load of 200 kN (thrust layouts obtained using internal and boundary node spacing of 0.5 m and 0.1 m; the boundary of the domain of strengthening measures is indicated in light blue with the nodal spacing there being 0.5 m; strengthening elements are highlighted in yellow; compression to tensile strength ratio of 1:100 in thrust layout; compression to tensile strength ratio of 100:100 in strengthening elements).

Further showing the form-dependence of the load-carrying capacity of masonry gravity structures, increasing the capacity of the strengthening (i.e., increasing the tensile capacity

of the tensile strap mentioned above) alone will not dramatically increase the load-carrying capacity of the structure. For that to happen, the keystone is now required to be joined to the adjacent blocks (at the intrados corners of the keystone block), with straps capable of carrying 7.41 kN tension at P=200 kN (Fig. 6.3c). This, along with the previous set of strengthening measures (though with the straps now increased to carry a tensile force of 32.8 kN), will 'geometrically lock' the failure mechanism, providing notionally an infinite load carrying capacity if the capacity of the strengthening straps continues to be increased and the blocks themselves do not fail in fracture or crushing.

Note that practical implementation of the theoretically obtained strengthening measures requires additional material as the theoretical length of the surface straps found above would tend to zero as the boundary node spacing used in TLO tends to zero; however, in practice, anchorage would be required to keep the straps in place. Similarly, locations where external strengthening elements join would require a mechanical joint. Furthermore, the possibility of having different materials as external, surface, and internal strengthening measures is recognized, for example, steel rods, CFRP straps, etc. To incorporate these practicalities, an extended cost function incorporating anchorage, joint and material costs can be used.

Similarly, it is possible to avoid certain types of strengthening measures altogether, for example, due to local availability issues for a given material leading to prohibitive economic and/or environmental costs. Fig. 6.4 presents an alternative solution where surface strengthening elements are eliminated. The solution is sub-optimal when only the volume of the strengthening elements is considered (i.e., disregarding the cost of fixing, etc.). Taking a hypothetical strength capacity of 100 $\mathrm{N/mm^2}$ in both compression and tension (and a nodal spacing of 0.01 m at block boundaries) the optimal volume of strengthening elements is 29,316 $\mathrm{mm^3}$ when surface strengthening is present (Fig. 6.3c) and 159,975 $\mathrm{mm^3}$ when surface strengthening is not present (Fig. 6.4), for a load capacity of 200 kN.

Note that the strengthening elements in Fig. 6.4 include compression elements. Although buckling failure is not explicitly considered, this can be accounted for e.g., by using circular hollow sections of sufficient stockiness. Furthermore, it is noted that in contrast to the optimal solution that connects the keystone block with the adjacent blocks (Fig. 6.3c), the solution in Fig. 6.4 connects the springing blocks with adjacent blocks; this, like the optimal solution, 'geometrically locks' the structural system giving a notional load carrying capacity of infinity if the strength of the strengthening elements can be increased without limit.

The above load capacities are of course only realizable if the masonry possesses infinite compression strength and the strengthening elements are composed of material possessing

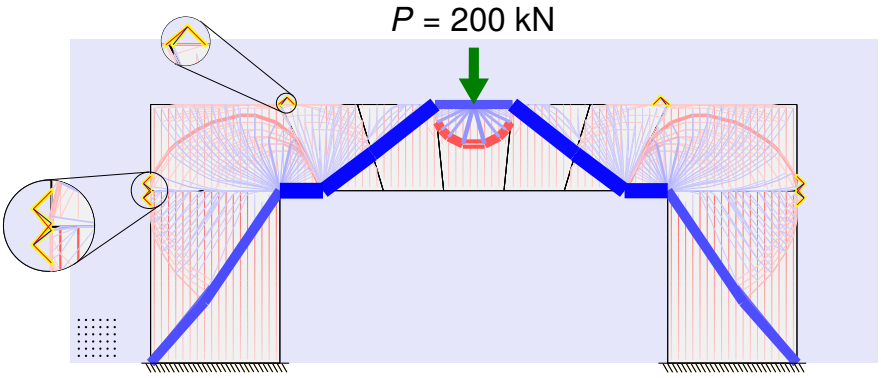

Figure 6.4: Strengthening a flat arch with only external elements: two distinct zones of strengthening are identified (see insets) where the springing blocks are connected to adjacent blocks.

sufficient tensile strength. Although the assumption of infinite strength is often reasonable for typical form-resistant structures, at the higher loads achieved when strengthening measures are employed, this assumption becomes less realistic as the working stresses are now significantly higher, leading to crushing of greater areas of material in compressive regions. Similarly, the tensile stresses in the masonry may exceed the finite tensile capacity of the material leading to fracture of the stone blocks.

The limited crushing strength can be accounted for by considering a thrust zone. This can be done by incorporating a node radius based on the forces connected to it (following [204]) and then moving the node to be fully contained within the structure. The volume minimization step for thrust layout visualization is in this case repeated until the maximum node movement is within a prescribed tolerance. However, note that in Fig. 6.3 and Fig. 6.4, although the thrust layout visualization suggests that stressed zones extend beyond the extent of the structure (e.g., see half of the main compressive thrust along the bottom-inner corner of the springing block being outside of the structure), this is due to scaling of force lines for visibility (e.g., in Fig. 6.3c the maximum calculated node radius (taking a compressive strength of 100 $\mathrm{N/mm^2}$ and a tensile strength of 1 $\mathrm{N/mm^2}$) is of the order of 1 mm, which is negligible in comparison to the dimensions of the structure).

6.3.2 Semicircular arch

As observed in the previous section, the theoretical optimal solution will often be an intuitively obvious one, that involves applying strengthening material to restrain the opening of hinges forming a mechanism. However, at increased load demands, the extended TLO procedure generates solutions that would not necessarily be obvious to a structural engineer.

Now consider a semicircular arch composed of 16 straight-edged voussoirs and subjected to a mid-span point load. The arch is of 10 m centreline radius and 1.1 m thickness. Voussoir material has a unit weight of 25 $\mathrm{kN/m^3}$ and a friction coefficient of 0.7. The maximum mid-span load that can safely be carried is 7.1 kN; see Fig. 6.5a.

The extended TLO formulation was used to identify the optimal placement of strengthening measures for the arch to carry loads in excess of its normal capacity; target loads of 15 kN and 75 kN were considered. To achieve the lower of these two target loads the intuitively obvious strengthening solution involving connecting the two blocks directly below the applied load is identified; see Fig. 6.5b. At the higher of these two target loads, an arrangement of strengthening measures that is less intuitively obvious is identified; see Fig. 6.5c. Here, the two blocks directly below the applied load are again connected but in this case attached to these are two compressive elements that apply forces to a tension cable running at mid-height; the latter restrains outward movement of the arch, at locations where the voussoirs are hinging at the intrados.

Furthermore, an edge clearance is considered here as a crude approach to account for the practicalities of providing connections near the corners of the voussoirs. This edge clearance also affects the form of the solution found. In this case, the strengthening measures are considered with an edge clearance of 0.67 m (1/3rd of the centreline length of voussoirs). If a lower edge clearance (say 0.4 m) was specified, then connecting the two blocks directly below the applied load would be optimal at the higher load as well. In a more refined formulation, the edge clearance can be replaced by considering embedment lengths and anchorage zones in an extended cost function, along with strengthening elements penetrating the stone masonry (i.e., one end not being outside and the other being inside the structure).

The same arch is now considered to demonstrate the capability of the extended TLO procedure to identify strengthening measures in the presence of various strengthening measure exclusion zones. In Fig. 6.6 outcomes for three different cases are shown: (a) unrestricted zone for strengthening elements; (b) a rectangular exclusion zone; and (c) a hexagonal exclusion zone. These are representative of the practical restrictions that might be present, e.g., to allow traffic to pass under the arch.

When an exclusion zone is introduced, preventing the solution obtained in Fig. 6.6a, additional sets of strengthening elements are introduced at the extrados, near the quarter-spans, where hinges are present at the intrados (Fig. 6.6b). As the exclusion zone is expanded, three distinct zones emerge: one at the intrados near the crown (where hinges occur at the extrados) and the others at the extrados at quarter spans (where hinges occur at the intrados);

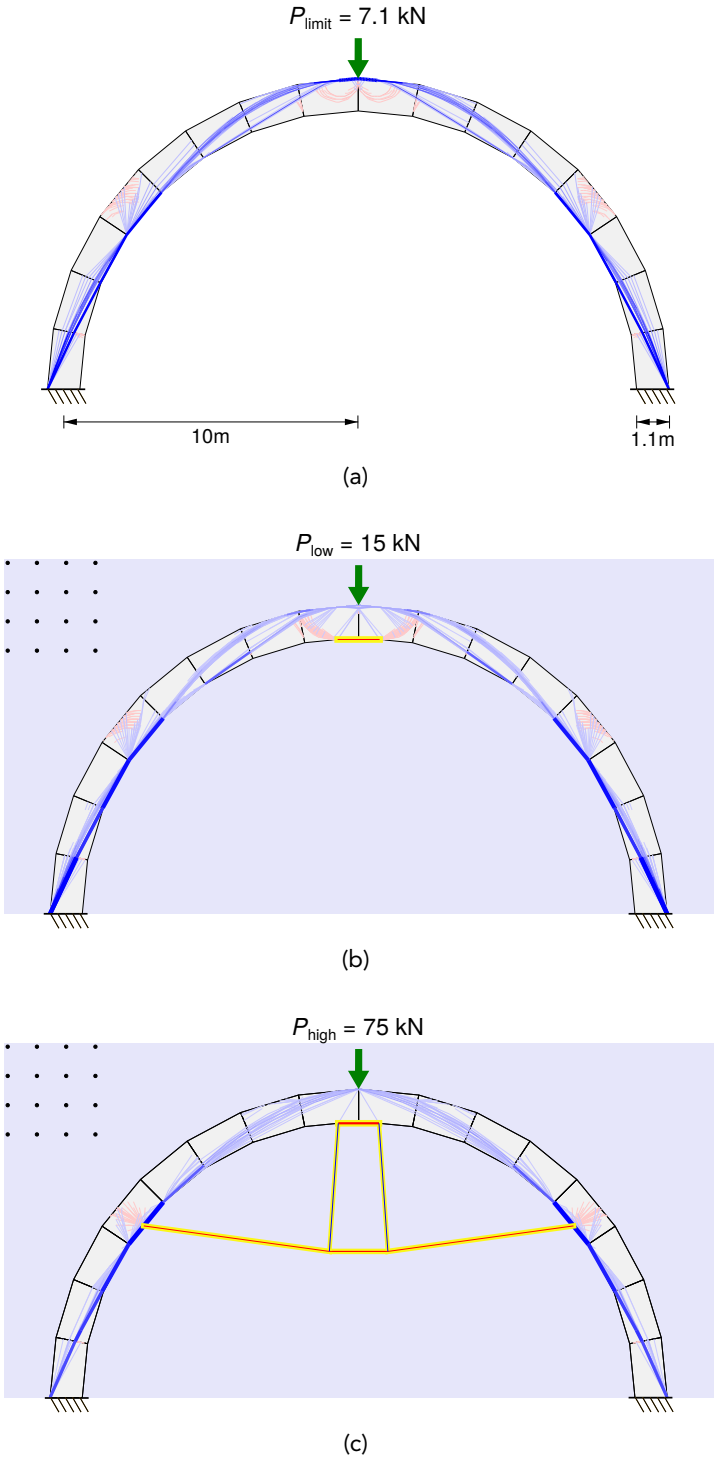

Figure 6.5: Strengthening a semi-circular arch: (a) the unreinforced arch at its collapse limit load of 7.1 kN; (b) the optimal strengthening measures to achieve a higher limit load, of 15 kN; and (c) the optimal strengthening measures to achieve a significantly higher limit load, of 75 kN (edge clearance of 0.67 m; thrust layouts obtained using internal and boundary node spacings of 0.2 m; for the strengthening measures a grid spacing of 1.0 m has been used).

see Fig. 6.6c. These strengthening measures effectively increase the depth of the section by introducing new tensile zones outside the masonry forming the arch. In relation to this, the

solution shown in Fig. 6.6a is particularly interesting as it combines these three zones in a single optimal solution. It can also be observed that the results obtained here correspond well with the results obtained by Gilbert [203], where a rigid block method was extended to find the optimal placement of strengthening elements for a semicircular arch.

6.3.3 Wall with openings subjected to seismic loading

A 3.0 m $\times$ 3.0 m masonry wall with a 1.0 m $\times$ 1.2 m opening and composed of 500 mm $\times$ 150 mm masonry units is considered. Masonry above the opening is supported by a flat arch of 300 mm in height and made of 6 blocks. The in-plane seismic capacity of the wall, assuming a quasi-static analysis, and the corresponding thrust layout were obtained using TLO; see Fig. 6.7.

The in-plane seismic capacity is determined as the maximum horizontal acceleration that can be safely carried, and in this case was found to be 0.33g, where g is the acceleration due to gravity. The thrust layout obtained (Fig. 6.7) indicates a significant thrust zone moving from the top-right of the opening to the bottom-right of the wall and two fanning tensile zones, one above the opening and one below, coinciding with the ends of the main thrust. The top-right and bottom-left corners of the opening have concentrations of compressive forces. Thus, the thrust layout provides a useful visualization of the state of stress within the structure, comparable to that which could be obtained using a finite element model, though without the need for material stiffness properties and at a much lower computational cost.

Now, the optimal placement of strengthening measures in the masonry wall is considered, in this case, if the maximum in-plane horizontal acceleration is to be increased to 0.45g. The thrust layout at the increased seismic demand is given in Fig. 6.8, where the strengthening measures are highlighted in yellow. As might be expected, the vertical portion of the main vertical thrust layout at the bottom-right of the wall is shorter, and individual movement of the blocks (see tensile-fans contained within blocks in Fig. 6.8) predominates as opposed to the movement of large sections of masonry observed at the seismic capacity (see tensile fans cutting across blocks in Fig. 6.7).

In this case, strengthening measures were only sought within the extent of the wall; i.e., no external strengthening measures were sought. It is interesting to note that the optimal strengthening measures found are a series of tensile connectors (see the elements highlighted in yellow in Fig. 6.8) where these connectors straddle across two adjacent blocks, stitching together the weak interface between them. These are reminiscent of the metal clamps ob-

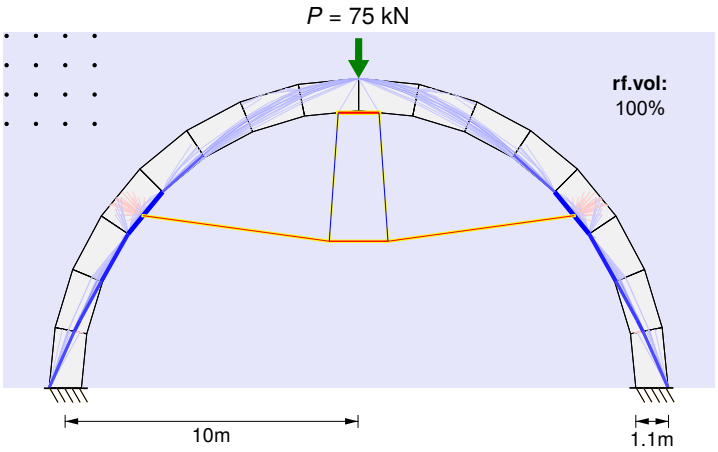

(a)

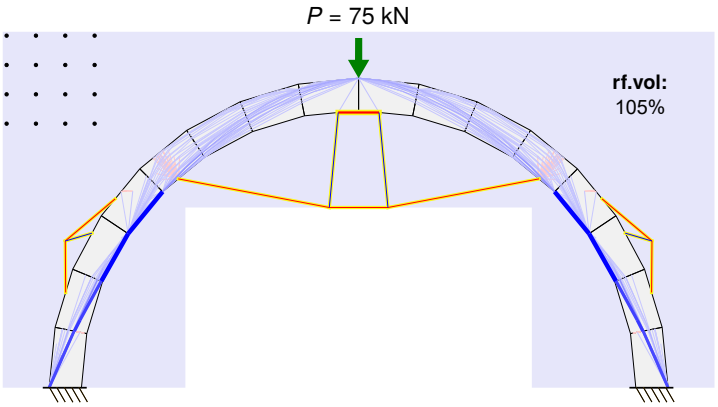

(b)

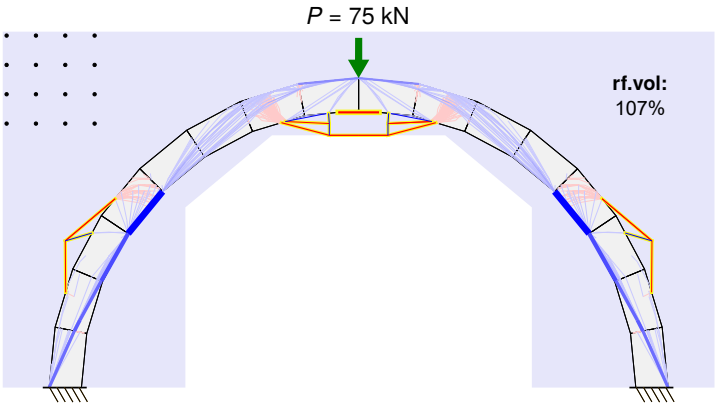

(c)

Figure 6.6: Change in optimal placement of strengthening with increasingly restrictive exclusion zone: (a) minimum volume strengthening elements with no exclusion zone; (b) solution with a rectangular exclusion zone; and (c) solution with a highly restrictive hexagonal exclusion zone - in this case, since the exclusion zones restrict the placement of strengthening elements, three distinct zones of strengthening appears. The total volume of strengthening measures in each case, as a percentage of the case (a), are noted (edge clearance of 0.67 m; thrust layouts considering an internal and boundary node spacings of 0.2 m, and the strengthening measures with a grid spacing of 1.0 m).

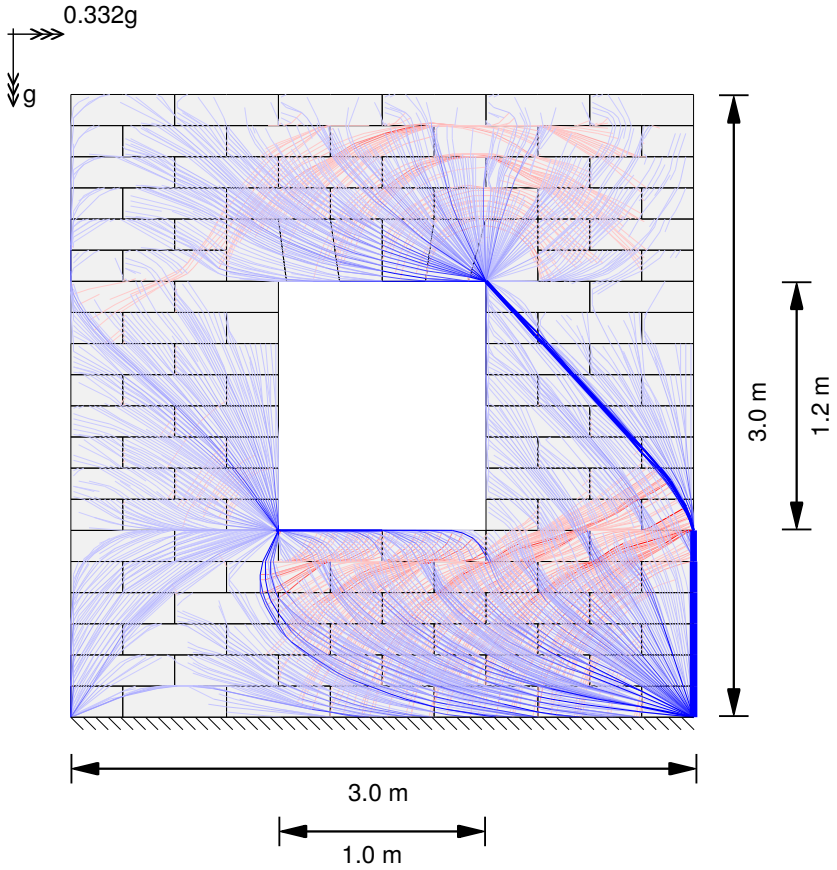

Figure 6.7: Seismic capacity of a masonry wall: thrust layout obtained using TLO, extended to account for seismic loading. The geometry and the limiting seismic action are as indicated, with individual blocks of 500 mm length and 150 mm height (thrust layouts obtained using internal and boundary node spacings of 0.025 m; tensile links scaled by a factor of 2 for clarity).

served in historical stone masonry construction, from the Incas in South America [205, 206] to the Greeks and Romans in ancient Europe [207, 208], to builders in far-East Asia [209]—see Fig. 6.9. These are now also used in the retrofit of ancient structures [210].

The optimal placement of strengthening measures was determined in a staged process where the problem was first solved with a coarser grid and then solved using a finer grid, now, the placement of strengthening measures is constrained within a limited zone based on the results of the first solve. This staged approach reduces the overall computational time and memory demand.

6.3.4 Design of a stone-beam

There has recently been renewed interest in stone masonry as a low embodied-carbon means of construction [156, 157]. However, it has been observed that the stone-beam cross-sections used in recent projects have sometimes been very large; having an external strengthening

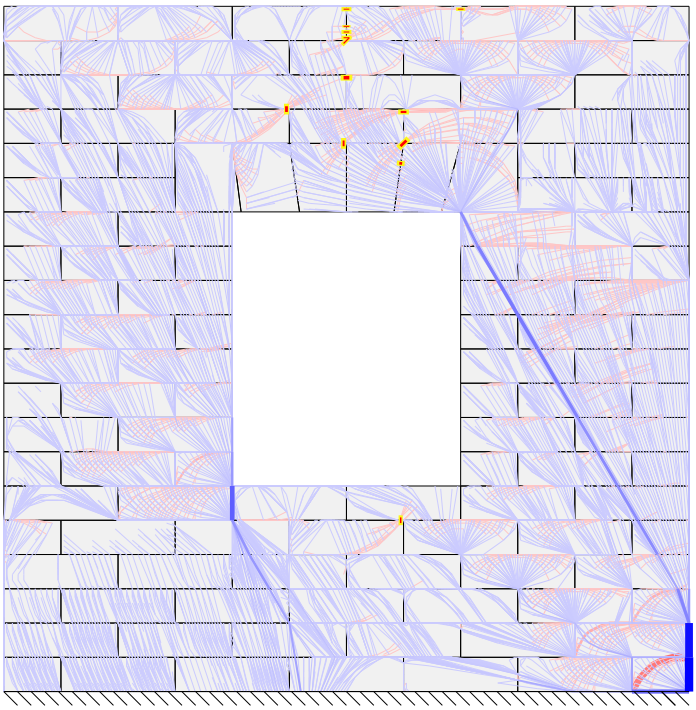

Figure 6.8: Strengthening of a masonry wall against seismic loading: optimal placement of strengthening measures and the corresponding thrust layout obtained using the extended TLO method for a masonry wall subjected to a seismic load of 0.450g, which is higher than its capacity (0.332g) (thrust layouts obtained using internal and boundary node spacings of 0.025 m; tensile links scaled by a factor of 2 for clarity).

domain could therefore reduce material usage.

A stone beam of 3.0 m span and 250 mm height and thickness is now considered. The beam is made of 11 blocks, including a keystone and two springing blocks. The block interfaces are inclined 15^o to the vertical, and the springing blocks are supported on a 225 mm ledge on either side. The stone has a unit weight of 25 $\mathrm{kN/m^2}$ and joints have a friction coefficient of 0.7.

A preliminary investigation with varying the number of blocks (3 to 15), block inclinations (0^o to 30^o), and friction coefficients indicated that an unrealistically high friction coefficient (>1.5) was required to enable the stone beam to stand on its own. The following design considers three load cases: a central point load, a 1/3rd span load, and a 2/3rd span load, each of which has a magnitude of 25 kN. The strengthening measures are restricted to a 250 mm deep zone below the stone blocks.

The optimal strengthening solution obtained includes two tensile cables starting and ending from stone blocks and hugging the edge of the strengthening zone at mid-span, creating the maximum lever arm there. Then a secondary set of 1 bar-2 cable systems prevent the opening up of individual joints between blocks.

(a) (b) (c)

Figure 6.9: Historical evidence of metal clamps in stone masonry: (a) Inca civilization example, in modern-day Bolivia (at Puma Punku); (b) example from ancient Greece; and (c) example from ancient China (Zhaozhou Bridge built in 600 CE).

6.4 Discussion

Masonry gravity structures are types of form-resistant structures, in that their load-carrying capacity is primarily determined by geometry (i.e., where the material is, as opposed to the strength of the material employed). This is also observed to be the case when the structure is strengthened via the addition of strengthening elements. As observed in the example of a flat arch on stone columns (Section 6.3.1) the first set of strengthening elements can increase the load-carrying capacity of the structure up to a point, with the strength of the extra elements in this case influencing the extra load carrying capacity. However, to further increase load capacity beyond this point strengthening elements need to be introduced elsewhere. Similar observations have been made in previous numerical studies of semicircular arches carried out by Basilio et al. [198], who note that "beyond a certain reinforcement width, insignificant load capacity increments are obtained". Load capacity can be increased by adding further sets of strengthening measures until the structure is 'geometrically locked', with a notional load capacity of infinity.

However, that infinite capacity is not always achievable or desired. A procedure to handle finite compressive strength via using a calculated nodal thickness was noted in Section 6.3.1; this is reasonable as the highly compressed regions are at the edges of the masonry, where hinges occur. However, handling the tensile strength limit accurately would require consideration of stress resultants from compressive and tensile forces intersecting at nodes, and also link overlaps; tensile forces in thrust layouts are observed in fan regions with tensile and compressive forces intersecting. Similarly, the strengthening measures required for higher load capacities may inhibit the ductility of the structure, diminishing the ability of a masonry gravity structure to adjust to changing boundary conditions. Further investigations, poten-

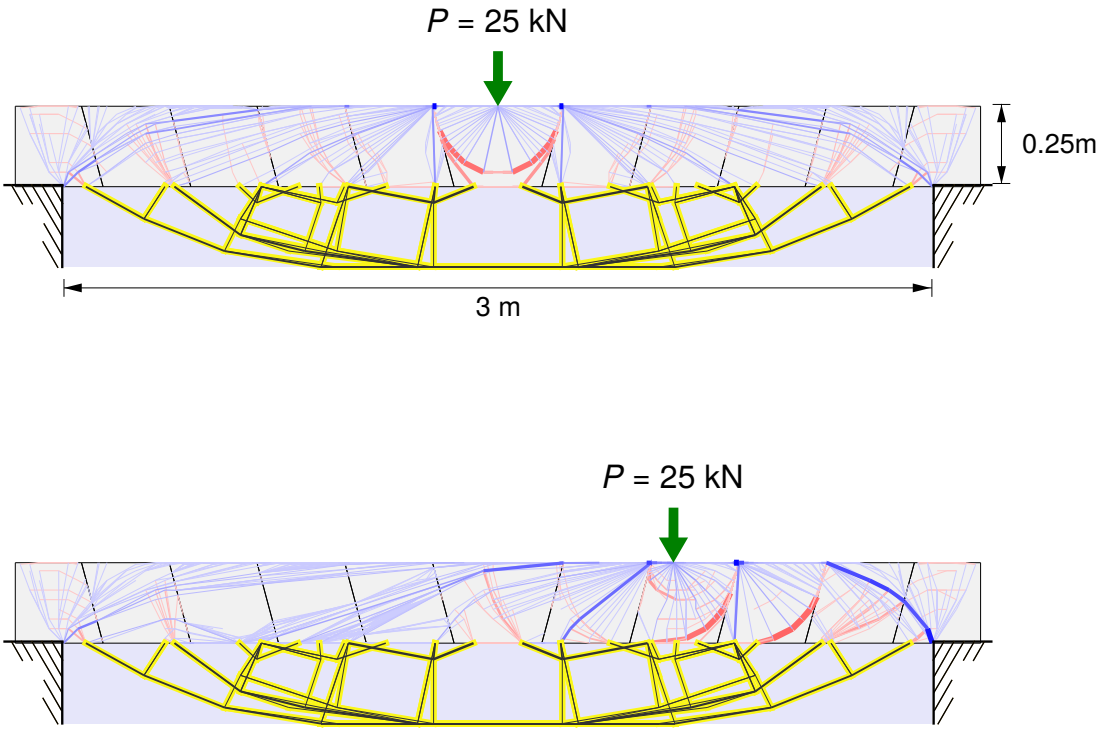

Figure 6.10: Design of a stone beam with external strengthening under multiple loads: (a) with a central point load of 25 kN; and (b) 1/3rd span loads of 25 kN, one at either side considered as separate load cases (thrust layouts considering an internal and boundary node spacings of 0.03 m; auxiliary strengthening structure indicated in black; tensile links scaled by a factor of 2 for clarity).

tially involving the dual kinematic solutions obtainable when solving the linear programming problem of extended TLO, will be required to incorporate this.

Two distinct patterns of placement were observed in the strengthening measures. In the first pattern (see the left column in Fig. 6.11) an additional load path is created to carry the extra external load applied, ΔP. Here the bending capacity is achieved by having an external tension element and increasing the lever arm of the section reduces the force and thus the cross-sectional area of the member involved. In contrast, the second pattern involves 'lifting up' of self-weight from an adjacent block to act as a counter-weight against the applied additional load; see Fig. 6.11, right column. In the optimal placement of strengthening elements observed in the current contribution (e.g., see Fig. 6.4) the fanning compression elements collapse to a single compression element as the ground structure grid is coarse; a subsequent optimization employing a locally refined grid is likely to produce the more optimal fan structure expected.

The requirement of anchorage provision, for both surface strengthening (Section 6.3.1) and external strengthening (Section 6.3.2) is noted. The forces to be resisted at these connection points can be obtained from the current extended TLO implementation and can feed

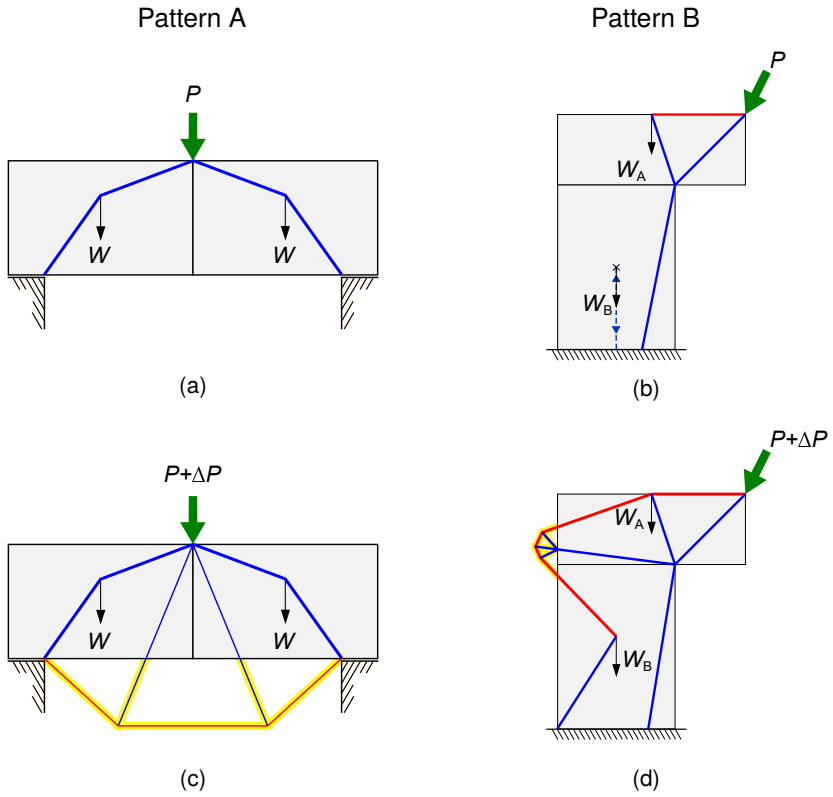

Figure 6.11: Patterns of optimal placement of strengthening measures: in pattern A (in the left column) an additional structure is formed to create a new load path to carry the extra loading ΔP, whereas, in Pattern B (in the right column) a new load path is created to lift up the self-weight from adjacent blocks. The strengthening elements added are highlighted in yellow.

into the process of designing the connections. Furthermore, constraints on edge clearance are also considered to account for the practicalities of providing sufficient pull-out resistance near the edges in the case of external strengthening elements. In the basic cost function used here, only the cost of the material is considered, though this can easily be extended to incorporate costs related to joint anchorage requirements.

The extended TLO procedure is not limited to determining the optimal placement of strengthening measures in masonry gravity structures, but can also potentially be used in the design of novel externally tensioned structures. These types of structures were first conceived by the French architect Viollet-lu-Duc [211], and later put into practice by Peter Rice at the Seville Expo in 1992 [212]; they have also recently been researched by Todisco et al. [213, 214]. When using the extended TLO formulation such structures can be designed by first defining the visually dominant compression field (i.e., the arrangement of masonry blocks), with the placement of the external strengthening elements (in both tension and compression) then sought via TLO. Various constraints may need to be added to generate visually striking

external member fields, since the optimal solutions may sometimes be obvious and hence not visually striking (e.g., Fig. 6.5b). Nonetheless, knowing the potential optimal volume of strengthening will be useful in justifying a balanced option; i.e., a visually striking solution that is within a reasonable margin of the optimal. A similar approach has been used to rationalize solutions in the interests of constructibility [15].

6.5 Conclusions

In this work, the thrust layout optimization (TLO) procedure for the analysis of masonry gravity structures has been extended to incorporate a domain of auxiliary strengthening measures, which may lie exterior to, interior to, or on the surface of a given structure. Specific conclusions are as follows:

- The TLO procedure has been extended to include a domain of auxiliary strengthening elements to provide a physics-based tool for determining the optimal placement of strengthening measures in masonry gravity structures. In addition, the extended process can handle seismic loading and multiple load cases, with force flows clearly visualized when strengthening elements are active.
- At low levels of loading, the optimal strengthening measures identified via TLO are likely to correspond to intuitively obvious solutions (e.g., surface strengthening to prevent the opening of hinges). However, at higher levels of loading, and/or with practical considerations taken account of, less intuitively obvious strengthening measures are likely to be identified. In this case, the corresponding thrust layout helps to rationalize these solutions.
- The addition of an auxiliary strengthening domain to the TLO makes it possible to design stone masonry structures with an external compression-tension structure. This provides a powerful physics-based means of exploring new structural systems.

Chapter 7

Discussion and Conclusions

7.1 Discussion

This thesis presents thrust layouts to represent force flows within form-resistant structures in equilibrium. In Chapter 4, prevalent notions of thrust lines are discussed and the benefits of thrust layouts over them are noted. However, generating thrust layouts by traditional means—i.e., physical models and graphic statics—is an involved process as now the topology of the thrust layout also needs to be decided a priori. Overcoming this, in Chapter 5, an automated procedure, termed thrust layout optimization (TLO), is presented for the generation of thrust layouts. In addition, TLO provides an opportunity to incorporate friction at block interfaces. Furthermore, the TLO procedure can be further extended to find an external strengthening domain to increase the load carrying capacity of the form-resistant structure.

Thrust layouts thus generated present advantages over the traditional thrust line method: (i) avoids the confusion present in traditional thrust lines and clearly demonstrates a force flow that stays within the bounds of the structure (if an equilibrium is indeed satisfied); (ii) gives better estimates of the exact collapse load (otherwise giving a lower bound solution); (iii) avoids the case specific pre-processing steps present in the traditional thrust line method, and is generally applicable to form-resistant structures.

While there are other useful techniques, such as the rigid block method, that exist for the estimation of the collapse load of block assemblies, a key advantage of thrust layouts lies in their highly visual nature. Traditional thrust lines give a single compression line of force flow, disregarding the tensile force that may be present in the real structure (e.g., bifurcation of thrust layouts around internal holes when a traditional thrust line would still run through it). In contrast, the rigid block method would give a failure mechanism, but not how the forces

flow inside the rigid blocks. Thrust layouts consider the possibility of limited tensile forces within the blocks, and the multitude of possible force flows (via the use of the underlying ground structure). This gives a much richer visualization of force flows, at a considerably lower computational cost and level of required user expertise compared to a non-linear finite element model. Arguably, thrust layouts give a designer a much more understandable picture of how a form-resistant structure carries loads.

It is further emphasised here that the thrust layout will only show one possible flow of forces within the structure: This may or may not reflect the actual internal stress state. Stresses within a structure are applied to areas whereas the thrust layout considers forces flowing along linear elements connected at nodes. Further, as infinite compression capacity is assumed this allows for compressive forces to pass through corners where blocks hinge against each other. When the working stresses in the structure are very low the corresponding stressed thicknesses are small and therefore the above idealization is reasonable. However, when the working stresses are closer to the material yield, this assumption becomes invalid and TLO will overestimate load capacity: When the assumption of infinite strength is valid, the TLO procedure will give the exact collapse load or a lower-bound solution.

As the TLO method solves a solid block system considering interfaces, there are some limitations arising from the kinematics at the interfaces. There are instances where although a valid equilibrium solution exists, the solution is not realistic. Consider 'the boy with the backpack' and ' Drucker's two block problem' in Fig. 7.1. Both these problems have equilibrium solutions, but neither is stable. In the case of the boy with the backpack, there exists a mechanically admissible virtual displacement system where the deformations are either contact separation, relative rotation about a point on the contact face, or a combination of the above (see Fig. 7.1a lower). Following Bagi [143], this violates the kinematic requirement for the structure to be safe. In contrast, the invalidity of the equilibrium solution in Drucker's two-block problem stems from the non-associativity of Coulomb friction. Here, an equilibrium solution giving a normal force at the frictionless contact between the two blocks will only be realisable if the smaller block on the inclined face has a friction response with dilation, therefore pushing the smaller block against the bigger block. In reality, with Coulomb friction present, and depending on the angle of friction and the inclination of the inclined surface, the smaller block will slide down (see Fig. 7.1b lower). Therefore, statics alone are not sufficient to verify the solution, and the relevant kinematics of the solution also need to be considered.

Furthermore, the TLO formulation uses transmissible loads to represent self-weight loads,

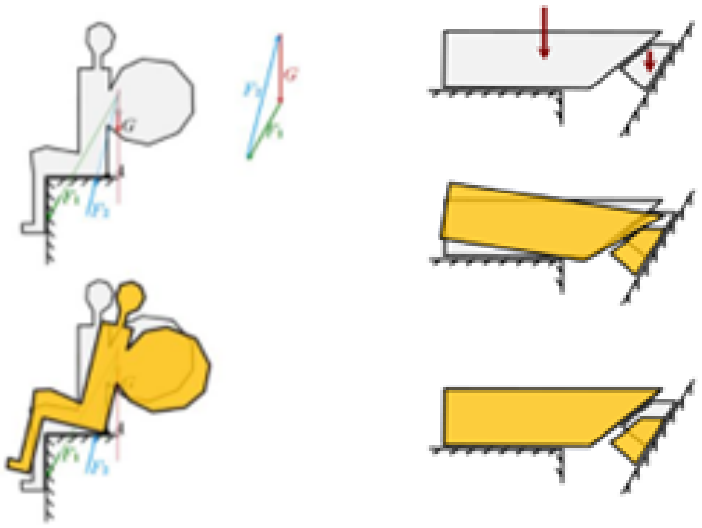

(a) (b)

Figure 7.1: Special cases of solid block systems: (i) "the boy with the backpack" problem following Or [215]; and (ii) "two-block problem" following Drucker [216].

so that force flows resembling traditional thrust lines can be realised. This, however, removes some of the important visual information, specifically that related to self-weight loads. However, this visual information can be added back to thrust layouts by plotting transmissible self-weight load vectors—i.e., force vectors indicating the force in the notional link required to move the self-weight either up or down from its original position to where it is transmitted to. Plotting of transmissible self-weights could also benefit traditional thrust lines, leading to potentially erroneous thrust lines being identified. Furthermore, a quasi-static seismic load can also be applied as a transmissible load set, now in the horizontal direction, and the corresponding seismic capacity (as a horizontal acceleration) and thrust layout can be obtained.

As a natural extension of the TLO, an extra set of ground structure nodes and links (i.e., an auxiliary strengthening domain) can be incorporated to represent potential strengthening measures that could be applied to form-resistant structures. This has been shown to be capable of determining optimal placement of strengthening measures—which in practice are primarily determined by expert opinion and rarely on physics-based models. Small increments of collapse load can be achieved by introducing strengthening measures to inhibit the formation of masonry hinges—i.e., the obvious solution. Furthermore, it is noted that the strengthened structure too retains the form-resistant nature until the structural system becomes 'geometrically locked', with a notional load capacity of infinity—i.e., closing one set of hinges would only increase the load capacity to a certain level and beyond that the increment of load carrying capacity of the strengthening elements would not increase the load carrying

capacity of the structure any further. Thus making the load carrying capacity of the structure form-dependent, and not strength-dependent. Once a structure is geometrically locked the failure in practice would inevitably be material strength dependent.

One key element of thrust layouts is that they recognise the limited but finite tensile strength of the block material making up the structure. Furthermore, it has been shown that the tensile strength requirement for the results to converge to the exact collapse load is very low. However, with the external strengthening measures pushing up both tensile and compressive forces within the structure, it will be required to calibrate the yield properties with experimental results. Nevertheless, the thrust layout would indicate where the forces are likely to cause fracture (due to tension) or crushing (due to compression).

However, there are limitations to the TLO formulation. The reliance of TLO on a linear programming solver implicitly results in the assumption of associative friction. This could be included in a modified version of the proposed procedure and would likely need to be considered for usage as a general tool. Similarly, the issue of increasing problem complexity as the number of blocks in the assembly is noted. It has been noted that this issue could be addressed by staged refinement of the model, starting with a coarse blocking pattern. This strategy can be used (and demonstrated in this thesis) for the determination of strengthening measures as well, where the areas to be strengthened can be first identified using a coarse grid.

7.2 Conclusions

From the study presented in this thesis, the following conclusions are drawn:

- Thrust layouts, which are networks of forces, are presented to visualize the flow of forces in equilibrium in form-resistant structures. They have benefits compared with traditional funicular thrust lines as they permit tensile links within blocks, but not across block interfaces, and require self-weight to be mobilized within corresponding blocks—thus, they explicitly consider the block stereotomy of form-resistant structures. Thrust layouts are superior to Moseley's line of resistance (which is also referred to as a line of thrust by some) in that they represent flows of forces where the lines correspond to force vectors. Therefore, thrust layouts are presented as an enhanced means of representing equilibrated forces in form-resistance structures, at the same time resolving the issues caused by the competing, and often confused, notions of thrust lines in use.

- Thrust layout optimization (TLO) is presented as a general numerical procedure to estimate the load carrying capacity of form-resistant structures and to visualize the force flow within a structure as a thrust layout. The rich visualization of forces provided by the thrust layouts and the possibility of plotting the load transmissibility provide useful information to a structural engineer on how form-resistant structures resist external loads. The procedure does away with the case specific pre-processing sometimes required when applying the traditional thrust line method and explicitly considers the interfaces and friction capacities therein. In contrast to sophisticated non-linear numerical models, which require significant computer time and user expertise, the TLO method relies only on the availability of a linear programming solver and physically meaningful parameters in order to obtain solutions, such that it appears better suited for application in general engineering practice.

- An extended TLO formulation provides a physics-based tool for the determination of optimal placement of strengthening elements in masonry gravity structures, where current practice requires intuition and/or expert opinion. The new methodology presented has the potential to identify locations for strengthening measures that are structurally efficient but not intuitively obvious. However, with the corresponding thrust layout plotted, how the structural system works becomes clearly explainable.

Chapter 8

Recommendations for Future Work

There is scope to improve on the methodologies presented in the thesis. Also, the research work described can be used as a foundation for new lines of investigation.

- **Improving user readiness:** while the proposed TLO procedure has been shown to be especially useful in analysing form-resistant structures, the efficiency of the specific implementation used in the current study can be further improved—efficient generation and management of self-weight data as transmissible load groups and the efficient management of ground structure node, link data are identified as potential areas for improvement. Currently, the transmissible load groups are generated taking a brute-force approach and general-purpose open-source packages are used for the management of ground structure data. A ready-to-use tool—like LayOpt [148]—where a user can build a block assembly in a GUI, along with more efficient solving of the LP problem, would allow wider adoption of the technique proposed.

- **Staged refinement of blocking patterns:** the rapidly increasing requirement of computational resources when solving large scale problems is noted. This could be potentially addressed by employing a refinement strategy where the structure is first analysed with a crude discretization and subsequently refined based on previous results. In the refinement stages, those block interfaces which have the potential to reduce the load capacity estimate are added to the model. These critical interfaces can potentially be identified by observing the thrust layouts—i.e., areas with tensile forces. In contrast, in areas where the blocks simply act as 'ballast', a coarser blocking to represent the effect of the self-weight would be sufficient. While the current implementation allows for manually staged refinement by the user, an automated refinement process would

be useful. Furthermore, studying different refinement strategies and interpretations of the results from coarser patterns can give further insights into the behaviour of form-resistant structures.

- **Incorporating friction constraints more realistically:** the TLO formulation could see further refinements, particularly related to friction. While the current implementation is using an associative law of friction, it is noted (in Section 3.1.2) that this could lead to over-estimation of load capacity. This is likely to be especially important when modelling 3D examples such as hemispherical domes. Load capacity over-estimation can be checked by incorporating a re-analysis step with a modified friction constraint, e.g. using the approach adopted by Gilbert et al. [150].

- **Improvements to geometry post-processing when using TLO:** a geometry post-processing procedure is implemented to improve the visual clarity of thrust layouts. While this proved effective for small scale problems, the improvement in visual clarity diminishes as the problem becomes larger. The problem being readily separated into sub-domains (i.e., blocks) makes it ideal for parallel-processing, thereby benefiting from improved efficiency. However, the major bottleneck with the geometry post-processing are the interface nodes which also carry transmissible self-weight loads—they are locked in place due to them being constrained by both the interface and the transmissible load line. Providing an effective way to split them and allow them to move independently (separately along the interface and the transmissible load line) would allow further clarity to be achieved in thrust layouts.

- **Generating rigid block mechanisms from TLO solutions:** the nature of LP problems is such that a dual problem is solved parallel to the primal one—i.e., a dual kinematic problem is solved while the static problem is being solved. Using the dual problem, it is possible to obtain a deformation field for the nodes in the underlying ground structure. When the dual deformations from the TLO solution are considered, the nodes along the thrust layout would move (flow) along the force path while the other nodes (i.e., nodes which are in the original ground structure but not part of the thrust layout) will deform giving an overall form similar to that of a rigid block mechanism. The 'flow' of nodes along the thrust layout gives indentation-like deformations in the blocks, where thrust lines (i.e., compression links in the thrust layout) pass from one block to the other. Addressing this to generate rigid block mechanisms would further improve the visual feedback from TLO.

- **A TLO formulation for a form-generation tool:** while thrust layouts improve upon thrust lines by explicitly considering block interfaces and tensile forces within blocks, TLO provides an analysis tool implementing the ideas of thrust layouts. While the analysis tool can be repeatedly applied to check, or even optimize, a design, a complementary design tool implementing thrust layouts would be an interesting potential new line for investigation. In this, several potential avenues of investigation are available: (1) following the idea of force networks for shells, and recent developments by Bołbotowski [116], but accounting for block stereotomy; (2) making use of optimal stress-regions (following Fairclough [217]), and studying the stress-regions identified from analysis problems, a ground structure based design problem may be formulated; (3) a ground structure formulation with explicit representation of interfaces in the ground structure, around the nodes which are representing potential blocks (and carrying transmissible loads).

- **Optimal strengthening measures with practical considerations:** the current work identifies the theoretical optimal locations of external strengthening measures while offering the potential for practical considerations to be accounted for via a richer cost function. Also, the need to consider the crushing and tensile strength limits of the material is noted. These aspects need further investigation taking practical considerations into account.

- **Externally tensioned structures:** there exist a handful of classic examples of externally tensioned form-resistant structures, designs of which were based on a structural designer's intuition and understanding of the structure. As case studies, it would be interesting to see how these structures compare with corresponding optimized structures obtained using extended TLO.

Appendix A

Journal Paper: *Shell Structures: Lessons in Structural Efficiency for Sustainable Construction* *

*Nanayakkara, K.I. (2020). 'Shell structures: lessons in structural efficiency for sustainable construction'. The Structural Engineer, 98(4): 8-17.

Shell structures: lessons in structural efficiency for sustainable construction

KAVINDA ISURU NANAYAKKARA
BSc, CPGS, MSc
PhD Student, University of Sheffield, UK (formerly at University of Moratuwa, Sri Lanka)

SYNOPSIS

Shells are a highly efficient, lightweight structural form that have been used in construction for thousands of years. Shell structures can be formed from a wide range of materials – from compressed earth to concrete – allowing local materials to be used in their construction. However, social and economic factors mean that local materials are often perceived as inferior to steel or concrete in developing countries.

In this article, stemming from his Pai Lin Li Travel Award in 2018, Isuru Nanayakkara looks at traditional technologies and modern approaches to lightweight shell construction to seek a better perspective on how shell technology can be appropriated to different local contexts.

Introduction

As we move towards a sustainable planet, the developing world is faced with the dilemma of a need for rapid expansion of housing and infrastructure on one hand and the constraints of sustainability on the other. However, a closer look at local strengths and technology elsewhere can lead to creative solutions.

Shells are a more efficient structural form than the widely used column–beam frames, which make use of bending strength and hence underutilise the structural capacity of materials. Superior structural efficiency allows shell structures to be lightweight, reducing the demand for materials. The wide range of possible material solutions – from compressed earth to concrete – allows for an appropriate local material to be used in the realisation of the structural form.

Shell structures are by no means a modern invention. Evidence of the earliest vaulted structures comes from Mesopotamia in 3000BC: a 5000-year-old Mesopotamian burial chamber with a barrel vault of approx. 1m span is on display at the Berlin Museum of Prehistory and Ancient History[1].

The Roman arch, the bridges and cathedrals of Renaissance Europe, Barcelona's *Modernisme* movement, and Guastavino vaulting on the east coast of the USA have left us with a rich collection of form-resistant shell structures. More modern examples include Hassan Fathy's reinvigoration of the Nubian technique, Heinz Isler, Frei Otto and Pier Luigi Nervi's compression-only shells, followed by Jacque Heyman's safe theorem giving a systematic approach to designing compression-only shells.

This article looks at traditional technologies (and adaptations thereof) and explores new frontiers in lightweight shell construction. An understanding of the sociocultural impacts of these structures, technologies and materials will give a better perspective on how technology can be appropriated to different local contexts.

Knowledge for this article was gathered from travels to India, Europe and the USA; the former two funded by

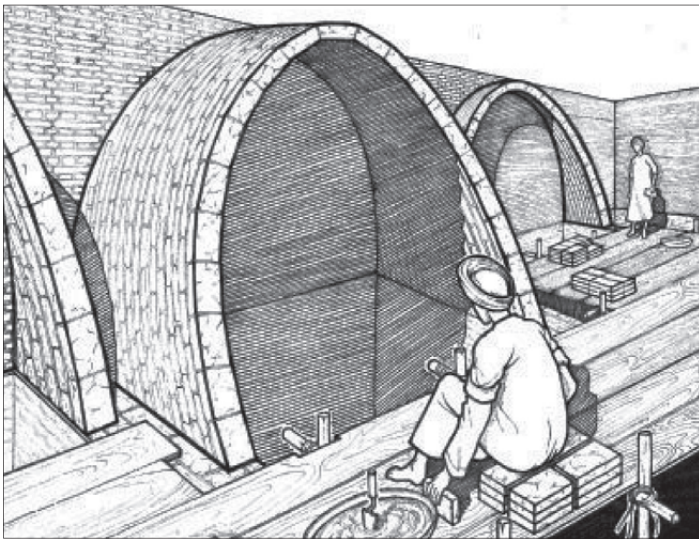

FIGURE 1: Nubian vaulting technique[2]

MAINI & DAVIS

the Pai Lin Li Travel Award presented by the IStructE Educational Trust.

Design philosophy: an exploration

The arch as a structural form came into being when beams were no longer able to bridge increasingly long spans. Vaults and domes may also have evolved for this reason, although some historians and architects suggest that domical roofs in cathedrals are suggestive of heaven or the realm of gods. Nonetheless, vaults and domes (the most common early shell geometries) were used for different functions and built from different materials in different places around the globe.

Nubian technique

Earthen structures as practised by the Auroville Earth Institute (AVEI), a partner institute of the UNESCO Chair of Earthen Architecture, are not necessarily a traditional Indian technology, but rather a mindful adoption of the Nubian technique, as popularised by Egyptian architect Hassan Fathy. However, significant improvements to the design methodology, production of material and construction have taken place at AVEI during its 30 years of existence.

The Nubian technique originated in southern Egypt, with the famous vaults of the granaries of the Ramesseum at Gourna testament to the success of the technique. The basis of the Nubian technique is that the earthen blocks adhere to each other with an earthen binder **(Figure 1)**[2]. The dryer blocks draw in water by capillary suction and the clay components of the soil act as an adhesive to bind the blocks.

Traditionally, the Nubian technique requires a back wall to mark the curve and 'lean' the first course of blocks. The vault is built as a sequence of arches slightly leaning on each other. The binder is a silty-clayey soil (traditionally from the Nile) and a binder layer of 10–15 mm is used with sun-dried earthen blocks.

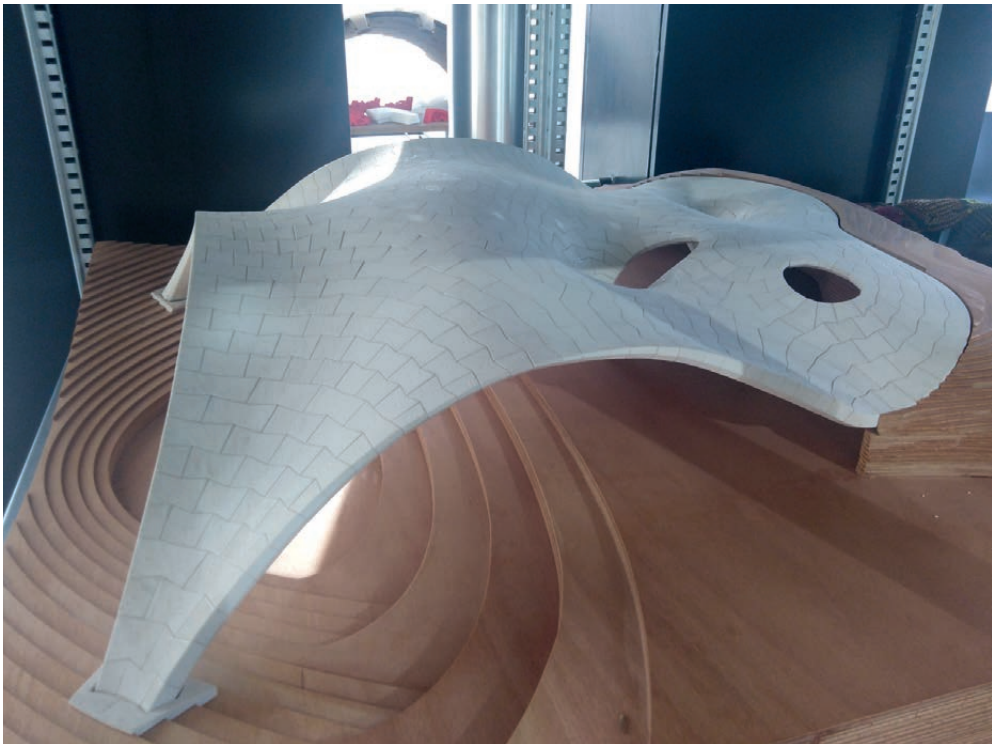

↑**FIGURE 2:** Model of proposed MLK Jr Pavilion in Austin, Texas

Catalan vaulting

In contrast to the heavy, thick masonry shells of the Nubian technique, Catalan vaulting (known as Guastavino vaulting in the USA) uses multiple layers of very thin tiles (usually three layers of 15–20mm thick tiles).

Catalan vaulting is also a free-spanning technique, using guides to define the geometry in space. This makes it an interesting technique to be used with free-form shells such as that proposed for the Martin Luther King (MLK) Jr Pavilion in Austin, Texas **(Figure 2)**. The first layer of a Catalan vault is built in space with a fast-setting gypsum mortar. The subsequent layers are built with the first layer acting as the formwork.

↙**FIGURE 3:** Guastavino vaulted ceiling at Oyster Bar in Grand Central Station, New York

> **CATALAN VAULTING IS ALSO A FREE-SPANNING TECHNIQUE**

There are many examples of Catalan vaulting in both Barcelona and the USA. Examples in Barcelona include Teatre La Massa (Rafael Guastavino), a factory building in Terrassa (Lluís Muncunill i Parellada), Palau de la Música Catalana (Lluís Domènech i Montaner) and Restaurant En Ville (Guastavino).

Examples in Boston include the Boston Public Library, the patio of the Boston Coast Guard building and Fariborz Maseeh Hall at MIT, while examples in New York City include the Municipal Building on Chambers Street, Queensboro Bridge, and the Oyster Bar at Grand Central Station **(Figure 3)**. All these US examples were designed and built by the Guastavino company.

Gaudí's forms following forces

With an understanding of the flow of forces, gained from his physical models, Antoni Gaudí was able to use the full

canvas of the three-dimensional (3D) space to produce some wonderful structures. Although one might be hesitant to call them shells, they follow the principle of form resistance.

Park Güell houses simple examples of forms following forces **(Figure 4)**, whereas La Sagrada Família, Colònia Güell, Casa Milà and Casa Batlló depict more elaborate expressions of this idea.

Similar yet different

All three traditions of shell structures – Roman, Nubian and Catalan – do the same fundamental thing: they carry loads primarily in compression. However, there are interesting differences in (i) how they account for variable loading, and (ii) how the lateral thrusts at supports are resisted.

Accounting for variable load

Like Roman arches, the heavy Nubian vaults have a much higher self-weight in comparison to variable loads. Also, these shell structures are typically used as roof structures rather than slab systems. Thus, the self-weight itself is the significant loading and the effects of variable action can be reasonably accounted for by having a 'safety margin' on the thickness of the shell.

> **ALL THREE TRADITIONS DO THE SAME FUNDAMENTAL THING: THEY CARRY LOADS PRIMARILY IN COMPRESSION**

Catalan vaults are used as slab systems **(Figure 5)** and have a much thinner shell. As such, the variable loading is a significant factor for the safety of the structure. Catalan vaulted floor slabs account for the variable loading by having vertical stiffeners **(Fig. 5c)**. Furthermore, the doubly curved shell is extremely stiff and is capable of safely carrying asymmetric loadings due to its multiple load paths. This was masterfully exploited by Guastavino **(Fig. 3)**.

The next generation of 'engineered' shells can be observed at the Institute of Lightweight Structures (ILEK) in Stuttgart: the SmartShell **(Figure 6)**. This 40mm thick timber shell of 10.28m span and 3.57m rise has three supports which can be actively controlled and one stationary support. The shell is sized to resist only the permanent actions. The variable loads are resisted by the active control of the structure at the supports **(Fig. 6b)**. A 0.4kN/m^2 additional load on one quadrant gives a maximum stress of 11.2MPa; by adjusting itself through active controls, the shell can reduce the maximum stress to 3.2MPa.

The hand-off point between the mass-resistant system and the active-control system (i.e. the material utilisation factor) is determined based on energy: the embodied energy of the material that resists permanent loads and the actuation energy required for active control of the structure. Further research on active-control structures continues at ILEK Stuttgart.

Resisting lateral thrust

The heavy masonry structures observed in Auroville (Nubian technique) and in traditional masonry structures (i.e. Roman arches) use masonry buttresses to safely carry the large horizontal thrusts created. In contrast, lightweight Catalan vault systems use steel tie rods **(Fig. 5a)** to carry the horizontal thrusts.

These tie-back techniques are observed in more modern projects by the Block Research Group (BRG) at ETH Zurich. The Armadillo Vault for the Venice Biennale in 2016 used steel support plates tied back with steel rods so as not to damage the historical floor of the exhibition hall. The ETH Zurich pavilion for the 2015 Ideas City festival in New York did not use any ties. The lighter weight of the vault (due to the material used) meant that the stability of the stack of timber pallets supporting the vault (tied together to act as a single unit) could be guaranteed by weighing down the timber pallets with ballast loads.

Gaudí took a different view of transferring the thrusts from heavy shells. Instead of traditional buttressing, which stays true to the concept of rectilinear spaces, he used inclined columns to support the random rubble vaulted viaducts at Park Güell **(Fig. 4)**. These are oriented so that the columns primarily resist axial loads and minimise bending moments.

Prinzip leichtbau

The lightweight principle presented by Frei Otto compares masses and how they can transmit forces. The ability to transmit forces (*Tra*) is quantified using the force that can be transmitted (*F*) and the length of the load path (*s*). This extends the concept of form and forces to include masses. With masses brought into the mix, it is now possible to relate form and forces to energy and cost – which are much easier parameters for the public and policy makers to comprehend.

In ILEK publication IL 24, Otto presents a parameter called *Bic* (with units g/Nm), which is the ratio of mass to *Tra*. An interesting observation from his study is that tension systems (e.g. cable nets)

FIGURE 4: Gaudí's forms following forces, Park Güell, Barcelona

a) Domed roof slab

b) Vaulted viaduct

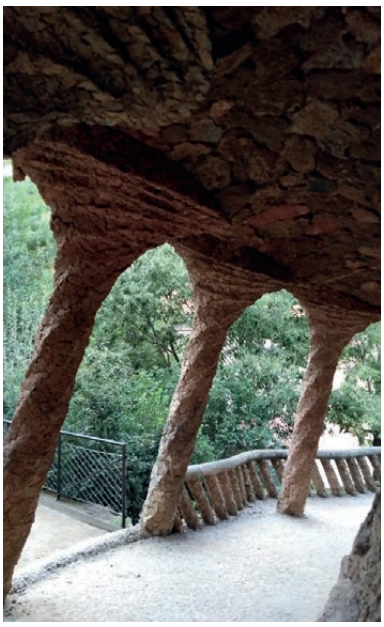

c) Tilted columns

will always give a lighter-weight solution than a compression-only solution (e.g. compression shell), although the latter still gives a positive *Bic* value.

This shows that compression-only shells are not the end of the path for optimising material usage – lighter-weight solutions can be found. However, considering the material at hand (e.g. materials with low tensile capacity) or other constraints, a compression-only solution may be the best one can aim for.

Design methodology: from intuition to the information age

Structural analysis of compression-only forms has evolved over the years. But all the methods of analysis observed during this study were based on one fundamental idea – Robert Hooke's observation of the hanging chain: 'as hangs the flexible cable, so but inverted stands the rigid arch'.

Physical models

Antoni Gaudí

Physical models are the most fundamental manifestation of Hooke's observation. Gaudí made extensive use of physical models **(Figure 7)** which are daring in their size and complexity, as are his realised structures.

Hanging-chain models are a more complex manifestation of Hooke's hanging chain. Different weights are attached to nodes to represent the loadings on the structure, due to self-weight or otherwise. Unlike Heinz Isler's models described later, the hanging-chain model is not rigidified, but the inversion is done on paper with the geometry measured from the hanging-chain model. Gaudí used a glass mirror to get a sense of the inverted shape generated.

Heinz Isler

Isler's physical models are much simpler. The scale model in **Figure 8** is a hanging-cloth model rigidified in plaster of Paris (gypsum plaster), which also include cables to resist the horizontal thrusts. It was built as a form-finding model for the Norwich Sports Village roof structures in the UK[3].

Frei Otto

ILEK – under Frei Otto's guidance – developed a systematic approach and expertise in using hanging-chain models for form-finding of compression-only structures. These approaches were developed for projects such as the Mannheim Multihalle and the Munich Olympic Stadium in Germany (the former is a timber gridshell and the latter a cable-net structure). Note that gridshells, although not fully solid, are considered shell structures and are designed to have minimum bending forces.

A 1:500 scale model (design model) was first built to get a sense of the size and the form of the structure. A 1:100 scale model (form-finding model) was then built to carry out a rigorous form-finding exercise and determine the final geometry. Playing around with these scale models gave a better understanding of the force flows and the final geometries were adjusted based on the understanding gained. Separate models were used to extract the geometry and member forces.

↑FIGURE 5: Catalan vaulted slab system in old weaving mill in Vilassar de Dalt, Spain

↓FIGURE 5: Stuttgart SmartShell

Three methods were developed at ILEK to take measurements of the geometry from a hanging-chain model. A measurement table with a pointer to drop a plumb line was the most basic method used. Measurements with a precision of ±0.1 mm are possible with this method. Aerial photogrammetry for cartography adjusted for close range was a more advanced method used. This can achieve a similar level of accuracy, but the technology of the day meant it was time-consuming and costly. Parallel light measurement was the third method used.

From line of thrust to thrust network

The concept of 'line of thrust' (or thrust line) has been attributed to Thomas Young (1817), Franz Joseph Ritter von Gerstner (1789), Méry (1840) and Henry Moseley (1835).

Jacque Heyman's safe theorem is the formalisation of Hooke's observation and concept of the line of thrust into the realm of limit state analysis. Heyman's safe theorem states that 'if a set of internal forces in a masonry structure can be found that equilibrate the external loads, and which lie everywhere within the masonry, then the structure is safe – safe in the sense that it cannot collapse under those loads (i.e. a lower-bound solution)'.

In 'The stone skeleton'[4], he describes this safe theorem and notes the corresponding uniqueness theorem with the additional requirement of the thrust line allowing '… the formation of sufficient hinges to transform the structure into a mechanism'.

At AVEI, Heyman's safe theorem is

used with Karl Culmann's graphic statics and James Clerk Maxwell's force and form duality to generate lines of thrust. With years of experience in design and construction, AVEI has developed its optimisation method. This is an empirical set of rules that can be used to optimise the thickness of vaults constructed of known geometries (e.g. segmental arch, pointed arch, equilateral arch, Egyptian arch).

The optimisation procedure relies on a fundamental understanding of hanging-chain models: if the line of thrust moves out of the middle third near the crown, increase the thickness near the support.

Since AVEI uses a 2D canvas as its design space, this methodology is only applicable to vaults – i.e. extrusions of 2D cross-sections. A 3D geometry, as in a dome, would have a 3D force flow. In a 1921 textbook on graphic statics, William S. Wolfe describes a graphical analysis method to analyse the equilibrium of domical shells by considering both meridional and hoop forces.

A full 3D analysis considering Heyman's safe theorem (and improvements thereof) is only possible using computers. The idea of a line of thrust then becomes a thrust network in the 3D case. In fact, the cable nets used by Gaudí (e.g. **Fig. 7**) are physical representations of force networks.

In his PhD thesis, Prof. Philippe Block presents thrust network analysis, which is a form-exploration tool where he merges Heyman's safe theorem and Clerk Maxwell's reciprocal diagrams. At BRG, thrust network analysis is implemented as a plugin for the Rhinoceros CAD platform – as RhinoVAULT – and in the open-source computation platform developed at BRG – COMPAS.

Both these tools facilitate analysis of 3D shells via evaluation of the equilibrium of a 3D force network representing the shell.

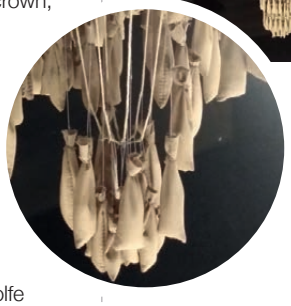

↑**FIGURE 7:** Hanging chain model of La Sagrada Familia, Barcelona

↘**FIGURE 8:** Heinz Isler's scale model for roof structure of Norwich Sports Village tennis court

It is important to note that thrust network analysis has been developed as a form-exploration tool, and as such is not only capable of analysing existing shell structures but also coming up with free-form compression-only shells – e.g. the Armadillo Vault. However, the form-exploration capabilities come at the cost of analysis being possible with parallel sets of loads only (e.g. gravity load).

Non-structural design aspects

The design requirements also include non-structural aspects. The possibility of building free-form structures – as opposed to the rectilinear footprints and elevations we are so used to – is one advantage of shell structures. In contrast, the acoustic performance of shells – reverberations and echo – could be either beneficial or problematic.

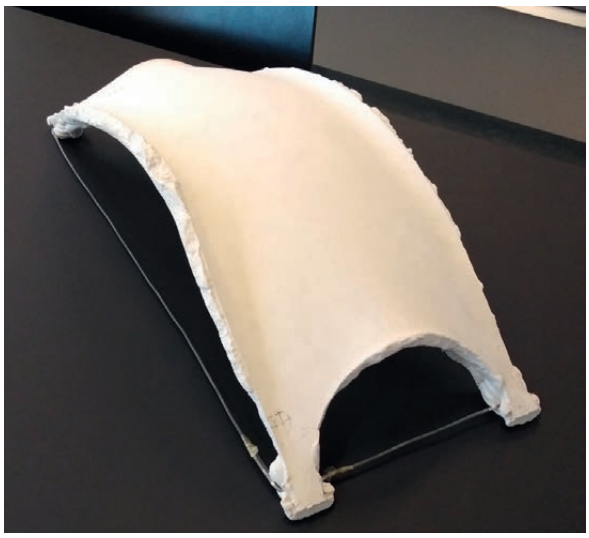

> **THE CABLE NETS USED BY GAUDÍ ARE PHYSICAL REPRESENTATIONS OF FORCE NETWORKS**

The MLK Jr pavilion **(Fig. 2)** and the Armadillo Vault by BRG are examples of the free-form possibilities of shell structures. Both these projects made use of the form-exploration capabilities of the software developed at BRG (RhinoVAULT and COMPAS). Maya Somaiya Library for the Shri Sharda English Medium School in Maharashtra, India, designed by Sameep Padora and Associates, is an example of RhinoVAULT being used by a group independent of BRG to design a free-form shell structure.

Raphael Guastavino Jr. was interested in acoustic architecture. Along with Wallace Clement Sabine – a professor of physics at Harvard – he improved the acoustics of the Catalan thin tiles and produced six patents related to acoustical innovations. The aim of these developments was to reduce reverberations by absorbing sound rather than reflecting it. This worked too well and was a problem in churches where the reverberation of sound is an important characteristic.

AVEI has also studied this problem, identifying three reasons for the high level of reverberations in vaults and domes: (i) the relatively large volume created by the vaulted structure; (ii) the propensity of the shape to reflect sound; and (iii) the surface quality of the materials of the shell interior.

At AVEI, Helmholtz resonators (single resonator absorbers) made of PVC pipes or clay pots are used to absorb sounds

↘**FIGURE 9:** Examples of clay pots or tube being used as resonator absorbers[2]

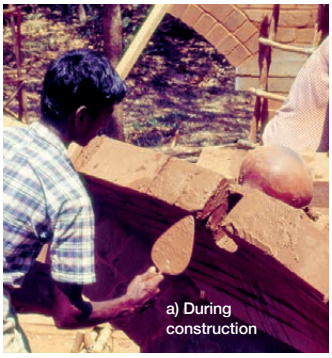

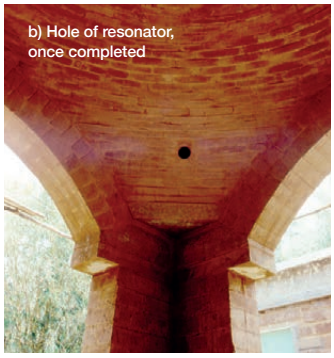

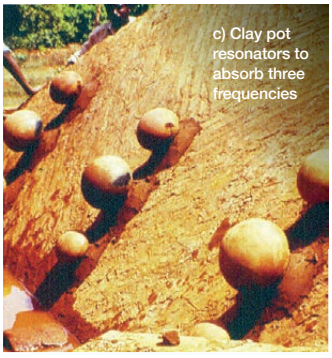

© DAVIS & MAINI

(Figure 9). This reduces echo in spherical domes and segments thereof. Echo is rarely an issue in other types of domes (e.g. pointed domes, groin vaults).

Construction: from earthen masonry to concrete and beyond

Material plays an integral role in compression-only structures. In fact, the need for a compression-only shell stems from the masonry itself not being able to carry significant tensile stresses.

Construction materials

Unbonded stone

Early Roman arches were made of unbonded dressed stones. BRG demonstrated the possibility of thin shells with unbonded dressed stones at the Venice Biennale in 2016 with the design and construction of the Armadillo Vault.

As well as highlighting possibilities with shell structures, the Armadillo Vault was a showcase for the material technology involved. The shell was discretised to blocks considering the principal stress directions and interlocking of blocks. The fabrication and assembly processes were also considered in the discretisation: smaller blocks would mean a longer construction time but larger blocks would be heavier and difficult to handle.

A five-axis CNC (computer numerical controlled) machining process was used to cut the limestone blocks to the required geometry. Considering the time constraints, the geometry was selected so that the extrados face was planar, requiring cutting in only one face. Further, all the contact faces were maintained as planar surfaces to enable a single cut with a circular saw. The curved intrados surface was formed by CNC cutting grooves at close spacings and then hacking away the resulting stone fins to give a rough surface.

> “ISLER’S SHELLS ARE A CLASSIC EXAMPLE OF THIN CONCRETE SHELLS

FIGURE 10: Wyss Garden Centre in Solothurn, Switzerland

Bonded masonry

Bonded masonry is used in both Catalan vaulting and Nubian vaulting technologies. But the blocks and the binder used are different and demonstrate the possibility of adopting a local material for construction of compression-only shells.

Catalan vaulting uses a thin burnt clay tile of 15–20mm thickness. The shell is typically of three layers, giving a shell thickness of less than 100mm, with a 10mm mortar layer between courses. The thinness of the tiles is essential to make full use of the optimal shape of the shell.

The construction process does not involve any formwork and the first layer of tiles acts as the formwork for subsequent layers. A system of guides is used to mark the geometry of the first layer (discussed further on). The first layer is built free standing and requires a fast-setting mortar. Gypsum mortar is used in Catalonia, where it is readily available.

In contrast, good-quality gypsum is not easy to come by in southern India (and in many other places) and would be expensive. The Nubian vaulting practised in Auroville therefore uses a completely different construction system: cement-stabilised and compressed earth blocks (CSEB) with a cement-stabilised clay mortar. The blocks are typically 9cm thick and the plan dimensions range from 19 × 9cm^2 to 39 × 9cm^2.

The construction proceeds without formwork. The clay mixture is applied to the block to be fixed, and the surface to which it is to be attached is wetted. Then

↑FIGURE 11: Glass dome at ILEK, University of Stuttgart

the block is placed. The block is pressed on with a repetitive left, to right, to left sliding motion. During this process, most of the clay mortar extrudes out from the sides. An excessive amount of mortar is initially used to guarantee a void-less bond.

Once a scratching sound is heard, the block can be released and will stay in place. For a skilled bricklayer this process will take less than 30 seconds. If the position of the block is not correct, the brick and the binder must be removed, and the surface cleaned before the block is re-laid. The block should not be tapped in to place as is done with regular masonry work.

The blocks are 5% cement stabilised if the soil is a sandy soil. Lime stabilisation is recommended for clayey soils. The blocks are cured under shade for two weeks and then for a further 4–6 months in the open before they are ready for use in construction.

The embodied energy of the blocks is shown to be less than 10% of that of fired bricks (6122.54MJ/m^3 for a fired brick and 548.32MJ/m^3 in CSEB bricks produced in Auroville). The blocks are also claimed to be 15–20% cheaper than fired bricks – although in a context where labour is cheap and good-quality soil is readily available.

The mortar used is also a cement-stabilised earthen mortar, typically stabilised 1.5 times more than the blocks. The mortar includes sand to reduce the effects of drying shrinkage. The mix proportions and the fluidity of the earthen mortar depend on the characteristics of the soil and the usage of the mix (e.g. type of vault). AVEI has developed guidelines for the mix proportions and simple *in situ* tests to check the consistency of the mortar.

Concrete shells

Isler's shells are a classic example of thin concrete shells. The Wyss Garden Centre in Solothurn, Switzerland was built in 1962 **(Figure 10)**. This is a geometric shell (with a thickness of 70mm), but has a cantilevered edge (with a maximum cantilevered length of 3.5m) which mimics the upturned lips observed in hanging-cloth models. These lips act as edge stiffeners, in lieu of bulky edge beams.

The twin, 31.6m long, 26.0m wide, three-point-supported, prestressed concrete shells at a highway service station in Deitingen, Switzerland (built in 1968) are another classic Isler shell. This shape was derived from a hanging-cloth model. The shells are 90mm thick and the doubly curved nature gives it a high load capacity.

Rosenstein Pavilion, built by ILEK, is a segmental concrete shell structure. The porosity of this 3cm thick shell is to give an illusion of a translucent material, while still being identified as a shell. The need for segmental shells came out of the limitations in constructing the shell as a single unit. Precast sections are bolted using M4 bolts along the connecting edges. The compression-only shell (under self-weight) guarantees that the bolts do not have to carry any bending.

The concrete shell floor system developed at BRG is a 2cm thick, unreinforced, doubly curved ribbed slab. The complex rib pattern is to activate the compression shell action, and external steel ties are used to resist the horizontal thrust. This system is found to result in a 70% cost reduction compared with conventional concrete slabs. However, the complex formwork required to achieve the rib pattern makes it more suitable for a repetitive floor footprint.

A full-scale prototype of the HiLo roof shell was constructed at ETH Zurich using fabric formwork supported on a cable net. Node markers of the cable net were used to monitor its

↘FIGURE 12: Blocks made of recycled beverage carton boards, used for BRG pavilion at Ideas City Festival 2015 in New York

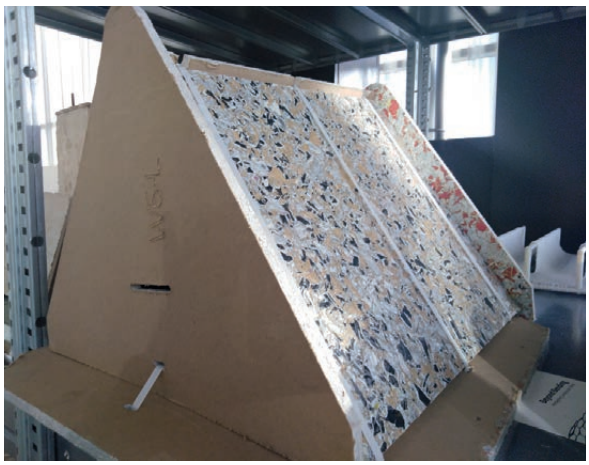

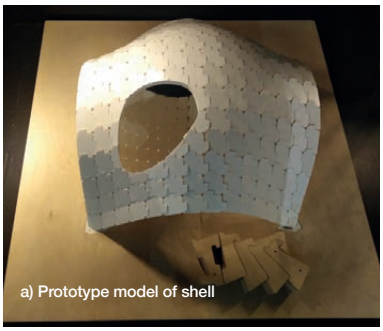
a) Prototype model of shell


b) Segment of timber block assembly


c) Single timber block

↑FIGURE 13: Surface expanded joinery system developed at IAAC

geometry, and to adjust the net if necessary. The adjustments were not straightforward, since the nodes do not move independently. Hence, a control algorithm was developed to determine the adjustments at the boundary such that the differences in node geometry – from planned to observed – are minimised.

A reinforcement net was provided and grade C90 concrete was used to reduce the likelihood of shrinkage cracking. Sprayed concrete was used to give the desired thicknesses of 3–12mm, as required. Once the concrete had set, both the cable net and fabric formwork were removed. The cable net was prepared for this specific project and is not readily reusable, but this method allows for greater control of shell geometry.

Glass shells

A few experimental shells were produced at ILEK in Stuttgart using glass as the construction material. The glass dome in **Figure 11** is a segmental spherical dome of 8.5m span and 6m radius, giving a rise of 176cm. The glass is 1cm thick, giving a slenderness ratio of 1:850, making its relative thickness smaller than that of an eggshell (0.3mm thick). The shell is of 44 panes of chemically tempered float glass bonded with a 10mm thick stiff adhesive and supported on a titanium ring fixed to a base by 32 stainless steel supports.

Recycled waste

BRG has previously completed a project using hollow blocks made of recycled beverage cartons: a temporary pavilion for the 2015 Ideas City festival in New York. The doubly curved shell covers an area of 20m^2 and consists of 442 unique blocks in 34 arches. The arches span between two stacks of ballasted wooden pallets. Triangular prismatic blocks were made from 9mm thick boards **(Figure 12)**, produced by ReWall by compressing shredded cartons without the addition of any binders. The blocks were CNC cut and then manually assembled and strapped.

Timber shells

The Institute for Advanced Architecture of Catalonia (IAAC) has developed a formwork-less construction system for shells with interlocking timber blocks **(Figure 13)**. The timber pieces are made by gluing together layers of plywood boards, cut in different shapes. The notches (or cuts) are to facilitate interlocking and to prevent blocks knocking each other at the edges.

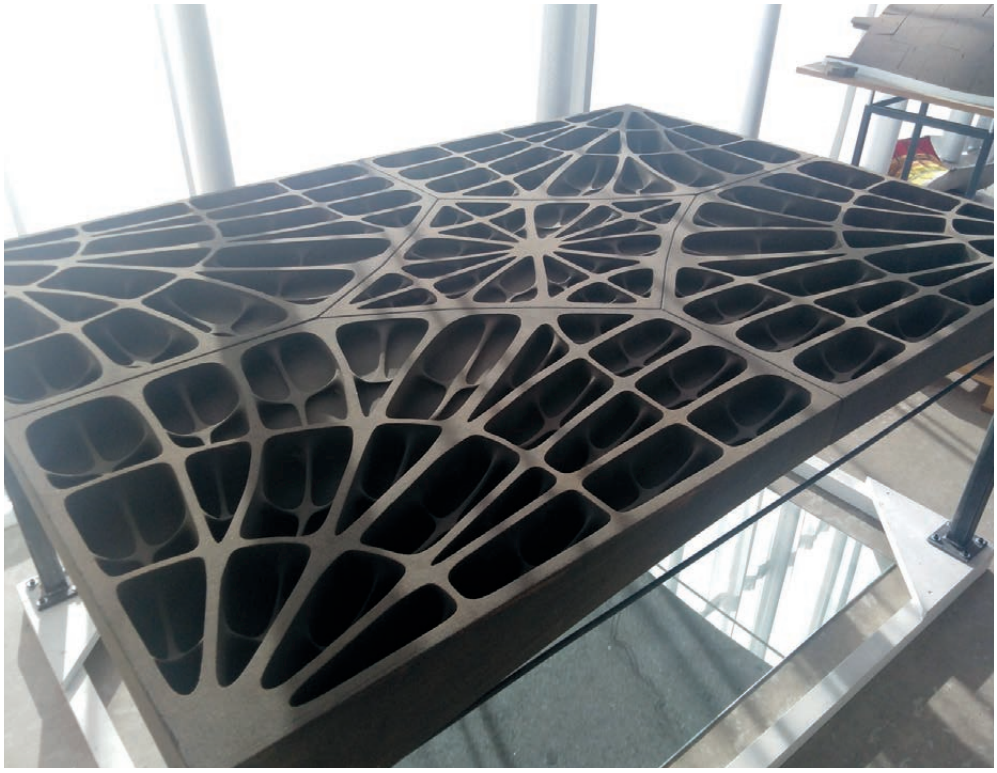

↑FIGURE 14: 3D printed slab system developed by BRG

3D printing

The compression-only shell floor system designed by BRG was first cast using concrete. This was subsequently tested with 3D printing, using a silica sand bonded by phenolic binders **(Figure 14)**. However, this technology is still in its infancy (with regards to building of structures) as the strength of the printed material is limited and integration of steel reinforcement during printing is difficult.

Formwork, falsework and free spans

Some type of formwork or falsework is required to keep track of the geometry of a shell during construction. Free-spanning construction techniques, such as the Nubian technique and Catalan vaulting, do not require any formwork, but guide work is required. Building free-form shapes with irregular geometries would require elaborate guide systems. However, in some cases, formwork is unavoidable as there are no intermediate stable geometries and the stability comes from the whole system working together (e.g. the voussoirs making up an arch).

Figure 15 shows guide work developed at AVEI for construction of prototype domes. The same technique has been used in various projects carried out by AVEI, including the segmental elliptical dome (22.16m span, 7.9m rise and 22.16m base diameter) for the Dhyanalinga Temple[5]. Although some early problems were encountered, regular checks with height surveys and extreme care with tape measurements


a) Segmental pointed dome


b) Cloister dome


c) Conical dome


d) Spherical dome

↑**FIGURE 15:** Compasses developed at AVEI

ensured that the dome was completed successfully, with an accepted tolerance of 2–3mm from the defined geometry.

A free-spanning technique inspired by the Nubian technique has been developed at AVEI. This distinguishes between horizontal courses – blocks laid in a length-by-width surface – and vertical courses – blocks laid in a breadth (or length)-by-height surface. This is made possible by the various block sizes manufactured at Auroville and the vaults generally having a wider base and a thinner crown.

The number of horizontal courses is based on the height of the leaning wall segment that can support its own weight, i.e. the moment of the horizontal courses about the vertical line passing through the intrados at the support should be balanced **(Figure 16)**. Beyond that, the vertical courses commence. The first vertical course requires a side wall to adhere to or temporary formwork to support it. The subsequent vertical courses can be built sequentially, providing safe load paths to the intermediate stages of construction.

The construction sequence needs to be decided during the design stage: the decision is based on equilibrium analysis, but the number and size of the blocks needs to be determined well before construction begins.

Different types of guide work for thin tile vaulting have been tested in various free-form shell construction projects. Simple guide work has been used for vaults (which are essentially extrusions of arches). Two steel frames are placed at either end of the longitudinal axis of the vault and guide strings are run between the two guide frames. This system was used in BRG's SUDU urban housing project in Ethiopia. A skeletal structure made of freely bent rebars was used as guide work for two Catalan free-form shells built at IAAC's Valldaura Labs and at the Universitat Politècnica de Catalunya in Barcelona.

In some cases, it is not possible to avoid formwork. In the New York pavilion project, BRG used temporary guide work supported on a moveable industrial lift to support the blocks. Once settled under self-weight, the thrusting between the blocks could keep them in place. A tensioned cable was also sent through the blocks (along the axis of the arch) as additional support.

The Armadillo Vault used timber skeletal formwork to support the stones until the keystone was placed and the shell was able to carry its own weight. The block placement was assisted by grooves in the blocks. A total station was used to locate the exact positions of the blocks and wooden shims were used to make finer adjustments to the position.

The shell started to carry its own weight only after the formwork was decentred and the blocks settled into their final positions. The decentring sequence was crucial as the decentring is equivalent to applying a large asymmetric load to the shell.

Formwork for the Armadillo Vault was placed on eleven independent scaffolding towers which allowed for a gradual and sequential decentring.

This was done in a circular pattern with stiffer parts decentred first. The scaffolds were lowered in stages of 0.4mm in each cycle. Falling of shims indicated that the shell was no longer supported by the formwork but was supporting its own weight. A final maximum settlement of the shell of 4mm was measured.

Socioeconomic dimensions

Structural efficiency or material technology alone do not determine the successful adoption of a construction system. Social and economic reasons can force out certain technologies, as evidenced by many historic events.

The rise of thin tile vaulting on the east coast of the USA was primarily due to the fire resistance characteristics of this construction – which timber structures of the day were unable to fulfil. The load-carrying capacity of the system was not a priority, although it had a superior load-carrying capacity due to its double curvature.

In a similar vein, the downfall of the Guastavino company and thin tile vaulting in the USA was not due to the introduction of a superior material or a structural system. In the 1940s, concrete was simply seen as 'the material of the future', although thin tile vaulting was a far superior load-carrying system.

In the current world of hyper-connectivity, the same can be observed in developing countries. People view concrete and steel construction – primarily using imported materials and technology – as 'modern' and regard earthen construction as 'poor quality'. This view neglects both the economies of using local materials and the local climatic conditions under which the earthen constructions are likely to perform far better (in terms of creating liveable spaces).

Auroville is an exception to this – or rather a case study of how people's mindset can play a role in wise adoption of technology. Auroville is a global village founded in southern India in 1968. It aspires to live by the four main ideas of the Auroville Charter: Auroville (i) belongs to no one in particular; (ii) is a place of unending education; (iii) is a bridge between the past and the future; and (iv) is a site of material and spiritual research.

This environment has created an ideal platform for the development of earthen construction technologies and their successful implementation. Many structures there are earthen shell structures using Auroville's take on the Nubian technique. Elsewhere in India – as in many parts of the developing world – earthen construction is looked down upon.

In contrast, Casa Milà is an example of structural efficiency and architectural beauty dictating the terms regardless of people's perceptions. People are said to have mocked this 'strange' house built for an elite family in Barcelona. But 100 years later, it is one of the main tourist attractions in the city. The proposed MLK Jr Pavilion project in Texas is an example of local availability being a primary reason for the choice of material. However, although these exceptions may exist – especially for marquee projects – people generally like to have new things: novelty is perceived as an indicator of quality.

The future: opportunities, possibilities and challenges

The many projects mentioned in this article demonstrate the potential of shell structures in producing aesthetically pleasing, efficient and sustainable structures. However, in many cases – apart from Auroville – these have been used mostly in landmark structures rather than everyday public spaces or domestic dwellings.

It remains possible – and necessary in view of the call for a sustainable construction industry – to make shell structures a more common structural form: from domestic dwellings to public spaces and landmark structures. The Stuttgart SmartShell demonstrates the potential to use shells in the next generation of structures: active-control structures.

However, there remain key challenges in using shells as structural systems. One of the main issues is the rigorous development of material technologies and simultaneous development of codes of practices. The variability of material properties and the vast range of possible material solutions will be a challenge in developing relevant codes of practices.

HAVE YOUR SAY

tse@istructe.org

@IStructE
#TheStructuralEngineer

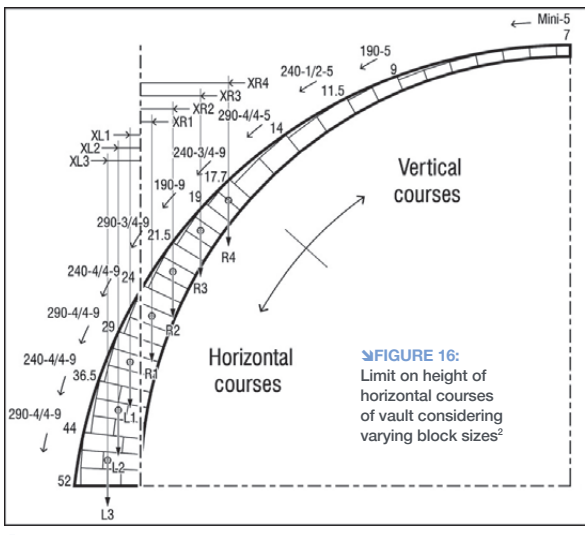

FIGURE 16: Limit on height of horizontal courses of vault considering varying block sizes[2]

MAINI & DAVIS

One of the key missing pieces in a fully earthen construction is the slab system. Catalan vaulting has demonstrated the potential of shells to be the structural component for an earthen slab system. However, Catalan vaulting may not be possible everywhere in the world. Other local material technologies need to be developed and tested, with earthen slab systems based on shell forms.

But the greatest challenge of all is how to convince engineers and the general public of the merits of using the structural efficiency of shell structures; that shells are not just part of history, but the future as well.

Conclusions

In conclusion, it is recognised that:

- there are several local traditions in building shell structures, which are practised around the globe
- various tools have been developed and used for analysis of shell structures, all of which can be traced back to Hooke's observation of a hanging chain
- the different material technologies used with shell structures include unbonded and bonded masonry, concrete, glass, timber, and even recycled materials and 3D printed materials. Allied construction methods have also been developed
- there is a genuine interest among researchers in showcasing the benefits of shell structures in moving towards a sustainable construction industry.

However, the biggest obstacles to more widespread use of shell structures appear to be:

- people's perception
- the lack of design freedom in rigid design and building codes.

REFERENCES

1) Kurrer K.-E. (2008) *The History of the Theory of Structures*, Berlin: Ernst and Sohn

2) Maini S. and Davis L. (2020) *Building with arches, vaults and domes: Training manual for architects and engineers*, Auroville: Auroville Earth Institute

3) Chilton J. (2000) *The engineer's contribution to contemporary architecture: Heinz Isler*, London: Thomas Telford

4) Heyman J. (1966) 'The stone skeleton', *Int. J. Solid. Struct.*, 2 (2), pp. 249–279

5) Maini S. (2011) *Dome of Dhyanalinga Temple*, Auroville: Auroville Earth Institute

Appendix B

Thrust Layout Optimization with Geometry Optimization Post-processing

A post-processing geometry optimization rationalization process (GO) for standard ground structure layout optimization (LO) was presented by He and Gilbert [113]. It is adapted here for the TLO procedure: changes were necessitated by the presence of transmissible self-weight loads and the interface node pairs. The GO process allows moving ground structure nodes—which are otherwise fixed in the LO and TLO processes—along with merging nodes in close proximity and creating nodes where links crossover resulting in thrust layouts with much improved visual clarity.

B.1 Mathematical Formulation

The variables (Annex B.1.1), objective function f (Annex B.1.2), and constraints g (Annex B.1.3) are first presented, followed by the analytical derivatives for gradient ∇f (Annex B.1.4), Jacobian ∇g (Annex B.1.5), and Hessian (Annex B.1.6). The derivations presented here make use of the connectivity matrix $\mathbf{C}$ which defines the connectivity of the underlying ground structure of the problem.

The connectivity matrix $\mathbf{C}$ is defined as

$$\mathbf{C_{ij}} = \begin{cases} 1 & \text{if link } i \text{ starts at node } j \\ -1 & \text{if link } i \text{ ends at node } j \\ 0 & \text{otherwise} \end{cases} . \tag{B.1}$$

Furthermore, the $diag()$ operation on a n dimensional vector $v = [v_1, v_2, \cdots, v_n]^T$ is defined as $diag(\mathbf{v}) = I \odot (\mathbf{v}\mathbf{1}^T)$. The expanded operation is presented as below in Eq. (B.2).

$$diag(\mathbf{v}) = I \odot (\mathbf{v}\mathbf{1}^T) \tag{B.2}$$

$$= \begin{bmatrix} 1 & 0 & \cdots & 0 \\ 0 & 1 & \cdots & 0 \\ \vdots & \vdots & \ddots & \vdots \\ 0 & 0 & \cdots & 1 \end{bmatrix} \odot \begin{bmatrix} v_1 \\ v_2 \\ \vdots \\ v_n \end{bmatrix} \begin{bmatrix} 1 & 1 & \cdots & 1 \end{bmatrix} \tag{B.3}$$

$$= \begin{bmatrix} 1 & 0 & \cdots & 0 \\ 0 & 1 & \cdots & 0 \\ \vdots & \vdots & \ddots & \vdots \\ 0 & 0 & \cdots & 1 \end{bmatrix} \odot \begin{bmatrix} v_1 & v_1 & \cdots & v_1 \\ v_2 & v_2 & \cdots & v_2 \\ \vdots & \vdots & \ddots & \vdots \\ v_n & v_n & \cdots & v_n \end{bmatrix} \tag{B.4}$$

$$= \begin{bmatrix} v_1 & 0 & \cdots & 0 \\ 0 & v_2 & \cdots & 0 \\ \vdots & \vdots & \ddots & \vdots \\ 0 & 0 & \cdots & v_n \end{bmatrix} \tag{B.5}$$

B.1.1 Variables

$$\mathbf{var} = \begin{bmatrix} \mathbf{x} & \text{(x-coordinates)} \\ \mathbf{y} & \text{(y-coordinates)} \\ \mathbf{a} & \text{(link area)} \\ \mathbf{q} & \text{(link force)} \\ \mathbf{q_n} & \text{(interface normal force)} \\ \mathbf{q_s} & \text{(interface shear force)} \\ \mathbf{w} & \text{(transmissible load)} \end{bmatrix}$$

B.1.2 Objective (f)

$$\text{vol} = \mathbf{a}^T\mathbf{l}, \tag{B.6}$$

where $\mathbf{l}$ is link length vector of the thrust layout.

Link length vector $\mathbf{l}$ forms the diagonal of the link length matrix $\mathbf{L}$, defined as follows:

$$\mathbf{L} = \sqrt{\mathbf{U}\mathbf{U} + \mathbf{V}\mathbf{V}}, \tag{B.7}$$

where

$$\begin{aligned} \mathbf{U} &= diag(\mathbf{C}\mathbf{x}), \\ \mathbf{V} &= diag(\mathbf{C}\mathbf{y}). \end{aligned} \tag{B.8}$$

B.1.3 Constraints (g)

Equilibrium

$$\mathbf{B}\mathbf{q} + \mathbf{B_n}\mathbf{q_n} + \mathbf{B_s}\mathbf{q_s} - \mathbf{w} = \mathbf{f}, \tag{B.9}$$

where

$$\mathbf{B} - \text{equilibrium matrix},$$
$$\mathbf{B_n}, \mathbf{B_s} - \text{equilibrium matrices for interface links},$$
$$\mathbf{f} - \text{external loads on nodes}.$$

Equilibrium matrix $\mathbf{B}$ can be computed as follows:

$$\mathbf{B} = \mathbf{E}\mathbf{L}^{-1} \tag{B.10}$$
$$\Rightarrow \mathbf{E} = \begin{bmatrix} \mathbf{C}^T\mathbf{U} \\ \mathbf{C}^T\mathbf{V} \end{bmatrix}. \tag{B.11}$$

Transmissible loads

$$\mathbf{H}\mathbf{w} = \bar{\mathbf{w}}, \tag{B.12}$$

where

$$\mathbf{H}_{ij} = \begin{cases} 1 & \text{if load component } j \text{ exists in load group } i \\ 0 & \text{otherwise} \end{cases}. \tag{B.13}$$

Group load vector $\bar{\mathbf{w}} = [\bar{w_1}, \bar{w_2}, ..., \bar{w_g}]^{\mathrm{T}}$, where g is the number of transmissible self-weight load groups.

Yield

$$-\sigma^{-}\mathbf{a} - \mathbf{q} \leq \mathbf{0}, \tag{B.14}$$
$$-\sigma^{+}\mathbf{a} + \mathbf{q} \leq \mathbf{0}, \tag{B.15}$$

where σ^+ and σ^- are limiting tensile and compressive stresses respectively.

Interface node

To ensure interface nodes ($\bar{x}_i$, $\bar{y}_i$) move along the interface, which is a line segment between $(x_{s,i}, y_{s,i})$ and $(x_{e,i}, y_{e,i})$:

$$\mathbf{T_a}\bar{\mathbf{x}} + \mathbf{T_b}\bar{\mathbf{y}} + \mathbf{T_c} = 0, \tag{B.16}$$

where

$$\mathbf{T_a} = diag([y_{s,i} - y_{e,i}]) \tag{B.17}$$
$$\mathbf{T_b} = diag([x_{s,i} - x_{e,i}]) \tag{B.18}$$
$$\mathbf{T_c} = [x_{s,i}y_{e,i} - x_{e,i}y_{s,i}]). \tag{B.19}$$

To ensure interface node pairs move together:

$$\mathbf{P}\bar{\mathbf{x}} = 0, \tag{B.20}$$
$$\mathbf{P}\bar{\mathbf{y}} = 0, \tag{B.21}$$

where

$$\mathbf{P}_{ij} = \begin{cases} 1 & \text{if nodes } i \text{ and } j \text{ are an interface pair with } i < j \\ -1 & \text{if nodes } i \text{ and } j \text{ are an interface pair with } i > j \\ 0 & \text{otherwise} \end{cases}. \tag{B.22}$$

Variable bounds

$$\mathbf{a}, \mathbf{w} \leq \mathbf{0}, \tag{B.23}$$

and

$$\mathbf{x_b} \leq \mathbf{x} \leq \mathbf{x_t}, \tag{B.24}$$

$$\mathbf{y_b} \leq \mathbf{y} \leq \mathbf{y_t}, \tag{B.25}$$

where

$$\mathbf{x_t}, \mathbf{x_b} - \text{upper and lower bounds of } x \text{ cordinates}, \tag{B.26}$$

$$\mathbf{y_t}, \mathbf{y_b} - \text{upper and lower bounds of } y \text{ cordinates}. \tag{B.27}$$

B.1.4 Gradient (∇f)

$$\nabla \text{vol} = \begin{bmatrix} \frac{\partial \text{vol}}{\partial \mathbf{x}} & \frac{\partial \text{vol}}{\partial \mathbf{y}} & \frac{\partial \text{vol}}{\partial \mathbf{a}} & \frac{\partial \text{vol}}{\partial \mathbf{q}} & \frac{\partial \text{vol}}{\partial \mathbf{q_n}} & \frac{\partial \text{vol}}{\partial \mathbf{q_s}} & \frac{\partial \text{vol}}{\partial \mathbf{w}} \end{bmatrix}^T, \tag{B.28}$$

where

$$\frac{\partial \text{vol}}{\partial \mathbf{x}} = \mathbf{C}^T diag\left(-\mathbf{r_1}\right) \mathbf{C}\mathbf{x}, \tag{B.29}$$

$$\frac{\partial \text{vol}}{\partial \mathbf{y}} = \mathbf{C}^T diag\left(-\mathbf{r_1}\right) \mathbf{C}\mathbf{y}, \tag{B.30}$$

$$\frac{\partial \text{vol}}{\partial \mathbf{a}}, \frac{\partial \text{vol}}{\partial \mathbf{q}} = \mathbf{0}, \tag{B.31}$$

$$\frac{\partial \text{vol}}{\partial \mathbf{q_n}}, \frac{\partial \text{vol}}{\partial \mathbf{q_s}} = \mathbf{0}, \tag{B.32}$$

$$\frac{\partial \text{vol}}{\partial \mathbf{w}} = \mathbf{0}, \tag{B.33}$$

and

$$\mathbf{r_1} = \left[\ldots \frac{a_i}{l_i} \ldots \right]. \tag{B.34}$$

B.1.5 Jacobian (∇g)

$$\text{Jacobian} = \begin{bmatrix} \frac{\partial \mathbf{Bq}}{\partial \mathbf{x}} & \frac{\partial \mathbf{Bq}}{\partial \mathbf{y}} & \mathbf{0} & \mathbf{B} & \mathbf{B_n} & \mathbf{B_s} & -\mathbf{I} \\ \mathbf{0} & \mathbf{0} & \mathbf{0} & \mathbf{0} & \mathbf{0} & \mathbf{0} & \mathbf{H} \\ \mathbf{0} & \mathbf{0} & -\sigma^{-}\mathbf{I} & -\mathbf{I} & \mathbf{0} & \mathbf{0} & \mathbf{0} \\ \mathbf{0} & \mathbf{0} & -\sigma^{+}\mathbf{I} & \mathbf{I} & \mathbf{0} & \mathbf{0} & \mathbf{0} \\ \mathbf{T_a} & \mathbf{T_b} & \mathbf{0} & \mathbf{0} & \mathbf{0} & \mathbf{0} & \mathbf{0} \\ \mathbf{P_I} & \mathbf{0} & \mathbf{0} & \mathbf{0} & \mathbf{0} & \mathbf{0} & \mathbf{0} \\ \mathbf{0} & \mathbf{P_I} & \mathbf{0} & \mathbf{0} & \mathbf{0} & \mathbf{0} & \mathbf{0} \end{bmatrix}, \tag{B.35}$$

where

$$\frac{\partial \mathbf{Bq}}{\partial \mathbf{x}} = \begin{bmatrix} \mathbf{C}^T diag\left(diag\left(\mathbf{r_2}\right)\mathbf{Cy}\right)\mathbf{VC} \\ \mathbf{C}^T diag\left(diag\left(-\mathbf{r_2}\right)\mathbf{Cx}\right)\mathbf{VC} \end{bmatrix}, \tag{B.36}$$

$$\frac{\partial \mathbf{Bq}}{\partial \mathbf{y}} = \begin{bmatrix} \mathbf{C}^T diag\left(diag\left(-\mathbf{r_2}\right)\mathbf{Cy}\right)\mathbf{UC} \\ \mathbf{C}^T diag\left(diag\left(\mathbf{r_2}\right)\mathbf{Cx}\right)\mathbf{UC} \end{bmatrix}, \tag{B.37}$$

and

$$\mathbf{r_2} = \begin{bmatrix} \dots & \frac{q_i}{l_i^3} & \dots \end{bmatrix}^T, \tag{B.38}$$

$$\mathbf{I} - \text{identity matrix.} \tag{B.39}$$

B.1.6 Hessian ($\nabla^2 f$, $\nabla^2 g$)

Lagrangian function:

$$f(\text{var}) + g(\text{var})^T \lambda \tag{B.40}$$

$$\Rightarrow \sigma_f \nabla^2 f(\text{var}) + \sum_i \lambda_i \nabla^2 g_i(\text{var}), \tag{B.41}$$

where

$$\nabla^2 f(var) = \begin{bmatrix} \frac{\partial^2 \text{vol}}{\partial \mathbf{x}^2} & & & & & & \\ \frac{\partial^2 \text{vol}}{\partial \mathbf{x}\partial \mathbf{y}} & \frac{\partial^2 \text{vol}}{\partial \mathbf{y}^2} & & & & & \\ \frac{\partial^2 \text{vol}}{\partial \mathbf{x}\partial \mathbf{a}} & \frac{\partial^2 \text{vol}}{\partial \mathbf{y}\partial \mathbf{a}} & \mathbf{0} & & & & \\ \mathbf{0} & \mathbf{0} & \mathbf{0} & \mathbf{0} & & & \\ \mathbf{0} & \mathbf{0} & \mathbf{0} & \mathbf{0} & \mathbf{0} & & \\ \mathbf{0} & \mathbf{0} & \mathbf{0} & \mathbf{0} & \mathbf{0} & \mathbf{0} & \\ \mathbf{0} & \mathbf{0} & \mathbf{0} & \mathbf{0} & \mathbf{0} & \mathbf{0} & \mathbf{0} \end{bmatrix}, \tag{B.42}$$

with

$$\frac{\partial^2 \text{vol}}{\partial \mathbf{x}^2} = \mathbf{C}^T diag\left(-\mathbf{r_1}\right)\mathbf{C} + \mathbf{C}^T diag\left(diag\left(\mathbf{r_3}\right)\mathbf{Cx}\right)\mathbf{UC}, \tag{B.43}$$

$$\frac{\partial^2 \text{vol}}{\partial \mathbf{y}^2} = \mathbf{C}^T diag\left(-\mathbf{r_1}\right)\mathbf{C} + \mathbf{C}^T diag\left(diag\left(\mathbf{r_3}\right)\mathbf{Cy}\right)\mathbf{VC}, \tag{B.44}$$

$$\frac{\partial^2 \text{vol}}{\partial \mathbf{x}\partial \mathbf{y}} = \mathbf{C}^T diag\left(diag\left(\mathbf{r_3}\right)\mathbf{Cy}\right)\mathbf{UC}, \tag{B.45}$$

$$\frac{\partial^2 \text{vol}}{\partial \mathbf{x}\partial \mathbf{a}} = diag\left(-\mathbf{r_4}\right)\mathbf{UC}, \tag{B.46}$$

$$\frac{\partial^2 \text{vol}}{\partial \mathbf{y}\partial \mathbf{a}} = diag\left(-\mathbf{r_4}\right)\mathbf{VC}, \tag{B.47}$$

and

$$\mathbf{r_3} = \begin{bmatrix} \dots & \frac{a_i}{l_i^3} & \dots \end{bmatrix}^T, \tag{B.48}$$

$$\mathbf{r_4} = \begin{bmatrix} \dots & \frac{1}{l_i} & \dots \end{bmatrix}^T. \tag{B.49}$$

$$\nabla^2 g_{(Eqm.,j)}(\mathsf{var}) = \begin{bmatrix} \frac{\partial^2(\mathbf{Bq})_j}{\partial \mathbf{x}^2} & & & & & & \\ \frac{\partial^2(\mathbf{Bq})_j}{\partial \mathbf{x}\partial \mathbf{y}} & \frac{\partial^2(\mathbf{Bq})_j}{\partial \mathbf{y}^2} & & & & & \\ \mathbf{0} & \mathbf{0} & \mathbf{0} & & & & \\ \frac{\partial^2(\mathbf{Bq})_j}{\partial \mathbf{x}\partial \mathbf{q}} & \frac{\partial^2(\mathbf{Bq})_j}{\partial \mathbf{y}\partial \mathbf{q}} & \mathbf{0} & \mathbf{0} & & & \\ \mathbf{0} & \mathbf{0} & \mathbf{0} & \mathbf{0} & \mathbf{0} & & \\ \mathbf{0} & \mathbf{0} & \mathbf{0} & \mathbf{0} & \mathbf{0} & \mathbf{0} & \\ \mathbf{0} & \mathbf{0} & \mathbf{0} & \mathbf{0} & \mathbf{0} & \mathbf{0} & \mathbf{0} \end{bmatrix}, \tag{B.50}$$

$$\frac{\partial^2(\mathbf{Bq})_j}{\partial \mathbf{x}^2} = \begin{bmatrix} (diag\,(\mathbf{C}[:,j])\,\mathbf{C})^T\, diag\,(-3\mathbf{r_5})\,\mathbf{CxVVC} \\ (diag\,(\mathbf{C}[:,j])\,\mathbf{C})^T\, diag\,(\mathbf{r_5})\,\mathbf{Cy}[2\mathbf{UU}-\mathbf{VV}]\mathbf{C} \end{bmatrix}, \tag{B.51}$$

$$\frac{\partial^2(\mathbf{Bq})_j}{\partial \mathbf{y}^2} = \begin{bmatrix} (diag\,(\mathbf{C}[:,j])\,\mathbf{C})^T\, diag\,(\mathbf{r_5})\,\mathbf{Cx}[2\mathbf{VV}-\mathbf{UU}]\mathbf{C} \\ (diag\,(\mathbf{C}[:,j])\,\mathbf{C})^T\, diag\,(-3\mathbf{r_5})\,\mathbf{CyUUC} \end{bmatrix}, \tag{B.52}$$

$$\frac{\partial^2(\mathbf{Bq})_j}{\partial \mathbf{x}\partial \mathbf{y}} = \begin{bmatrix} (diag\,(\mathbf{C}[:,j])\,\mathbf{C})^T\, diag\,(\mathbf{r_5})\,\mathbf{Cy}[2\mathbf{UU}-\mathbf{VV}]\mathbf{C} \\ (diag\,(\mathbf{C}[:,j])\,\mathbf{C})^T\, diag\,(\mathbf{r_5})\,\mathbf{Cx}[2\mathbf{VV}-\mathbf{UU}]\mathbf{C} \end{bmatrix}, \tag{B.53}$$

$$\frac{\partial^2(\mathbf{Bq})_j}{\partial \mathbf{x}\partial \mathbf{q}} = \begin{bmatrix} diag\,(\mathbf{C}[:,j])\, diag\,(\mathbf{r_6})\,\mathbf{CyVC} \\ diag\,(\mathbf{C}[:,j])\, diag\,(-\mathbf{r_6})\,\mathbf{CxVC} \end{bmatrix}, \tag{B.54}$$

$$\frac{\partial^2(\mathbf{Bq})_j}{\partial \mathbf{y}\partial \mathbf{q}} = \begin{bmatrix} diag\,(\mathbf{C}[:,j])\, diag\,(-\mathbf{r_6})\,\mathbf{CyUC} \\ diag\,(\mathbf{C}[:,j])\, diag\,(\mathbf{r_6})\,\mathbf{CxUC} \end{bmatrix}, \tag{B.55}$$

with

$$\mathbf{r_5} = \begin{bmatrix} \cdots & \frac{q_i}{l_i^5} & \cdots \end{bmatrix}^T, \tag{B.56}$$

$$\mathbf{r_6} = \begin{bmatrix} \cdots & \frac{1}{l_i^3} & \cdots \end{bmatrix}^T. \tag{B.57}$$

and $\mathbf{C}[:,j]$ denoting the j^{th} column of matrix $\mathbf{C}$.

Hessians of the remaining constraints are null matrices:

$$\nabla^2 g_{(TrLoads.)}(\mathsf{var}) = \mathbf{0}; \tag{B.58}$$

$$\nabla^2 g_{(Yield)}(\mathsf{var}) = \mathbf{0}; \tag{B.59}$$

$$\nabla^2 g_{(NodeMove.)}(\mathsf{var}) = \mathbf{0}. \tag{B.60}$$

B.2 Procedure

The GO process presented by He and Gilbert [113] was adapted for the TLO procedure—see Fig. B.1. A new step of 'split lines' (Section B.2.1) is added while the 'merge and move process' (Section B.2.2) is adapted for the TLO process. The 'filter process' and 'crossover process' (Section B.2.3) largely follow the original form with only minor changes.

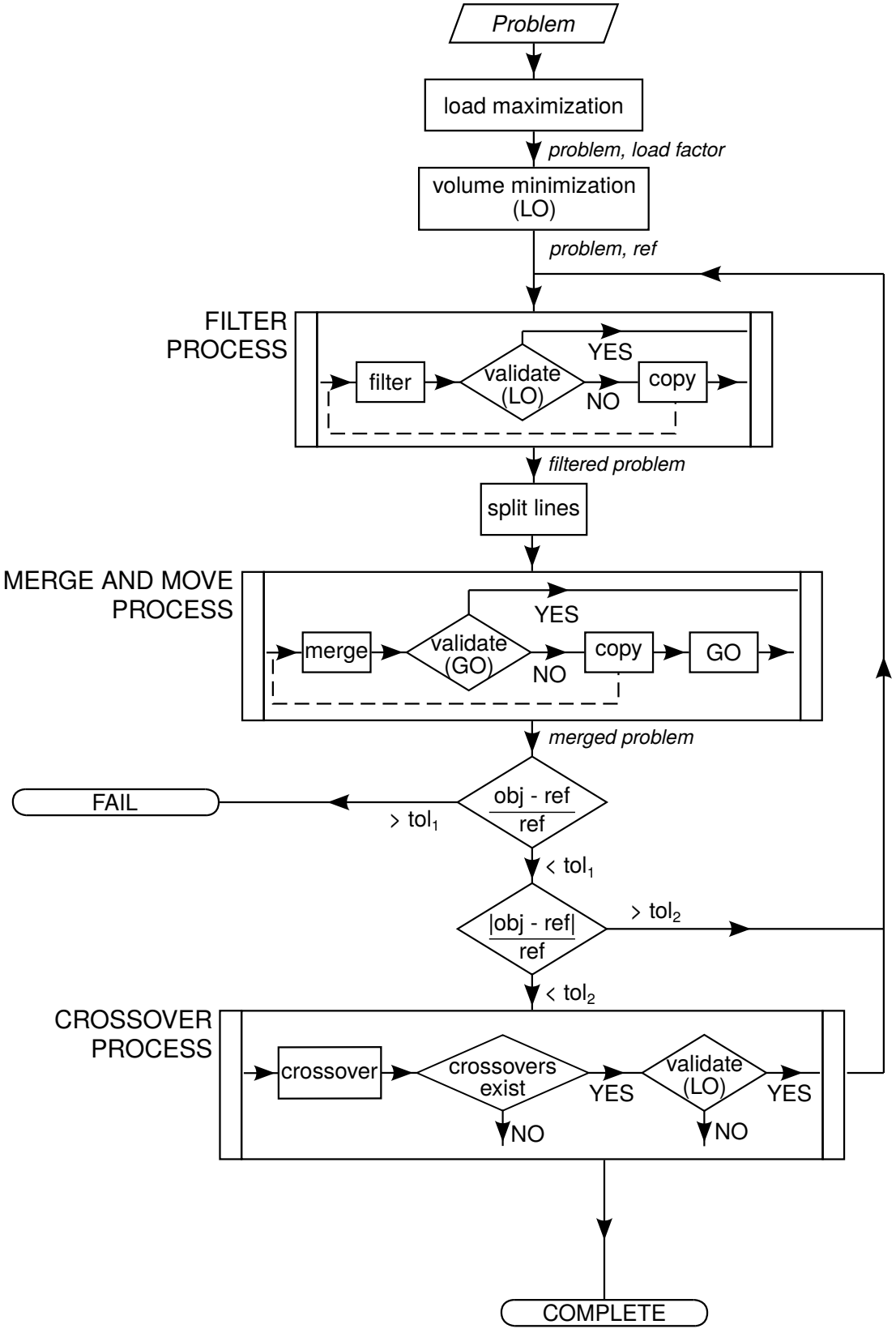

Figure B.1: Flowchart of the geometry optimization (GO) post-processing process for TLO.

B.2.1 Split-lines

TLO process uses transmissible self-weight loads to mimic the traditional funicular thrust lines, where self-weight loads are allowed to move along their lines of action so they can be attached to the funicular. To recreate this behaviour in the geometry optimization post-processing procedure, new nodes are created in the 'split lines' step to allow the transmissible self-weight loads to be attached to the thrust line. New nodes are created where the links in the thrust layout intersect transmissible load lines.

B.2.2 Node merge and move process

The presence of transmissible self-weight loads and interface node pairs put additional constraints on the node merge and move process. The merge and move behaviour are dictated by the nature of the nodes attempted to be merged—e.g., do they carry transmissible self-weights, are they part of an interface node pair, etc. A classification of nodes is presented in Fig. B.2—the figure also summarises move and merge constraints on the nodes, and if they are allowed to be filtered out during the filtering process.

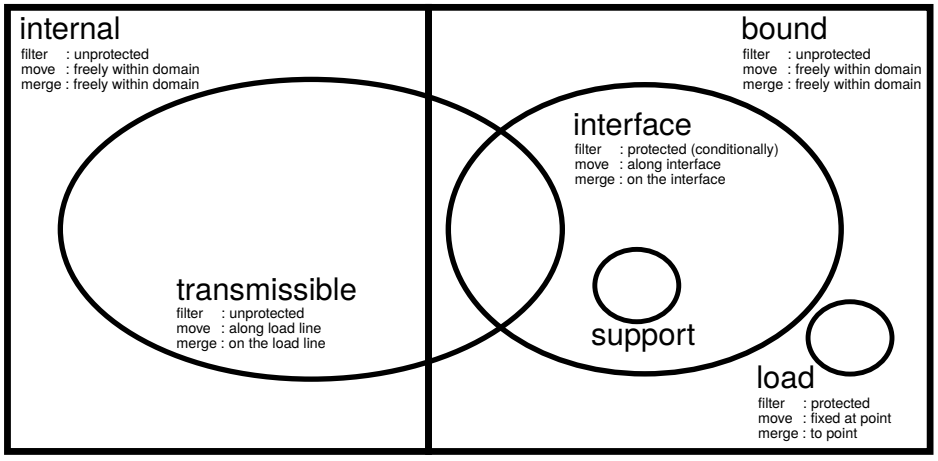

Figure B.2: Classification of nodes in the underlying ground structure of a TLO problem. Move, merge, and filter constraints for the geometry optimization post-processing step is also noted.

A given node in the ground structure of a TLO problem will be either an internal or a bound node—bound nodes are at the boundary of the corresponding block. All nodes have the default setting of being unprotected against being filtered out and are free to move and merge within the block (domain).

At the start of the GO process, all internal nodes will carry transmissible loads as they are created to discretize the self-weight of the block. However, new internal nodes not carrying self-weight are created in the crossover process. Transmissible loads will also be mobilized at some of the bound nodes—i.e., if they are on a load line.

Where bound nodes are at a common boundary between two blocks, they are called interface nodes—interface nodes are in pairs, one belonging to each of the blocks sharing the common interface (boundary). Interface nodes are also protected against being filtered, on the condition they have interface forces above a given threshold—interface nodes having interface forces below the threshold are reclassified as bound nodes (i.e., the interface is

opening up). Support nodes are interface nodes—each supported node shares its nodal location with a block—but does not carry transmissible loads. External loads are applied only at the boundary of the structure and are not allowed to be filtered out or moved.

The merge process is simplified by only considering two nodes at a time. Two nodes lying within a pre-defined merge radius are selected at in turn and merged, if a valid merge can be carried out. This continues until no two mergeable nodes are within the merge radius. Furthermore, only nodes within the same block are considered for merging.

The possible scenarios of node combinations and how the nodes are merged is summarized in Table B.1. Also noting that interface and transmissible load nodes constrained on a line, and loaded nodes are fixed to a point, 5 types of potential combinations are noted—although only 3 of them would result in a merge and move occurring.

Table B.1: Node merge combinations for GO with TLO: five types of node combinations considered based on the constraints applied on different node types. Free nodes include unconstrained internal and bound nodes.

	free	interface	transmissible	load	
Type 1	2				merge to mean point
Type 2	1 1 1	1	1	1	move bound node to the constrained node
Type 3		1 1	1 1	1 1	no merge
Type 4		2	2		merge to mean point, if line constraints are consistent
Type 5				2	no merge

If the two nodes are free to move and merge (i.e., unconstrained nodes), they will be merged to a node at the midpoint between the two (Type 1 in Table B.1). If only one of the nodes is an unconstrained node, the unconstrained node will move (and merge) to the constrained node (Type 2 in Table B.1). If the two nodes are of different constraint types no merge is carried out (Type 3 in Table B.1). If the two nodes are of the same constraint type, a merge might be possible: if the two nodes are in the same interface or the transmissible load line, then a merge is possible (Type 4 in Table B.1); no merge is possible with two externally loaded points (Type 5 in Table B.1).

Note that a pair of interface nodes are merged only when both the pair and its duals are mergeable: when interface pairs are merged, the corresponding dual pair should also be merged—interface node pairs move together and thus, merge together.

B.2.3 Filter and crossover processes

A filtering process following He and Gilbert [113] is used. Links having forces below a threshold value are removed—to further simplify the problem unconnected nodes are also removed and transmissible load groups updated. To ensure that the link is not structurally significant, albeit being a lower force, a validation is carried out where a volume minimization (LO without

GO) is carried out and checked if the volume of the reduced problem is within a tolerance of the original volume.

The crossover process creates new nodes where links cross each other and this follows the process of He and Gilbert [113]. In the case of TLO, gives rise to internal nodes that are not carrying self-weight loads (i.e., internal nodes without the transmissibility constraint).

Appendix C

Conference Paper: *Thrust Layout Optimization for the Analysis of Historic Masonry Structures**

*Nanayakkara, I., Liew, A., Gilbert, M. (2024). 'Thrust Layout Optimization for the Analysis of Historic Masonry Structures'. In: Endo, Y., Hanazato, T. (eds) Structural Analysis of Historical Constructions. SAHC 2023. RILEM Bookseries, vol 46. Springer, Cham.

Thrust Layout Optimization for the Analysis of Historic Masonry Structures

Isuru Nanayakkara(✉), Andrew Liew, and Matthew Gilbert

Department of Civil and Structural Engineering, The University of Sheffield, Sheffield S1 3JD, UK
kiunanayakkara1@sheffield.ac.uk

Abstract. Historic masonry structures form an important part of the world's collective cultural heritage. Many methods have been developed for assessing the load carrying capacity of masonry gravity structures, from simple hanging chain representations to much more complex non-linear finite element models, though tools that can provide rapid and reliable assessments are still sought after. Here, a new automated procedure, termed thrust layout optimization (TLO) is presented. This is designed to overcome limitations of the traditional thrust line method, and more recently developed computer based alternatives such as the thrust network analysis (TNA) method. The new procedure is capable of automatically identifying admissible thrust lines in masonry gravity structures comprising general arrangements of masonry blocks, without the need to specify in advance the form of the thrust line or thrust network layout. As well as providing a rapid assessment of load carrying capacity, the TLO method provides a clear visual presentation of load paths. Also, sliding friction can be accounted for and large-scale problems involving complex geometries can be tackled, as demonstrated via various examples described in this contribution.

Keywords: Thrust Line Analysis · Masonry Structures · Computational Analysis

1 Introduction

Historic masonry structures form an important part of the world's collective cultural heritage—ranging from the grand arches of the Sassanian Empire in the 3rd Century AD to Saint Peter's Basilica in Rome in the 17th Century AD [1]. Assessment of their load carrying capacity and making any necessary corrective measures to strengthen them is necessary for the preservation of this cultural heritage [2].

Thrust lines generated by funiculars—from physical models (e.g., hanging chain models [3]), graphical methods (e.g., [4]), or numerical methods (e.g., particle spring models [5])—have been extensively used in the analysis of masonry gravity structures such as arches, buttresses and gothic apses (in 2D) as well as in vaults and domes (in 3D). The usage of funicular thrust lines stems from Hooke's observation of hanging chains—'as hangs the flexible cable, so but inverted stands the rigid arch' [6]. From

Y. Endo and T. Hanazato (Eds.): SAHC 2023, RILEM Bookseries 46, pp. 626–638, 2024.
https://doi.org/10.1007/978-3-031-39450-8_52

this, it follows that if one can find a catenary form (with the appropriate loading and support conditions) that can be contained within the masonry gravity structure under consideration, then that structure will be safe under those loads and support conditions. This was further formalised by Heyman in his eponymous 'safe theorem', formulated as a limit analysis problem [7].

More recently, computer based methods implementing finite element models and limit analysis approaches have also been used for the analysis of masonry structures. While traditional linear elastic finite element models are of limited use for the analysis of masonry structures, non-linear finite element methods can be applied but are computationally expensive and demand higher levels of user expertise [2]. Limit analysis approaches, which directly model the collapse limit state, have been more popular and have seen significant improvements over the years. Building on the work of Kooharian [8] and Heyman [7], Livesley [9] proposed a rigid block limit analysis method, later extended by others (e.g., [10–12]). However, rigid block methods require explicit modelling of constituent units, or taking a macro-block approach (e.g., [13]): While the former can be time-consuming to model and solve when the blocks are numerous, the latter runs the danger of overestimating the stability when the failure planes do not coincide with actual interfaces between blocks.

A resurgence of computer based implementation of graphic static models has been observed. This has primarily been due to the popularity of the thrust network analysis (TNA) procedure developed by Block and Ochsendorf [14], building on work by O'Dwyer [15]. TNA can be used to evaluate the safety of masonry gravity structures by computing a geometric safety factor, or by considering limiting horizontal thrusts at the supports [16]. However, the dependence of the results obtained on the topology of the initially defined thrust network remains an issue.

Thrust line method have inherent limitations, regardless of the mode of implementation. Apart from the explicit limitations of unlimited friction capacity (which is not a reasonable assumption for flying buttresses [17]), there are ambiguities related the way tension is treated (although the solution is purported to be compression only, it does implicitly assume tension to allow material below the thrust line to be 'lifted up'), and case specific modifications (such as the need to determine an inclined crack in masonry buttresses [18]). Also, there are acknowledged limitations in using funiculars as thrust lines, where the method implicitly assumes vertical cuts, disregarding the actual block stereotomy [19–21]. Furthermore, when complex geometries are involved (e.g., consider a gothic cathedral) it is often necessary to analyse parts of the structure separately and to then combine these to check overall stability, a somewhat cumbersome process [18].

In this work, a new computational means of identifying admissible thrust lines in masonry gravity structures is proposed to overcome the aforementioned issues. The proposed procedure takes advantage of powerful layout (or 'topology') optimization techniques that have already been successfully used to automate the so-called 'strut and tie' method of design for reinforced concrete structures, where the goal is to identify tensile and compressive force paths in deep beams and other elements, enabling efficient layouts of tensile reinforcement to be identified [22]. In a traditional unreinforced masonry structure, the goal is somewhat different, with the priority being to identify compressive force paths, with self-weight effects handled appropriately. In the present

contribution it will be shown that a formulation employing truss layout optimization [23, 24], used in tandem with transmissible loads [25–27], can be built upon to directly identify compressive force paths and to establish margins of safety. It will be shown that this requires the introduction of interfaces to represent weak masonry joints, thereby allowing both tensile and sliding failures to be modelled, as well as changes to the optimization objective function.

The present paper is organized as follows. In Sect. 2 identifying the shortcomings in the funicular thrust lines, thrust layouts are proposed; thrust layout optimisation procedure to automatically obtain thrust layouts is formulated in Sect. 3 and is then applied to typical examples of historical masonry structures in Sect. 4; conclusions are drawn in Sect. 5.

2 Thrust Layouts

Although funicular thrust lines have been successfully used in applying Heyman's safe theorem to masonry gravity structures, Heyman himself later noted some limitations of the thrust line method [19–21]. Specifically, funicular thrust lines implicitly assume vertical cuts, disregarding the actual stereotomy of the constituent blocks, thus allowing for the possibility of self-weight loads being 'lifted up' across weak interfaces. Furthermore, the treatment of tensile strength in the funicular thrust lines is not clear—although the solution visualised is compression only, implicitly the self-weight of masonry lying below the thrust line is lifted up to this. Also, whereas the block material possesses some limited tensile strength, the interfaces have negligible tensile strength, and thus need to be treated differently.

The two simple examples shown in Fig. 1 and Fig. 2 demonstrate how these errors can lead to incorrect results. In Fig. 1, as vertical cuts are assumed instead of the actual cut, which is horizontal, the funicular thrust line predicts a higher collapse load than that can be carried by the assembly. This is by allowing the self-weight of the bottom block to be lifted across the tension-weak interface. This is clearer when the tensile lines are drawn from the centres of mass of the blocks to the thrust line—it is evident that the tensile link from the bottom block cuts across the weak interface between blocks.

In Fig. 2, although a compression only thrust line cannot be constructed, an equilibrium solution exists as demonstrated by the force flow plotted in (b). This force flow is now allowed to carry tensile forces within the block but not across weak interfaces between blocks. Note that the force T in the tensile link introduced (5 force units, horizontal) is significantly less than the implicit tension pulling the self-weight of the top block (40 force units, vertical). And there is no reason for these two tensile forces to be treated any differently.

Following these observations, the following rules are applied to correct funicular thrust lines and to arrive at thrust layouts:

- self-weight forces are only allowed to be transmitted within a given block (when attempting to attach itself to the thrust layout);

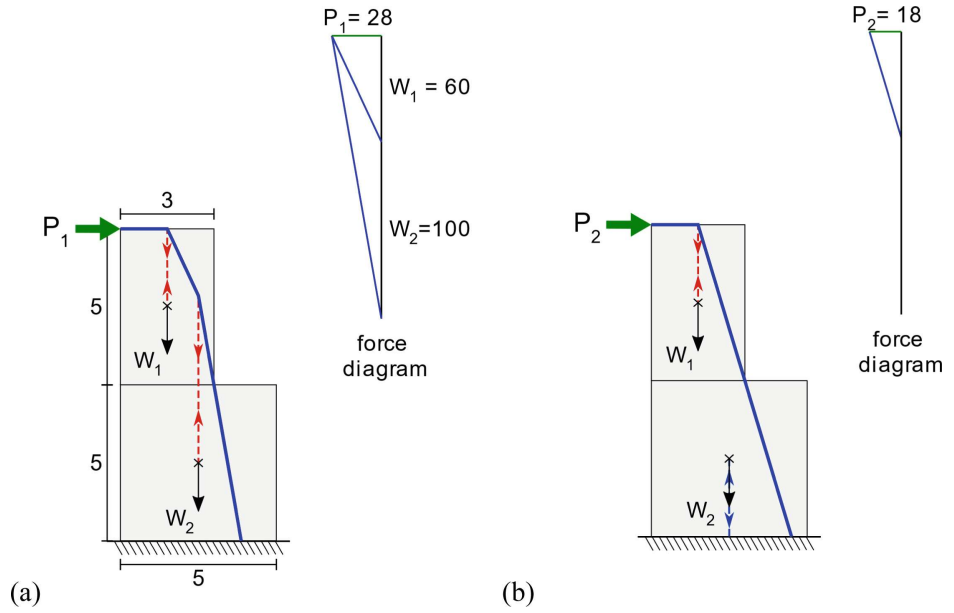

Fig. 1. Constraining load transmissibility in funicular thrust lines: (a) the funicular thrust line generated from graphic statics disregards the weak interface between blocks and implicitly assumes a tensile link across it, overestimating load capacity; (b) the self-weight of the bottom block is not pulled across the weak interface, but is allowed to be carried by the supports, giving the exact collapse load (compression and tension links in blue and red respectively; the geometry is as indicated; unit weight of 2 units and width of 2 units considered).

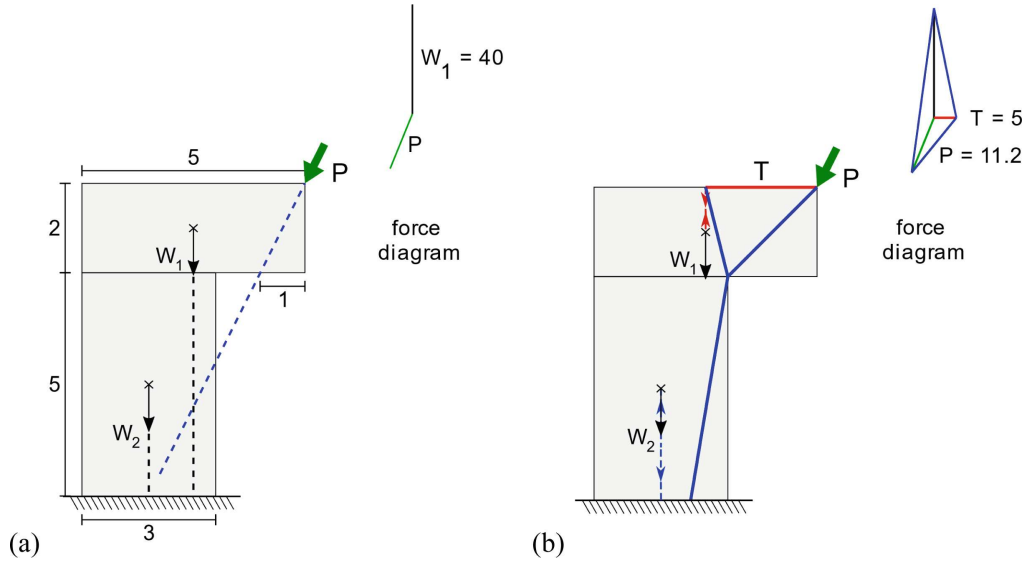

Fig. 2. Incorporating tension explicitly in thrust lines: (a) a valid thrust line cannot be drawn if only compressive links are allowed; (b) a thrust layout contained within the structure can be constructed with the help of a tensile link (the geometry is as indicated; unit weight of 2 units and width of 2 units considered).

- links carrying tensile forces are permitted within blocks (but not across weak interfaces).

Thrust layouts give a valid representation of the equilibrium of individual blocks making up the structure, while respecting the weak interfaces that exist between blocks, and visualising a (possible) force flow within the structure.

3 Thrust Layout Optimisation (TLO)

A relationship exists between graphic statics (GS) and ground-structure layout optimisation (LO), in their application to pin jointed structures. GS enforces equilibrium at nodes and allows exploration of a design space by letting nodes move, thereby changing the geometry of the structure (which is usually of pre-defined topology). Similarly, LO too enforces equilibrium at nodes; however, in this case, the nodal coordinates are usually fixed but a fully connected ground-structure is considered (i.e., all possible members connecting all the pin joints are considered first). And thereafter, in LO, member yield strengths are imposed to enable a minimum volume structure to be found. Given this relationship between the two methods, LO appears to be a viable candidate to automate the generation of thrust layouts, albeit some modifications are required.

Direct application of the LO process would generate a 'truss-like' force flow within a masonry structure, but (i) would fail to recognise the weak interfaces in masonry gravity structures, and (ii) self-weights fixed at nodes would not generate force flows resembling typical thrust lines. To address these issues, interface nodes representing weak masonry bonds can be introduced and self-weight loads can be allowed to move along their lines of action via the use of 'transmissible' loads contained within a given block. Using the two block assembly in Fig. 3, the proposed thrust layout optimization (TLO) process is now described in more detail (see [28] for additional details).

Interface nodes share the same physical location at a weak interface, but with each being associated with one of the adjacent blocks. This gives rise to node pairs that are each connected via a normal force q_n and a shear force q_s, respectively aligned perpendicular and parallel to the interface (Fig. 3b). The weak interface is enforced by constraining the normal force to always be compressive, and the shear force to be limited by the normal force and the friction coefficient between blocks at the interface.

Transmissible loads have previously been used in conjunction with the standard ground structure layout optimisation procedure [25–27]. These are loads that are shared across multiple nodes lying along a given vertical line of action when self-weight loads are involved. To respect the weak block interfaces, the transmissibility is restricted to the extents of a given block (Fig. 3c).

When assessing the stability of a masonry gravity structure, a common goal is to seek the magnitude of applied load that can be applied before collapse occurs. To achieve this, the collapse load factor (the multiplier on a given load required to initiate failure) is sought. This can be achieved by maximizing the load factor subject to equilibrium and yield constraints, using the defined ground structure and set of transmissible self-weight loads—resulting in the formulation given in Eq. (1) below:

$$\max \lambda \quad \mathbf{q},\ \mathbf{q_n},\ \mathbf{q_s},\ \mathbf{w},\ \lambda \tag{1a}$$

$$\text{s.t. } \mathbf{Bq} + \mathbf{B_n q_n} + \mathbf{B_s q_s} - \mathbf{w} - \lambda \mathbf{f} = \mathbf{0} \tag{1b}$$

$$\mathbf{Hw} = \hat{\mathbf{w}} \tag{1c}$$

$$\mathbf{q} \leq q_{\max}^{\mathrm{t}} \mathbf{1} \tag{1d}$$

$$\mathbf{q_n} \leq \mathbf{0} \tag{1e}$$

$$\mu \mathbf{q_n} \leq \mathbf{q_s} \leq -\mu \mathbf{q_n} \tag{1f}$$

$$\mathbf{w} \geq \mathbf{0} \tag{1g}$$

$$\lambda \geq 0 \tag{1h}$$

where λ is the load factor on the externally applied loads; $\mathbf{B}$ is a $2n \times m$ matrix containing direction cosines of links, $\mathbf{q} = [q_1, q_2, \ldots, q_{\mathrm{m}}]^{\mathrm{T}}$ is a vector of internal member forces, with $q_{\max}^{\mathrm{t}}$ being the maximum tensile force allowed. Also $\mathbf{f} = [\mathrm{f_{1x}}, \mathrm{f_{1y}}, \mathrm{f_{2x}}, \mathrm{f_{2y}}, \ldots, \mathrm{f_{nx}}, \mathrm{f_{ny}}]^{\mathrm{T}}$ is a vector of external applied loads and $\mathbf{B_n}$ and $\mathbf{B_s}$ are interface equilibrium matrices of size $2n \times p$ (where p is the number of interface node pairs) containing direction cosines on the basis of notional zero-length members oriented respectively perpendicular and parallel to the corresponding interface; $\mathbf{q_n} = [q_{\mathrm{n},1}, q_{\mathrm{n},2}, \ldots, q_{\mathrm{n,p}}]^{\mathrm{T}}$ is the interface normal force vector and $\mathbf{q_s} = [q_{\mathrm{s},1}, q_{\mathrm{s},2}, \ldots, q_{\mathrm{s,p}}]^{\mathrm{T}}$ is the interface shear force vector; $\mathbf{w} = [0, w_1, 0, w_2, \ldots, 0, w_{\mathrm{n}}]^{\mathrm{T}}$ is the nodal self-weight load vector (note that as self-weight loads are applied in the vertical direction, only vertical equilibrium constraints are affected); $\hat{\mathbf{w}} = [\hat{w}_1, \hat{w}_2, \ldots, \hat{w}_{\mathrm{g}}]^{\mathrm{T}}$ is the load group vector, where g is the number of transmissible self-weight load groups in the problem, with $\hat{w}_{\mathrm{i}}$ being the total load applied in transmissible load group i. Finally, $\mathbf{H}$ is a binary matrix that specifies which nodal load components in $\mathbf{w}$ belong to which load group in $\hat{\mathbf{w}}$, where $\mathbf{H}$ is of size $g \times 2n$ and is given by:

$$H_{ij} = \begin{cases} 1; \textit{if load component } j \textit{ exist in load group } i \\ 0; \textit{otherwise} \end{cases}. \tag{2}$$

Thus, the factor on externally applied loads is maximized under the constraints of (i) static equilibrium at nodes, Eq. (1b) and Eq. (1c); (ii) a maximum tensile force allowed within blocks, Eq. (1d), with no tensile forces allowed across weak interfaces, Eq. (1e); and (iii) interface friction force limited by friction coefficient, Eq. (1f). Additionally, the constraint in Eq. (1g) is needed to avoid spurious solutions from being identified [26]. The linear nature of the objective function and constraints means that the problem can be solved using an efficient linear programming (LP) solver.

Finally, although solving Eq. (1) will determine the collapse load factor, the associated solution may include spurious self-equilibrating force networks, since these are not explicitly penalized in Eq. (1). This will in turn lead to thrust layouts that are not visually clear. To address this, a volume minimization post-processing step can be performed, with the computed load factor constrained to lie at the value found in the load evaluation step. This is carried out using the basic layout optimization formulation (i.e., that typically used for trusses), with interface nodes and transmissible self-weights now also included in the model. Outcomes from the process are shown in Fig. 3d–e. A further post processing geometry optimization rationalization step (after [29]) can help further improve the visual clarity of the force flow; see Fig. 3f. Furthermore, in addition to the thrust lines obtained via the TLO process (shown in Fig. 3d–f), the vertical self-weight vectors hidden by the assumed transmissibility of self-weight loads can also be optionally plotted to provide additional visual information; see Fig. 3g.

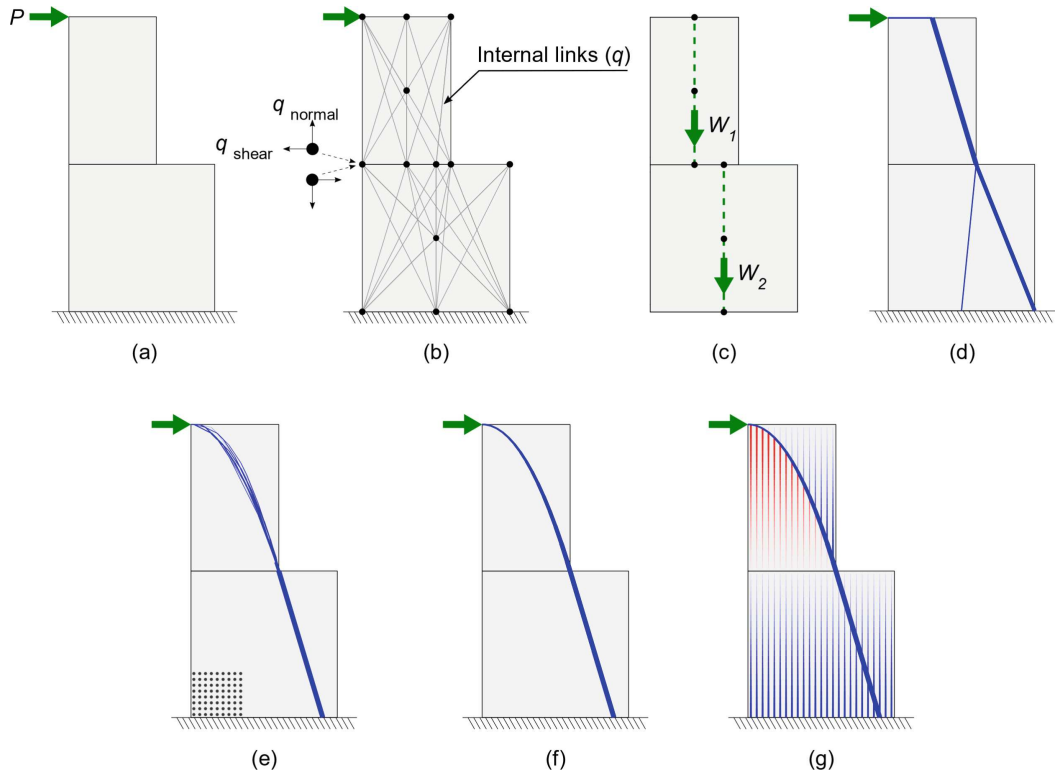

Fig. 3. Application of proposed thrust layout optimization (TLO) procedure to a simple two block problem: (a) geometry of blocks and location of external load P and support; (b) problem discretized via nodes and links; (c) masonry self-weight represented by transmissible loads W_1 and W_2; (d) collapse load and thrust layout found by solving the associated layout optimization problem; (e) thrust layout obtained when using a finer resolution nodal grid (as indicated); (f) thrust layout obtained after also performing a post-processing geometry optimization rationalization step; (g) layout with transmissible self-weight vectors also plotted—compression and tensile transmissible self-weight vectors are shown in blue and red, respectively, with line thicknesses indicating the magnitude of the forces.

4 Examples

A set of three examples are provided to showcase the potential of TLO in the analysis of historic masonry gravity structures—(i) an arch with holes; (ii) a flying buttress; and (iii) a section of a gothic cathedral.

4.1 Segmental Arch

A segmental arch having equally sized voussoirs, with three ornamental internal holes positioned on the arch centreline is considered (see Fig. 4). The arch is subjected to an off-centre point load. A friction coefficient of 1 is assumed to eliminate sliding failures.

A funicular thrust line (see Fig. 4a) contained fully within the structure, and not passing through the holes, would give a very conservative estimate of the collapse load (P of 27.6 kN). Recognizing the likely limited, albeit finite, tensile strength of the masonry voussoirs, the funicular thrust line can instead be restrained to lie within the structure only at weak interfaces between the blocks (see Fig. 4b). This, now, gives a much higher collapse load, P of 57.4 kN. However, the thrust line no longer stays within the arch section, thus making the status of the force flow and hence the validity of the solution unclear.

Now, the corresponding thrust layout optimization solution (see Fig. 4c) gives a collapse load P of 58.1 kN. This, while slightly higher than that estimated via the thrust line method, makes the load path clearer. While the force flow remains entirely within the structure, the presence of tensile forces where the thrust line would move out of the structure, and the bifurcation of the thrust line around the internal holes are clearly visualised (Additionally, this justifies constraining the thrust line only at weak interfaces in Fig. 4b). The slight increase in collapse load arises due to a situation akin to that in Fig. 2—where the tensile links in the first voussoir pulls back its self-weight and does not correspond to a location of the thrust line moving out of the structure. The same collapse load estimated by TLO is also predicted by the rigid block method (Fig. 4d). However, this method does not provide information on the force flow within the structure, whereas TLO provides a valuable perspective on how forces flow in masonry gravity structures.

4.2 Flying Buttress

In the traditional thrust line method, it is generally assumed that no sliding failures will occur, which can be unsafe, particularly in the case of flying buttresses [17]. However, limited friction capacity at block interfaces can readily be accounted for via the interface nodes in TLO. This leads to a more realistic visualisation of the force flow within masonry gravity structures of the sort shown in Fig. 5.

The flying buttress of Mallorca Cathedral, as presented by [30], is considered. It is subjected only to its self-weight. The thrust line in Fig. 5a (reproduced from [30]) gives a thrust line passing through the bottom corner of the head of the flyer to a point on the base support, while touching both the extrados and intrados along the way; this would lead to a collapse only if the abutments spread enough to enable formation of a ‘snap through’ collapse mechanism. Now considering the angle of incidence of thrust at supports (i.e., the angle between the thrust and the perpendicular to the support), at the

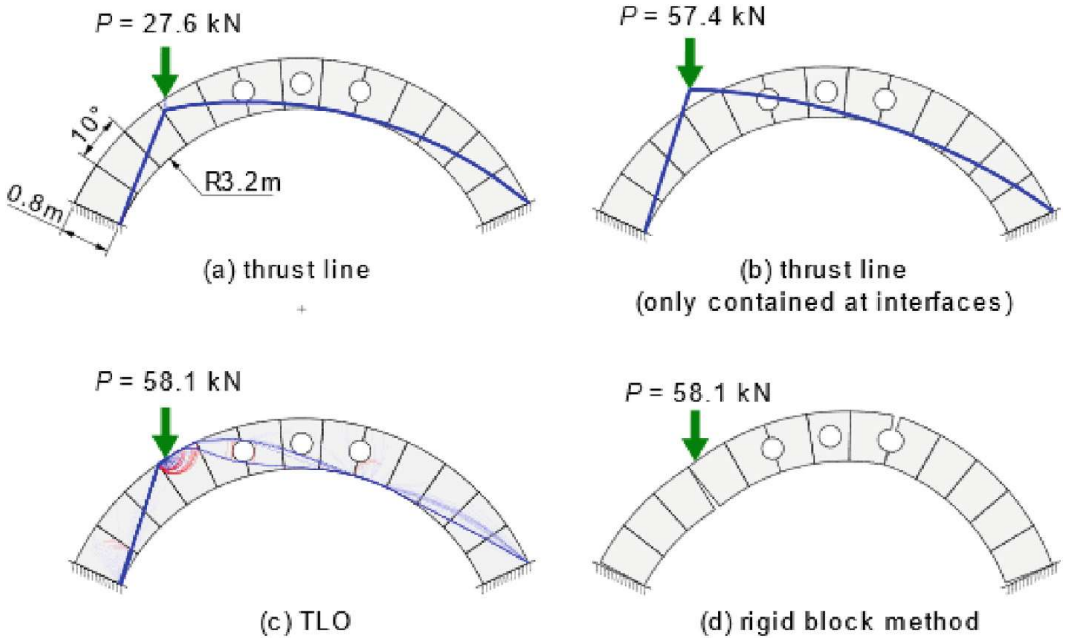

Fig. 4. Segmental arch - solutions obtained via: (a) traditional thrust line method; (b) thrust line method with thrust constrained at block interfaces only; (c) TLO, showing force flows confined to areas where material is present; (d) rigid block method, showing collapse mechanisms only (arch span: 5.80 m, rise 1.85 m, width 0.1 m, unit weight: 25 kN/m^3; circular voids on arch centreline at locations indicated have diameter of 0.35 m; collapse load P in kN applied 0.72 m from left support; thrust lines obtained assuming self-weight lumped at block centroids; thrust layouts obtained using internal and boundary node spacings of 0.05 m and $q^{\mathrm{t}}_{\max} = 250$ N; thrust layout tensile force line thickness scaled by a factor of 2 for emphasis).

flyer head it is 47.6° and at the base it is 13.4°. Although the thrust line is fully contained within the structure, the friction angle of the material (assumed to be 40° in this case) is not sufficient to avoid sliding failure at the flyer head.

Considering the stereotomy of the blocks and limited friction capacity of the material via TLO, a more realistic force flow can be found (see Fig. 5b). The resulting thrust layout indicates that the load will be carried primarily by the arch ring, giving a shallower angle of incidence for the thrust at the head. As a result, the horizontal thrust and the vertical reaction at base are increased. This would in turn increase the loading on the elements carrying those reaction forces—e.g., a masonry buttress.

4.3 Gothic Cathedral

TLO can also be used to analyse more complex structures, rapidly providing information on load carrying capacity and internal force flows. To demonstrate this, a section of a gothic cathedral is considered.

Thus, a gothic cathedral section—inspired by Tortosa Cathedral in Tarragona, Spain [31]—is now considered. It has two side aisles, at either side of the nave, all of which having barrel vaulted roofs and a set of single flying buttresses above. The nave is of 10.96 m span and the aisles are of 4.71 m and 3.92 m span, while the roofs of the nave

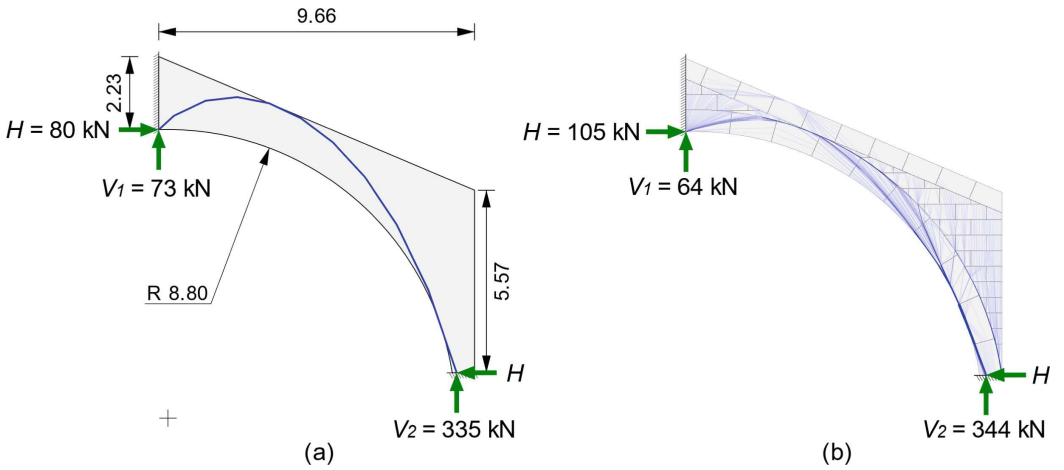

Fig. 5. Flying buttress - subjected only to its self-weight, is assessed via (a) traditional thrust line method (reproduced from [30]); (b) TLO, considering actual stereotomy and friction capacity limited by a friction coefficient of 0.85 (horizontal (H) and vertical (V_1 and V_2) support reactions are as indicated; thrust layouts obtained using internal and boundary node spacings of 0.05 m).

and side aisles are at 23.68 m, 17.04 m, and 11.15 m, respectively, from ground level. Buttress piers are of 20.36 m and 14.12 m in height. The section considered for the analysis has varying widths; buttress piers are of 2 m width, flying buttresses of 1 m width, and the vaulted roof of 6m width, as indicted in Fig. 6. The cathedral is built using stone of unit weight 18 kN/m^3, while the ballast filling of the vaulted roof has a unit weight of 15 kN/m^3 (see Fig. 6). A friction angle limit of 40° is assumed for all interfaces.

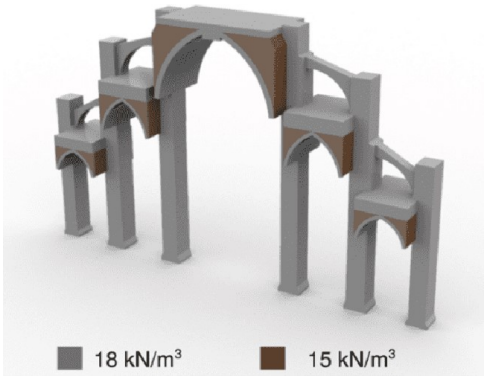

Fig. 6. Gothic cathedral: width and unit weight variation of the assessed section. Width of the flying buttresses, piers and vaults are 1m, 2 m, and 6 m respectively. Unit weight of stone (in grey) is 18 kN/m^3 and unit weight of ballast fill (in brown) is 15 kN/m^3.

The gothic cathedral is assessed under a point load applied on the keystone of the nave barrel vault. The block discretization indicated in Fig. 7 is used. The ground-structure was in this case made up of 43,192 nodes, 4,038,868 internal links and 12,962 interface

node pairs. The corresponding CPU times were 55 s for the load evaluation step, and 263 s for the volume minimization postprocessing step.

The resulting thrust layout is shown in Fig. 7, where the left and the right hand sides of the figure use different cut-off limits for the forces plotted; on the left only forces greater than $f_{max}/100$ are plotted, while on the right forces greater than $f_{max}/10000$ are plotted, where f_{max} is the maximum thrust in the thrust layout. As the cut-off is increased the main elements of the thrust layout emerge. Note that when only the higher forces are plotted (left hand side) no thrust lines appear on the flying buttresses, since the forces present in these are small, particularly when no external applied loads are present.

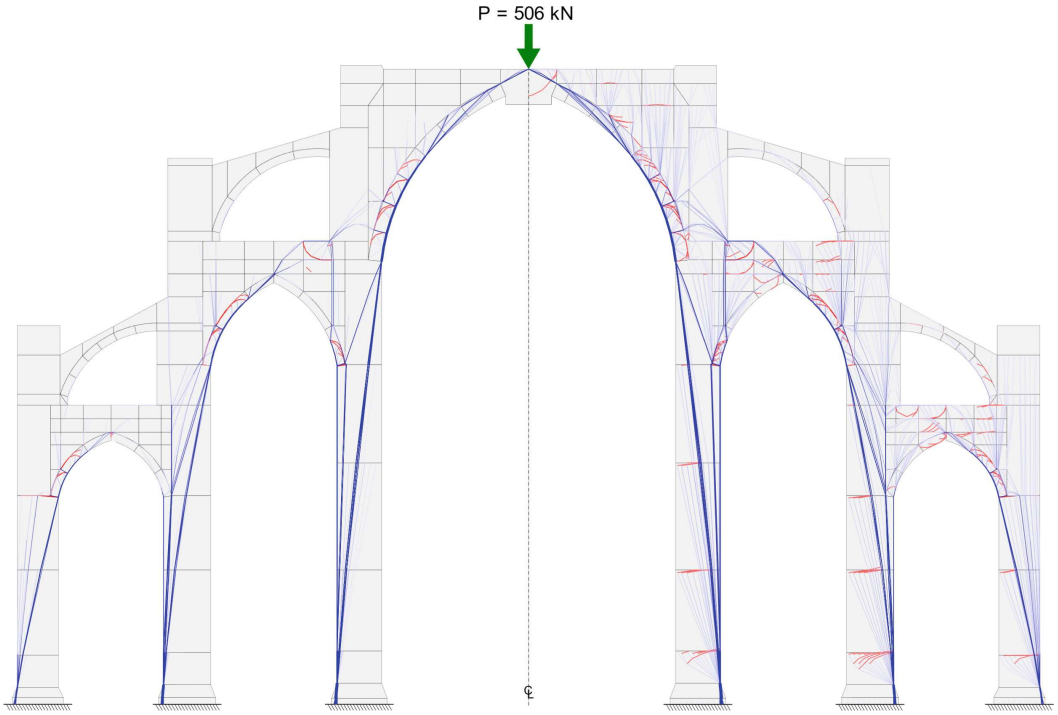

Fig. 7. Gothic cathedral: thrust layout for load applied on the keystone of nave vault. On the left hand side, forces lower than 1/100 of f_{max} are cut off and on the right forces lower than 1/10000 of f_{max} are cut off (tensile link thickness scaled by a factor of 2 for emphasis; q^t_{max} of 10 kN, boundary node spacing of 0.05 m and internal node spacing of 0.2 m).

5 Concluding Remarks

A new procedure has been developed that allows both the safety of masonry gravity structures to be evaluated and the transmission of internal forces to be clearly visualized. The procedure builds on the truss layout optimization with transmissible loads formulation, using this to model self-weight, and with interfaces included in the formulation to model weak masonry joints. The new procedure is herein termed thrust layout optimization (TLO).

Although the traditional thrust line analysis method has proved useful for many years, it has some limitations. For example, block stereotomy is not considered, leading to self-weight being 'lifted up' across weak interfaces. Also, the treatment of tensile forces is not clear. Thrust layouts—where transmissibility of self-weights is restrained and the limited, albeit present, tensile strength of the block material is made use of—are presented here. Furthermore, the TLO process proposed to obtain thrust layouts readily incorporate limiting friction at block interfaces.

The thrust layouts identified via TLO provide a rich visual representation of force flows in masonry gravity structures. The procedure takes on board the limited tensile capacity of masonry blocks and makes no prior assumptions about the topology of thrust layouts. This enables visualisation of forces flowing around internal holes, with the force flows associated with blocks rocking about vertices often resembling classical Michell structures; more familiar funicular thrust line solutions can also be identified. It is also possible to plot transmissible self-weight vectors, eliminating ambiguity as to how self-weight forces are mobilized.

References

1. Kurrer, K.E.: The History of the Theory of Structures, 2nd edn. Ernst & Sohn, Berlin (2008)
2. Roca, P., Cervera, M., Gariup, G., Pela', L.: Structural analysis of masonry historical construction. Classical and advanced approaches. Arch. Comput. Methods Eng. **17**, 299–325 (2010)
3. Graefe, R.: The catenary and the line of thrust as a means for shaping arches and vaults. In: Addis, B. (ed.) Physical Models: Their Historical and Current Use in Civil and Building Engineering Design, pp. 79–126. Ernst & Sohn (2021)
4. Paris, V., Ruscica, G., Roberti, G.M.: Graphical modelling of hoop force distribution for equilibrium analysis of masonry domes. Nexus Netw. J. **23**, 855–878 (2021)
5. Kilian, A., Ochsendorf, J.: Particle-spring systems for structural form finding. J. Int. Assoc. Shell Spat. Struct. **46**(147), 77–84 (2005)
6. Heyman, J.: The Masonry Arch. Ellis Horwood, Chichester (1982)
7. Heyman, J.: The stone skeleton. Int. J. Solids Struct. **2**, 249–279 (1966)
8. Kooharian, A.: Limit analysis of voussoir (segmental) and concrete arches. J. Am. Concr. Inst. **24**, 317–328 (1952)
9. Livesley, R.K.: Limit analysis of structures formed from rigid blocks. Int. J. Numer. Meth. Eng. **12**, 1853–1871 (1978)
10. Ferris, M., Tin-Loi, F.: Limit analysis of frictional block assemblies as a mathematical program with complementarity constraints. Int. J. Mech. Sci. **43**, 209–224 (2001)
11. Orduña, A., Lourenço, P.B.: Cap model for limit analysis and strengthening of masonry structures. J. Struct. Eng. **129**, 1367–1375 (2003)
12. Gilbert, M., Casapulla, C., Ahmed, H.M.: Limit analysis of masonry block structures with non-associative frictional joints using linear programming. Comput. Struct. **84**, 873–887 (2006)
13. Casapulla, C., Portioli, F., Maione, A., Landolfo, R.: A macro-block model for in-plane loaded masonry walls with non-associative Coulomb friction. Meccanica **48**(9), 2107–2126 (2013). https://doi.org/10.1007/s11012-013-9728-5
14. Block, P., Ochsendorf, J.: Thrust network analysis: a new methodology for three dimensional equilibrium. J. Int. Assoc. Shell Spat. Struct. **48**, 167–173 (2007)
15. O'Dwyer, D.: Funicular analysis of masonry vaults. Comput. Struct. **73**, 187–197 (1999)

16. Avelino, R.M., Iannuzzo, A., Van Mele, T., Block, P.: Assessing the safety of vaulted masonry structures using thrust network analysis. Comput. Struct. **257**, 106647 (2021)
17. Nikolinakou, M.-K., Tallon, A.J., Ochsendorf, J.A.: Structure and form of early Gothic flying buttresses. Revue Européenne de Génie Civil **9**(9–10), 1191–1217 (2005)
18. Huerta, S.: The safety of masonry buttresses. Proc. Inst. Civil Eng. Eng. Hist. Herit. **163**, 3–24 (2010)
19. Heyman, J.: La coupe des pierres. In: Kurrer, K.E., Lorenz, W., Wetzk, V. (eds.) Proceedings of the 3rd International Congress on Construction History, Cottbus, Germany, pp. 807–812 (2009)
20. Ochsendorf, J.: The masonry arch on spreading supports. Struct. Eng. **84**(2), 29–35 (2006)
21. Alexakis, H., Makris, N.: Limit equilibrium analysis of masonry arches. Arch. Appl. Mech. **85**(9–10), 1363–1381 (2014). https://doi.org/10.1007/s00419-014-0963-6
22. Xia, Y., Langelaar, M., Hendriks, M.A.N.: A critical evaluation of topology optimization results for strut-and-tie modelling of reinforced concrete. Comput. Aided Civil Infrastruct. Eng. **35**, 850–869 (2020)
23. Dorn, W.S., Gomory, R.E., Greenberg, H.J.: Automatic design of optimal structures. J. Mech. **3**, 25–52 (1964)
24. Gilbert, M., Tyas, A.: Layout optimization of large-scale pin-jointed frames. Eng. Comput. **20**, 1044–1064 (2003)
25. Darwich, W., Gilbert, M., Tyas, A.: Optimum structure to carry a uniform load between pinned supports. Struct. Multidiscip. Optim. **42**, 33–42 (2010)
26. Lu, H., Tyas, A., Gilbert, M., Pichugin, A.V.: On transmissible load formulations in topology optimization. Struct. Multidiscip. Optim. **64**(1), 23–37 (2021). https://doi.org/10.1007/s00158-021-02932-0
27. Fuchs, M.B., Moses, E.: Optimal structural topologies with transmissible loads. Struct. Multidiscip. Optim. **19**, 263–273 (2000)
28. Nanayakkara, K.I.U., Liew, A., Gilbert, M.: Application of thrust layout optimization to masonry structures. Proc. Royal Society A 20230053 (2023). https://doi.org/10.1098/rspa.2023.0053
29. He, L., Gilbert, M.: Rationalization of trusses generated via layout optimization. Struct. Multidiscip. Optim. **52**(4), 677–694 (2015). https://doi.org/10.1007/s00158-015-1260-x
30. Fuentes, P.: Mechanics of flying buttresses: the case of the cathedral of Mallorca. J. Mech. Mater. Struct. **13**(5), 617–630 (2018)
31. Lluís i Ginovart, J., Jover, A.C.: Design and medieval construction: the case of Tortosa cathedral (1345–1441). Constr. Hist. **29**(1), 1–24 (2014)

Bibliography

[1] UK structural engineers declare climate & biodiversity emergency. URL https://www.structuralengineersdeclare.com/. [Online] Accessed on: July 02, 2020.

[2] UK architects declare climate and biodiversity emergency. URL https://www.architectsdeclare.com/. [Online] Accessed on: July 02, 2020.

[3] United Nations Environment Programme. *Global Status Report for Buildings and Construction: Towards a Zero-emission, Efficient and Resilient Buildings and Construction Sector*. United Nations Environment Programme, Nairobi, 2022.

[4] United Nations. The 17 goals, . URL https://sustainabledevelopment.un.org/?menu=1300. [Online] Accessed on: September 05, 2020.

[5] M. Corradi, A. Borri, G. Castori, and K. Coventry. Experimental analysis of dynamic effects of FRP reinforced masonry vaults. *Materials*, 8(12):8059–8071, 2015.

[6] L.K. Davis, M. Varma, and S. Maïni. Sharanam: Case study of a 15 meter span earthen conical vault. *Structures*, 18:10–19, 2019.

[7] There's no place like homes: Re-use and recycle to reduce carbon. Technical report, Historic England, 2020.

[8] W. Darwich, M. Gilbert, and A. Tyas. Optimum structure to carry a uniform load between pinned supports. *Structural and Multidisciplinary Optimization*, 42(1):33–42, 2010.

[9] A. Tyas, A.V. Pichugin, and M. Gilbert. Optimum structure to carry a uniform load between pinned supports: Exact analytical solution. *Proceedings of the Royal Society A: Mathematical, Physical and Engineering Sciences*, 467(2128):1101–1120, October 2011.

[10] A. Liew, R. Avelino, V. Moosavi, T. Van Mele, and P. Block. Optimising the load path of compression-only thrust networks through independent sets. *Structural and Multidisciplinary Optimization*, 60(1):231–244, 2019.

[11] E. Allen and W. Zalewski. *Form and Forces: Designing efficient, expressive structures*. Wiley, 2009.

[12] P. Block and L. Lachauer. Three-dimensional funicular analysis of masonry vaults. *Mechanics Research Communications*, 56:53–60, 2014.

[13] M. Gilbert and A. Tyas. Layout optimization of large-scale pin-jointed frames. *Engineering Computations*, 20(8):1044–1064, 2003.

[14] L. He and M. Gilbert. Rationalization of trusses generated via layout optimization. *Structural and Multidisciplinary Optimization*, 52(4):677–694, 2015.

[15] L. He, M. Gilbert, P. Shepherd, J. Ye, A. Koronaki, H.E. Fairclough, B. Davison, A. Tyas, J. Gondzio, and A.G. Weldeyesus. A new conceptual design optimization tool for frame structures. In *Proceedings of the IASS Annual Symposium*, Boston, USA, July 2018.

[16] United Nations. What is climate change?, . URL https://www.un.org/en/climatechange/what-is-climate-change. [Online] Accessed on: June 19, 2023.

[17] R. Lindsey and L. Dahlman. Climate change: Global temperature. URL http://www.climate.gov/news-features/understanding-climate/climate-change-global-temperature. [Online] Accessed on: June 19, 2023.

[18] United Nations. Causes and effects of climate change, . URL https://www.un.org/en/climatechange/science/causes-effects-climate-change. [Online] Accessed on: June 19, 2023.

[19] O. Jack, E. Caitlyn, C. Davide, H. Michael, H. Jonathan, J. Sally, N. Liliana, N. Amy, O. Vargas, S. Simon, S. Zita, S. Dominic, and Y. Walz. Interconnected disaster risks. Technical report, United Nations University - Institute for Environment and Human Security (UNU-EHS), Bonn, Germany, 2021.

[20] Climate change 2021: Summary for all. Technical report, IPCC- Working Group I Technical Support Unit, 2022.

[21] City of Darebin. Climate emergency declaration. URL https://www.darebin.vic.gov.au/Waste-and-environment/Sustainability/Energy-and-climate/Climate-emergencydeclaration. [Online] Accessed on: June 19, 2023.

[22] National adaptation plan of Bangladesh (2023-2050). Technical report, Ministry of Environment, Forest and Climate Change, Government of the People's Republic of Bangladesh, October 2022.

[23] European Parliament. The European Parliament declares climate emergency, November 2019. URL https://www.europarl.europa.eu/news/en/press-room/20191121IPR67110/the-european-parliament-declares-climate-emergency. [Online] Accessed on: June 19, 2023.

[24] Health declares - climate crisis is a health crisis, (n.d.). URL https://healthdeclares.org/. [Online] Accessed on: June 19, 2023.

[25] Engineers declare climate and biodiversity emergency, (n.d.). URL https://www.engineersdeclare.com/. [Online] Accessed on: June 19, 2023.

[26] L.H. McHugh, M.C. Lemos, and T.H. Morrison. Risk? crisis? emergency? implications of the new climate emergency framing for governance and policy. *WIREs Climate Change*, 12(6), 2021. [Online] Accessed on: June 19, 2023.

[27] United Nations. Paris Agreement, 2015.

[28] Climate change act 2008. URL https://www.legislation.gov.uk/ukpga/2008/27/part/1/crossheading/the-target-for-2050/2019-06-27. [Online] Accessed on: June 19, 2023.

[29] UK housing: Fit for the future? Technical report, Committee on Climate Change, 2019.

[30] Climate change 2022: Mitigation of climate change. Technical report, Intergovernmental Panel on Climate Change, 2022.

[31] M. Salvadori and R. Heller. *Structure in Architecture*. Prentice-Hall Inc., New Jersey, USA, 1965.

[32] R. Graefe. The catenary and the line of thrust as a means for shaping arches and vaults. In B. Addis, editor, *Physical Models: their historical and current use in civil and building engineering design*, chapter 3, pages 79–126. Ernst & Sohn, 2021.

[33] K.I. Nanayakkara. Shell structures: lessons in structural efficiency for sustainable construction. *The Structural Engineer*, 98(4):8–17, 2020.

[34] The Institution of Structural Engineers. Shell structures from Catalan to Mapungubwe, 2019. [Online Video]. Available: https://www.youtube.com/watch?v=aZUDpAdqOX4.

[35] J. Heyman. The stone skeleton. *International Journal of Solids and Structures*, 2(2): 249–279, 1966.

[36] P. Block, M. DeJong, and J. Ochsendorf. As hangs the flexible line: Equilibrium of masonry arches. *Nexus Network Journal*, 8(2):13–24, October 2006.

[37] G. Poleni. *Memorie istoriche della gran cupola del tempio vaticano*. Stamperia del Seminario, Padua, Italy, 1748.

[38] S. Huerta. Galileo was wrong: The geometrical design of masonry arches. *Nexus Network Journal*, 8(2):25–52, 2006.

[39] J. Heyman. *The Masonry Arch*. Ellis Horwood, Chichester, UK, 1982.

[40] K.E. Kurrer. *The History of the Theory of Structures: From Arch Analysis to Computational Mechanics*. John Wiley & Sons, 2012.

[41] A.A. Markou and G. Ruan. Graphic statics: Projective funicular polygon. *Structures*, 41: 1390–1396, July 2022.

[42] D.C. Drucker, W. Prager, and H.J. Greenberg. Extended limit design theorems for continuous media. *Quarterly of Applied Mathematics*, 9(4):381–389, 1952.

[43] K. Bagi. Statics of fan vaulting: current state of knowledge and open issues. *Proceedings of the Royal Society A: Mathematical, Physical and Engineering Sciences*, 477 (2246):20200893, February 2021.

[44] E.T. Onat and W. Prager. Limit analysis of arches. *Journal of the Mechanics and Physics of Solids*, 1(2):77–89, January 1953.

[45] A. Kooharian. Limit analysis of voussoir (segmental) and concrete arches. *Journal of the American Concrete Institute*, 24(4):317–328, 1952.

[46] P. Fuentes. Mechanics of flying buttresses: the case of the cathedral of mallorca. *Journal of Mechanics of Materials and Structures*, 13(5):617–630, 2018.

[47] M.K. Nikolinakou, A.J. Tallon, and J.A. Ochsendorf. Structure and form of early gothic flying buttresses. *Revue Européenne de Génie Civil*, 9(9-10):1191–1217, 2010.

[48] A. Bacigalupo, A. Cavicchi, and L. Gambarotta. A simplified evaluation of the influence of the bond pattern on the brickwork limit strength. *Advanced Materials Research*, 368: 3495–3508, 2012.

[49] V. Beatini, G. Royer-Carfagni, and A. Tasora. A regularized non-smooth contact dynamics approach for architectural masonry structures. *Computers & Structures*, 187:88–100, 2017.

[50] S. Chen and K. Bagi. Crosswise tensile resistance of masonry patterns due to contact friction. *Proceedings of the Royal Society A: Mathematical, Physical and Engineering Sciences*, 476(2240):20200439, 2020.

[51] J. Heyman. Why ancient cathedrals stand up. *Ingenia*, (10):19–23, 2001.

[52] J. Ochsendorf. *Collapse of Masonry Structures*. PhD thesis, University of Cambridge, Cambridge, UK, 2002.

[53] D. O'Dwyer. Funicular analysis of masonry vaults. *Computers & Structures*, 73(1):187–197, 1999.

[54] J. Heyman. Leaning towers. *Meccanica*, 27:153–159, 1992.

[55] S. Huerta. The safety of masonry buttresses. *Proceedings of the Institution of Civil Engineers - Engineering History and Heritage*, 163(1):3–24, 2010.

[56] J.A. Ochsendorf. The masonry arch on spreading supports. *The Structural Engineer*, 84(2):29–35, 2006.

[57] J. Heyman. La coupe des pierres. In K.E. Kurrer, W. Lorenz, and V. Wetzk, editors, *Proc. 3rd Int. Congr. Constr. Hist.*, pages 807–812, Cottbus, Germany, May 2009.

[58] H. Alexakis and N. Makris. Limit equilibrium analysis of masonry arches. *Archive of Applied Mechanics*, 85:1363–1381, 2015.

[59] P. Block and J. Ochsendorf. Thrust Network Analysis: A new methodology for three-dimensional equilibrium. *Journal of the International Association for Shell and Spatial Structures*, 48(3):167–173, 2007.

[60] H.J. Schek. The force density method for form finding and computation of general networks. *Computer Methods in Applied Mechanics and Engineering*, 3(1):115–134, 1974.

[61] M. J. Clerk. On reciprocal figures and diagrams of forces. *The London, Edinburgh, and Dublin Philosophical Magazine and Journal of Science*, 27(182):250–261, 1864.

[62] S. Pellegrino and C.R. Calladine. Matrix analysis of statically and kinematically indeterminate frameworks. *International Journal of Solids and Structures*, 22(4):409–428, 1986.

[63] D. Veenendaal and P. Block. Comparison of form-finding methods. In *Shell Structures for Architecture*, pages 129–144. Routledge, 2014.

[64] A. Kilian and J. Ochsendorf. Particle-spring systems for structural form finding. *Journal of the International Association for Shell and Spatial Structures*, 46(148):77–84, 2005.

[65] S. Bagrianski and A.B. Halpern. Form-finding of compressive structures using prescriptive dynamic relaxation. *Computers & Structures*, 132:65–74, 2014.

[66] A. Liew, D. Pagonakis, T. Van Mele, and P. Block. Load-path optimisation of funicular networks. *Meccanica*, 53(1-2):279–294, 2018.

[67] R. Oval, M. Rippmann, T.V. Mele, O. Baverel, and P. Block. Patterns for masonry vault design. In *Proceedings of IASS Annual Symposia*, Hamburg, Germany, September 2017.

[68] R. Oval, M. Rippmann, R. Mesnil, T.V. Mele, O. Baverel, and P. Block. Topology finding of structural patterns. In *Advances in Architectural Geometry 2018*, pages 342–363, Gothenburg, Sweden, September 2018.

[69] R. Oval, R. Mesnil, T.V. Mele, P. Block, and O. Baverel. Rule-based topology finding of patterns towards multi-objective structural design. In *Proceedings of IASS Annual Symposia*, Barcelona, Spain, October 2019.

[70] R. Oval, M. Rippmann, R. Mesnil, T. Van Mele, O. Baverel, and P. Block. Feature-based topology finding of patterns for shell structures. *Automation in Construction*, 103:185–201, 2019.

[71] J.K. Wight and J.G. MacGregor. *Reinforced Concrete: Mechanics and Design*. Pearson, 6th edition, 2012.

[72] P. Roca, A. Viviescas, M. Lobato, C. Díaz, and I. Serra. Capacity of shear walls by simple equilibrium models. *International Journal of Architectural Heritage*, 5(4-5):412–435, 2011.

[73] P. Foraboschi and A. Vanin. Non-linear static analysis of masonry buildings based on a strut-and-tie modelling. *Soil Dynamics and Earthquake Engineering*, 55:44–58, 2013.

[74] F. Palmisano and A. Elia. Shape optimization of strut-and-tie models in masonry buildings subjected to landslide-induced settlements. *Engineering Structures*, 84:223–232, 2015.

[75] M. Angelillo, E. Babilio, and A. Fortunato. Singular stress fields for masonry-like vaults. *Continuum Mechanics and Thermodynamics*, 25(2):423–441, March 2013.

[76] A. Baratta and O. Corbi. On the equilibrium and admissibility coupling in NT vaults of general shape. *International Journal of Solids and Structures*, 47(17):2276–2284, August 2010.

[77] F. Fraternali. A thrust network approach to the equilibrium problem of unreinforced masonry vaults via polyhedral stress functions. *Mechanics Research Communications*, 37(2):198–204, 2010.

[78] Y.C. Chiang and A. Borgart. A form-finding method for membrane shells with radial basis functions. *Engineering Structures*, 251:113514, January 2022.

[79] F. Barsi, R. Barsotti, S. Bennati, and T. Ciblac. Investigating the relation between thrust networks and thrust surfaces for masonry domes subjected to vertical loads: A case study. *International Journal of Architectural Heritage*, pages 1–19, 2022.

[80] T. Mitchell, W. Baker, A. McRobie, and A. Mazurek. Mechanisms and states of self-stress of planar trusses using graphic statics, part I: The fundamental theorem of linear algebra and the Airy stress function. *International Journal of Space Structures*, 31(2-4):85–101, 2016.

[81] M. Konstantatou, W. Baker, T. Nugent, and A. McRobie. Grid-shell design and analysis via reciprocal discrete Airy stress functions. *International Journal of Space Structures*, 37(2):150–164, June 2022.

[82] R.K. Livesley. Limit analysis of structures formed from rigid blocks. *International Journal for Numerical Methods in Engineering*, 12(12):1853–1871, 1978.

[83] R.K. Livesley. A computational model for the limit analysis of three-dimensional masonry structures. *Meccanica*, 27(3):161–172, 1992.

[84] F. Portioli and L. Cascini. Large displacement analysis of dry-jointed masonry structures subjected to settlements using rigid block modelling. *Engineering Structures*, 148:485–496, 2017.

[85] M. Gilbert and C. Melbourne. Rigid-block analysis of masonry structures. *Structural Engineer*, 72(21):356–361, 1994.

[86] P. Block, T. Ciblac, and J. Ochsendorf. Real-time limit analysis of vaulted masonry buildings. *Computers & Structures*, 84(29):1841–1852, 2006.

[87] P.B. Lourenço and J.G. Rots. Multisurface Interface Model for Analysis of Masonry Structures. *Journal of Engineering Mechanics*, 123(7), 1997.

[88] L. Pelà, M. Cervera, and P. Roca. An orthotropic damage model for the analysis of masonry structures. *Construction and Building Materials*, 41:957–967, 2013.

[89] P. Roca, M. Cervera, G. Gariup, and L. Pela'. Structural analysis of masonry historical constructions. classical and advanced approaches. *Archives of Computational Methods in Engineering*, 17(3):299–325, 2010.

[90] H.R. Lotfi and P.B. Shing. Interface model applied to fracture of masonry structures. *Journal of Structural Engineering*, 120(1):63–80, January 1994.

[91] P.B. Lourenço, G. Milani, A. Tralli, and A. Zucchini. Analysis of masonry structures: review of and recent trends in homogenization techniques. *Canadian Journal of Civil Engineering*, 34(11):1443–1457, 2007.

[92] G. Milani, P.B. Lourenço, and A. Tralli. Homogenised limit analysis of masonry walls Part I: Failure surfaces. *Computers & Structures*, 84(3):166–180, 2006.

[93] E. Milani, G. Milani, and A. Tralli. Limit analysis of masonry vaults by means of curved shell finite elements and homogenization. *International Journal of Solids and Structures*, 45(20):5258–5288, 2008.

[94] Cundall (Peter) Associates Virginia water (England). UDEC - A generalised distinct element program for modelling jointed rock. Technical report, 1980.

[95] G.H. Shi and R.E. Goodman. Two dimensional discontinuous deformation analysis. *International Journal for Numerical and Analytical Methods in Geomechanics*, 9(6):541–556, 1985.

[96] M. Ma, A. Pan, M. Luan, and J. Gebara. eismic analysis of stone arch bridges using discontinuous deformation analysis. In *Proceedings of the 11th World Conference on Earthquake Engineering*, 1996.

[97] J.V. Lemos. Discrete element modeling of masonry structures. *International Journal of Architectural Heritage*, 1(2):190–213, 2007.

[98] A.M. D'Altri, V. Sarhosis, G. Milani, J. Rots, S. Cattari, S. Lagomarsino, E. Sacco, A. Tralli, G. Castellazzi, and S. de Miranda. Modeling strategies for the computational analysis of unreinforced masonry structures: Review and classification. *Archives of Computational Methods in Engineering*, August 2019.

[99] A. Munjiza, D. Owen, and N. Bicanic. A combined finite□discrete element method in transient dynamics of fracturing solids. *Engineering Computations*, 12(2):145–174, 1995.

[100] I.H.P. Mamaghani, O. Aydan, and Y. Kajikawa. Analysis of masonry structures under static and dynamic loading by discrete finite element method. *Doboku Gakkai Ronbunshu*, 1999(626):1–12, 1999.

[101] M. Akbarzadeh, T. Van Mele, and P. Block. On the equilibrium of funicular polyhedral frames and convex polyhedral force diagrams. *Computer-Aided Design*, 63:118–128, 2015.

[102] M. Konstantatou, P. D'Acunto, and A. McRobie. Polarities in structural analysis and design: n-dimensional graphic statics and structural transformations. *International Journal of Solids and Structures*, 152-153:272–293, 2018.

[103] P. D'Acunto, J.P. Jasienski, P.O. Ohlbrock, C. Fivet, J. Schwartz, and D. Zastavni. Vector-based 3D graphic statics: A framework for the design of spatial structures based on the relation between form and forces. *International Journal of Solids and Structures*, 167: 58–70, 2019.

[104] C. Millar, A. McRobie, and W. Baker. A Graphical Method for Determining Truss Stability. *Journal of the International Association for Shell and Spatial Structures*, 61(4):285–295, December 2020.

[105] A. McRobie, C. Millar, D. Zastavni, and W. Baker. Graphical Stability Analysis of Maillart's Roof at Chiasso. *Structural Engineering International*, 32(4):538–546, October 2022.

[106] A. McRobie. Maxwell and Rankine reciprocal diagrams via Minkowski sums for two-dimensional and three-dimensional trusses under load. *International Journal of Space Structures*, 31(2-4):203–216, June 2016.

[107] A. McRobie, M. Konstantatou, G. Athanasopoulos, and L. Hannigan. Graphic kinematics, visual virtual work and elastographics. *Royal Society Open Science*, 4(5):170202, May 2017.

[108] W.S. Dorn, R.E. Gomory, and H.J. Greenberg. Automatic design of optimal structures. *Journal de Mécanique*, 3:25–52, 1964.

[109] T.J. Pritchard, M. Gilbert, and A. Tyas. Plastic layout optimization of large-scale frameworks subject to multiple load cases, member self-weight and with joint length penalties. In *6th World Congresses of Structural and Multidisciplinary Optimization*, Rio de Janerio, Brazil, June 2005.

[110] T. Zegard and G.H. Paulino. Grand—ground structure based topology optimization for arbitrary 2d domains using matlab. *Structural and Multidisciplinary Optimization*, 50(5): 861–882, 2014.

[111] T. Sokół. A 99 line code for discretized michell truss optimization written in mathematica. *Structural and Multidisciplinary Optimization*, 43(2):181–190, 2011.

[112] L. He, M. Gilbert, and X. Song. A Python script for adaptive layout optimization of trusses. *Structural and Multidisciplinary Optimization*, 60(2):835–847, 2019.

[113] L. He and M. Gilbert. Rationalization of trusses generated via layout optimization. *Structural and Multidisciplinary Optimization*, 52:677–694, 2015.

[114] M. Gilbert, W. Darwich, A. Tyas, and P. Shepherd. Application of large-scale layout optimization techniques in structural engineering practice. In *Proceedings of the 6th World Congress of Structural and Multidisciplinary Optimization*, Rio de Janeiro, Brazil, June 2005.

[115] Y. Jiang, T. Zegard, W.F. Baker, and G.H. Paulino. Form-finding of grid-shells using the ground structure and potential energy methods: A comparative study and assessment. *Structural and Multidisciplinary Optimization*, 57(3):1187–1211, March 2018.

[116] K. Bołbotowski. Optimal vault problem – form finding through 2D convex program. *Computers & Mathematics with Applications*, 109:280–324, March 2022.

[117] H.E. Fairclough, M. Gilbert, A.V. Pichugin, A. Tyas, and I. Firth. Theoretically optimal forms for very long-span bridges under gravity loading. *Proceedings of the Royal Society A: Mathematical, Physical and Engineering Sciences*, 474(2217):20170726, 2018.

[118] M. Rippmann, L. Lachauer, and P. Block. Interactive vault design. *International Journal of Space Structures*, 27(4):219–230, December 2012.

[119] M.B. Fuchs and E. Moses. Optimal structural topologies with transmissible loads. *Structural and Multidisciplinary Optimization*, 19(4):263–273, 2000.

[120] H. Lu, A. Tyas, M. Gilbert, and A.V. Pichugin. On transmissible load formulations in topology optimization. *Structural and Multidisciplinary Optimization*, 64:23–37, 2021.

[121] P. Martínez, P. Martí, and O.M. Querin. Growth method for size, topology, and geometry optimization of truss structures. *Structural and Multidisciplinary Optimization*, 33:13–26, 2006.

[122] M.P. Bendsøe. Optimal shape design as a material distribution problem. *Structural Optimization*, 1(4):193–202, December 1989.

[123] M.P. Bendsøe and N. Kikuchi. Generating optimal topologies in structural design using a homogenization method. *Computer Methods in Applied Mechanics and Engineering*, 71(2):197–224, 1988.

[124] K. Suzuki and N. Kikuchi. A homogenization method for shape and topology optimization. *Computer Methods in Applied Mechanics and Engineering*, 93(3):291–318, 1991.

[125] I. Lochner-Aldinger and A. Schumacher. Homogenization method. In S. Adriaenssens, P. Block, D. Veenendaal, and C. Williams, editors, *Shell Structures for Architecture: Form Finding and Optimization*, chapter 17, pages 211–224. Taylor & Francis - Routledge, 2014.

[126] G. Rozvany. The SIMP method in topology optimization - theoretical background, advantages and new applications. In *8th Symposium on Multidisciplinary Analysis and Optimization*, Long Beach, USA, September 2000.

[127] G.I.N. Rozvany, M. Zhou, and T. Birker. Generalized shape optimization without homogenization. *Structural Optimization*, 4(3):250–252, 1992.

[128] Y.M. Xie and G.P. Steven. A simple evolutionary procedure for structural optimization. *Computers & Structures*, 49(5):885–896, December 1993.

[129] P. Tanskanen. The evolutionary structural optimization method: theoretical aspects. *Computer Methods in Applied Mechanics and Engineering*, 191(47-48):5485–5498, 2002.

[130] O. Querin, G. Steven, and Y. Xie. Evolutionary structural optimisation (ESO) using a bidirectional algorithm. *Engineering Computations*, 15(8):1031–1048, 1998.

[131] X. Huang and Y.M. Xie. A further review of ESO type methods for topology optimization. *Structural and Multidisciplinary Optimization*, 41(5):671–683, 2010.

[132] Y. Ding. Shape optimization of structures: A literature survey. *Computers & Structures*, 24(6):985–1004, January 1986.

[133] M.Y. Wang, X. Wang, and D. Guo. A level set method for structural topology optimization. *Computer Methods in Applied Mechanics and Engineering*, 192(1-2):227–246, 2003.

[134] N. Guarín-Zapata. An illustration of the level-set method, 2018. [Online] San Francisco: Wikimedia Foundation. Available from: https://en.wikipedia.org/wiki/Level-set_method#/media/File:Level_set_method.png [Accessed: accessed 10 August 2023].

[135] K.E. Kurrer. *The History of the Theory of Structures: Searching for Equilibrium*. Wiley, 2 edition, 2018.

[136] J.A. Ochsendorf and P. Block. Designing unreinforced masonry. In E. Allen and W. Zalewski, editors, *Form and Forces: Designing Efficient, Expressive Structures*, chapter 8, pages 215–245. Wiley, 2009.

[137] J. Chilton and C.C. Chuang. Rooted in nature: Aesthetics, geometry and structure in the shells of Heinz Isler. *Nexus Network Journal*, 19(3):763–785, 2017.

[138] V. Paris, G. Ruscica, and G. Mirabella Roberti. Graphical modelling of hoop force distribution for equilibrium analysis of masonry domes. *Nexus Network Journal*, 23(4): 855–878, 2021.

[139] J. Heyman. Equilibrium of masonry arches. *Proceedings of the Institution of Civil Engineers - Engineering and Computational Mechanics*, 163(3):129–133, 2010.

[140] J. Ochsendorf. The masonry arch on spreading supports. *The Structural Engineer*, 84 (2):29–35, May 2006.

[141] N. Grillanda, A. Chiozzi, G. Milani, and A. Tralli. NURBS solid modeling for the three-dimensional limit analysis of curved rigid block structures. *Computer Methods in Applied Mechanics and Engineering*, 399:115304, 2022.

[142] F. Marmo. Archlab: a matlab tool for the thrust line analysis of masonry arches. 8(1): 26–35, 2021.

[143] K. Bagi. When Heyman's Safe Theorem of rigid block systems fails: Non-Heymanian collapse modes of masonry structures. *Int J Solids Struct*, 51(14):2696–2705, July 2014.

[144] T.E. Boothby. Analysis of masonry arches and vaults. *Progress in Structural Engineering and Materials*, 3(3):246–256, 2001.

[145] H. Moseley. *The Mechanical Principles of Engineering and Architecture*. Longman, Brown, Green, and Longmans, New York, 1843.

[146] M. Milankovitch. Theorie der druckkurven. *Zeitschrift für Mathematik und Physik*, 55: 1–27, 1907.

[147] F. Foce. Milankovitch's Theorie der Druckkurven: Good mechanics for masonry architecture. *Nexus Network Journal*, 9(2):185–210, 2007.

[148] H.E. Fairclough, L. He, T.J. Pritchard, and M. Gilbert. LayOpt: An educational web-app for truss layout optimization. *Structural and Multidisciplinary Optimization*, 64(4): 2805–2823, October 2021.

[149] K.I.U. Nanayakkara, A. Liew, and M. Gilbert. Application of thrust layout optimization to masonry structures. *Proceedings of the Royal Society A: Mathematical, Physical and Engineering Sciences*, 479(2273):20230053, May 2023.

[150] M. Gilbert, C. Casapulla, and H.M. Ahmed. Limit analysis of masonry block structures with non-associative frictional joints using linear programming. *Computers & Structures*, 84(13-14):873–887, 2006.

[151] T. Michiels, R. Napolitano, S. Adriaenssens, and B. Glisic. Comparison of thrust line analysis, limit state analysis and distinct element modeling to predict the collapse load and collapse mechanism of a rammed earth arch. *Engineering Structures*, 148:145–156, 2017.

[152] F. Loccarini, G. Ranocchiai, T. Rotunno, and M. Fagone. Experimental and numerical analyses of strengthened rammed earth masonry arches. *Computers & Structures*, 239: 106329, 2020.

[153] J. Valentino, M. Gilbert, M. Gueguin, and C.C. Smith. Limit analysis of masonry walls using discontinuity layout optimization and homogenization. *International Journal for Numerical Methods in Engineering*, 124(2):358–381, 2023.

[154] N.A. Nodargi and P. Bisegna. A unifying computational approach for the lower-bound limit analysis of systems of masonry arches and buttresses. *Engineering Structures*, 221: 110999, 2020.

[155] M. Fantin and T. Ciblac. Extension of thrust network analysis with joints consideration and new equilibrium states. *International Journal of Space Structures*, 31(2-4):190–202, June 2016.

[156] A. Lenczner. Speaking stone – a retrospective look at the stone arch design for the Padre Pio church, Italy. *Structural Engineer*, 98:30–39, 2020.

[157] S. Webb. Stone rises. *RIBA Journal*, 127:52–54, 2020.

[158] J.V. Lemos. Discrete element modeling of masonry structures. *International Journal of Architectural Heritage*, 1(2):190–213, 2007.

[159] M. Ferris and F. Tin-Loi. Limit analysis of frictional block assemblies as a mathematical program with complementarity constraints. *International Journal of Mechanical Sciences*, 43(1):209–224, 2001.

[160] A. Orduña and P.B. Lourenço. Cap model for limit analysis and strengthening of masonry structures. *Journal of Structural Engineering*, 129(10):1367–1375, 2003.

[161] N.A. Nodargi, C. Intrigila, and P. Bisegna. A variational-based fixed-point algorithm for the limit analysis of dry-masonry block structures with non-associative Coulomb friction. *International Journal of Mechanical Sciences*, 161–162:105078, October 2019.

[162] M. Gilbert. Gross displacement mechanism analysis of masonry bridges and tunnel linings. In *Proc. 11th Int. Brick Block Mason. Conf.*, pages 473–482, Shanghai, China, October 1997.

[163] A. Iannuzzo, A. Dell'Endice, T. Van Mele, and P. Block. Numerical limit analysis-based modelling of masonry structures subjected to large displacements. *Computers & Structures*, 242:106372, 2021.

[164] C. Casapulla, F. Portioli, A. Maione, and R. Landolfo. A macro-block model for in-plane loaded masonry walls with non-associative coulomb friction. *Meccanica*, 48(9):2107–2126, 2013.

[165] P. Block and J. Ochsendorf. Thrust network analysis: a new methodology for three-dimensional equilibrium. *Journal of the International Association for Shell and Spatial Structures*, 48(3):167–173, 2007.

[166] R. Maia Avelino, A. Iannuzzo, T. Van Mele, and P. Block. Assessing the safety of vaulted masonry structures using thrust network analysis. *Computers & Structures*, 257:106647, 2021.

[167] C. Melbourne and M. Gilbert. The behaviour of multiring brickwork arch bridges. *The Structural Engineer*, 73(3):39–47, 1995.

[168] Y. Xia, M. Langelaar, and M.A.N. Hendriks. A critical evaluation of topology optimization results for strut-and-tie modeling of reinforced concrete. *Computer-Aided Civil and Infrastructure Engineering*, 35(8):850–869, 2020.

[169] G. Milani and M. Bruggi. Simple homogenization-topology optimization approach for the pushover analysis of masonry walls. *International Journal of Architectural Heritage*, 12(3):395–408, 2018.

[170] Robert McNeel and Associates. *Rhinoceros: modeling tools for designers (version 6.0)*, 2020. [Computer software].

[171] G. Van Rossum and Python Software Foundation. *Python (version 3.7)*, 2021. [Computer software].

[172] S. Van Der Walt, C. Colbert, and G. Varoquaux. The NumPy array: a structure for efficient numerical computation. *Computing in Science & Engineering*, 13(2):22–30, 2011.

[173] S. Gillies. *Shapely (version 1.7.0)*, 2021. [Computer software].

[174] MOSEK ApS. *MOSEK Fusion API for Python (version 9.1.8)*, 2021. [Computer software].

[175] M. Botsch, S. Steinberg, S. Bischoff, and L. Kobbelt. Openmesh-a generic and efficient polygon mesh data structure. In *OpenSG Symposium*, Darmstadt, Germany, January 2002.

[176] A.A. Hagberg, D.A. Schult, and P.J. Swart. Exploring network structure, dynamics, and function using NetworkX. In G. Varoquaux, T. Vaught, and J. Millman, editors, *Proceedings of the 7th Python in Science Conference (SciPy2008)*, pages 11–15, Pasadena, USA, August 2008.

[177] LimitState Ltd. *LimitState:GEO (version 3.5.g)*, 2021. [Computer software].

[178] C. Smith and M. Gilbert. Application of discontinuity layout optimization to plane plasticity problems. *Proceedings of the Royal Society A: Mathematical, Physical and Engineering Sciences*, 463(2086):2461–2484, 2007.

[179] M. Gilbert, C.C. Smith, and T.J. Pritchard. Masonry arch analysis using discontinuity layout optimisation. *Proceedings of the Institution of Civil Engineers - Engineering and Computational Mechanics*, 163(3):155–166, 2010.

[180] T. Lewinski, T. Sokół, and C. Graczykowski. *Michell structures*. Springer, 2018.

[181] V. Beatini, G. Royer-Carfagni, and A. Tasora. The role of frictional contact of constituent blocks on the stability of masonry domes. *Proceedings of the Royal Society A: Mathematical, Physical and Engineering Sciences*, 474(2209):20170740, 2018.

[182] Y. Korany, R.L.S. Drysdale, and S.E. Chidiac. Retrofit of unreinforced masonry buildings: The state-of-the-art. In *Proceedings of the 9th Canadian Masonry Symposium*, Fredericton, Canada, June 2001.

[183] T. Manzouri, M.P. Schuller, P.B. Shing, and B. Amadei. Repair and retrofit of unreinforced masonry structures. *Earthquake Spectra*, 12(4):903–922, November 1996.

[184] P.D. Gkournelos, T.C. Triantafillou, and D.A. Bournas. Seismic upgrading of existing masonry structures: A state-of-the-art review. *Soil Dynamics and Earthquake Engineering*, 107428:903–922, October 2022.

[185] E. Rovithis and K. Pitilakis. Seismic assessment and retrofitting measures of a historic stone masonry bridge. *Earthquakes and Structures*, 10:645–667, March 2016.

[186] C. Modena, G. Tecchio, C. Pellegrino, F. da Porto, M. Donà, P. Zampieri, and M.A. Zanini. Reinforced concrete and masonry arch bridges in seismic areas: Typical deficiencies and retrofitting strategies. *Structure and Infrastructure Engineering*, 11(4): 415–442, April 2015.

[187] A. Bayraktar, S. Bayraktar, and E. Hökelekli. Strengthening techniques for masonry domes: A review. *International Journal of Space Structures*, 38(1):30–39, March 2023.

[188] R. Chmielewski and L. Kruszka. Application of selected modern technology systems to strengthen the damaged masonry dome of historical St. Anna's Church in Wilanów (Poland). *Case Studies in Construction Materials*, 3:92–101, December 2015.

[189] J. Heyman. The strengthening of the west tower of ely cathedral. *Proceedings of the Institution of Civil Engineers*, 60(1):123–147, November 1976.

[190] P. Aghabeigi and S. Farahmand-Tabar. Seismic vulnerability assessment and retrofitting of historic masonry building of Malek Timche in Tabriz Grand Bazaar. *Engineering Structures*, 240:112418, August 2021.

[191] A. Ascıkouglu, Ö. Avcsar, P.B. Lourenço, and L.C. Silva. Effectiveness of seismic retrofitting of a historical masonry structure: Kütahya Kurs unlu Mosque, Turkey. *Bulletin of Earthquake Engineering*, 17(6):3365–3395, June 2019.

[192] V. Gattulli, G. Lampis, G. Marcari, and A. Paolone. Simulations of FRP reinforcement in masonry panels and application to a historic facade. *Engineering Structures*, 75: 604–618, 2014.

[193] M.R. Valluzzi, C. Modena, and G. de Felice. Current practice and open issues in strengthening historical buildings with composites. *Materials and Structures*, 47(12): 1971–1985, 2014.

[194] M.R. Valluzzi, M. Valdemarca, and C. Modena. Behavior of brick masonry vaults strengthened by FRP laminates. *Journal of Composites for Construction*, 5(3):163–169, 2001.

[195] S. Huerta. Mechanics of masonry vaults: The equilibrium approach. In *Historical Constructions*, pages 47–69, 2001.

[196] J. Heyman. *The Stone Skeleton: Structural Engineering of Masonry Architecture*. Cambridge University Press, Cambridge, UK, 1997.

[197] F. Fraternali, G. Carpentieri, M. Modano, F. Fabbrocino, and R. Skelton. A tensegrity approach to the optimal reinforcement of masonry domes and vaults through fiber-reinforced composite materials. *Composite Structures*, 134:247–254, 2015.

[198] I. Basilio, D. Oliveira, and P. Lourenço. Optimal frp strengthening of masonry arches. In *13th International Brick and Block Masonry Conference*, Amsterdam, July 2004.

[199] T.D. Krevaikas and T.C. Triantafillou. Computer-aided strengthening of masonry walls using fibre-reinforced polymer strips. *Materials and Structures*, 38(1):93–98, January 2005.

[200] M. Bruggi and A. Taliercio. Optimal strengthening of no–tension structures with externally bonded reinforcing layers or ties. *Structural and Multidisciplinary Optimization*, 55(5):1831–1846, May 2017.

[201] M. Bruggi, G. Milani, and A. Taliercio. Design of the optimal fiber-reinforcement for masonry structures via topology optimization. *International Journal of Solids and Structures*, 50(13):2087–2106, June 2013.

[202] G. Carpentieri, M. Modano, F. Fabbrocino, L. Feo, and F. Fraternali. On the minimal mass reinforcement of masonry structures with arbitrary shapes. *Meccanica*, 52(7): 1561–1576, 2017.

[203] M. Gilbert. Limit analysis applied to masonry arch bridges: State-of-the-art and recent developments. In *5th International Conference on Arch Bridges*, Madeira, Portugal, 2007.

[204] L. He, M. Gilbert, T. Johnson, and T. Pritchard. Conceptual design of AM components using layout and geometry optimization. *Computers & Mathematics with Applications*, 78(7):2308–2324, October 2019.

[205] S. Uhland, H. Lechtman, and L. Kaufman. Assessment of the As-Cu-Ni system: An example from archaeology. *Calphad*, 25(1):109–124, March 2001.

[206] A. Vranich. Reconstructing ancient architecture at Tiwanaku, Bolivia: The potential and promise of 3D printing. *Heritage Science*, 6(1):65, December 2018.

[207] Ž. Nikolic, L. Krstevska, P. Marovic, and H. Smoljanovic. Experimental investigation of seismic behaviour of the ancient Protiron monument model. *Earthquake Engineering & Structural Dynamics*, 48(6):573–593, 2019.

[208] L. Krstevska, Ž. Nikolic, and M. Kustura. Shake Table Testing of Two Historical Masonry Structures for Estimation of Their Seismic Stability. *International Journal of Architectural Heritage*, 15(1):45–63, January 2021.

[209] H. Kim. A Study of Stone-joint Metal Clamps in China and Korea during the 6th-8th Centuries. *The Silk Road*, 18, 2020.

[210] Ž. Nikolic, L. Krstevska, H. Smoljanovic, and N. Živaljic. Modelling of the Influence of Metal Connectors on the Resistance of Historical Dry-Stone Masonry Structures. *International Journal of Architectural Heritage*, 14(10):1468–1483, November 2020.

[211] A. Rueda Márquez De La Plata and P.A. Cruz Franco. A simulation study to calculate a structure conceived by Eugène Viollet-le-Duc in 1850 with finite element analysis. *Materials*, 12(16):2576, August 2019.

[212] P. Rice and A. Lenczner. Pabellon del Futuro Expo '92 Seville. *The Arup Journal*, 27(3), 1992.

[213] L. Todisco, C. Fivet, H.C. Peiretti, and C. Mueller. Design and exploration of externally post-tensioned structures using graphic statics. In *Proceedings of the International Association for Shell and Spatial Structures (IASS) Symposium 2015*, Amsterdam, 2015.

[214] L. Todisco, E. Stocks, J. León, and H. Corres. Enhancing the Structural Performance of Masonry Structures by Post-Tensioning. *Nexus Network Journal*, 20(3):671–691, December 2018.

[215] Y. Or. *Frictional equilibrium postures for robotic locomotion*. PhD thesis, Technion - Israel Institute of Technology, Haifa, Israel, 2007.

[216] D.C. Drucker. Coulomb friction, plasticity, and limit loads. Technical Report 85, 1953.

[217] H.E. Fairclough. *Layout Optimization of Structures: Novel Methods and Applications*. PhD thesis, the University of Sheffield, Sheffield, UK, 2019.